

Papers presented to the
**NINETEENTH SYMPOSIUM
ON ANTARCTIC METEORITES**



May 30-June 1, 1994

NATIONAL INSTITUTE OF POLAR RESEARCH,
TOKYO

国立極地研究所

Papers presented to the
NINETEENTH SYMPOSIUM
ON ANTARCTIC METEORITES



May 30-June 1, 1994

NATIONAL INSTITUTE OF POLAR RESEARCH,
TOKYO

国立極地研究所

Monday, May 30, 1994

0900 - 1200 Registration Auditorium (6th Floor)

0925 - 0930 Opening Address **Takao Hoshiai**
Director-General
National Institute of
Polar Research

* Speaker

Chairmen: Ikeda Y. and Miura Yasunori

- 1 0930 - 0945 **Nishio F*., Fujita H. and Higashi A.**
Comparison on model study and field survey for meteorite mass concentration and age of ice in Allan Hills & Yamato meteorite ice field
- 2 0945 - 1000 **Miura Yasunori, Iancu G.O.*, Iancu G., Yanai K. and Haramura H.**
Meteoritics aspects in Romania
- 3 1000 - 1015 **Miura Yasunori***
Orbits and collision types of impact materials to the earth
- 4 1015 - 1030 **Nakamura T.*, Tomeoka K., Sekine T. and Takeda H.**
Shock metamorphism of CK and CV chondrites inferred from experimentally produced shock features of Allende
- 5 1030 - 1045 **Noguchi T.***
Comparison of petrology and mineralogy of the PCA 91082 and the Yamato-793495 (CR) chondrites: On the phyllosilicate clasts
- 6 1045 - 1100 **Ichikawa O.* and Ikeda Y.**
Petrology of Yamato-8449 chondrite (CR)
- 7 1100 - 1115 **Ikeda Y.* and Kimura M.**
Alkali-lime reactions of Allende chondrules I: Alteration of chondrules with known oxygen-isotope compositions
- 8 1115 - 1130 **Kimura M.* and Ikeda Y.**
Alkali-lime reactions of Allende chondrules II: Ca-rich phases in chondrules
- 9 1130 - 1145 **Kojima T.*, Yada S. and Tomeoka K.**
Ca-Al-rich inclusions in three Antarctic CO3 chondrites, Y-81020, Y-82050 and Y-790992: Record of low-temperature alteration
- 10 1145 - 1200 **Kojima H.*, El Goresy A. and Yanai K.**
Chemically different populations of hibonites and perovskites in a CAI from Y-791601: Evidence for an extraneous origin
- 11 1200 - 1215 **Zinovieva N.G.*, Mitreikina O.B. and Granovsky L.B.**
K-rich object in the matrix of the ordinary chondrite Raguli (H3-4)
- 1215 - 1315 Lunch Time

Chairmen: Kimura M. and Nagahara H.

- 12** 1315 - 1330 **Fujita T.* and Kitamura M.**
Origins of the lithic fragments in the unequilibrated ordinary chondrites, Julesburg (L3) and Y-790448 (LL3)
- 13** 1330 - 1345 **Yanai K.* and Kojima H.**
Chondritic breccia consisting of mixed two ordinary chondrite components
- 14** 1345 - 1400 **Yamaguchi A. and Takeda H.***
Mineralogical study of recrystallized clastic matrix in the Yamato-74356 monomict eucrite
- 15** 1400 - 1420 **Pun A.* and Papike J.J.**
Unequilibrated eucrites Y-74450, Y-793548, Y-82210, and Pasamonte: Pyroxene REE systematics and major, minor, and trace element zoning
- 16** 1420 - 1435 **Saiki K.* and Takeda H.**
The origin of cumulate eucrite deduced from magma differentiation simulation
- 17** 1435 - 1450 **Yanai K.***
Comparative studies of three angrites; Angra dos Reis, LEW87051 and Asuka-881371 meteorites
- 18** 1450 - 1505 **Murae T.*, Yamori A. and Kawashima N.**
Comparison of shock induced carbonaceous matter from C60/70 fullerene with kerogen-like organic matter in carbonaceous chondrites
- 1505 - 1530 Tea Time
- 19** 1530 - 1550 **Bridges J.C.*, Franchi I.A., Hutchison R., Alexander C.M.O'D. and Pillinger C.T.**
A feldspar-nepheline achondrite clast in Parnallee with possible links to ureilites
- 20** 1550 - 1610 **Lauretta D.S.* and Fegley B., Jr.**
Kinetics and grain growth mechanism for troilite formation on iron metal in H₂-H₂S gas mixtures
- 21** 1610 - 1625 **Imae N.* and Kitamura M.**
Troilite formation reaction between metallic grain and S-rich gas in chondrites
- 1630 - 1730 Business meeting

Chairman: Fujimaki H.

Tuesday, May 31, 1994

Chairmen: Tsuchiyama A. and Fukuoka T.

- 22 0930 - 0945 **Tsuchiyama A.*, Fujimoto K. and Uyeda C.**
Evaporation experiments of metallic iron into vacuum
- 23 0945 - 1000 **Koga A.* and Nagahara H.**
Magnesium isotopic fractionation in the olivines from Allende chondrules and isolated grains caused by evaporation in the solid state
- 24 1000 - 1015 **Nagahara H.* and Ozawa K.**
Kinetics of evaporation and reaction with hydrogen of forsterite
- 25 1015 - 1030 **Sasaki S.*, Nagahara H., Kitagami K. and Nakagawa Y.**
Heating during solar nebula formation and Mg isotopic fractionation in CAI
- 26 1030 - 1045 **Togashi S.*, Kamioka H., Ebihara M. Yanai K. and Kojima H.**
Trace elements of Antarctic meteorites by INAA (I)
- 27 1045 - 1105 **Kallemeyn G.W.* and Rubin A.E.**
Loongana 001 and Coolidge: A new carbonaceous chondrite grouplet
- 28 1105 - 1120 **Torigoye N.*, Tatsumoto M. and Yanai K.**
The U-Th-Pb and Sm-Nd isotopic systematics of MET 78008 ureilite
- 29 1120 - 1135 **Morikawa N.* and Nakamura N.**
Chemical fractionations of primitive achondrites and their implications for melting processes
- 30 1135 - 1150 **Okano O.* and Katayama H.**
Shock-induced melt mixing of L and LL materials in Y-793533
- 31 1150 - 1205 **Zinovieva N.G.*, Mitreikina O.B. and Granovsky L.B.**
Melted nature of ordinary chondrites: Experimental data and structural-petrological evidence of liquid immiscibility process during chondrule formation
- 1205 - 1300 Lunch Time

Chairmen: Nakamura N. and Takaoka N.

- 32 1300 - 1315 **Fukuoka T.***
Chemistry of the lithic inclusions in Yamato-75097, -793241 and -794046 meteorites
- 33 1315 - 1330 **Nakamura N.*, Morikawa N., Kojima H., Misawa K. and Yanai K.**
Zonal distributions of REE in the Y-75097 inclusion and their implications for the early formation and metamorphism

- 34** 1330 - 1345 **Nagao K.* and Miura Yayoi**
Noble gas isotopic compositions in the Yamato-75097 inclusion revealed by stepwise heating experiment
- 35** 1345 - 1400 **Misawa K.*, Nakamura N., Fujita T., Kitamura M. and Yurimoto H.**
REE abundances and Mg isotopic compositions of Allende barred olivine chondrules
- 36** 1400 - 1415 **Kano N.*, Yamakoshi K. and Matsuzaki H.**
Isotopic, chemical and textural properties of acid residues from various meteorites (II)
- 37** 1415 - 1430 **Ozaki H.* and Ebihara M.**
Rhenium, osmium and iridium in Antarctic unequilibrated ordinary chondrites
- 38** 1430 - 1445 **Kong P.*, Ebihara M. and Endo K.**
Preliminary study of element distribution trends in metallic fractions of an Antarctic ordinary chondrite ALH77231.51 (L6)
- 39** 1445 - 1500 **Mitreikina O.B., Zinovieva N.G.* and Granovsky L.B.**
Magmatic replacement processes in ureilites
- 1500 - 1530 Tea Time
- 40** 1530 - 1545 **Miura Yasunori***
Shocked carbon materials with CVD-diamond shapes
- 41** 1545 - 1600 **Takaoka N.***
Enrichment and fractionation of noble gases in bubbles
- 42** 1600 - 1615 **Kiyota K.* and Sugiura N.**
Nitrogen isotope measurement of UOCS by a laser probe method
-- Special Lecture (I) --

Chairman: Nakamura N.

- 43** 1615 - 1715 **Weisberg M.K.* and Prinz M.**
The CR chondrite clan

1730 - 1930 Reception Lecture Room (2F)

Wednesday, June 1, 1994

Chairmen: Kaneoka I. and Ebihara M.

- 44** 0930 - 0945 **Kong P.* and Ebihara M.**
Interrelation of parents and daughters of extinct nuclides in meteorites
- 45** 0945 - 1000 **Honda M.***
Low energy cosmogenic products in meteorites
- 46** 1000 - 1020 **Englert P.A.J.***
Cosmic ray tracks and cosmogenic ^{53}Mn in meteorites
- 47** 1020 - 1035 **Kaneoka I.*, Nagao K. and Takeda H.**
 ^{40}Ar - ^{39}Ar analyses of Juvinas fragments
- 48** 1035 - 1050 **Sugiura N.* and Zashu S.**
Nitrogen isotopic composition of CK chondrites
- 49** 1050 - 1105 **Miura Yayoi N.* and Sugiura N.**
Heavy nitrogen in a SNC orthopyroxenite ALH84001
- 50** 1105 - 1120 **Ozaki K.*, Takaoka N., Motomura Y. and Nagao K.**
Bubbles as a candidate for a noble gas trapping site:
Yamato-74063
- 51** 1120 - 1135 **Sugiura N.*, Higuchi Y. and Sakaguchi T.**
Accretion of fine particles: Experimental study under the atmospheric pressure
- 52** 1135 - 1150 **Takaki S.*, Yamanaka C. and Ikeya M.**
Optically stimulated luminescence of meteorite
- 1150 - 1300 Lunch Time

Chairmen: Sugiura N. and Fujimaki H.

- 53** 1300 - 1315 **Yamanaka A.*, Funaki M. and Nagai H.**
Magnetic properties of high petrologic grade L-LL chondrites, Tenham, Tuxtuac, Willard and Forrest B
- 54** 1315 - 1330 **Zbik M.* and Gostin V.A.**
Electronmicroscopical study of the distal ejecta layer from Flinders Ranges in South Australia
- 55** 1330 - 1350 **Lin W.***
Infrared absorption of the diaplectic glass
- 56** 1350 - 1410 **Zbik M.* and Gostin V.A.**
Morphology of Antarctic cosmic dust spherules, and comparison to spherules from the Tunguska catastrophe
- 57** 1410 - 1425 **Futagami T.***
Studies on cosmic matter in the deep sea core sample
- 58** 1425 - 1440 **Matsuzaki H.* and Yamakoshi K.**
Poynting-Robertson Effect and cosmogenic ^{26}Al in deep-sea stony spherules

Chairman: Fujimaki H.

- 59** 1440 - 1540 **Mittlefehldt D.W.* and Lindstrom M.M.**
ALH84001 orthopyroxenite: Comparison with other martian meteorites and Yamato 75032-type and LEW88xxx ferroan diogenites

Abstract only

- 60 Akai J.**
TEM-AEM examination on impact glass from Henbury meteor crater in Australia
- 61 Bérczi Sz. and Lukács B.**
Icy meteorites on Antarctica?
- 62 Bruno J.C., Fernandes A.A.R. and Scorzelli R.B.**
Microstructure analysis of the Yamato 791694 Antarctic meteorite
- 63 Bourdin E., Thomassin J.H., Le Coustumer P., Abrioux M.F. and Nakashima S.**
Experimental alteration of a meteoritic model-glass in different media
- 64 Hiroi T., Zolensky M.E. and Lipschutz M.E.**
Mineralogy and spectroscopy of heated Allende meteorite and a K-type asteroid 221 EOS
- 65 Thomassin J.H., Le Coustumer P. and Patrier P.**
Mineralogy and ultrastructure of some alteration products of Y-86032 meteorite
- 66 Kubovics I.**
NASA lunar petrographic thin section set in Hungary: Should Japan, NIPR prepare thin section set of Antarctic meteorites for education?
- 67 Marakushev A.A.**
Two stage evolution of the terrestrial planets recorded in diamond-bearing chondrites
- 68 Miura Yasunori**
Carbon-14 data of heterogeneous meteorites at high-energy-SIMS
- 69 Nayak V.K.**
The opaque minerals in impactite glasses from the lunar impact crater, India

Monday, May 30, 1994

<i>0900 - 1200</i>	<i>Registration, 6th Floor</i>
<i>0925 - 0930</i>	<i>Opening address, Auditorium</i>
<i>0930 - 1625</i>	<i>Symposium, Auditorium</i>
<i>1630 - 1730</i>	<i>Business meeting</i>

Comparison on model study and field survey for meteorite mass concentration and age of ice in Allan Hills & Yamato Meteorite Ice Field

Fumihiko NISHIO¹⁾, Hitoshi FUJITA²⁾ and Akira HIGASHI³⁾

1) Hokkaido University of Education

2) Sannei Co. Ltd.

3) Emeritus Prof. of Hokkaido University

In order to estimate the meteorite concentration and the age of ice in the Meteorite Ice Field near the Yamato Mountains and the Allan Hills bare ice field, the meteorite mass concentration and age of ice are computed based on the ice flow model proposed by Whillans(1983).

This study also aims to understand the flow behavior of ice sheets which are obstructed by nunataks in the coastal mountains. Such barrier effects give rise to form bare ice fields under some favorable conditions, like those near the Yamato Mountains and Allan Hills in Antarctica, where large amount of accumulated meteorites were found since last more than two decades ago.

We developed a model of the flow, by comparing the one by Whillans' equation, and the one by Azuma and others. These models are basically the same, constructed from the flow law of ice and the continuity equation (steady state model), but differs in a way of introducing the divergence of the ice flow around the nunataks near mountains.

Computational results obtained from our improved model, on the surface velocity, the surface strain rate, the particle trajectory in the ice, the isochrons of ice age, are all shown as functions of the distance from the mountain in many graphical outputs under various boundary conditions. The mass concentration of meteorites on the bare ice field computed with the preceding results under various infall rates, and the age of ice are also shown in the same way.

Comparisons with the actual concentration of meteorites recently measured in the Yamato and Allan Hills bare ice fields gave a reasonable value of the infall rate of meteorites, some $20 \sim 45 \times 10^{-6} \text{kg/km}^2\text{a}$. Age of ice measured by that of included tephra in ice, or terrestrial age of some meteorites in both the Yamato and Allan Hills by the isotopic method roughly coincide with those obtained by the computer model calculation.

Data of the meteorite concentration and the terrestrial ages of meteorites collected on the bare ice fields in Yamato Mountains and Allan Hills have been published recently. Collection of meteorites carried out in the area of the width of 10 km and the distance of 25 km upstream from the Massif A, Yamato Mountains was described by Nishio et al. (1987), and Allan Hills are in an abstract by Nishio (1988). In these works, histograms of the meteorite mass concentration vs distance from the nunataks were drawn. For comparison with such curves, histograms were converted to smooth curves with some average operations. If such an actual observational curve can be fitted with an estimated meteorite mass concentration distribution curve with a given infall

rate, and that infall rate is reasonable, the validity of the model can be proved. As we have two sites of meteorite collection sites in Antarctica, the infall rate thus estimated should be equal each other in the order of the global value of it.

In addition to the check in the meteorite concentration distribution described above, another check can be done with the age of surface ice in comparison with the terrestrial age of meteorites at Yamato bare ice field (Nishiizumi et al., 1989) and with the uranium series dating of tephra included in ice at Allan Hills bare ice field (Fireman, 1989). Actual practices of the comparisons stated above will be described below.

Derivation of infall rates from the comparison of observed data with computational results

a) Yamamoto Mountains

There are two peaks in the meteorite mass concentration distribution graph.

One is near the massif A and the other is near the Motoi nunatak which is approximately 15 km upstream from the Massif A. It is a problem how we deal with these two peaks.

First, Two nunataks are considered as one large barrier against the flow of ice sheet. Then, the peak which seems to be obstructed by Motoi Nunatak is moved downward, and was added Massif A peak. Then the peak is smoothed by averaging with weights. This distribution of meteorites concentration is compared with the calculated one to estimate a range of possible infall rates. The calculated results are given under boundary conditions which fit the Yamato bare ice field, with $X_{eq} = 40$ km. Since the peak fit to the curves of $15 \sim 25 \times 10^{-6}$ kg/km²a

$$f = 15 \sim 25 \times 10^{-6} \text{ kg/km}^2\text{a}$$

Secondly, two nunataks are recognized as two independent obstruction of ice flow. Two peaks are smoothed and compared with the computed concentration distribution which give us the value of f in the same unit.

$$f_a = 10 \sim 15 \times 10^{-6} \text{ kg/km}^2\text{a}$$

for the Massif A.

$$f_m = 15 \sim 22.5 \times 10^{-6} \text{ kg/km}^2\text{a}$$

for Motoi nunatak.

However, since two nunataks are considered as two independent barrier against ice flow, approximately a half of 10 km sampling width is contributing to each barriers. Therefore, the above estimated infall rates must be doubled to evaluate real values. Consequently, they are

$$f_a = 20 \sim 30 \times 10^{-6} \text{ kg/km}^2\text{a}$$

for the Massif A

$$f_m = 15 \sim 22.5 \times 10^{-6} \text{ kg/km}^2\text{a}$$

for Motoi nunatak.

b) Allan Hills

The same procedure described for a case of Yamato Mountains is carried out for the Allan Hills meteorite ice field. In this case, we see a distinguished peak in the histograms of the meteorite concentration (30 kg/km²). It is a problem how to consider this high peak which may eliminate other columns in the histograms when it is smoothed. However, if we see the number distribution of meteorites shown by a solid line in the histogram diagram, this peak corresponds to one or two in number. This indicates that the high peak of mass concentration is likely to cause by an exceptionally large meteorite. Therefore, we delete this peak from the data. Then, the remained data are smoothed as were done before, to obtain such a shape.

When this curve is fitted to computational result which is obtained for boundary conditions of Allan Hills ($X_{eq} = 40$ km, $A_b = -5$ cm, $A_c = 10$ cm), the infall rate for the fitted curve is,

$$f = 25 \sim 37 \times 10^{-6} \text{ kg/km}^2\text{a}$$

This curve of the infall rate agrees with those obtained for Yamato Mountains. Recently, rough estimate of the infall rate in the order of $15 \times 10^{-6} \text{ kg/km}^2\text{a}$ was obtained from the collection of meteorites in the Sør Rondane Mountains (private communication, H. Fujita, 1990). These values of $15 \sim 45 \times 10^{-6} \text{ kg/km}^2$ a coincide well with the global value hitherto recognized.

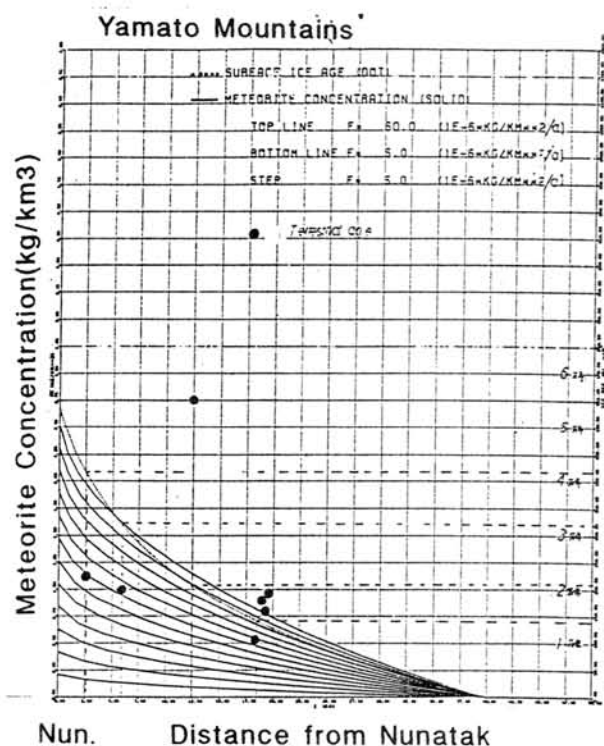


Figure 1

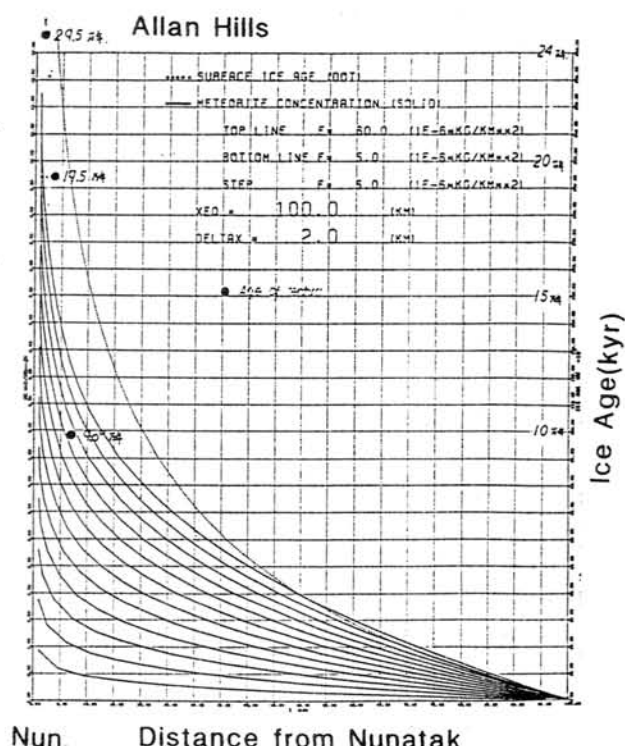


Figure 2

Age of surface ice

a) Yamato Mountains

Nishiizumi et al. (1990) determined terrestrial ages of several meteorites found in Yamato bare ice field. The data are plotted on a graph of the age of surface ice computed with the same conditions in the preceding subsection (see Fig. 1). The terrestrial age of a meteorite found in the vicinity of 20 km from the nunatak agrees well with the computed curve, although those for other meteorites agree only in the order of magnitude.

b) Allan Hills

In Allan Hills meteorite ice field, the ice age was determined from the tephra imbedded in ice (Fireman, 1989). Also one meteorite which was found imbedded in ice near the surface of Allan Hills bare ice field was measured by (Nishiizumi, 1989). These data are plotted on the graph of computed age of the surface ice near Allan Hills. Although agreement is not necessarily well, but they are roughly in the same order of magnitude (see Fig. 2).

We can now conclude that the model proposed as Model-W offers considerably fair estimates of the meteorite mass concentration distribution and of the age of the surface ice under an assumption of the steady state of the ice sheet.

REFERECES

- Auzma, N., Nakawo, M., Higashi, A. and Nishio, F. (1985): Flow pattern near Massif A in the Yamato bare ice field estimated from the structures and the mechanical properties of a shallow ice core. Mem. of Natl. Inst. Polar Res., Special Issue, No. 39.
- Fireman, E. L. (1989): Uranium series dating of tephra banded Allan Hills Ice. Proc. NIPR Symp. Antarct. Meteorites. 2, 335-343.
- Nishio, F., Ohmae, H., Mori, K., Osada, K. and Uratsuka, S. (1987): Collection of Yamato and Sør Rondane Meteorites in the 1986-87 field season, Antarctica. Abstract for the 12th Symp. on Antarctic Meteorites, 8-10, June 1987, NIPR, p1-2.
- Nishio, F. (1988): Comparison of meteorite concentration and age of ice in the Allan Hills and the Meteorite Ice Field near the Yamato Mountains. Abstract for the 13th Symp. on Antarctic Meteorites. 7-9, June, 1988, NIPR, p1.
- Nishiizumi, K., Jull, A. J., Bonani, G., Suter, M., Wolfli, W., Elmore, D., Kubik, P. W. and Arnold, J. R. (1989): Age of Allan Hills 82102, a meteorite found inside the ice. Nature, Vol. 340, No. 6234, pp550-552.
- Nishiizumi, K., Elmore, D. and Kubik, P. W. (1990): Update on terrestrial ages of Antarctic Meteorites. Earth and Planetary Sciences Letters.
- Whillans, I. M., and Cassidy, W. A. (1983): Catcha falling star: Meteorite and old ice. Science, Vol. 222, p55-57.

METEORITICS ASPECTS IN ROMANIA

Yasunori MIURA¹, Gabriel O. IANCU^{1, 2}, Gabriela IANCU¹, Keizo YANAI³ and Hiroshi HARAMURA³

¹ Faculty of Science, Yamaguchi University, Yoshida, Yamaguchi 753, Japan.

² Department of Mineralogy and Geochemistry, "Al. I. Cuza" University, Copou Bld. no. 20A, 6600 Iasi, Romania.

³ Department of Antarctic Meteorites, National Institute of Polar Research, Kaga, Itabashi-ku, Tokyo, 173, Japan.

The purpose of this paper is to discuss briefly about all data known up to now, concerning Romanian meteorites, meteors or some other aspects related to meteoritics science in Romania.

1. METEORITES: Throughout Romania, 10 meteorites (9 fallen and 1 found) were pointed, registered and investigated, as shown in Table 1.

Table 1. Romanian Meteorites

No.	Name	Date of fall	Place of fall	Total weight	Class and type	Others
1.	Buzau	1714, January	Buzau, Muntenia	?	?	Lost
2.	Tirgoviste	1774, shower	Tirgoviste, Muntenia	?	?	Lost
3.	Madaras	1852, September 4, 16.30hrs. , shower	Madaras, Transylvania	22.7kg	chondrite L3, xenolithic	In this study
4.	Cacova	1857, May 19, 08.00hrs.	Cacova, Banat	577g	chondrite L6, veined	
5.	Ohaba	1857, October 10, 00.15hrs.	Ohaba, Transylvania	16.25kg	chondrite H5, veined	
6.	Jadani	1875, March 31, 15.00-16.00hrs. , shower	Jadani, Banat	552g	chondrite H5	
7.	Moci	1882, February 3, 16.00hrs. shower	wide area around Moci Transylvania	300kg	chondrite L6 ? veined	In this study
8.	Sopot	1927, April 27, 12.00-13.00hrs. , shower	Sopot, Oltenia	958g	chondrite, not classified	
9.	Tauti	1937, July or August, shower	Tauti, Transylvania	21kg	chondrite L6	In this study
10.	Tuzla?	Found?	Tuzla? , Dobrogea	236g?	chondrite L6	

Although the preliminary note of Maxim (1967) and the Catalogue of Meteorites published by British Museum refer to most of Romanian meteorites, these papers doesn't include correct informations concerning the samples kept outside or in Romania respectively. We present below a brief revised catalogue of these meteorites, some new results obtained at Yamaguchi University, Japan, regarding Tauti, Moci and Madaras chondrites and few considerations concerning the possibility of finding other Romanian meteorites by studying the founding process of the Antarctic meteorites.

1.1 BRIEF CATALOGUE OF ROMANIAN METEORITES

1) BUZAU (Buzau District, Muntenia)

Fallen date: 1714, January. No information about the weight, number of individual specimens and type of this chondrite in literature.

All the mass fallen was sent for analysis by Const. Brîncoveanu (the prince of Muntenia) from Bucharest to S. Köleséri, a scientist from Cluj-Napoca. Unfortunately the meteorite was lost and nobody knows where is now this material.

- 2) TIRGOVISTE (Dîmbovita District, Muntenia)
 Fallen date: 1774 (no data about the month and day of the fall), shower.
 An eye witness saw several fragments of this meteorite but informations about the weight, number of individual specimens and type of this chondrite doesn't exist in literature because all material was lost.
- 3) MADARAS (Mures District, Transylvania)
 Fallen date: 1852, September 4, 16.30 hrs. , Shower. Chondrite (L3), xenolithic.
 After the appearance of a luminous meteor and detonations, a shower of many stones fell, of which the largest weighed about 10kg and the total weight was about 22.7kg. The biggest sample, in size of a human head, fell into a swamp and was not found.
 Main mass found is kept in Germany: 3kg Humboldt Univ. , Berlin and 1.7kg Tübingen Univ. Museum.
 Samples kept in Romania: Cluj-Napoca Univ. , Miner. Mus. , 192g + 1 thin section.
 Other samples: 9g, Austria, Naturhist Museum, Vienna {[L4374]}; 1.8kg, Hungary, Nat. Mus. , Budapest; 613g, Russia, Acad. Sci. , Moscow; 538g, India, Mus. Geol. Surv. India, Calcutta; 569g, U. S. A. , Arizona State Univ. , Tempe; 449g, U. S. A. , Field Mus. Nat. Hist. , Chicago; 335g, U. S. A. , U. S. Nat. Mus. , Smithsonian Inst. , Washington; 247g, U. S. A. , Univ. of California, Los Angeles; ?g, U. S. A. , Miner. Mus. of Harvard Univ. , Harvard; 651.75g, England, British Museum, London {[33909], 565g and fragments, 3g; [33188], 65.75g most of a stone; [90270], 18g; [96270], 2 thin sections}.
- 4) CACOVA (Caras Severin District, Banat)
 Fallen date: 1857, May 19, 08.00hrs. Chondrite (L6), veined.
 After detonations, a stone of 577g (510g?) was seen to fall by 5 shepherds.
 Main mass is kept in Austria: 327g, Naturhist. Mus. Vienna.
 No samples in Romania.
 Other samples: 9g, Germany, Humboldt Univ. , Berlin; 4.9g, U. S. A. , Arizona State Univ. , Tempe; 150g, England, British Museum, London {[35166]}.
- 5) OHABA (Alba District, Transylvania)
 Fallen date: 1857, October 10, 00.15 hrs. Chondrite (H5), veined.
 After appearance of fireball, followed by detonations, a stone of 16.25kg was found by a priest.
 Main mass is kept in Austria: 15.75kg, Naturhist. Mus. Vienna.
 Samples kept in Romania: 3g + 1 thin section, Cluj-Napoca Univ. , Mineral. Mus.
 Other samples: 46g, U. S. A. , Arizona State Univ. , Tempe; 7g, U. S. A. , Field Museum Nat. Hist. , Chicago; 39.75g, England, British Museum, London {[55530], 29.75g; [34588], 10g}.
- 6) JADANI (Timis District, Banat)
 Fallen date: 1875, March 31, 15.00-16.00 hrs. , Shower. Chondrite (H5).
 After detonations, a shower of stones fell, of which only 9 small ones were found, totaling 552g, the largest weighing 152g. It is believed that the main mass was not found.
 Main mass found is kept in Hungary: 223g, Budapest Nat. Mus.
 Samples kept in Romania: 4g, Cluj-Napoca Univ. , Mineral. Mus.
 Other samples: 44g, Austria, Naturhist Museum, Vienna; 14g, France, Mus. d'Hist. Nat. , Paris; 14g, U. S. A. , Field Mus. Nat. Hist. , Chicago; 13g, U. S. A. , U. S. Nat. Mus. , Smithsonian Inst. , Washington; 13.5g, England, British Museum, London {[52274], complete stone}.
- 7) MOCI (Cluj District, Transylvania)
 Fallen date: 1882, February 3, 16.00 hrs. , Shower. Chondrite (L6?), veined.
 After appearance of luminous meteor and detonations, a shower of stones fell on a wide area (15 km length and 3 km width) which includes Moci, Ghiris, Vaida Camaras, Barai, Visea, Coasta, Tauseni, Palaica and Chesau villages (Cluj District, Transylvania). The number of fragments has been estimated at 3000 and the total weight at about 300kg, the largest stone weighing about 56kg.
 Main mass found is kept in Austria: 70kg, Naturhist. Mus. Vienna.
 Samples kept in Romania: 1) Cluj-Napoca Univ. , Miner. Mus. , 63 pieces (total weight =43.142kg, including a stone of 35.7kg); 2) Bucharest Univ. Miner. Mus. , 3 pieces (no information about their weight); 3) Aiud,

Natural Sci. Mus. , 6 pieces (1 is weighing 76.2g; no information about the weight of the other 5 samples); 4) Dej, Natural Sc. Collection of "Andrei Muresanu" High School, 1 piece Coasta (no information about its weight). Other samples: 21kg, Hungary, Nat. Mus. , Budapest, 8.25kg, Eötvös Loránd Univ. , Budapest and 0.5kg, Reform College, Debreczen; 3.37kg, France, Mus. d'Hist. Nat. , Paris; 1.596kg, Denmark, Univ. Geol. Mus. , Copenhagen; 1kg, Germany, Univ. Mus. , Bonn; 672g, Scotland, Royal Scottish Mus. , Edinburgh; 615g, Czech Republic, Nat. Mus. , Prague; 6kg, U. S. A. , Field Mus. Nat. Hist. , Chicago; 7kg, U. S. A. , U. S. Nat. Mus. , Smithsonian Inst. , Washington; 1.3kg, U. S. A. , Univ. Mus. , Harvard; 1kg, U. S. A. , Amer. Mus. Nat. Hist. , New York; 1kg, U. S. A. , Univ. Mus. , Yale; 14.6675kg, England, British Museum, London {[54772], 8635g complete stone from Olah Gyéres; [54773], 4630g complete stone from Chesau(Keszu); [54647], 826g nearly complete stone from Barai (Báré); [54648], 276g complete stone from Barai (Báré); [54651], 123.5g from Barai (Báré);[54649], 81g complete stone from Gyulatelke; [54775], 27.5g from Vaida Camaras (Vajda-Kamaras); [54774], 25g from Palaica (Palatka); [54776], 20.5g from Marokháza; [54650], 17.5g complete stone from Visea (Visa); [54777], 5.5g from Visea (Visa); [1964,568], thin section}.

8) SOPOT (Dolj District, Oltenia)

Fallen date: 1927, April 27, 12.00 - 13.00 hrs. , Shower. Chondrite (not classified yet).

After detonations, eight stones totaling 958g were collected over an area measuring 12 km from east to west. It is believed that the main mass fell was not found.

All the samples are kept in Romania: 1) 4 fragments (main mass found) weighing 953.287g, Craiova, Muzeul Regional al Olteniei; 2) 22g + 1 thin section, Cluj-Napoca Univ. , Mineral. Mus.

9) TAUTI (Bihar District, Transylvania)

Fallen date: 1937, July or August, Shower. Chondrite (L6).

After three explosions and a bright bolide, a 20kg stone fell at Tauti (Bihar District Transylvania), and two other stones of about 0.5kg each fell at Gura Suvelului, about 6km S. of Tauti. After discovery, the principal sample broke in several pieces (the real number is unknown). Mr. Lajos from Tauti village, collected all the pieces, mixed them and distributed to some friends or relatives.

No information about the place where is kept the main mass (could be Lajos family).

Samples from this meteorite are kept only in Romania: 1) Bucharest, Geol. Mus. , 1 piece (no information about its weight); 2) Oradea (Bihar District, Transylvania) Natural Sci. Mus. , 2 pieces (1 is weighing 80.35g; no information about the weight of the other sample) and D. Sandrutiu-Private Collection, 2 pieces (no information about their weight); 3) Ineu (Arad District, Banat), 2 pieces in Junior-High School Collection (no information about their weight).

There is also a Romanian sample from Tuzla (236g, found meteorite, chondrite L6?) in the collection of the British Museum (Natural History), but in Romania nothing is known as to fall or find, concerning this chondrite.

1.2 NEW DATA REGARDING TAUTI, MOCI and MADARAS CHONDRITES

Table 2. Samples used in this study

SAMPLES	SIZE	PROVENANCE
Madaras - 1	Thin Section	Naturhist Mus. Vienna, Austria
Moci - 1	1.3g (1.4x1.0x0.5 cm)	Naturhist Mus. Vienna, Austria
Moci - 2	2.69g (1.4x1.0x1.0 cm)	Naturhist Mus. Vienna, Austria
Moci - 3	2.3g (2.5x1.5x0.4 cm)	Naturhist Mus. Vienna, Austria
Moci - 4	2.8g (3.0x1.4x0.3 cm)	Naturhist Mus. Vienna, Austria
Moci - 5	76.29g (3.0x4.0x4.0 cm)	Natural Sci. Mus. Aiud, Romania
Moci - 6	2.18g (1.5x1.2x0.5 cm)	Miner. Mus. of Cluj Univ. , Romania
Tauti - 1	80.35g (2.5x5.0x3.0 cm)	"Tarii Crisurilor" Mus.Oradea, Romania

Eight samples representing Madaras, Moci and Tauti meteorites were investigated in this study for shock minerals and classification respectively, as listed in Table 2.

1) Tauti meteorite: Although classified as L6 chondrite by British Museum, only one scientific paper was written about this chondrite by Savu (1937) who analyzed 1 sample from Bucharest, Geological Museum of Romania by using optical and bulk chemical analyses. To check the homogeneity of Tauti meteoritic shower, we analyzed an other sample: Tauti - 1 (see Table 2)

without any analytical data reported before. The interpretation of bulk composition made by Dr. Haramura on this sample indicate also the chemical group of Tauti meteorite as L chondrite. By optical and EPMA studies we found that the petrographic class of this fragment is L6: poorly defined chondrules, recrystallized matrix, igneous glass absent, plagioclase-like dark microcrystalline grains in matrix, brecciated texture, shocked veins, almost uniform compositions of olivine (mean deviation: 1.9%) and pyroxene (mean deviation: 2.7%), orthorhombic state of low Ca pyroxene and kamacite and taenite present (>20%). We analyzed also by X-ray powder diffractometry the composition of the black shocked veins (one of these looks like glass) and found representative peaks for forsterite, enstatite, hypersthene and ringwoodite. The latest mineral was found in only four L6 chondrites (Tenham, Coorara, Catherwood and Coolamon) and we will make other experimental investigations to confirm or not his presence.

2) Moci meteorite: 6 fragments of Moci Meteorite (as shown in Table 2) without analytical data reported up to now were investigated also in this study. Although the analyses are still in progress the most interesting results obtained so far are presented as follows: 1. The interpretation of bulk composition made by Dr. Haramura on Moci - 5 fragment indicate the chemical group of Moci as L chondrite. Described before as L6 chondrite we found however for Moci - 5 and Moci - 6 fragments well-defined barred olivine and fibrous pyroxene chondrules and readily delineated chondrules, kamacite grains (one of this with Neumann bands), recrystallized matrix, absence of igneous glass and secondary feldspar developed in grains <50- μ m. Mean deviation of olivine and pyroxene from this samples, measured by EPMA is 1.9% and 2.1% respectively; 2. By X-ray powder analyses for Moci - 5, we found representative peaks for ringwoodite but further investigations should be carried out because we didn't find purple grains by optical analyses.

3) Madaras meteorite: Optical analyses of Madaras - 1 (see Table 2) reveals anomalous dark like-chondrules made mainly by troilite, kamacite and microcrystalline grains of olivine and pyroxene. EPMA analyses of these grains indicate 19%Fs and 34%Fa respectively.

1.3 THE POSSIBILITY OF FINDING OTHER ROMANIAN METEORITES

It is well known that in Antarctica, many meteorites fallen in different places of the snow fields were found in certain locations ablated near obstacles due to transportation mechanism of the ice flow. The glacial activity was also present in Romania during Pleistocene. Valley glaciers, moraines, glacial lakes and piedmont glaciers were described in Carpathians Mts. (i. e. Meridionali Mts. , which cross the country from East to West). Because of the glacial movement from North to South, it's possible that this mountains could be obstacles for meteorites fallen? in Northern part of Romania in that period. On other chance is to discover meteorites originated from the snowed mountains in piedmonts, periglacial deposits, glacial lakes and brooks from Meridionali Mts.

2. METEORS: An extremely bright meteor was observed over many Romanian localities on January 1, 1906 but no meteorite of recoverable size was found in that time.

3. IMPACT CRATERS?: No impact craters were discovered so far in Romania. Shatter cones, rocks melted by intense heat and pressure and shocked minerals as coesite, stishovite or shocked quartz were not reported also. Due to the complex geological structure of the Romanian territory, with an active subduction front in the past and many orogenic movements, is probable that impact craters (if ever existed) to be destroyed during the time.

ACKNOWLEDGMENTS: We are grateful to Dr. G. Kurat from Naturhist Museum, Vienna, Mrs. A. Herta from Natural Sci. Mus. , Aiud, Mrs. M. Popa from "Tarii Crisurilor" Mus. , Oradea and Mrs. D. Pop from Mineral. Mus. of Cluj-Napoca Univ. for providing the samples used in this study.

REFERENCES: 1. Bedeleian I. et al. (1979), *The catalogue of the meteoritic matters collection from the Mineralogical Museum of the University of Cluj-Napoca*, Studia Univ. Babes-Bolyai, Geologia-Geographia, XXIV, 2, 3-23; 2. Graham A. L. et al. (1985), *Catalogue of Meteorites with special reference to those represented in the collection of the British Museum (Natural History)*, 4th ed. (rev. and enl.), British Museum (Natural History), pp. 234; 3. Maxim I. A. (1968), *Meteorites and Meteoritic Materials in Romania, Preliminary Note to the Meteorite Catalogue of Romania*, Studia Univ. Babes-Bolyai, ser. Geol. - Geogr. 1, 3-6 (in Romanian language, with Russian and English abstract); 4. Stanciu V. and Stoicovici E. (1943), *The Meteorites of Romania*, Rev. Muz. Mineral. Geol. al Univ. din Cluj la Timisoara, vol. VII, No. 1-2, 3-34 (in Romanian language, with French abstract)

ORBITS AND COLLISION TYPES OF IMPACT MATERIALS TO THE EARTH

Yasunori MIURA

Faculty of Science, Yamaguchi University, 753, Japan

1. Introduction

Sensitive and clear relation between orbit of meteorite and time-of-fall has been reported by many scientists (cf. Hutchison and Grahm, 1992; Wetherill and Chapman, 1988). But type and group of meteorites are difficult to classify clearly into A.M. type (midnight to noon) or P.M. type (noon to midnight), though almost all the meteorites are belonging to P.M. type (i.e. 67% = $100 \times 362/544$ in the world; 72% = $100 \times 18/24$ in Japan). But there are no reports on relation among orbits of meteoroids (clockwise or anticlockwise), collision types (retrograde, or prograde), and impact materials. Impact materials in this paper mean meteorite (collected on the Earth) and meteoroids (including meteors, and impact materials from planetesimals or planetary bodies).

The main purpose of the present paper is to discuss the origin and orbits of impact materials.

2. Orbits of meteoroids and observed fall time

Retrograde orbit shows clockwise rotation (i.e. opposite direction to the Earth) and head-on collision with half with time from midnight to noon (A.M. type). High impact velocity (ca. 70km/sec) of retrograde orbit is mainly due to speedy orbit with opposite direction and main source of force by the Sun.

Therefore, retrograde collision may occur the following impact materials (Table I; Miura et al., 1993, 1994; Miura, 1994):

- (a) Giant impact of planetary size: The moon formation can be explained by giant impact between proto-Earth and planetesimals (or Mars-size planetary bodies) with opposite and oblique impacts. It is not sure that these impact materials are formed directly or indirectly to the Moon (i.e. fission or accretion). If the moon was formed by fission process, the cratering rate during an intense bombardment on the Moon (ca. 4.0 b.y.) can be explained as re-collision of impact fragments to the near-side of the Moon and all surface of the Earth. There could be found these impact fragments both on the Moon and Earth.

- (b) Anomalous fall of meteorites: Sikhote-Alin iron meteorite and Pasamonte stony meteorite reveal anomalous fall with huge fireball and spiral flight on the atmosphere.
- (c) Few survival of meteorites: High impact velocity give impact materials with little chance of survival. The Tunguska event occurred at 0:16 a.m., 1908 is belonging to the same category of retrograde impact.

Prograde orbit shows anticlockwise rotation (i.e. the same direction to the Earth) with half time from noon to midnight (i.e. P.M. type). Most meteoroids after travelling around the Sun hit to the Earth with low impact velocity. The slower the impact velocity, the greater the chance of impact materials surviving to the Earth rather than burning up in the atmosphere (by retrograde orbit).

The following impact materials can be found at the prograde collision (Table 1; Miura et al., 1993, 1994; Miura, 1994):

- (a) Almost all meteorites: Various sizes of stone and iron meteorites can be classified into the prograde collision.
- (b) Antarctic meteorites: Almost all meteorites generally concentrate to the Equatorial region by gravitational focussing. The fall of meteorites to the poles can be explained by (a) radial orbit near the Earth by deflection of Earth's gravity, and (b) "slower" velocity of meteoroids near poles of the Earth.
- (c) SNC meteorites: Impact materials from planetary bodies produce both orbits of clockwise and anticlockwise rotations. But the impact materials with retrograde orbit cannot be survived by the before-mentioned reason. Thus small fragments of SNC meteorites can be observed as prograde orbit as a result (both at poles and equator).
- (d) Lunar meteorites: Lunar impact meteorites can be explained by the same collision type as SNC meteorites from origin of planetary surface. The lunar meteorite found near the Antarctica should be explained by the gravitational focussing.

Table 1. Orbits and collision types of impact materials to the Earth.

Orbit	Collision type	Examples	Others
1. Clockwise:	Retrograde	1) Iron meteorites	Sikhote-Alin
	Head-on	(Okano, Lowicz, Pitts,	
	A.M. (from midnight)	Zaisho, Yarydnyly)	
	G. Force by the Sun	2) Stone meteorites	Allende
		(Pasamonte)	(Spiral orbit)
		3) Tunguska	Shock wave
		4) Collision of Proto-	The Moon (?)
		Earth (to form the	
		Moon)	
2. Anticlockwise:	Prograde	1) Stone & iron	Jilin, Kokubunji
	P.M. (from noon)	meteorites	Mihonoseki etc.
	G. Force by the Earth	2) Antarctic meteorites	(Shower)
		3) SNC meteorites	(Equator & Pole)
		4) Lunar meteorites	(near the Pole)

3. Summary

The present results are summarized as follows:

- (a) Impact materials to the Earth can be explained as two major rotation orbits of clockwise (retrograde) and anticlockwise (prograde) with falling-times of A.M. and P.M. falling types, respectively.
- (b) Retrograde collision is giant impact and anomalous fall of meteorite with few survival of meteorites.
- (c) The moon formation can be explained by giant impact between proto-Earth and planetesimals (or Mars-size planetary bodies) with opposite and oblique impacts. If the moon was formed by fission process, the cratering rate during an intense bombardment on the Moon (ca. 4.0 b.y.) can be explained as re-collision of impact fragments to the near-side of the Moon and every surface of the Earth.
- (d) Tunguska event of A.M. type is belonging to the same category of retrograde impact without tiny fragments.
- (e) Prograde collision is found in almost all meteorites, Antarctic meteorites, and SNC and lunar meteorites with smaller size.

- (f) The fall of meteorites to the poles can be explained by (i) radial orbit near the Earth by deflection of Earth's gravity, and (ii) slower velocity of meteoroids near poles of the Earth.
- (g) Impact materials from planetary bodies (e.g. Mars) produce both orbits of clockwise and anticlockwise rotations. Small fragments of SNC meteorites can be observed as prograde orbit both at poles and equator as a result.
- (h) Lunar impact meteorites can be explained by the same collision type as SNC meteorites from origin of planetary surface. The lunar meteorite found near the Antarctica can be explained by the gravitational focussing.

References

- Hutchison R. and Graham A. (1992): Meteorites. pp.60.
Miura Y. et al. (1993): Shock Waves, Japan-1994, 259-264.
Miura Y. et al. (1994): LPSC XXV (LPI,USA), 25, 915-916.
Miura Y. (1994): (submitted).
Wetherill G.W. and Chapman C.R. (1988): Meteorites and Early Solar System 38-44.

SHOCK METAMORPHISM OF CK AND CV CHONDRITES INFERRED FROM EXPERIMENTALLY PRODUCED SHOCK FEATURES OF ALLENDE.

T. Nakamura¹, K. Tomeoka², T. Sekine³ and H. Takeda⁴

(1) Department of Earth and Planetary Sciences, Faculty of Science, Kyushu University, Hakozaki, Fukuoka 812, (2) Department of Earth and Planetary Sciences, Faculty of Science, Kobe University, Nada, Kobe 657, (3) National Institute for Research in Inorganic Material, Tukuba, Ibaragi 305, (4) Mineralogical Institute, Faculty of Science, University of Tokyo, Hongo, Tokyo 113

Introduction

Carbonaceous chondrites commonly show a variety of shock features that probably resulted from impacts on/between planetesimals in the early solar system. Such impacts might have affected mineralogical and chemical properties of planetesimals. We can obtain informations about the nature of the impact through studying shock metamorphism of carbonaceous chondrites. Studies of experimentally shock-loading on carbonaceous chondrites [1, 2] and related chondritic materials [3, 4] have shown that degree of the shock metamorphism is controlled by several physical parameters; shock intensity, initial temperature and porosity of the sample, and impact frequency. It is known that shock pressures generate two major effects: mechanical compression and post-shock heating. Basically degree of the two effects increases with increasing shock intensity. But, the latter effects is particularly enhanced if the pre-shock temperature is high [1, 2] and thus, shock effects at high temperature considered to be quite different from those at low temperature. In this study, we discuss conditions for shock metamorphism experienced by CK and CV chondrites by comparing shock features of two CK (Y-693 and Y-82104) and a CV (Efremovka) chondrites with experimentally reproduced shock features of Allende.

Results

Shock experiments

High-temperature shock experiments on the Allende CV chondrite were performed with experimental conditions (equilibrated shock pressures and pre-heated temperatures) as follows; 11GPa initially at room temperature (R. T.) and 300 °C, 21GPa at R. T., 300 °C and 600 °C. Detailed mineralogical and petrological results obtained from these shock experiments have been described in [1, 2].

Chondrules, which were more or less spherical before shock loading, are uniformly flattened and show preferred orientation. The degree of chondrule flattening at constant pressures is proportional to the temperatures of pre-heated samples. This may be resulted from increase of plasticity of components (silicate and metal-sulfide grains and mesostasis glass) in chondrules at high temperature. Olivine and low-Ca pyroxene in chondrules show shock-induced deformation characteristic of mostly S3 level based on the shock-classification scheme for

chondrites proposed by Stöffler et al. [5]. Important features produced by the high-temperature shock experiments are: (1) blackening of chondrules due to intrusion of Fe-S or Fe-Ni-S melt into fine fractures of chondrules, (2) generation of numerous subround or irregularly-shaped grains (10 to 30 μm) of glassy material rich in Ca and Si in the matrix, and (3) segregation of Fe-S melt in areas $\sim 400 \mu\text{m}$ in the matrix. The features (1) and (2) are observed in both recovery samples pre-heated to 300°C and 600°C, but the degree of blackening and the density of glassy grains are much greater in the 600°C sample than in the 300°C one. The feature (3) is observed only in the 600°C sample.

CK chondrites

Y-693 and Y-82104 show nearly the same degree of shock metamorphism. Olivine in both chondrules and matrix exhibit moderate to strong undulatory extinction and planar fractures. Extensive blackening occurs throughout the matrix and on the margins of chondrules. Olivine, low- and high-Ca pyroxene, and plagioclase are uniformly blackened due to dispersed tiny ($<10 \mu\text{m}$) magnetite and pentlandite grains. Glassy to microcrystalline material, which is round to elliptical in shape and 200 - 700 μm in diameter, occurs in the matrix; it is probably a localized shock-induced melt.

Efremovka CV chondrite

Most chondrules show remarkable flattening in preferred orientation like those in the Leoville CV chondrite [6]. Olivine in chondrules commonly show planar fractures and exhibit strong undulatory extinction. A few olivine grains show mosaic extinction. Mesostasis glass is devitrified. Metal-sulfide grains in chondrules are partially melted to form network-like veins within chondrules, resulting in weak blackening in chondrules. Some CAIs show weak blackening on their periphery that is caused by intrusion of Fe-S melt from exterior of CAIs. All these characteristics are mostly consistent with those reported by Scott et al. [7].

SEM observations show the matrix of Efremovka is similar in texture with that of Leoville [6]: both are strongly compacted and each olivine grain can not be distinguished in SEM images. But, a notable difference is found: subround or irregularly-shaped glassy materials rich in Ca and Si occur in the matrix of Efremovka. They are closely resemble in both texture and composition with those observed in experimentally shocked Allende at high temperature.

Discussion and conclusions

The extensive blackening of the recrystallized matrix and the presence of a localized shock-induced melt indicate that the CK chondrites have suffered from intense thermal effects during shock compression. Rubin [8] pointed out that the blackening in CK chondrites was produced by shock metamorphism. However, shock features in the CK chondrites we studied show that they have experienced shock pressures not greater than that for S3 level ($>20 \text{ GPa}$), which may be too low

to generate enough heat for producing the shock-induced melt and the extensive blackening. The results of our shock experiments indicate that the blackening occurs at pressures of S3 level only when the sample was pre-heated to temperature higher than 300°C. Thus, it is presumed that the temperature of the CK chondrites would have been already elevated when it was shocked. We believe that CK chondrites have experienced shock pressure during high-temperature period when they were thermally metamorphosed. Metamorphic temperatures are estimated by Geiger and Bischoff [9] to be 550 - 650°C and 650 - 800°C for type 4 and 5 CK chondrites, respectively. If the CK parent bodies had been heated to such high temperatures, shock pressures of S3 level or even S2 may have been enough for generating the blackening and the shock-induced melt. This may explain why the blackening is observed in many CK chondrites that show characteristics of relatively weak shock levels (S2 ~ S3) [7, 8].

Shock effects of CV chondrites are quite different from those of CK chondrites. Our shock experiments on Allende show that the foliations of highly flattened chondrules in some CV chondrites [7] might have been produced by shock pressures of S3 level [1]. Leoville shows remarkable chondrule flattening and matrix compaction but metal-sulfide grains appears not to have melted, suggesting that it has experienced shock effects at low temperature [6], although some components (CAIs) are thought to have been hot when Leoville was shocked [10]. Efremovka shows weak blackening of chondrules and generation of glassy grains in the matrix, indicating that its post-shock temperature might be higher than that of Leoville. The degree of the blackening in Efremovka appears to be comparable to that in experimentally shocked Allende at 21 GPa and 300°C. But, Efremovka shows shock features of olivine assigned to S4 level (20~35 GPa), whereas the shocked Allende shows those assigned to S3 level (10~20 GPa). It is known that post-shock temperatures increase with increasing shock intensities. Thus, the higher post-shock temperature in Efremovka might be raised by a strong shock pressure of S4 level.

Acknowledgments

We thank Drs. H. Nagahara and G. J. MacPherson for loaning a thin section of Efremovka.

References: [1] Nakamura T. et al. (1993) *Meteoritics*, 28, 408. [2] Nakamura T. et al. (1994) *LPSC XXV*, 969-970. [3] Katamura M. et al. (1992) in *high-pressure Res.: Appl. to Earth and Planet. Sci.* (eds. Shono Y. and Manghnami M. H.), 330-340. [4] Schmitt et al. (1993) *Meteoritics*, 28, 431. [5] Stöffler et al. (1991) *GCA*, 55, 3845-3867. [6] Nakamura T. et al. (1992) *EPSL*, 114, 159-170. [7] Scott E. R. D. et al. (1992) *GCA*, 56, 4281-4293. [8] Rubin A. E. (1992) *GCA*, 56, 1705-1714. [9] Geiger T. and Bischoff A. (1991) *Meteoritics*, 26, 337. [10] Caillet C. et al. (1993) *GCA*, 57, 4725-4743.

COMPARISON OF PETROLOGY AND MINERALOGY OF THE PCA 91082 AND THE YAMATO-793495 (CR) CHONDRITES: ON THE PHYLLOSILICATE CLASTS

Takaaki NOGUCHI

Dept. of Earth Sci., Ibaraki University, Bunkyo 2-1-1, Mito 310, Japan

Introduction PCA 91082 was tentatively classified as a CR chondrite, because the amount of matrix of this meteorite is much lower than the other CR chondrites (Mason, 1993). I investigate this meteorite and the Yamato (Y)-793495 chondrite which was described as a member of the CR group (Weisberg et al., 1993), by a scanning electron microscope (SEM), an electron microprobe analyzer (EPMA). Here I report "phyllosilicate clasts" in these chondrites.

Phyllosilicate clasts in PCA 91082 and Y-793495 There are some phyllosilicate clasts in PCA 91082. A phyllosilicate clast is observed also in Y-793495. They are different from "dark inclusions" or "dark clasts" in the other CR chondrites (e. g. Weisberg et al., 1993; Bischoff et al., 1993; Endreß et al., 1993). "Dark inclusions" or "dark clasts" are considered as consolidated inclusions of matrix materials of CR chondrites, although there is an argument about the petrographic features and chemical composition of the dark inclusions or clasts (e. g. Weisberg et al., 1993; Bischoff et al., 1993; Endreß et al., 1993). On the other hand, these phyllosilicate clasts are composed mainly of phyllosilicates with small amount of fine-grained (submicron in size) opaque minerals. BEI photographs of phyllosilicate clasts reveal that some clasts are composed of relatively large phyllosilicates and the interstices of them are filled finer phyllosilicates, although the phyllosilicate clasts do not always show the similar texture as described above.

The Si-Mg-Fe diagrams show that the Fe/(Fe+Mg) ratios of phyllosilicates decrease in the following order; phyllosilicates in chondrules, matrices, and phyllosilicate clasts. Compositional differences among these components are wider in PCA 91082 than in Y-793495. In PCA 91082, the ranges of Fe/(Fe+Mg) ratios of these three components are 0.9 ~ 0.65, 0.7 ~ 0.35, and 0.4 ~ 0.2, respectively. In Y-793495, those are 0.75 ~ 0.5, 0.7 ~ 0.4, and 0.5 ~ 0.25, respectively. Especially, phyllosilicates in a phyllosilicate clast in PCA 91082 have similar composition to phyllosilicates in CI chondrites (Tomeoka and Buseck, 1988) on a (Si+Al)-Mg-Fe diagram.

CaO wt % of spot analyses of a phyllosilicate clast in PCA 91082 show interesting correlations between S wt %. Although most of analyses are plotted near the origin, there can be seen two trends. First one shows various CaO content and low S content. On the other hand, there is a positive correlation between CaO and S wt % in the second one. But there is a negative correlation between FeO and S contents. These relations indicate that the high S contents in some analyses do not result from the higher abundance of Fe-bearing sulfides (or sulfates) but a component which includes both Ca and S. The atomic ratio between Ca and S of gypsum and anhydrite is 1. However, the ratio suggested from spot

analyses of the phyllosilicate clast is higher than 1. Therefore, a Ca-carbonate component may be associated with a Ca-sulfate component. This is the first discovery of a clast including a Ca-sulfate component from a CR chondrite.

Implication for the aqueous alteration processes As noted above, there is an argument whether there is a compositional differences between "dark inclusions" and host matrix in CR chondrites or not. This study shows that there is a compositional difference between "phyllosilicate clasts" and matrices. Phyllosilicates in phyllosilicate clasts are more magnesian than host matrix. Phyllosilicates in heavily altered CM chondrites and some heavily altered carbonaceous chondrites like Y-86720 are more magnesian than those in weakly altered CM chondrites (e. g. Zolensky et al., 1993). This compositional difference results from the participation of magnesian olivine and pyroxene in aqueous alteration process. Therefore, texture and composition of the phyllosilicate clast suggest that some phyllosilicate clasts in PCA 91082 and Y-793495 seem to have been chondrules which suffered severe aqueous alteration. After aqueous alteration, constituent components which experienced different degrees of aqueous alteration were agglomerated. This interpretation is plausible because CR chondrites are breccias (e. g. Weisberg et al., 1993; Bischoff et al., 1993). Because compositional range of phyllosilicates in Y-793495 is narrower than that in PCA 91082, modification of original compositions of phyllosilicates in each constituents perhaps occurred after agglomeration of the chondrite.

Phyllosilicates in a phyllosilicate clast in PCA 91082 have similar composition to those in CI chondrites and are associated with a Ca-sulfate component. Ca-sulfate is reported from CI chondrites (e. g. Richardson, 1978). Ca-sulfate and more common Mg-sulfate in CI chondrites were formed during aqueous alteration on the meteorite parent body. Probably the phyllosilicate clast in PCA 91082 also suffered aqueous alteration on the meteorite parent body. According to Zolensky et al. (1993), temperature (50~150 °C) and water/rock ratio of aqueous alteration of CI and CR are similar, but fO_2 of aqueous alteration of CI reaches higher than that of CR. However, because the phyllosilicate clast in PCA 91082 contains a Ca-sulfate component and contains only a small amount of Fe-sulfide component, this clast probably experienced aqueous alteration under higher fO_2 and lower fS_2 conditions like CI chondrites.

References Bischoff, A. et al. (1993) *Geochim. Cosmochim. Acta*, 57, 1587-1603. Endreß, M. et al. (1994) *Meteoritics*, 29, 26-40. Mason, B. (1993) *Antarctic Meteorite Newsletter*, 16. ed. by R. Score and M. Lindstrom. pp. 22. Richardson, S. M. (1978) *Meteoritics*, 13, 141-159. Tomeoka, K. and Buseck, P. (1988) *Geochim. Cosmochim. Acta*, 52, 1627-1640. Weisberg, M. K. et al. (1993) *Geochim. Cosmochim. Acta*, 57, 1567-1586. Zolensky, M. et al. (1993) *Geochim. Cosmochim. Acta*, 57, 3123-3148.

Petrology of Yamato-8449 Chondrite (CR)

Osamu Ichikawa * and Yukio Ikeda **

* Department of Polar Science, The Graduate University for Advanced Studies,
National Institute of Polar Research, 1-9-10 Kaga, Itabashiku, Tokyo, 173, Japan

** Department of Earth Sciences, Ibaraki University, Mito 310, Japan

Introduction The Yamato-8449(Y-8449) chondrite is an Antarctic carbonaceous chondrite which was previously classified as an E4, but is a CR (Renazzo-type) chondrite. CR chondrites have been studied by several researchers; the bulk chemical analyses of CR chondrites (Renazzo and Al Rais) were carried out by McSween (1979), Fe-Ni alloys in three CR chondrites were studied by Lee *et al.* (1992), petrologic, geochemical, and oxygen isotopic studies in eight CR chondrites were done by Weisberg *et al.* (1993), and matrix of CR chondrites (Renazzo and EET87770) was analyzed by Zolensky *et al.* (1993). In order to clarify the characteristics of Y-8449, we present the detailed petrography and mineralogy of Y-8449, and discuss the petrogenesis.

Petrography Y-8449 is composed of chondrules, isolated minerals, and matrix. Most of chondrules are 0.5 to 1.1 mm in diameter, and abundant types of chondrules are porphyritic olivine (PO), porphyritic olivine pyroxene (POP), and porphyritic pyroxene (PP) chondrules. Only one barred olivine (BO) chondrule and one cryptocrystalline microchondrule were observed. Groundmass glass in some chondrules is replaced by phyllosilicates in the peripheral portions of chondrules.

Olivine, low-Ca pyroxene, and Fe-Ni metal occur as isolated minerals in Y-8449. Two types of isolated olivine are observed; one type is ferroan (Fo₃₀₋₈₀) olivine grains free from inclusions, and the other type is magnesian (Fo₉₈₋₁₀₀) ones including high-Ca pyroxene, plagioclase, phyllosilicate, Fe-Ni metal, and/or spinel. For convenience, the former is called ferroan olivine fragments, and the latter is called magnesian olivine fragments.

Matrix of this meteorite is composed of fine-grained phyllosilicates smaller than several micrometers.

Mineralogy Olivine in chondrules is forsteritic olivine (Fo₉₂₋₉₉), and does not show distinct chemical zoning. These olivine contain 0.1-1.2 wt.% Cr₂O₃ and 0.1-1.18 wt.% MnO. Ferroan olivine fragments show distinct zoning from magnesian cores to ferroan rims. These olivines contain 0.1-0.47 wt.% Cr₂O₃ and 0.1-0.6 wt.% MnO. Magnesian olivine fragments contain 0.1-0.21 wt.% Cr₂O₃ and 0.1-0.1 wt.% MnO. Pyroxene in Y-8449 contain high chromium contents (0-3.5 wt.%). Phyllosilicate occurs in chondrules, as irregular inclusions in magnesian olivine fragments, and in Y-8449 matrix. The chemical compositions of phyllosilicates in Y-8449 chondrules and matrix are plotted between the compositional ranges of chlorite and talc. But the chemical composition of phyllosilicate in magnesian olivine fragments is similar to chlorite (or serpentine).

Chromite occurs only in one ferroan olivine fragment. Carbonate(calcite) occurs only in chondrule No. 16. A silica mineral occurs in the center of chondrule No. 11. Fe-Ni metals are classified into two types; one type has an exsolution texture, and the other type has a massive texture. The massive Fe-Ni metal in Y-8449 occurs in chondrule interior, chondrule rim, and matrix. The difference in occurrence corresponds to the difference in metal chemical composition; Co content (wt.%) of chondrule interior metal is the highest among them, P content (wt.%) of chondrule rim metal is the highest among them, and Cr content (wt.%) of matrix metal is the highest among them.

Discussion In Y-8449, groundmass glass and phenocrystic enstatite in chondrule No. 12 are replaced by phyllosilicates in the chondrule rim. The precursor of these phyllosilicates must have been the groundmass glass and phenocrystic enstatite. We calculated the normative composition of the groundmass glass, and aqueous alteration reaction to produce the phyllosilicates in chondrule No. 12 may have been as follows; $[12Ab+4An+19Qz+2En+Wo]$ (glass) + $69.456FeO + 56.96H_2O + 5CO_2 + 44.32En \rightarrow 4.24Chl + 11.52Talc + 5Calcite + 0.48 Na_2O$, where FeO, H₂O and CO₂ in the reactants were introduced into the chondrule to produce the phyllosilicates, and alkali components in the products were lost from the chondrule.

References McSween H.Y. (1979) Rev. Geophys. Space Phys., 17, 1059-1078. Lee M.S., Rubin A.E., and Wasson J.T. (1992) Geochim. Cosmochim. Acta 56, 2521-2533. Weisberg M.K., Prinz M., Clayton R.N., and Mayeda T.K. (1993) Geochim. Cosmochim. Acta 57, 1567-1586. Zolensky M., Barrett R., and Browning L. (1993) Geochim. Cosmochim. Acta 57, 3123-3148.

Alkali-lime Reactions of Allende Chondrules I: Alteration of Chondrules with Known Oxygen-isotope Compositions

Y. Ikeda and M. Kimura, Dept. of Earth Sciences, Ibaraki University, Bunkyo 2-1-1, Mito 310.

Most of Allende chondrules experienced various degrees of anhydrous alteration after lithification of chondrule liquid droplets (Ikeda and Kimura, 1985; Kimura and Ikeda, 1992); some chondrules have altered rims, and others have altered groundmasses. The altered rims and groundmasses contain nepheline, sodalite, and ferroan olivine with minor amounts of Ca-rich phases such as grossular, hedenbergite, etc. The nepheline (or sodalite) occurs in an alteration texture replacing mesostasis plagioclase and groundmassic glass in chondrules, resulting in the devitrified dark groundmasses of Allende chondrules. The main reaction for the replacement of plagioclase or glass by nepheline is: $\text{CaAl}_2\text{Si}_2\text{O}_8 + 2\text{Na} = 2\text{NaAlSiO}_4 + \text{Ca}$.

Most of CAI's (Ca- and Al-rich inclusions), especially fine-grained CAI's, and AOP's (amoeboid olivine inclusions) in carbonaceous chondrites also experienced various degrees of anhydrous alteration similar to that of chondrules (Ikeda, 1982).

The problem we take interest in is whether the alteration reaction took place in the solar nebula or in the Allende parent body. In order to clarify this problem, we petrologically studied alteration degrees of twelve Allende chondrules with known oxygen-isotope compositions.

Allende chondrules form an oxygen-isotope mixing line in three isotope diagram, which differs from the Allende inclusion line (Clayton et al., 1983). If alteration of chondrules took place in the Allende parent body at the same time as that of inclusions, then chondrules with higher degrees of alteration should have oxygen isotope compositions which deviate more from the Allende chondrule line, and are nearer to the Allende inclusion line than those with lower degrees of alteration.

The twelve Allende chondrules show various degrees of anhydrous alteration; some chondrules contain clean glass in the cores and seem not to

have experienced any alteration except the peripheral portions, but others have devitrified dark groundmasses in the cores and consist mainly of nepheline and ferroan olivine with minor relic magnesian olivine and pyroxene. However, all chondrules, including both highly-altered and less-altered ones, have their oxygen-isotope compositions which plot on the Allende chondrule line and never deviate from the chondrule line toward the inclusion line. One chondrule has a highly-altered rim and a less-altered core, and the oxygen isotope compositions of the rim and core plot on the same chondrule line. These facts suggest that the alteration of Allende chondrules to produce nepheline and ferroan olivine took place in the solar nebula prior to their accretion onto the Allende parent body. The anhydrous alteration may have been caused by reactions of chondrules with an oxidized nebular gas in various degrees and probably took place in a gas-chondrule reservoir which was different from a gas-inclusion reservoir for alteration of CAI's and AOI's.

Ikeda (1982) Mem. Natl. Inst. Polar Res., 25, 34-65.

Ikeda and Kimura (1985) Meteoritics, 20, 670.

Kimura and Ikeda (1992) Abs. 17 Symp. Antarc. Meteorites, 31-33.

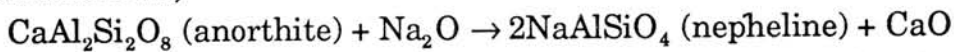
Clayton et al. (1983) "Chondrules and their Origins" ed. by E.A.King, Lunar and Planetary Institute, Houston.

Alkali-lime reactions of Allende chondrules II: Ca-rich phases in chondrules.

KIMURA Makoto and IKEDA Yukio

Department of Earth Sciences, Ibaraki University, Bunkyo 2-1-1, Mito 310.

Ikeda [1] and Ikeda and Kimura [2] found some zoned chondrules in Allende (CV3) and ALH-77003 (CO3) chondrites; groundmass of these chondrules shows zonation from clean and CaO-rich (anorthite-normative) glass in the center, to devitrified and Na₂O-rich (nepheline-normative) margin. It is probable that such zoning formed by introduction of Na₂O from the solar nebular gas and loss of CaO from chondrules. A possible alkali-lime reaction to form nepheline from glass is as follows;



Later Kimura and Ikeda [3] reported sodalite as well as nepheline in devitrified groundmasses of many Allende chondrules, and found that most of chondrules in Allende experienced the alkali-lime reaction.

Here we report a detailed mineralogical and petrological study of 58 Allende chondrules using a scanning electron microscope. The purpose of this study is to clarify the distribution and behavior of Ca during the alkali-lime reaction. Chondrules studied here cover various types of chondrule texture, size, shape and mineralogy.

Nepheline occurs in all chondrules studied here. Sodalite occurs in 38 chondrules. Nepheline and sodalite replace primary anorthite-normative glass and plagioclase (An₇₀₋₉₅). The abundances of nepheline and sodalite are various among chondrules; several chondrules have these minerals only in the peripheral parts, like zoned chondrules. On the other hand, primary glass and plagioclase in some chondrules were totally replaced by nepheline and sodalite. Olivine and Ca-rich pyroxene phenocrysts do not show any reaction texture. Ca-poor pyroxene phenocrysts often show a replacement texture by ferroan olivine.

Allende chondrules have magnesian high-Ca pyroxene in groundmass. In addition, five kinds of Ca-rich silicate phases are noticed: hedenbergite, andradite, grossular, kirschsteinite and wollastonite. These five Ca-rich phases occur intimately with nepheline and sodalite in groundmass, although their abundances are below about 2-3% of those of nepheline and sodalite. They are usually smaller than 10 microns in size, and have irregular shapes. The occurrence indicates that the five Ca-rich phases formed within groundmass as secondary minerals. However, the Ca-rich phases do not occur in all chondrules studied here. Fifteen chondrules have only nepheline as a secondary mineral. Fourteen

chondrules have nepheline and sodalite without the Ca-rich phases. Thus, secondary mineral assemblages are grouped as follows (number of chondrule is in parenthesis);

nepheline (15)

nepheline + sodalite (14)

nepheline + sodalite + hedenbergite (18)

nepheline + sodalite + hedenbergite + andradite (4)

nepheline + sodalite + hedenbergite + andradite + grossular (4)

nepheline + sodalite + hedenbergite + andradite + kirschsteinite (1)

nepheline + sodalite + andradite + kirschsteinite (1)

nepheline + sodalite + hedenbergite + andradite + wollastonite (1)

These secondary mineral assemblages are not correlated with primary features of chondrules such as texture, size, mineralogy of phenocryst, abundance of groundmass, and compositions of glass and plagioclase.

Hedenbergite is usually poor in MgO (Fs_{40-50}) and Al_2O_3 (0.2% $>$). Wollastonite and andradite are nearly pure in composition. Grossular, smaller than 5 microns in size, always occurs in association with andradite, and seems to contain andradite component (10% $<$). Kirschsteinite has about 20% monticellite component. These Ca-rich phases are commonly observed as secondary minerals in CAIs in Allende and other carbonaceous chondrites (*e.g.*, Hashimoto and Grossman [4]), which supports that chondrule as well as CAI suffered a secondary reaction.

Nepheline usually has about 10% anorthite component that is much lower than CaO contents of primary glass and plagioclase. Most of primary CaO should have been redistributed during the alkali-lime reaction. However, 29 chondrules studied here do not have any secondary Ca-rich phases. On the other hand, hedenbergite, andradite, grossular, kirschsteinite and wollastonite were secondarily originated in the other chondrules, with an introduction of FeO probably from outside of chondrules. However, the low abundances of these Ca-rich phases can not explain the amount of CaO which is lost from primary glass and plagioclase. Therefore, primary CaO must have been mostly lost from chondrules during the alkali-lime reaction.

References: [1] Ikeda Y. (1982) Mem. Natl. Inst. Polar Res., 25, 34-65. [2] Ikeda Y. and Kimura M. (1985) Meteoritics, 20, 670. [3] Kimura M. and Ikeda Y. (1992) Abs. 17 Symp. Antarc. Meteorites, 31-33. [4] Hashimoto A. and Grossman L. (1987) GCA, 51, 1685-1704.

**Ca-Al-RICH INCLUSIONS IN THREE ANTARCTIC CO3 CHONDRITES,
Y81020, Y82050 AND Y790992: RECORD OF LOW-TEMPERATURE
ALTERATION**

Tomoko Kojima*, Satomi Yada and Kazushige Tomeoka

Department of Earth and Planetary Sciences, Faculty of Science, Kobe University, Nada,
Kobe 657

* Also Mineralogical Institute, Faculty of Science, University of Tokyo, Hongo, Tokyo 113

INTRODUCTION

Ca-Al-rich inclusions (CAIs) in CV3 carbonaceous chondrites have been extensively studied, but much less work has been done on those in CO3 chondrites. Previous studies have revealed that CAIs in some CO3 chondrites contain considerable amounts of low-temperature phases such as nepheline and sodalite, which were formed by replacing primary phases during low-temperature (<1000 °C) alteration [1,2]. Here we report the results of our petrographic and scanning electron microscope studies on CAIs in three Antarctic CO3 chondrites, Y81020, Y82050 and Y790992. The present study reveals that CAIs in these meteorites contain variable amounts of nepheline. Nepheline increases in amount in the order Y81020<Y82050<Y790992, representing three different degrees of alteration.

RESULTS

Y81020

37 CAIs are observed within ~25mm² total area on a polished thin section. They range in diameter from 25 to 680 μm, but most are <300 μm. Among them, 20 inclusions are single concentric objects or aggregates of concentric objects, composed of cores of spinel with or without melilite and minor perovskite, surrounded by rims of fassaite and aluminous diopside. The rest include 10 olivine (Fo₁₀₀₋₉₈)-rich inclusions, 4 unrimmed anorthite-pyroxene inclusions, 2 CaAl₄O₇-bearing inclusions, and 1 hibonite-pyroxene inclusion. Almost all of the CAIs are free of nepheline. Spinel is nearly Fe-free (<1.0 FeAl₂O₄ mol. %) and melilite is gehlenitic (mostly Ge₈₅₋₉₉). Besides these minerals, an unidentified Na-Al-Fe-rich phase (~5.8 Na₂O wt. %, ~60 Al₂O₃ wt. %, ~30 FeO wt. %) is found in two CaAl₄O₇-bearing inclusions, and Ca-rich phase, probably calcite, is found in an olivine-rich inclusion. Both Na-Al-Fe-rich phase and Ca-rich phase have not been reported from CAIs in CO3 chondrites. The Na-Al-Fe-rich phase may have been formed during alteration of CAIs, but we cannot preclude the possibility that the Ca-rich phase resulted from terrestrial weathering.

Y82050

38 CAIs, 20 to 500 μm in diameter, are observed within ~25mm² total area. Most of them contain variable amounts nepheline and sodalite; some contain only minor amounts (<5

vol.%) but others contain up to 80 vol. %. Nepheline and sodalite commonly coexist with fine grains of troilite. 5 inclusions (200 to 280 μm in diameter) are concentric objects having 20 to 40 vol. % of melilite-rich areas, resembling the unique melilite- and spinel-rich inclusion in Y791717 (Fig.4 in ref.[2]). From their textures, it is evident that nepheline and sodalite were formed by replacing primary phases such as melilite and fassaite. Within the unaltered (melilite-rich) areas, spinel is Fe-poor ($<10 \text{ FeAl}_2\text{O}_4$ mol. %), while in the altered (nepheline-rich) areas spinel is Fe-rich and commonly shows Fe-Mg zoning (20 to 50 FeAl_2O_4 mol. %). Rims of diopside remain unaltered even within the altered areas. 5 inclusions are olivine-rich, in which olivine shows strong Fe-Mg zoning (Fo_{99} in the core and Fo_{50} in the rim). In a heavily altered inclusion, Fe-rich monticellite ($\text{Fe}_{0.7}\text{Mg}_{0.3}\text{CaSiO}_4$) is found.

Y790992

30 CAIs, 30 to 300 μm in diameter, are observed within $\sim 25 \text{ mm}^2$ total area. All of them contain major variable amounts (10~80 vol. %) of nepheline, sodalite and troilite. The amounts of these secondary phases are larger than those in the Y82050 CAIs. The texture and mineralogy of the CAIs most resemble those in Y791717 [2]. Among the CAIs in Y790992, 13 inclusions show concentric textures consisting of Fe-rich spinel cores (45~65 FeAl_2O_4 mol. %) with fine-grained porous mixture of secondary phases, surrounded by rims of aluminous diopside. Although they texturally resemble the concentric, melilite-rich inclusions in Y81020, they contain much less amounts of melilite and fassaite. In some inclusions, minor amounts of ilmenite (FeTiO_3) and ilvospinel (Fe_2TiO_4) occur with perovskite. 6 inclusions contain large amounts of Fe-rich ($\text{Fo}_{60\sim 50}$) olivine.

DISCUSSION

The present study reveals that, despite textural similarity, there are considerable differences in mineralogy between CAIs in the three CO chondrites, which probably reflects different degrees of alteration. Most CAIs in Y81020 are melilite- and spinel-rich concentric objects with pyroxene rims, while CAIs in Y790992 contain almost no melilite but abundant nepheline, sodalite and troilite. Melilite is known to be the most susceptible to alteration among the primary phases in CAIs [2,3]. Thus, it is probable that some CAIs in Y790992 were once melilite-rich, but melilite was consumed to form nepheline and sodalite. Along with the alteration, spinel and olivine were probably enriched in Fe. Perovskite was replaced by ilmenite and ilvospinel . All of these features suggest that considerable amounts of Na and Fe were introduced simultaneously during the low-temperature alteration. Based on the amounts of secondary phases, we interpret that the degree of alteration increases in the order Y81020 < Y82050 < Y790992. Mean Fe-contents in spinel and olivine in CAIs increase in the same order, being consistent with the interpretation that Fe was added with the alteration. CAIs in another Antarctic CO3 chondrite, Y791717, are reported to be also rich in nepheline and poor in

melilite [2]. The alteration degree of CAIs in Y791717 appears to be equivalent or slightly less than that of CAIs in Y790992.

It is widely believed that the secondary phases in CAIs from CV3 and CO3 chondrites were formed by reaction of primary phases with a Na-, Fe- and Cl-rich nebular gas at low temperature [e.g. 4-6]. Greenwood et al. (1992) [7] investigated CAIs in four non-Antarctic CO chondrites, and suggested that the degree of alteration of CAIs is correlated with metamorphic grade. Based on thermoluminescence (TL) sensitivity measurements, Y81020, Y82050 and Y791717 (data for Y790992 is currently unavailable) are all classified into metamorphic grade 3.3 [8]. Thus, our results appear to provide no support for the conclusion by Greenwood et al. [7]. However, Scott and Jones (1990) [9] showed that metamorphic grades for CO3 chondrites determined by TL method often differ considerably from those petrographically determined, on which Greenwood et al. [7] was based. Therefore, further petrographical studies on these four Antarctic CO3 chondrites may be necessary to verify whether the degree of alteration on CAIs is related to metamorphic grade or not.

REFERENCES

- [1] Davis A. M. (1985) Lunar Planet. Sci. XVI, 165-166 (abstract).
- [2] Tomeoka K., Nomura K. and Takeda H. (1992) Meteoritics 27, 136-143.
- [3] MacPherson G. J., Wark D. A. and Armstrong J. T. (1988) In Meteorites and the Early Solar System (Univ. Arizona Press), 746-807.
- [4] MacPherson G. J., Grossman L., Allen A. M. and Beckett J. R. (1981) Proc. Lunar Planet. Sci. Conf. 12B, 1079-1091.
- [5] Wark D. A. (1981) Lunar Planet. Sci. XII, 145-1147 (abstract).
- [6] Hashimoto A. and Grossman L. (1987) Geochim. Cosmochim. Acta 51, 1685-1704.
- [7] Greenwood R. C., Hutchison R., Huss G. R. and Hutcheon I. D. (1992) Meteoritics 27, 229 (abstract).
- [8] Sears D. W. G., Batchelor J. D., Lu J. and Keck B. D. (1991) Proc. NIPR Symp. Antarct. Meteorites 4, 319-343.
- [9] Scott E. R. D. and Jones R. H. (1990) Geochim. Cosmochim. Acta 54, 2485-2502.

CHEMICALLY DIFFERENT POPULATIONS OF HIBONITES AND PEROVSKITES IN A CAI FROM Y-791601: EVIDENCE FOR AN EXTRANEIOUS ORIGIN: Hideyasu Kojima¹, Ahmed El Goresy² and Keizo Yanai¹; ¹National Institute of Polar Research, Tokyo 173, Japan; ²Max-Planck-Institut für Kernphysik, P.O.Box 103980, D-69029 Heidelberg, Germany

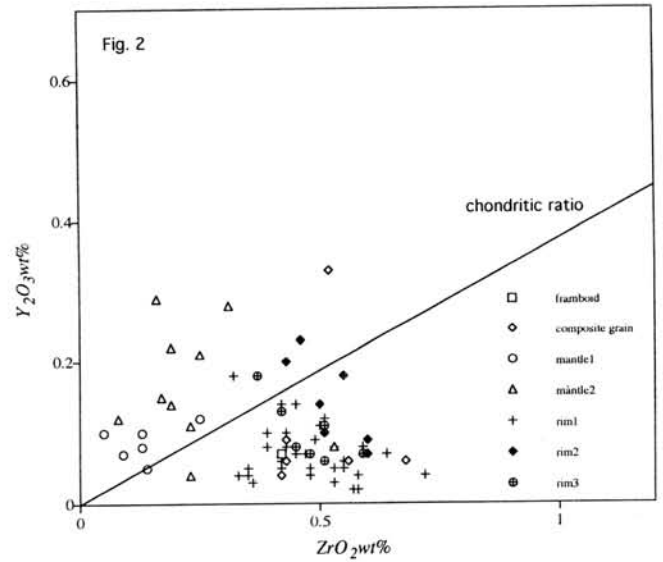
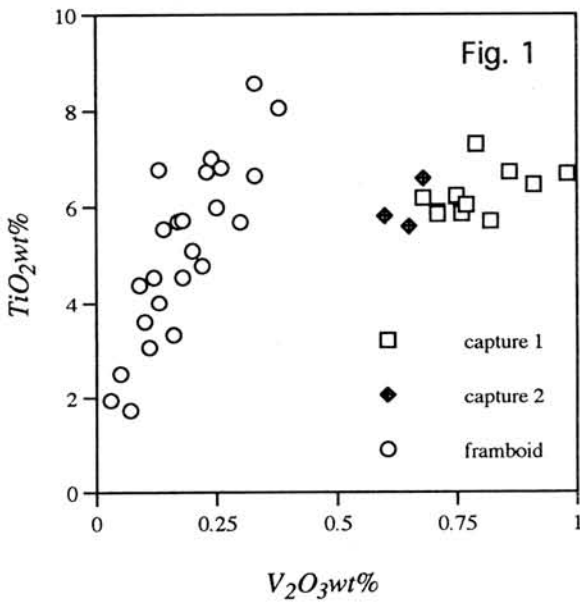
A petrographic and EPMA study revealed the presence of different populations of perovskites and hibonites in CAI from the Y-791601 CV3 chondrite. Some of them probably are of extraneous origin. This CAI(YM1) is very large (2 cm in length) and has a core-mantle structure. The core consists mainly of loosely packed coarse spinels with anorthite, fassaite, diopside and grossular in their interstices. The mantle consists of melilite (Ak₉) with minor spinel, hibonite and perovskite. A few euhedral grains of corundum, several μm in size, are found in the melilite mantle. The narrow rims are developed as successive layers on the outermost mantle. In thin section YM1 (Y-791601,51-1) is quadrilateral in shape and lacks mantle and rim in both elongated sides. It seems that the spinel core lies between the two mantles (mantle 1 and mantle 2). The mineral assemblage resembles type A CAI (CTA), however, the abundance of spinel and melilite and the textural features differ from type A.

Three distinct populations of hibonites were encountered: a) in the rim sequence, b) in spinel framboids, and c) in captured multiphase fragments. Two type C assemblages consisting of hibonite and spinel occur along with a spinel framboid in mantle 1. Hibonites in captured fragments are rich in V₂O₃ (0.6 - 1.0%). In contrast, hibonites in spinel framboids are depleted in V₂O₃ ($\leq 0.4\%$). These hibonites display a positive correlation between V₂O₃- and TiO₂- contents (Fig. 1). This results suggests that the hibonite populations originated from different sources.

There are three categories of perovskites: a) in the rim sequence, b) as a composite grain, and c) subhedral grains in the melilite mantle. Perovskites forming the innermost rim with spinel and hibonite are heterogeneously distributed. Here, three domains enriched in perovskite are encountered: rim 1 consisting of perovskite and spinel, rim 2 and 3 consisting of perovskite, hibonite, and spinel. The composite grain is amoeboid in shape and consists of a bright and a dark portion on BEI image. Two chemically different perovskite types were found: (1) perovskite with higher than chondritic

ZrO₂/Y₂O₃ ratios, (2) perovskite with lower than chondritic ZrO₂/Y₂O₃ ratios (Fig. 2). Type 1 perovskites either condensed from a reservoir with non chondritic ZrO₂/Y₂O₃ ratio or were formed by fractional condensation[1]. Perovskites in the rims show negative relationship between Y₂O₃ and ZrO₂ and mainly belong to type 1. This indicates that the perovskites in rims did not crystallize from the host CAI liquid and are probably condensates and extraneous to CAI. The composite grain also belongs to type 1. The bright portion is higher in ZrO₂ than the dark one. These results are indicative of a very complex formation history of the composite grain. Single grains and aggregates of perovskite in the mantle belong to type 2. Type 2 perovskites have Y₂O₃/ZrO₂ ratios similar to those obtained from crystal/liquid fractionation experiments[2]. In these perovskites the abundance of Sc₂O₃ is positively correlated with both ZrO₂ and Al₂O₃.

[1] Zinner, E. and El Goresy, A.(1994): LPS XXV, 1557-1558. [2] Simon S. B. et al.(1994): GCA 58, 1525-1536



K-RICH OBJECT IN THE MATRIX OF THE ORDINARY CHONDRITE RAGULI (H3-4)

Zinovieva N.G., Mitreikina O.B. and Granovsky L.B.

Moscow State University, Geological Faculty, Department of Petrology, Moscow 119899,
Russia

The meteorite Raguli is an unequilibrated ordinary chondrite H3-4 (1; 10). It consists of olivine-pyroxene and pyroxene-olivine chondrules of granular, barred or porphyritic texture, which are embedded in a sulfide-metallic matrix.

Detailed petrological research on the sample of the Raguli chondrite has been carried out by the scanning electron microscope CamScan-4DV with energy-dispersive analyzer AN 10000. The matrix material has been studied the most attentively. In general it consists of kamacite, taenite and troilite with a few crystals of olivine, pyroxene and whitlockite, and fragments of chondrules and chondrule minerals. Now, in addition, a K-rich object in the matrix has been found. Such K-rich objects have not been described previously in ordinary chondrites. The presence of K-feldspar was revealed in silicate inclusions in iron meteorites (8), in nakhlites (3) and rare K-feldspar grains in ordinary chondrite regolith breccias (2). K-rich objects are also known in LL (11) and H (12) chondrites, but they are typically silicate-rich and poor in Fe and Ni compared to the host. Moreover, cryptocrystalline K-feldspar or potassium glass occur in the interstices between idiomorphic crystals of olivine and, to a lesser extent pyroxene, in these objects.

The K-rich object in the matrix of Raguli consists of idiomorphic crystals of K-feldspar and sodic plagioclase, cemented by kamacite. The entire irregularly shaped K-rich object is 300x400 μm in size, has the sharp boundary with both the chondrules and sulfide-metallic material of the matrix and occurs between chondrules and has a concentric, bi-zonal structure (Fig. 1).

The external 30-80 μm -thick rim consists of small (up to 5 μm) plagioclase crystals (Table 1, N 1) of irregular or tabular shape, and rare < 5 μm -size grains of K-feldspar (Table 1, N 2). The kamacite cementing grains of plagioclase and K-feldspar together contains no more than 5% of Ni content. The kamacite is highly oxidized by weathering and it contains < 2% of the silica content. Rare grains of troilite and whitlockite also occur in the assemblage. The internal part of this K-rich object consists of ~50 μm -size idiomorphic crystals of K-feldspar (Table 1, N 4), surrounded by a 3 - 5 μm rim (Fig. 2) of plagioclase (Table 1, N 3). The kamacite of the central part contains as much silica content as the kamacite in the rim but the amount of Ni content is less (< 2%).

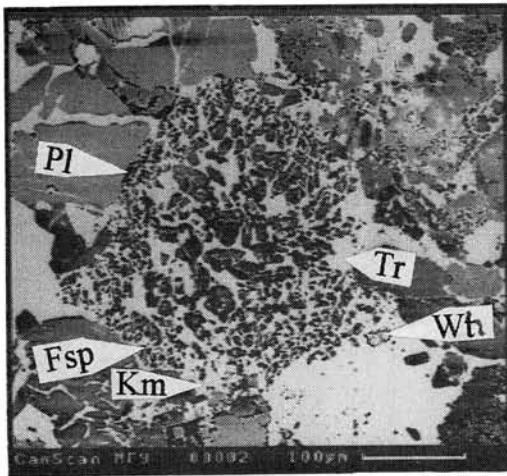


Fig. 1. Structure of the K-rich object in the matrix the Raguli chondrite. Km - kamacite, Tr - troilite, Wh - whitlockite, Pl - plagioclase, Fsp - K-feldspar, Ol - olivine.

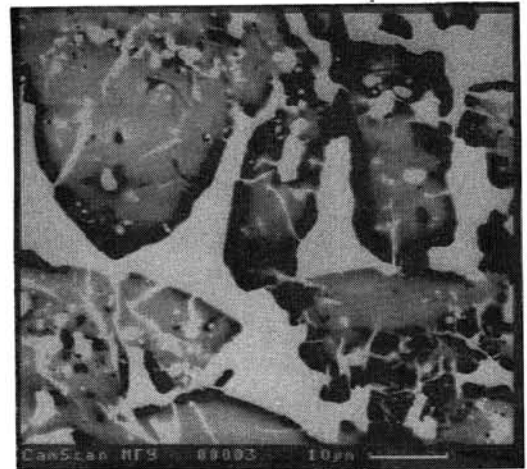


Fig. 2. Idiomorphic crystals of K- of feldspar (gray), surrounded by a rim of almost pure albite (black), cemented by kamacite (white).

TABLE 1.

Ranges and average compositions of feldspars of the K-rich object.

N	An		Ab		Or		n
	Range	Av.	Range	Av.	Range	Av.	
1	8.8-10.6	9.3	82.4-88.4	87.0	2.8-7.0	3.7	6
2	5.2-8.9	7.0	11.7-19.0	15.1	75.9-80.2	77.9	4
3	5.0-5.9	5.4	86.6-92.7	89.4	3.3-7.6	5.2	6
4	2.7-6.7	3.9	5.7-10.8	7.5	85.8-90.7	88.7	7

n - number of analyzed grains; 1 - plagioclase and 2 - K feldspar of the external part of the K-rich object; 3 - plagioclase and 4 - K-feldspar of the internal part of the K-rich object.

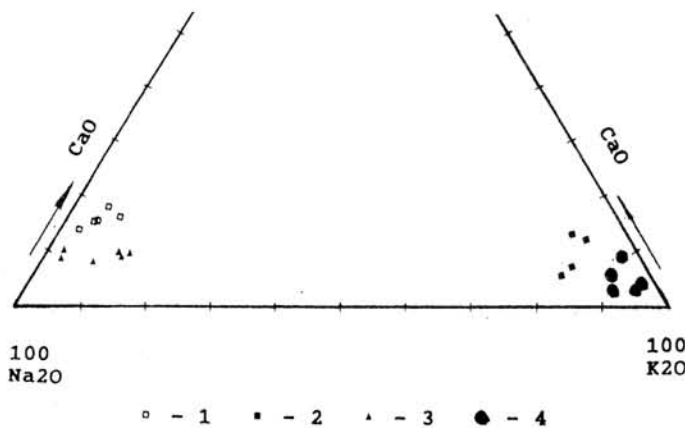


Fig. 3. The diagram of compositions (weight %) of plagioclase and K-feldspar. 1 - plagioclase and 2 - K-feldspar of the external part of the K-rich object; 3 - plagioclase and 4 - K-feldspar of the internal part of the K-rich object.

Comparing compositions of K-feldspar and plagioclase in the central and the outer parts of the K-rich object we see (Fig. 3) that the K-feldspar of the rim is rich in Na and Ca. Plagioclase of the rim is rich in calcium and poor in potassium in comparison with the plagioclase of the central part of the object. The more fine-grained texture of the rim formed by more basic plagioclase and K-feldspar rich in Na and Ca testify (4) to higher temperature of crystallization of the rim than in the central part of K-rich object. The crystallization of the central part started with the formation of idiomorphic grains of K-feldspar, and when almost all potassium is absorbed by this phase a rim of almost pure albite forms around the grains. The central part, rich in K in comparison with Na, was formed at a lower temperature. The final process in this sequence of formation was the crystallization of the kamacite.

It was shown above that:

the K-rich object has the irregular, interstitial shape submitted to the boundaries of the chondrules;

there is the sharp boundary with both the chondrules and the matrix;

there is the concentric bi-zoned structure with the fine-grained rim and the grained core;

the assemblage of the rim is more high temperature in comparison with the assemblage of the central part. These facts all together are in accordance with properties of crystallization of the melts. Everything mentioned above let us make the following conclusions: the K-rich object crystallized from the melt, the crystallization followed for a decreasing temperature and the K-rich object solidified after the chondrules.

Detailed petrological research on the ordinary chondrite Raguli doesn't allow us to explain the molten formation of the K-rich object as by the impact-melting in situ because we couldn't find sings of impact metamorphism in the minerals both the chondrules and the matrix, as by removing the impact metamorphosed object in the matrix because the subordination of the morphology and zonal structure of the K-rich object to the chondrule boundaries shows that it was formed in situ. May be easier to explain the formation of this object according the idea of liquid immiscibility of chondrite melt (6, 7). The possibility of liquid immiscibility of chondrite melt was shown by experimental melting of the ordinary chondrite Tsarev (5; 13, 14). The existence of the sharp boundary between the K-rich object and both the chondrules and the matrix as well as the sequence of crystallization from the boundary to the center in the K-rich object and subordination of the morphology and zonal structure of the K-rich object to the chondrule boundaries let us suppose that the K-rich object was formed by liquid immiscibility

Acknowledgements - This work was supported by International Science Foundation (ISF) and Russian Fund of Fundamental Researches (RFFR), Project 94-05-16942.

- REFERENCES: (1) Baryshnikova G.V., Charitonova V.Ya. and Barsukova L.D. (1982) *Meteoritika* **40**, 10-15, (in Russian). (2) Bischoff A., Rubin A. E., Keil K. and Stoffler D. (1983) *Earth Planet.Sci. Lett.* **66**, 1-10. (3) Bunch T.E. and Ried A.M. (1975) *Meteoritics* **10**, 303-315. (4) Ghiorso M.S. (1984) *Contrib. Mineral. Petrol.* **87**, 282-296. (5) Marakushev A.A. and Bezmen N.I. (1983) *Evolution of meteorite substance of planets and magmatic series*. Nauka. 184 pp., (in Russian). (6) Marakushev A.A., Granovsky L.B., Zinovieva N.G. and Mitreikina O.B. (1992) *Space Petrology*. Moscow University. 325 pp., (in Russian). (7) Mitreikina O.B., Zinovieva N.G. and Granovsky L.B. (1992) *Vestnik Moskovskogo Universiteta, seriya geologiya* **1**, 38-48, (in Russian). (8) Olsen E. and Mueller R.F. (1964) *Nature* **201**, 596,597. (9) Ramdohr P. (1960) *Die Erzminerale und ihre Verwachsungen*. Akademie - Verlag. 1132 pp. (10) Stroganov I.A., Barsukova L.D. and Kononkova N.N. (1994) *Meteoritika* **51**, (in press, in Russian). (11) Wlotzka F., Palme H., Spettel B., Wanke H., Fredriksson K. and Noonan A.F. (1983) *Geochim. Cosmochim. Acta* **47**, 743-757. (12) Wlotzka F., Spettel B. and Pedroni A. (1991) *Meteoritics* **26**, 308. (13) Zinovieva N.G., Mitreikina O.B., Granovsky L.B. (1994) *LPS XXV*. (14) Zinovieva N.G., Mitreikina O.B., Granovsky L.B. (1994) *LPS XXV*.

Origins of the lithic fragments in the unequilibrated ordinary chondrites, Julesburg(L3) and Y-790448(LL3).

Takashi Fujita and Masao Kitamura

Department of Geology and Mineralogy, Faculty of Science, Kyoto University, Sakyo Kyoto 606-01.

Lithic fragments included in two unequilibrated ordinary chondrites, Y-790448(LL3) and Julesburg (L3) were studied mineralogically. The composition and textures of the fragments imply that they were originated from the grand-parent body of the chondritic meteorites.

It has been reported that various kinds of non-chondrule lithic fragments are observed in the unequilibrated ordinary chondrites, and that some fragments had igneous origin (e.g., Hutchison, 1992; Kitamura et al. 1990). However, it needs further studies to elucidate the genetic relation between the igneous fragments and the other chondritic textures. In this study, lithic fragments found in the two unequilibrated ordinary chondrites, Y-790448(LL3) and Julesburg(L3) were studied by comparing them to chondrules and relict precursors.

1) Julesburg(L3)

Host rock of the Julesburg chondrite show the preferred orientation of ellipsoidal chondrules, which reflect the post-accretional shock metamorphism (e.g., Sneyd et al., 1988; Nakamura et al., 1990). However, the composition of the silicate minerals still preserve the unequilibrated conditions.

Textures of the fragments

Two types of lithic fragments were observed in the Julesburg chondrite (Figs. 1a and 1b). One type (Fragment A: 3X1.5 mm. Fig. 1a) is composed of olivine, pyroxene, and mesostasis of a few 100s mm in sizes. Olivine grains show the reverse zoning in their rim region. Pyroxenes show the zoning from enstatite or pigeonite to augite (En₄₉₋₈₁Fs₉₋₂₄Wo₄₋₄₁).

Another type (Fragment B: 3x4mm. Fig. 1b) is mainly composed of olivines of a several 100mms to a few mms showing nearly the same extinction direction. The interstices of the olivine grains are filled with pyroxenes (En₅₂₋₈₀Fs₁₉₋₂₄Wo₃₋₂₆) and mesostasis. The mesostasis have anorthitic composition and include silica grains. The rim of the olivines in the fragment also show the reverse zoning patterns.

Dusty olivine textures reported as relict of the precursor materials (Nagahara, 1981; Rambaldi, 1981) are observed in a few chondrules. Figure 2a and 3a show the compositions of the pyroxene and olivine grains in the dusty relict, chondrules, and lithic fragments respectively. The pyroxenes of the fragments are Fe-richer than those of the chondrules. In the fig. 3a, the histograms of the relict and fragments show the peaks of nearly the same olivine compositions.

Origin of the fragments

Although the two fragments do not have holocrystalline textures, the large clastic shape of the fragments, coarse grain sizes, especially coarse Ca-rich pyroxenes, and anorthitic composition of the mesostasis are dissimilar to the chondrules in the host rock. It is possible that the mesostasis of the fragments experienced remelting process. The chondrule olivines of the host rock show the normal zoning texture. Therefore, the reverse zoning texture in the rims of the olivine grains are interpreted not to be formed by the post-accretional shock metamorphism but to be originated from the pre-accretional reheating process. It is possible that the texture was formed during the deformation process of the parent body of the fragment. The similarities of the olivine composition between relict and the fragment implies the possibility that precursors of the chondrules and the lithic fragments are derived from the same parent body.

2) Y-790448 (LL3)

The textures of matrix and chondrules of the Y-790448 chondrite indicates the least metamorphosed texture. In the chondrites, two types of lithic fragments were also observed.

Textures of the fragments

One type (Fragment A: 200x300 mm. Fig.1c) is composed of olivine, Ca-rich pyroxene (En67-79Fs13-18Wo8-18) of a few 100 mms in sizes. In the rim, olivine and pyroxenes show section-like surfaces, which implies that the fragment was formed from larger rock. Although the size of fragment is not so large, the holocrystalline texture and the occurrence of the coarse Ca-rich pyroxene grain is different from the chondrules in the host rock.

Another type (Fragment B: 2.5X3 mm. Fig.1d) is also composed of olivine, Ca-rich pyroxene (En53-63Fs20-23Wo13-27), and plagioclase(An83-88Ab12-17) but show the different texture. The core of the fragment show the barred olivine like texture, in which the olivines with a thickness of a few tens mms are aligned to the same direction. The interstices of the olivine is filled with pyroxene and plagioclase. The core is rimmed by granular textures of the same mineral component. Concentration of small chromite grains is observed in the core-rim boundary of the fragment. Although compositional difference is not so distinct between core and rim, the texture indicates the discontinuity of the formation process. The texture of the fragment is similar to a kind of barred olivine chondrule which is related to basaltic rocks (Hutchison,1992).

Origin of the fragments

In the host rock of the Y-790448, dusty relict of olivine and pyroxene are observed. Figs. 2b and 3b show the composition of the pyroxene and olivine in the relict, chondrules and two lithic fragments. In this chondrite, the composition of the fragments are not identical to the relict precursors. On the other hand, relicts and two fragments comprise a compositional trend. In olivines, the trend from Fe-poor olivine to Fe-rich olivine, and in pyroxenes, the trend from Ca-Fe-poor enstatite to Ca-Fe-rich augite are observed. The trend implies the possibility that the precursor of relict grains and the two types of lithic fragments were formed by fractional crystallization process in a same parent body. This interpretation is consistent with the origin of precursor estimated from the fine fragments in the UOCs (Fujita and Kitamura,1992).

Summary: Implication to the origin of chondritic materials.

The result of the study suggest that the precursor of the chondrules and the lithic fragments are genetically related. The result is identical to the previous report on the lithic fragment in the Moorabie (L3) chondrite. This interpretation is consistent with the shock impact origin of the chondritic meteorite (Kitamura,1990; Kitamura et al.,1992) suggesting that chondritic component was formed by the impact deformation of grand-parent body.

References

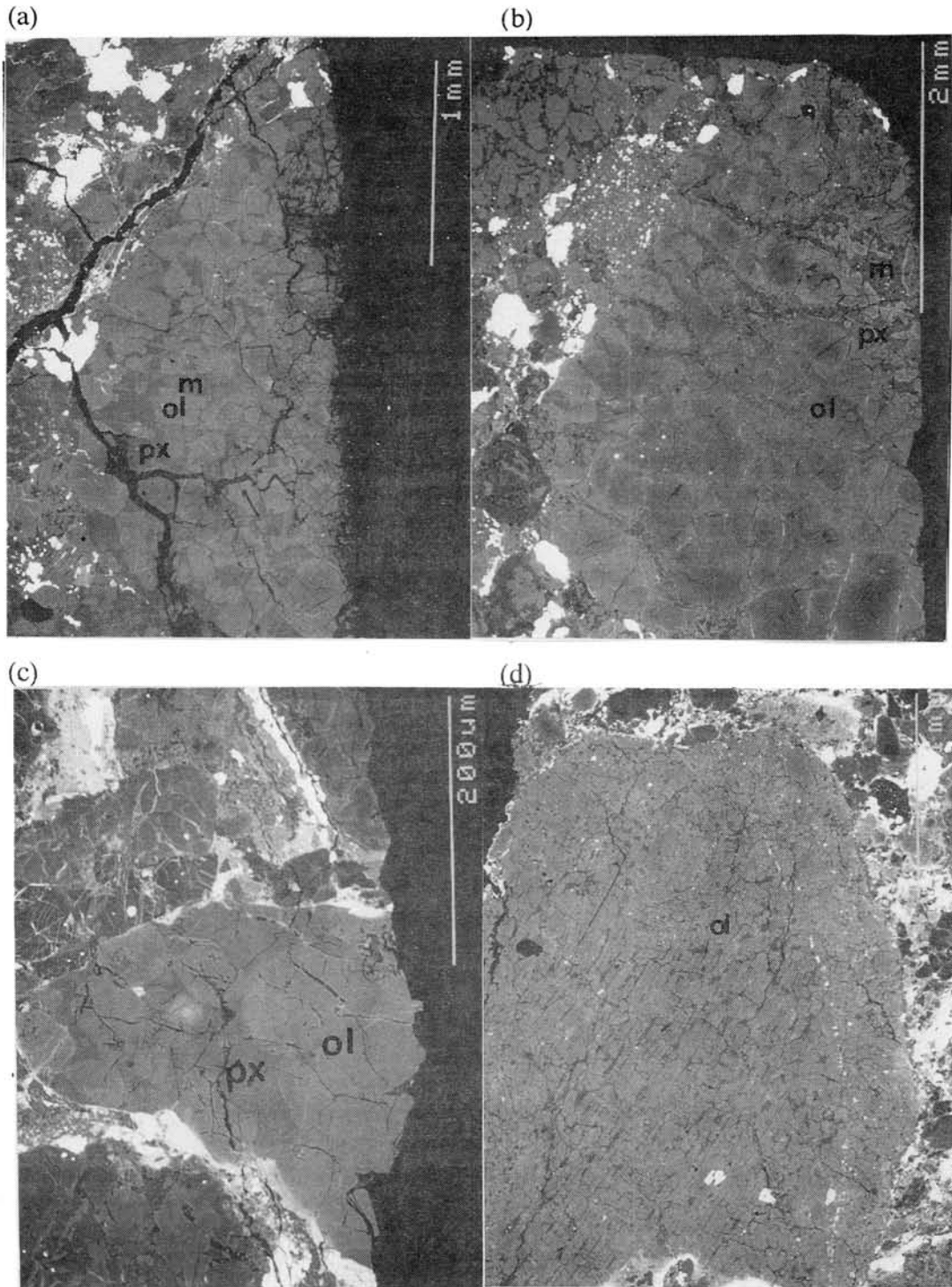
- Fujita,T. and Kitamura,M. (1992): Papers presented for the 17th symposium on Antarctic meteorites,34-35.
 Fujita,T. and Kitamura,M.(1993): Papers presented for the 18th symposium on Antarctic meteorites,15-18.
 Hutchison,R. (1992): *J. Volcanol. Geotherm. Res.*, **50**, 7-16.
 Kitamura,M., Tsuchiyama,A., Watanabe,S., Syono,Y. and Fukuoka,K. (1992): High-pressure research: Application to Earth and Planetary sciences, Syono,Y. and Manghn,M.H. eds. Terra Scientific Publishing Company,Tokyo,p333-340.
 Kitamura ,M.(1990):*Proc.23th ISAS Lunar Planet. Symp.*,223-225
 Kitamura,M., Okamoto,Y. and Watanabe,S. (1990): Papers presented for the 15th symposium on Antarctic meteorites, 36-37.
 Nagahara,H. (1981): *Nature*,**292**,135-136.
 Nakamura,T., Tomeoka,K., and Takeda,H. (1990): *Proc. 23th ISAS Lunar Planet. Symp.*, 188-193.
 Rambaldi,E.R.(1981): *Nature*, **292**, 558-561.
 Sneyd,D.S., McSween,H.Y.,Jr.,sugiura,N.,Strangway,D.W., and Nord,G.L.,Jr.(1988): *Meteoritics*,**23**,139-149.

Fig. 1

Backscattered electron images of the lithic fragments. (a) Type A in the Julesburg, (b) Type B in the Julesburg, (c) Type A in the Y-790448, d) Type B in the Y-790448.

ol: olivine, px: pyroxene. m: mesostasis.

In the right side of the fig.d, white spots of chromite grains are observed on the boundary of the barred-olivine like core and granular rim.



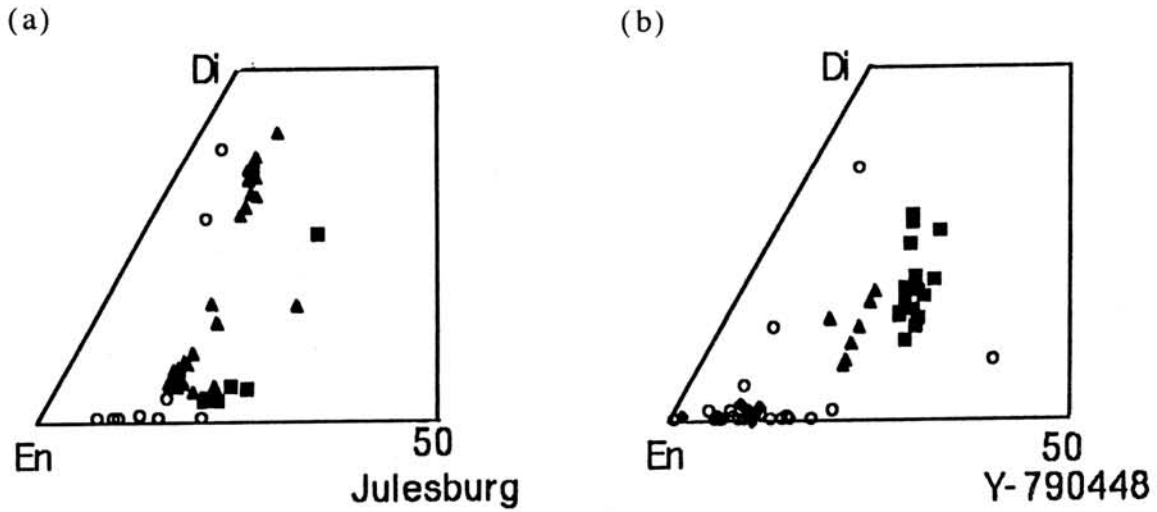


Fig. 2 Compositions of the pyroxenes plotted on the quadrilaterals. (a) Julesburg, (b) Y-790448. solid triangles: fragment A, solid squares: fragment B, solid diamonds: relicts, open circles: chondrules.

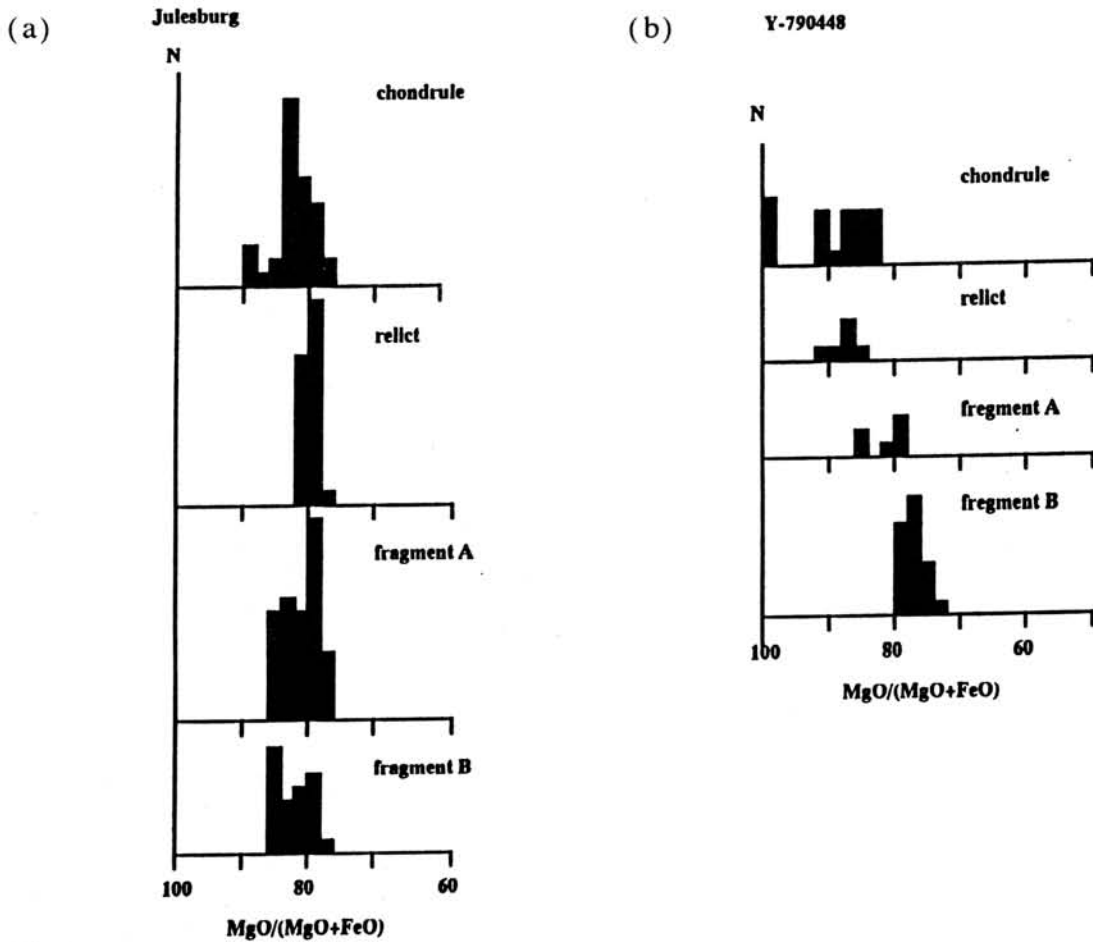


Fig.3 Histograms of $MgO/(MgO+FeO)$ mol content of the olivines in the (a) Julesburg and (b) Y-790448.

CHONDRITIC BRECCIA CONSISTING OF MIXED ORDINARY CHONDRITE COMPONENTS. Keizo Yanai and Hideyasu Kojima, Department of Antarctic Meteorites, National Institute of Polar Research, 9-10, Kaga 1-chome, Itabashi-ku, Tokyo 173, Japan.

Two Antarctic meteorites Yamato-8424 and Yamato-86745 have been identified as the chondritic breccia consisting of mixed components of the ordinary chondrites. Yamato-8424 is a regolith breccia that is homogenized mixture of mostly H and LL chondritic components. Yamato-86745 is a typical breccia consisting of LL clasts within homogenized L and LL with H chondritic matrices. The both breccias consist of same mineral assemblages of ordinary chondrites such as olivine, pyroxene, Fe-Ni metal, troilite with trace of plagioclase.

Yamato-8424(Y-8424): Y-8424 is a small irregular shaped stone(mostly complete) weighing 9 grams[1] and it is covered with a dull-black fusion crust. The surface of the stone shows a dark brown to brown to do weathering effect, however the interior(sawing surface) is very fresh with relatively large and very fresh Fe-Ni metal grains in dark grey fine material.

In the thin section (Fig.1), Y-8424 shows typical regolith breccia consisting mainly of fine-grained matrix and less amount of mineral fragments. The mineral fragments are olivines, pyroxenes and Fe-Ni metals ranging 0.2-0.4 mm, excepting 1 mm Fe-Ni metal grain (center of bottom in Fig.1). The matrix is fine grains under 50 μ m, consisting of olivines, pyroxenes, troilites, Fe-Ni metals and traces of plagioclases within very fine recrystallized. Most troilites distributed as under 30 μ m grains along the grain boundaries in the whole section. Some relatively large fragments may be traced as parts of chondrules. Therefore it indicates that the specimen is originally chondrite.

The result of the EPMA analyses of constituent minerals show an unusual features such as Fig.2. Olivines and low-Ca pyroxenes in both

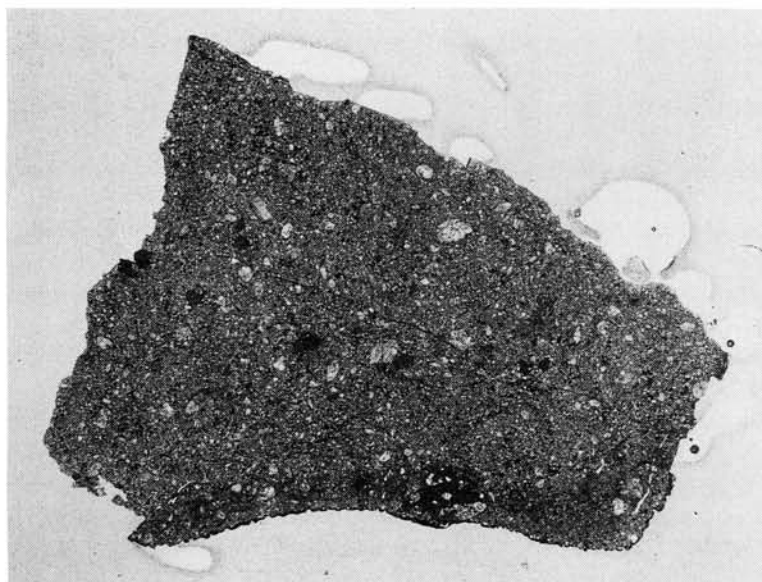


Fig. 1 Photomicrograph of the thin section of Yamato-8424, regolith breccia of H and LL chondrite mixture. Field view is 6.5 mm.

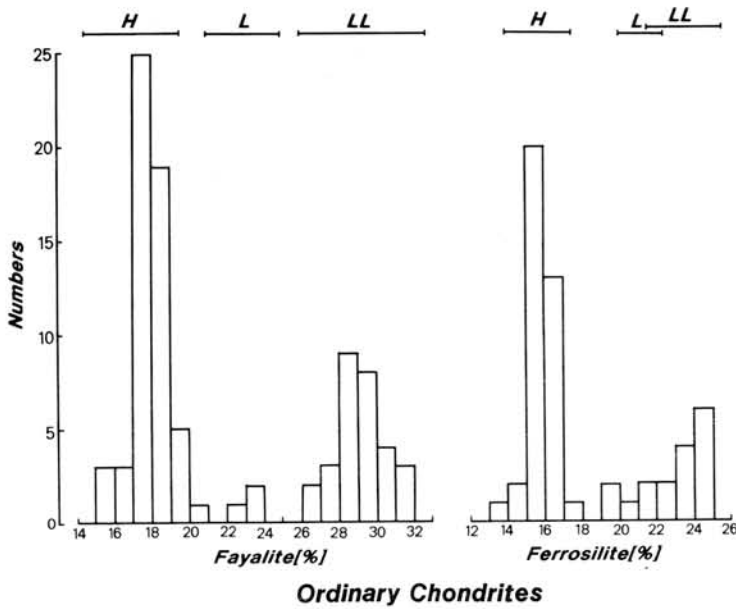


Fig. 2 Frequencies of olivine (fayalite %) and orthopyroxene (ferrosilite %) compositions which correspond to H, L and LL chondrites.

mineral fragments and fine grains in matrix, appear as the bimodal frequency patterns in their compositions. Olivines are recognized three groups for their compositions such as an average composition Fa17.5, Fa23.0 and Fa28.7. Especially two remarkable peaks of them are conspicuous and they are corresponded to those of H and LL chondrite groups. Low-Ca pyroxenes are comprised largely two compositional groups such as an average composition Fs15.8 and Fs22.8, and they are also corresponded to H chondrite group and L-LL groups. Both olivines and pyroxenes derive from at least two chondrite groups, and they distribute uniformly in the whole section as mixture.

Yamato-86745(Y-86745): Y-86745 is 11.8 g in original weight and almost 3/4 stone covered by a dull-black fusion crust, with grey interior. The surface of the stone is a dark brown to grey to do weathering effect, but the interior (sawing surface) is relatively fresh with shiny Fe-Ni metal grains in pale grey fine material.

In the thin section (Fig.3), Y-86745 shows typical breccia consisting of dark grey matrix and slightly rounded clast. Clasts are chondritic without any chondrules and show slightly brecciated texture with few black veinlets. Those clasts consist mainly of olivine and pyroxene with Fe-Ni metal and troilite, and traced opaques. The mineral assemblage resembles to metal less ordinary chondrite. The matrix consist of mineral fragments (olivine, pyroxene and Fe-Ni metal) with dark material, therefore the matrix seem to be originated from chondritic meteorite.

The EPMA analyses of constituent minerals show the two different patterns as Fig.4. Olivine and pyroxene in the clasts are average composition Fo30.1 and Fs24.1 respectively, which are corresponded to those of LL group ordinary chondrite. On the other hand, olivine in matrix is a wide compositional range including those of all ordinary chondrites. Especially most of olivines are ranged between L and LL chondrite groups. Therefore the matrices resemble to originated from the both L and LL groups. However pyroxene in matrix is average composition Fs24.6 (correspond to LL group) without wide compositional range.

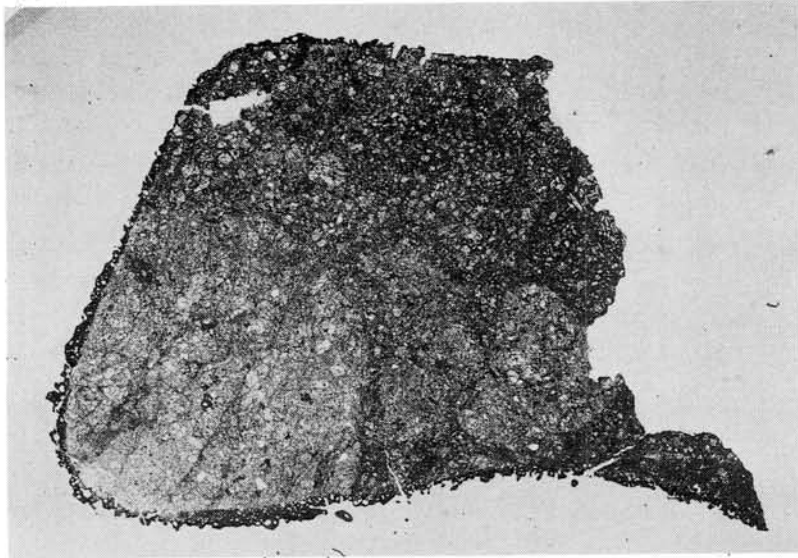


Fig. 3 Photomicrograph of the thin section of Yamato-86745, typical breccia of mostly L and LL chondrite mixture. Field view is 10 mm.

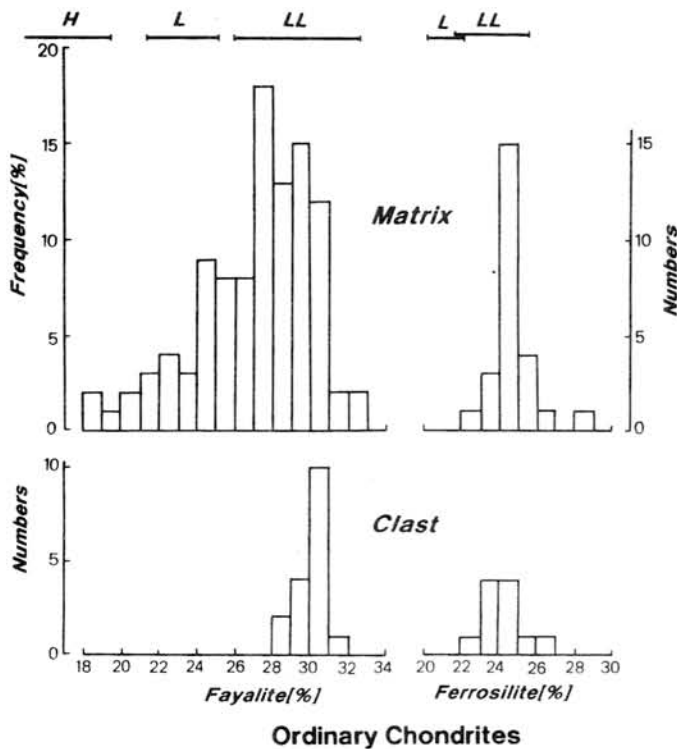


Fig. 4 Frequencies of olivine and pyroxene in matrices and clasts of Yamato-86745 breccia. Olivine compositions in matrices ranged through those of H to LL chondrites.

The textures and unusual compositional patterns indicate that Yamato-8424 and Yamato-86745 are the regolith breccia and typical breccia respectively, and those meteorites are the mixture of the different chondritic materials. The mixing of the chondritic materials should be carried out on their parent bodies before the breaking of them. It seems that the both breccias had been formed by the mixing on the surface of the chondritic parent bodies where occurred the intense bombardments of the ordinary chondrite bodies, during the early stage of the solar system.

[1] Yanai and Kojima (1993) Lunar Planet. Sci. XXIV, 553-554.

MINERALOGICAL STUDY OF RECRYSTALLIZED CLASTIC MATRIX IN THE YAMATO 74356 MONOMICT EUCRITE. ^{1,2}Akira Yamaguchi and ²Hiroshi Takeda.

¹Planetary Geosciences, Dep. of Geology and Geophysics, SOEST, Univ. of Hawaii at Manoa, Honolulu, HI 96822, USA and ²Mineralogical Institute, Faculty of Science, University of Tokyo, Hongo, Tokyo 113, Japan.

Introduction. Eucrites are the meteoritic record of basaltic volcanism at a very early stage in the evolution of the solar system. Many eucrites are monomict breccias composed predominantly of a single lithic type with homogenized host pigeonites of uniform composition and fine lamellae of exsolved augite. They are often called "ordinary eucrites" in an analogous sense that the term equilibrated ordinary chondrite is used. The effects of the thermal events are also recorded in the clastic matrix as well as the pigeonite crystals in the clast [1].

The polymict eucrites had been common among the early Antarctic meteorite collections [2] and the Yamato (Y) 74356 is the first monomict eucrite found in Antarctica and has been identified as a single equilibrated eucrite [3]. Subsequently, more monomict eucrites such as Y792510 and Y791186 have been recovered from Antarctica [2]. Y74356 has not been studied in detail except that it contained homogenized pyroxenes [3]. During our comparative studies between lunar and eucritic granulites, we found that Y74356 has completely recrystallized clastic matrix similar to lunar granulites [1]. To gain better understanding of early thermal events on the HED parent body, we investigated Y74356 by mineralogical techniques and compared it with other Antarctic monomict eucrites.

Samples and Methods. A sample of Y74356 used in this study is a potted bat made from a chip from the National Institute of Polar Research (NIPR). A polished thin section (PTS) has been made and examined by an optical microscope and a scanning electron microscope (SEM) JEOL JSM-840A equipped with an energy dispersive spectrometer (EDS) and a Kevex Super 8000 system. Four PTSs of Y792510 and Y91186 made from parts of the chips used for the isotopic studies were examined for comparison. Chemical compositions of minerals in these PTSs were obtained by electron probe microanalysis (EPMA) with the JEOL 8600 Superprobe at Geol. Inst., Univ. of Tokyo and a JEOL JCSA-733 at the Ocean Research Institute, Univ. of Tokyo.

Results. The Y74356 eucrite (PTS Y74356,10) is matrix-rich recrystallized breccia, composed of coarse grained (<0.3x0.7 mm) (CC) clasts, granulitic pyroxene (GP) clasts, mineral fragments and granoblastic clastic matrix. The CC clasts are composed of pigeonite and lath-shaped plagioclase and have tiny (<30 μ m in diameter) chromite. The granulitic clasts are composed of fine grained (<80 μ m in diameter) polygonal pigeonite, augite, ilmenite and minor other minerals. Mesostasis area is not observed in this PTS.

Microscopic observation of a clastic matrix in Y74356 displays granoblastic texture. The clastic matrix is dominated by two lithologies. One lithology is relatively dark zone composed of pyroxene and plagioclase and their modal abundances are similar to the ordinary eucrites. Second lithology is light colored zone, in which more feldspathic fragments predominate. Forms of small crystals are anhedral and equant and boundaries form smooth curves that approach 120° triple point juncture. Pore space (ca. 10 %) in the form of intergranular cavities occur sporadically.

The pigeonite crystals in the CC clasts and many fragments have closely-spaced (001) augite lamellae and have cloudy and dusty core and transparent rim. Tiny chromite crystals less than 30 μm are often located along the line of grain or subgrain boundaries of pigeonites. The GP clasts have transparent pyroxenes. Chemical compositions of pyroxene of the whole PTS fall along a single tie line in the pyroxene quadrilateral ranging from $\text{Ca}_4\text{Mg}_{38}\text{Fe}_{58}$ to $\text{Ca}_{37}\text{Mg}_{31}\text{Fe}_{32}$ (bulk composition: $\text{Ca}_8\text{Fe}_{36}\text{Fe}_{56}$).

The most plagioclase crystals are transparent, but sometimes dusty inclusions are located at the subgrain boundary in the crystals. The crystals show sharp or very weakly undulose extinction. The chemical variation in the CC clasts and the fragments is preserved in the ranges from An_{86} to An_{94} , which is smaller in the range than those of other monomict eucrites. Small plagioclase crystals in the GP clast have high Na spots (An_{70}).

Minor minerals include ilmenite, chromite, a silica mineral, and Fe metal. Troilite is not found in this PTS. The chemical compositions of tiny chromites at grain boundary of the pyroxene crystals are $\text{Fe}_{6.8-7.9}\text{Mg}_{0.2}\text{Mn}_{0.1}\text{Cr}_{6.2-7.5}\text{Al}_{1.2-2.2}\text{Ti}_{1.0-2.1}\text{O}_{24}$, which is close to the values of the ordinary eucrites. There are thin (<10 μm in thickness) ilmenite lamellae in a large (100 μm in diameter) chromite crystal in one of the GP clasts.

Y792510 consists of brecciated plagioclase and pyroxene crystals up to 1 mm in length, and lithic clasts up to 3 mm across. These fragments are angular and generally less shocked than the surrounding material. Throughout the section the pyroxene and feldspar crystals show distorted twin lamellae, shear deformation, and clouding, but no maskelynite was seen. The pyroxenes contain extensive fine exsolution lamellae and partly inverted to Opx. The matrix grain size is highly variable, ranging from 0.02 to 0.2 mm. No granulitic area has been detected.

Discussion. The most remarkable feature of Y74356 is a galanoblastic matrix and granulitic clasts which are easily distinguishable by an optical microscope. Such texture is formed by solid state annealing and recrystallization. The degree of recrystallization of the clastic matrix is higher than any other ordinary eucrites such as Millbillillie, Juvinas, Stannern [1] and Y792510. Such breccia as Y74356 can be called a granulitic breccia.

Light colored feldspathic zone in the matrix might be a crushed single plagioclase crystal, indicating in-situ brecciation. In contrast, Millbillillie which has granulitic matrix [4], are well mixed with all kind of fragments.

Y74356 has more than 10 % pore space. The large pore space may be interpreted as recrystallization of matrix with pores. Such texture is often observed in highly metamorphosed lunar breccias (lunar granulites) [5]. In contrast to the porous clastic matrix of Y74356, the complex matrix of Millbillillie may be formed by recrystallization after welding to reduce the pore space subsequent to the mixing of melt and clastic materials [4].

completely homogenized Mg/Fe ratios of the host pigeonite with a scale of about 1.1 mm (PTS size) and cloudy pyroxene indicate that metamorphic degree of pyroxene is type 5 [6]. Also, the Na-Ca variations in the matrix plagioclase are less than those of other ordinary eucrites, indicating more equilibration of the plagioclase. The ilmenite lamellae in a large chromite may have been formed by subsolidus annealing. All mineral chem-

istries are consistent with the matrix recrystallization. The facts suggest that the matrix recrystallization occurred at the same time or after the equilibration of pigeonite.

The GP clasts are similar to the GP areas of the Juvinas eucrite [7], but the Juvinas GP areas are mostly found as parts of pyroxene crystals in the lithic clast, and their matrices contain acicular plagioclase crystals. The Y792510 matrix does not show a granulitic texture in spite of the partial inversion of pigeonite to orthopyroxene. Prolonged subsolidus annealing only may not produce the granulitic matrix.

The history of Y74356 can be summarized as follows: (1) Primary crystallization of the CC clast pyroxene and plagioclase. (2) Brecciation to produce clastic matrix. (3) Extensive thermal metamorphism to recrystallize the clastic matrix. The matrix regions in Y74356 can be classified as a granulitic breccia. The GP clast might be formed as the same time as the brecciation event 2, such as shock mosaicism. There is possibility of thermal event before stage 2, because such event might be erased by stage 3. If stage 3 is subsequent to stage 2, the heat source may be derived from an impact cratering event.

The textural feature of the matrix of Y74356 is similar to lunar granulitic breccia such as 79215 [1], which was formed by recrystallization of the polymict breccias by heating at temperature over 1000°C for long periods of time [8]. The effects in the lunar granulitic breccias could have resulted from burial at a depth of several km, possibly during an earlier period of even higher impact flux, accompanied by heat flow from the lunar interior [5]. The presence of eucritic granulite, Y74356 indicates that nearly the same extensive thermal events as the moon have been effective in the early history of the HED parent body.

In conclusions, (1) Y74356 eucrite is the first example of granulitic breccia found in the Antarctic eucrites; (2) the degree of recrystallization of the clastic matrix is the highest among the eucrites; and (3) the surface of the small asteroid such as the HED parent body or 4 Vesta experienced extensive thermal metamorphism comparable to the early moon.

We thank NIPR for the samples, and T. Ishii, H. Yoshida, O. Tachikawa and M. Otsuki for their technical assistance. This work was supported in part by a Grant-in-Aid for Scientific Research from the Japanese Ministry of Education, Science and Culture.

References: [1] Yamaguchi A. and Takeda H. (1994) Lunar Planet. Sci. 15, 1525-1526. [2] Takeda H. (1991) Geochim. Cosmochim. Acta 55, 35-47. [3] Takeda H. (1979) Icarus 40, 455-470. [4] Yamaguchi A. et al. (1994) Meteoritics in press. [5] Warner et al. (1977) Proc. Lunar Planet. Sci. Conf. 7th, 2379. [6] Takeda H. and Graham A. L. (1991) Meteoritics 26, 129-134. [7] Takeda H. and Yamaguchi A. (1991) Meteoritics 26, 400-401. [8] Taylor G. J. et al. (1991) Lunar Source Book, A user's guide to the moon, ed. by Heiken G. H., Vaniman D. T. and French B. M., Cambridge Univ. Press, 183.

UNEQUILIBRATED EUCRITES Y-74450, Y-793548, Y-82210, and Pasamonte: PYROXENE REE SYSTEMATICS AND MAJOR, MINOR, AND TRACE ELEMENT ZONING. Aurora Pun and J.J. Papike, Institute of Meteoritics, Dept. Earth & Planetary Sciences, University of New Mexico, Albuquerque, NM 87131-1126, USA

We are evaluating the minor and trace element concentrations in the pyroxenes of a few Yamato unequilibrated eucrites and Pasamonte. Pasamonte is a characteristic member of the main group eucrites, and has recently been redescribed as a polymict eucrite [1]. We are evaluating the Pasamonte eucrite as a basis of comparison to the Yamato eucrites. Our Pasamonte sample contained eucritic clasts with textures ranging from subophitic to moderately coarse-grained. This study concentrates on pyroxenes from an unequilibrated, moderately coarse-grained eucrite clast in Pasamonte. Our Yamato eucrites, Y-74450, 74-6, Y-82210, 61-4, and Y-793548, 51-2 are all polymict eucrites from the collections of the NIPR. We have also selected moderately coarse grained unequilibrated eucrites clasts from these sections for our study.

Major, minor and trace element analyses were measured for zoned pyroxenes in the eucritic clasts of Pasamonte and the Yamato meteorites. The major and minor element zoning traverses were measured using the JEOL 733 electron probe with an Oxford-Link imaging/analysis system. Complimentary trace elements were then measured for the core and rim of each of the grains by SIMS. The trace elements analyzed consisted of eight REE, Sr, Y, and Zr. These analyses were performed on a Cameca 4f ion probe at the UNM/SNL Ion Microprobe Facility, a joint operation of the Institute of Meteoritics, UNM and Sandia National Laboratories.

The results of the CI Chondrite normalized (average CI, [2]) trace element analyses for several grains from the Yamato samples and from Pasamonte are shown in Figure 1. The Eu abundance in the cores of the pyroxenes from Pasamonte represent the detection limit and therefore, the (- Eu) anomaly is a minimum. Examples of the major and minor element zoning patterns from a single pyroxene grain in Pasamonte and a single pyroxene from Y-74450 are shown in Figure 2. Major and minor element patterns are typical for igneous zoning. Pyroxene cores are Mg enriched, whereas the rims are enriched in Fe and Ca. Also, Ti and Mn are found to increase, while Cr and Al generally decrease in core to rim traverses. The cores of the pyroxenes are more depleted in the REE than the rims.

Using the minor and trace element concentrations of bulk Pasamonte from [5, 6] and the minor and trace element concentrations from the cores of the pyroxenes in Pasamonte measured in this study, we calculated

partition coefficients (D 's) between pyroxene and melt ($C_{\text{pyx}}/C_{\text{bulk}} = D$). This calculation assumes that bulk Pasamonte is representative of a melt composition. Calculated D 's are shown in Table 1. In our future attempts to back calculate the compositional characteristics of eucritic melts from pyroxene compositions, we anticipate using these calculated partition coefficients and others we plan to determine specifically for Yamato -74450.

Acknowledgments: We thank the NIPR for providing the Yamato thin sections. We thank M. N. Spilde for technical assistance on the electron probe and G. Fowler and G. Layne for technical assistance on the SIMS. This work was supported by NASA grant NAGW-3347 (J.J.P.) and NGT-70223 (NASA-GSRP training grant for A.P.).

References: [1] Metzler K., Bobe K.-D., Palme H., Spettel B., and Stoffler D. (1994) *LPSC XXV*, 901-902. [2] Anders. E. and Grevesse N. (1989) *GCA*, **53**, 197-214. [3] Papike J.J., Shearer C.K., and Shimizu N. (1988) *LPSC XIX*, 901-902. [4] Shearer C.K., Papike J.J., Simon S.B., and Shimizu N. (1989) *GCA*, **53**, 1041-1054. [5] Shimizu H. and Masuda A. (1986) *GCA*, **50**, 2453-2460. [6] McCarthy T.S., Erlank A.J., and Willis J.P. (1973) *EPSL*, **18**, 433-442.

Figure 1

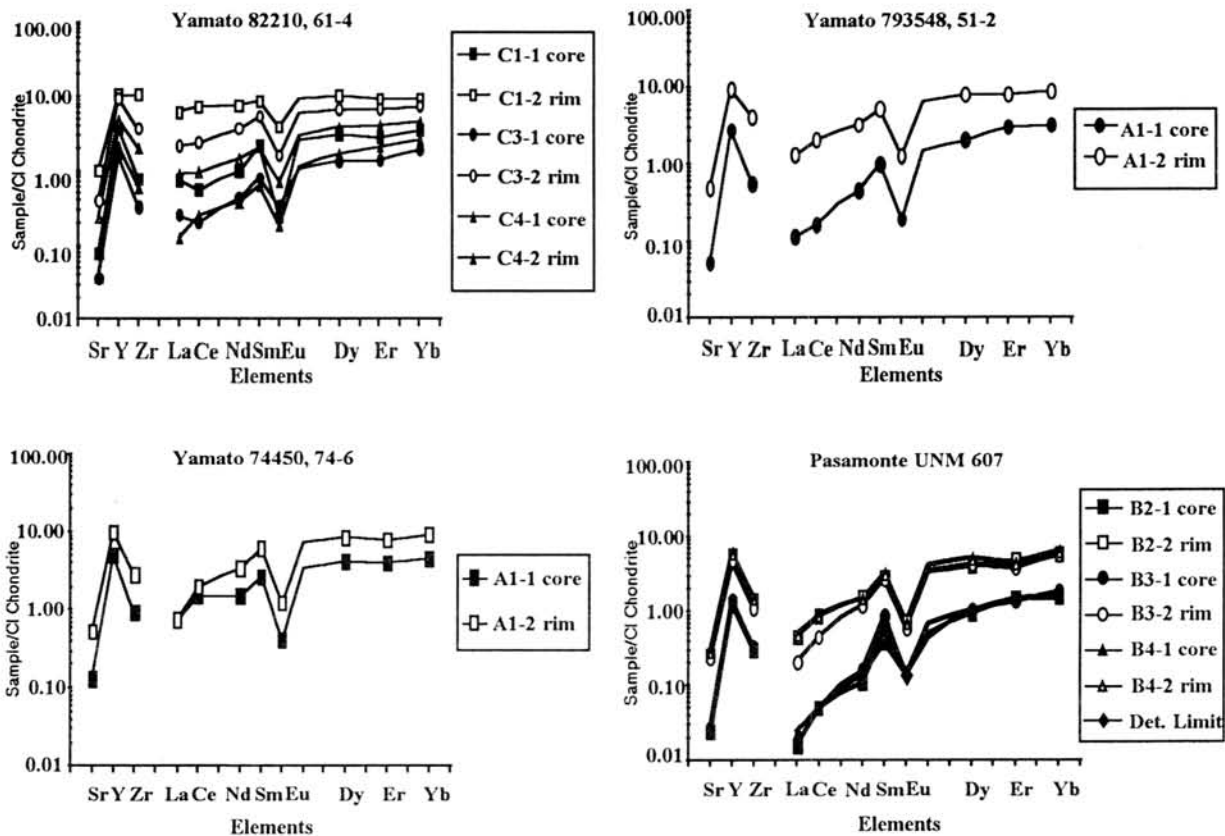


Figure 2

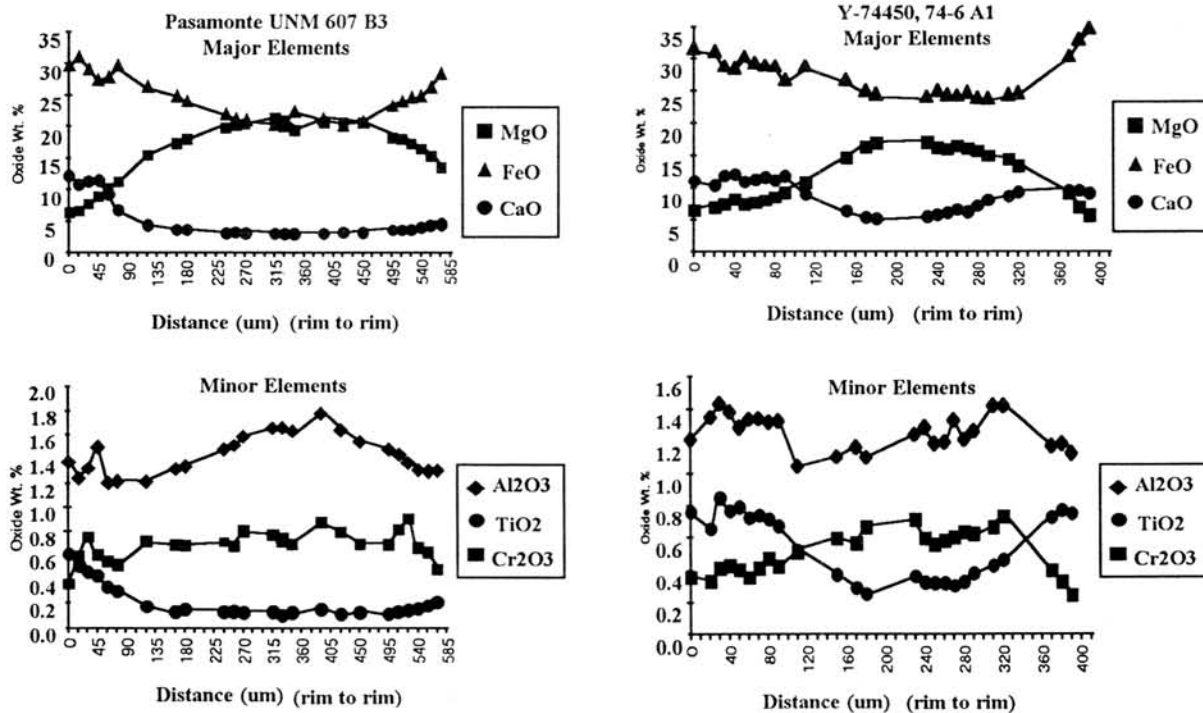


Table 1.
Pasamonte

Element	Calculated D
La	0.001
Ce	0.004
Nd	0.010
Sm	0.042
Dy	0.070
Er	0.104
Yb	0.129
Y	0.119
Sr	0.003
Zr	0.023
Al	0.118
Ti	0.312
Cr	2.242
Wo _{pyx}	5.98

THE ORIGIN OF CUMULATE EUCRITE DEDUCED FROM MAGMA DIFFERENTIATION SIMULATION

Kazuto Saiki and Hiroshi Takeda

Mineralogical Institute, Faculty of Science, University of Tokyo, Hongo, Tokyo 113, Japan

Introduction: Cumulate eucrites have bulk compositions between diogenites and eucrites. Many models had been constructed to explain the origin of eucrite. They are roughly separated to two groups: "Crystal fractionation models" [1,2] and "Partial melting models" [3]. Previous models, however, could not produce cumulate eucrite which has suitable chemical compositions. That's why the origin of ordinary eucrite and cumulate eucrite are usually discussed separately. Bartels and Grove mentioned "Ordinary eucrites produced by partial melting near the surface of HED parent body and cumulate eucrites are likely produced from parent magmas by fractionation in plutonic environments within the parent body, with the production of very iron-rich ($Mg\# = 20$) residual liquids." [4]. The study of polymict eucrite Y791439, however, shows that ordinary to cumulate eucrites were located adjacent in the parent body crust, and there were many kinds of cumulate eucrites existed at one region [5]. It is important to keep in mind that there should be the genetic link between ordinary eucrites and cumulate eucrites.

Methods: In order to obtain a better understanding of the origin of cumulate eucrites, we examined following three kinds of calculation: Equilibrium liquid calculation (Work A), Mafic element fractionation with/without trapped liquid (Work B), and Fractional crystallization with trapped liquid (Work C). In work A, we calculated equilibrium liquid coexisting with pyroxenes in polymict eucrite Y791439 and some other eucrites, and plotted the data on Fig.1 focusing the Fe# of liquid and solid phase. Mg/Fe partition coefficient is not so sensitive to temperature, so it can be treated as constant in this work. In work B, we simulated the fractional crystallization of mafic elements. Fe#s of liquid and instantaneous solid in fractional crystallization process were calculated and plotted on Fig.2. This simulation only handled Fe and Mg. For the calculation, partition coefficient of pyroxene is applied. On the early stage olivine also crystallized. In the equation: $(Mg/Fe)_{liq} = (Mg/Fe)_{sol} / K$, partition coefficient (K) of olivine is about 3.2, and pyroxene is about 3.4. These difference did not affect on the result severely. Initial Fe# was taken from Y7308 howardite bulk composition. In work C, we simulated fractional crystallization with trapped liquid. For the calculation we adopted the modified Bottinga-Weill two-lattice melt model and applied Nielsen-Dungan crystal/liquid partition coefficients [6]. Saturated phases were determined by Longhi's liquidus boundary equations [7]. We made a program (MAGDIF.C) for examining physical processes such as: crystal fractionation, solid-liquid remixing, and transport of elements from one system to another. Starting material was 1:10 mixture of Serra de Magé and Juvinas compositions. This material was estimated as a candidate for 90% fractionated liquid at Fig. 2B.

Results: The results of work A are shown in Fig.1. The liquids equilibrated with most of cumulate eucrites has more Fe-rich compositions than ordinary eucrites. Cumulate eucrites are too Fe-rich, if they are cumulus from the magma of ordinary-eucritic compositions. The results of maximum fractionation of mafic elements are shown in Fig.2A. In this process, crystals were completely separated from liquid. When the Fe# of fractionated pyroxene reaches to Fe# of cumulate eucrite (Fe# = 40-50), there is over 10 vol % liquid remained. And the remnant liquid has Fe# over 80. The results of fractional crystallization with trapped liquid are shown in Fig.2B. In this case, Fe-rich cumulate eucrite can be produced without Fe-rich liquid. When the amount of trapped liquid is around 50%, Fe-rich cumulate-eucritic (Fe# = 45-55) could be produced from ordinary-eucritic liquid (Fe# = 60-65). For the work C, the path of solid compositions with 50% trapped liquid is shown in Fig.3. When the mol fractionation reaches to 5%, the compositions of liquid get close to those of Juvinas and the compositions of fractionated solid with trapped liquid get close to those of Serra de Magé. The solid compositions were slightly more Si-poor than we had expected.

Discussion: The results of work A show that the liquid coexisting with cumulate eucrites is too Fe-rich. Cumulate eucrites are used to be regarded as cumulus from evolved Fe-rich liquid. But there is no such Fe-rich clast in the HED meteorites. If we apply "partial melting model", the liquid produced from the cumulate eucrite is too Fe-rich for eucrite. Some cumulate eucrites especially Fe-rich ones may not be cumulus but slightly evolved liquid itself solidified slowly under an ordinary eucrite scarf. However, there still remains one problem in this hypothesis. If such cumulate-eucritic liquid should exist, some Mg-rich liquid would flow over the scarf and solidify as Mg-rich lava-like eucrite. Such eucrite has not been reported. The results of work B suggest the cumulus includes large amount of residual liquid (50%), cumulate eucrite (Fe# = mean 45-50) could crystallize from ordinary eucritic liquid (Fe# = mean 60-65). For the mixing process of solid and liquid, convection is of course available. But it is not clear whether there is sufficient convection or not, because the gravity on the HED parent body is very low. So liquid trapping process is more simple. If there are the variable amount of trapped liquid, many kind of cumulate eucrite could be produced. The results of work C suggested that cumulate eucrites may be produced by fractional crystallization with trapped liquid. The calculated cumulate eucrite has slightly Si-poor compositions. This is an effect of crystallized olivine component. We must examine reaction process of olivine in next work. Saturated phase and chemical compositions of crystals would change according to conditions such as: cooling rate, amount of minor elements, oxygen fugacity, and so on. This simulation, however, could propose one possible process. For examining the complex physical process, this kind of simulation work would be useful.

We thank Dr. John Longhi for giving us useful information in simulation work. This work is supported by Fellowships of the Japan Society for the Promotion of Science for Japanese Junior Scientists.

References

[1] Mason B. (1962) *Meteorites* (New York: Wiley), 116-119. [2] Ikeda Y. and Takeda H. (1985) *Proc. Lunar Planet. Sci. Conf. 15th*, in *J. Geophys. Res.*, 90, C649-C663. [3] Stolper E. (1977) *Geochim. Cosmochim. Acta*, 41, 587-611. [4] Bartels and Grove (1991) *Proc. Lunar Planet. Sci. 21st*, pp. 351-165. [5] Saiki K., Tagai T., and Takeda H. (1992) *Meteoritics* (abstract) 27, 284. [6] Nielsen R. L. and Dungan M. A. (1983) *Contrib. Mineral. Petrol.*, Vol. 84, pp.310-326. [7] Longhi J. and Pan V. (1988) *Proc. Lunar Planet. Sci. Conf. 18th*, pp. 459-470. [8] BVSP (Basaltic Volcanism Study Project) (1981) *Basaltic Volcanism on the Terrestrial Planets*. Pergamon, New York. 1286pp.

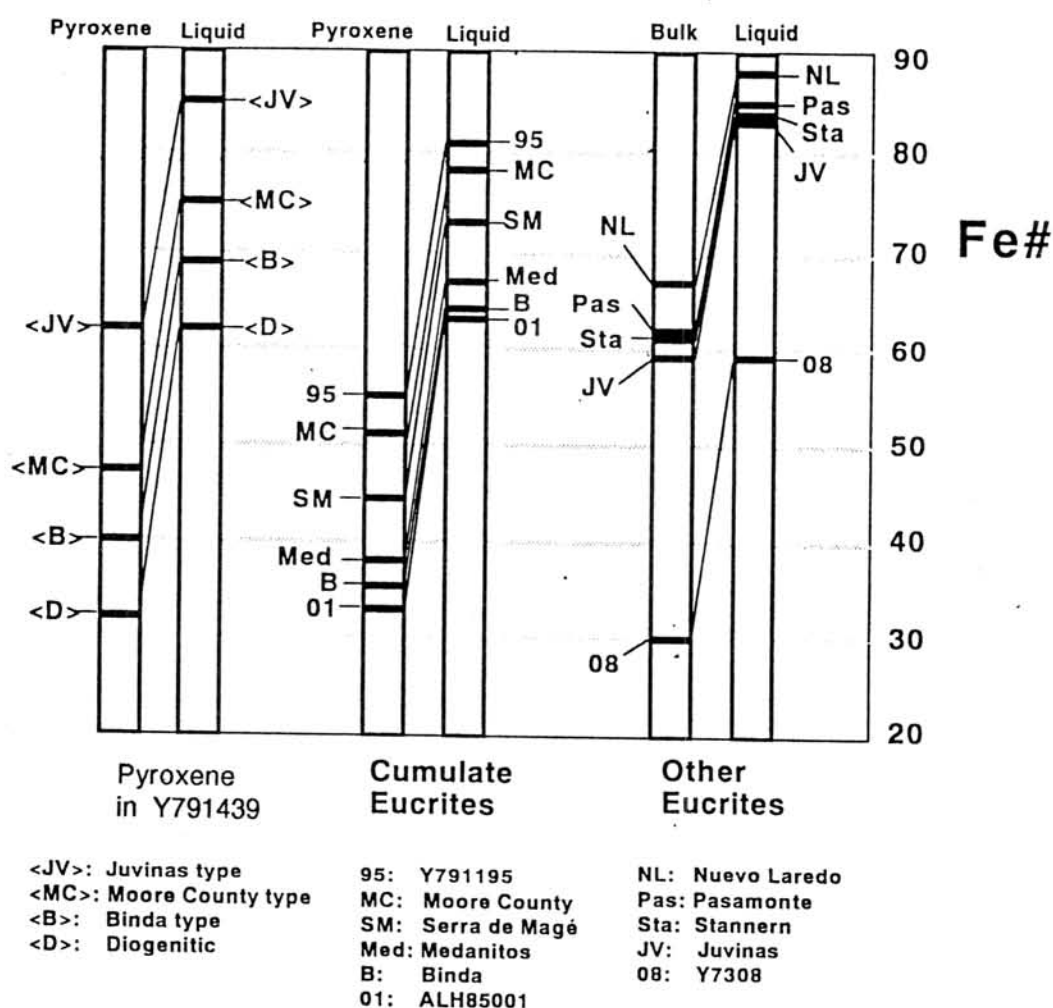
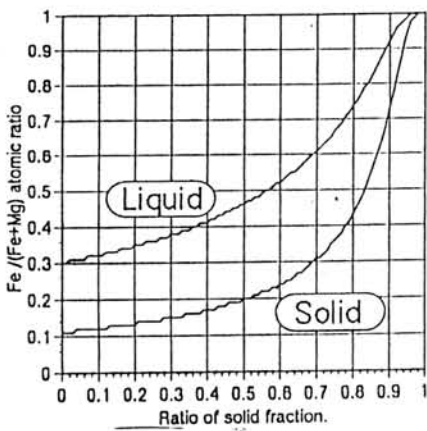
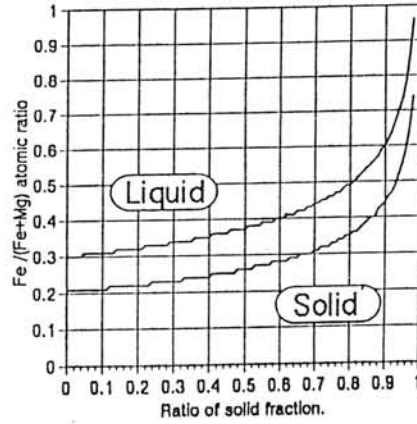


Fig.1 Fe# chart of eucrites and estimated liquids equilibrated with their pyroxene or bulk composition. The chemical composition data of Y791439, ALH85001, Medanitos and Y791195 are obtained in this study. Bulk chemical compositions of Y7308 is taken from Ikeda & Takeda (1985) [2] and those of the other meteorites are taken from BVSP (1981) [8].

Fig.2 Fractional crystallization of mafic minerals.



Case.A Complete separation of crystals from liquid.



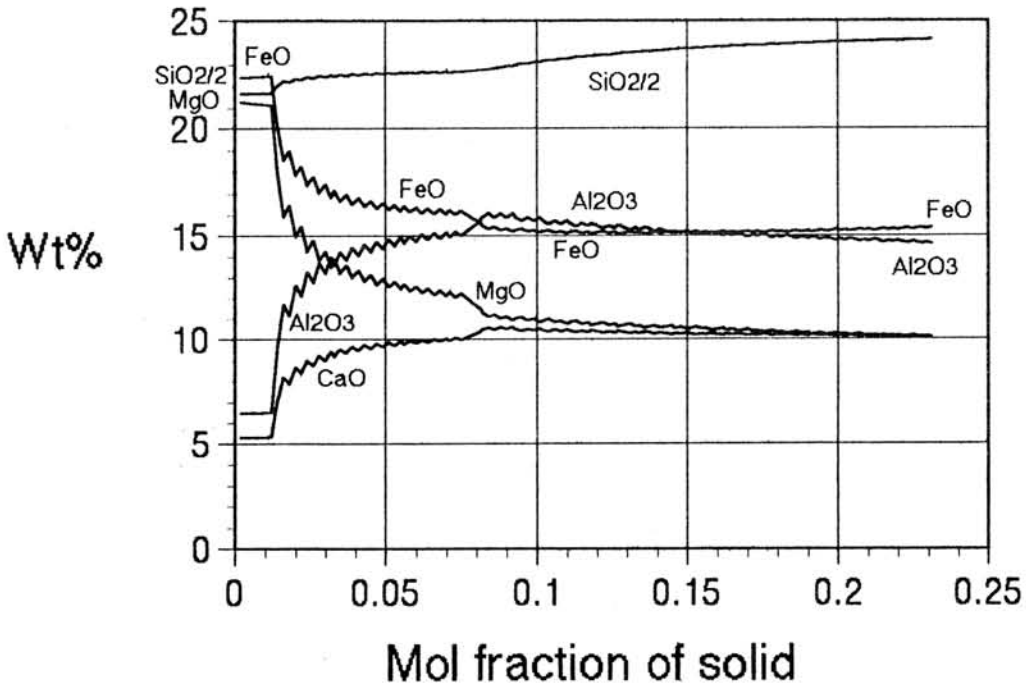
Case.B 50% trapped liquid exists with cumulus.

Liquid — Fe# of liquid.

Solid — Fe# of instantaneous solid composition (ISC).
(When trapped liquid exists, that is mixed composition of ISC and trapped liquid)

Ratio of fraction — mol ratio of solid phase.
(including trapped liquid)

Fig.3 Chemical compositions of fractionated solid with 50% trapped liquid.



COMPARATIVE STUDIES OF THREE ANGRITES; ANGRA DOS REIS, LEW87051 AND ASUKA-881371 METEORITES. Keizo Yanai, Department of Antarctic Meteorites, National Institute of Polar Research, 9-10, Kaga 1-chome, Itabashi-ku, Tokyo 173, Japan.

Three angrites; Angra dos Reis(ADOR), Lewis Cliff 87051(LEW87051) and Asuka-881371(A-881371) meteorites are studied in comparatively on their mineral assemblages, textures and compositions. ADOR is non-Antarctic meteorite and fell in Rio de Janeiro (22°58'S and 44°19'W), Brazil in 1869. Two others are Antarctic meteorites have been found on Lewis Cliff Ice Tange (84°17'S and 161°00'E), the Transantarctic Mountains in 1987 and in the Sør Rondane Mountains (72°50'S and 24°30'E), Queen Maud Land in 1988, respectively. Therefore the three localities are over 6,000 km (between Antarctic and non-Antarctic angrites) and over 2,500 km (between both Antarctic angrites) at a distance.

Angra dos Reis: ADOR meteorite is about 1.5 kg in original weight. Under 0.8 g fragmental pieces were provided to author for this study. Thin section and wet chemical analysis have been down using these samples. ADOR is an ultramafic igneous rock consisting of fassaite pyroxene with minor olivine, and accessory minerals. Accessory minerals are magnesian kirschsteinite, spinel, whitlockite, metallic Ni-Fe, troilite, and very rare plagioclase (An86), celsian, baddeleyite and titanian magnetite [1]. The petrographically, ADOR shows granular texture of pyroxene with little variation in grain size (Fig.1). Fassaite pyroxene occurs in two textural pattern such as more coarse grains (weakly porphyritic) and fine grains looks like groundmass. In composition, pyroxene is quite homogeneous titanian fassaite which is average composition $En_{33}Fs_{12}Wo_{55}$ containing 9-10% Al_2O_3 and 2% TiO_2 . Olivine is also homogeneous which is Fo_{48-52} containing 1.2-1.7% CaO (Fig.2).

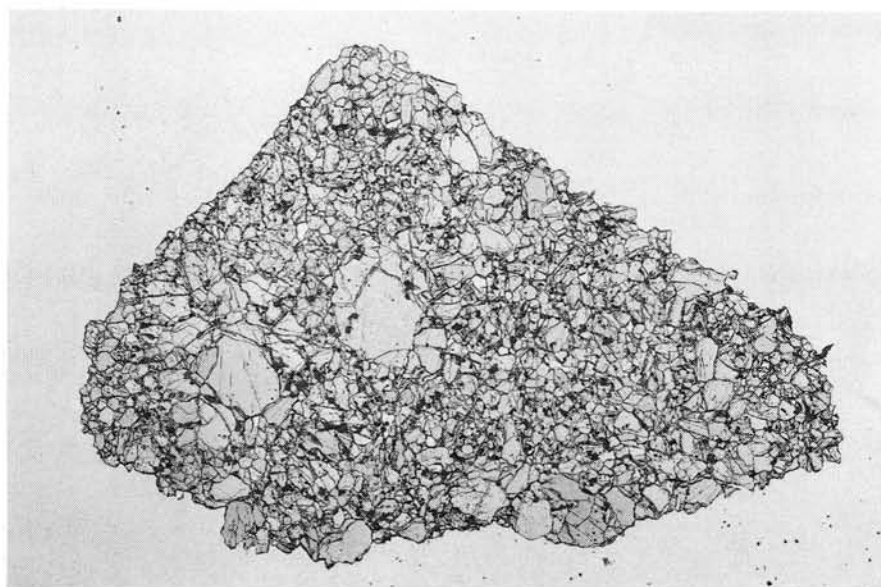


Fig. 1. Photomicrograph of thin section of Angra dos Reis meteorite. Field view is 9 mm. ADOR is a granular texture of pyroxene with minor olivine. Porphyritic crystals are fassaite pyroxene as same composition as groundmass fassaite pyroxene. Plan polarized light.

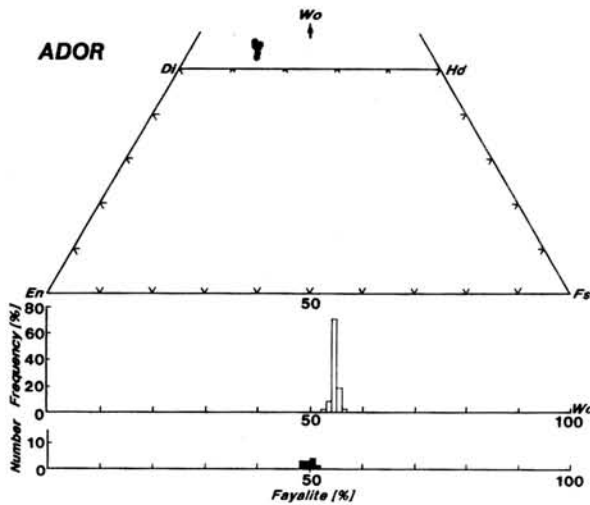


Fig. 2. Compositions of pyroxene and olivine of ADOR are almost homogeneous.

LEW87051: LEW87051 is 0.6 g in original weight and it is an individual stone with completely covered with black fusion crust [2]. The petrographically, this specimen shows typical porphyritic texture of olivine grains with subequal amount of groundmass plagioclase laths and interstitial pyroxene with little opaque. Plagioclase laths, 0.02 x 0.3 mm, are well subparallel arrangement (Fig.3). Pyroxene is titanian fassaite pyroxene showing weakly pleochroic of purplish tint, which ranged En1-29, Fs21-55 and Wo44-53 (average composition Wo50.2). Olivine contains variable composition ranged from Fo8-91, with a strong mode at approximately Fo18-25 (average Fo21). Those compositional ranges are corresponded with Fe-rich rim to Mg-rich core (Fig.4). Plagioclase is almost pure anorthite (An99-100).

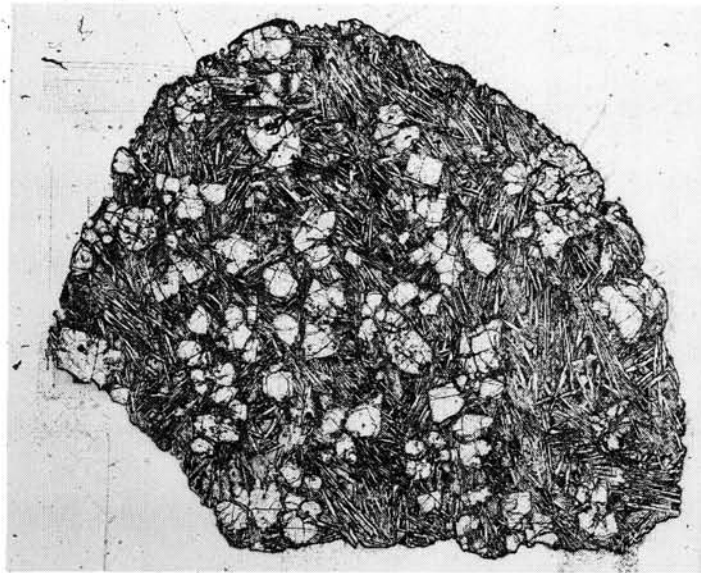


Fig. 3. Photomicrograph of the thin section of LEW87051 meteorite. Field view is 5 mm. LEW87051 is a typical porphyritic texture of olivine with plagioclase laths and interstitial fassaite pyroxene. Plan polarized light.

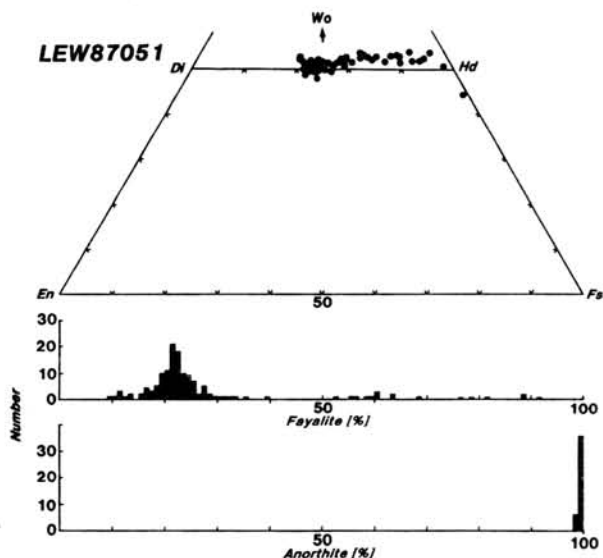


Fig. 4. Compositions of olivine, pyroxene and plagioclase of LEW87051. Olivine and pyroxene show a wide compositional ranges, but plagioclase is completely homogeneous (pure anorthite).

Asuka-881371: Asuka-881371 is 11 grams in original weight and it is an individual rounded stone almost completely covered with dull black fusion crust. Pale green, relatively coarse olivine crystals can be seen on the exposed face of the interior. Asuka-881371 is an unbrecciated, igneous rock showing typical ophitic (doleritic) texture with porphyritic olivine crystals. Asuka-881371 consists mainly of olivine, intergranular pyroxene (fassaite) and

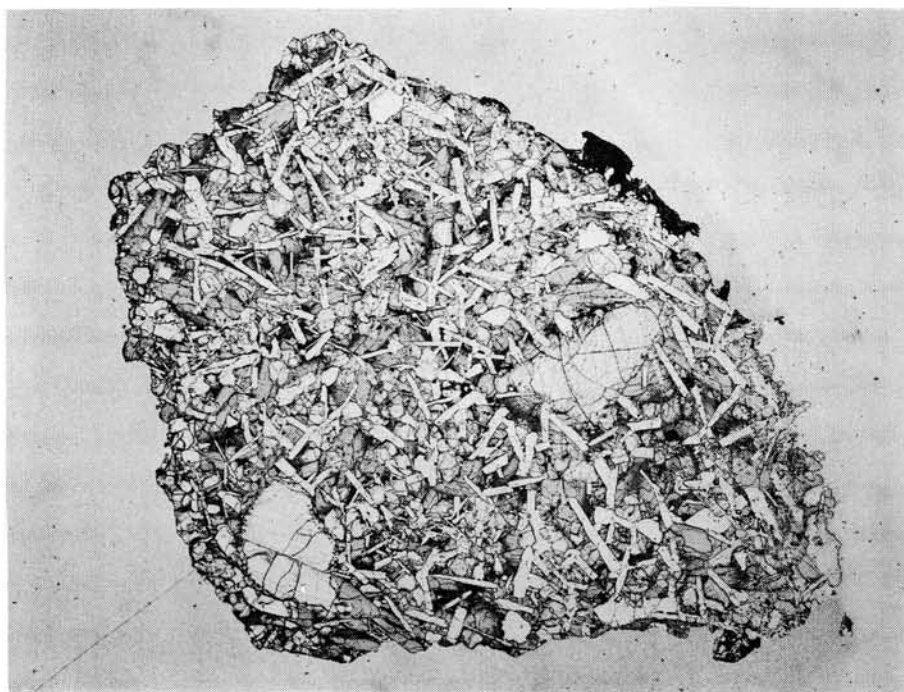


Fig. 5. Photomicrograph of the thin section of Asuka-881371 meteorite. Field view is 9 mm. A-881371 is an unbrecciated, igneous rock with an ophitic (doleritic) texture of coarser porphyritic olivine, granular olivine, prismatic plagioclase and intergranular fassaite pyroxene. Plan polarized light.

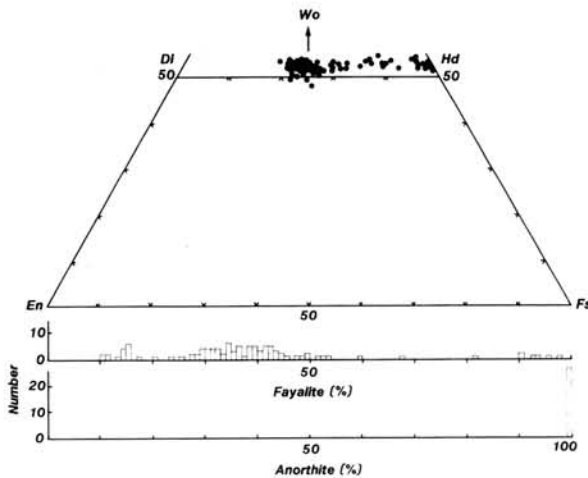


Fig. 6. Compositions of olivine, pyroxene and plagioclase of A-881371 are a wide range except plagioclase.

euhedral plagioclase with traced opaque and spinel (Fig.5). Olivine is present in three textural pattern such as porphyritic olivines (possible xenocryst), euhedral olivines and groundmass olivines. Those olivines are in remarkable compositional variations. The mode of Asuka-881371 is roughly 5% porphyritic olivine, 24% euhedral olivine in the groundmass, 20% fassaite pyroxene, 36% plagioclase and 15% Ca-olivine (kirschsteinite) in the groundmass and under 1% in other phases including ilmenite and apatite.

Pyroxene is titanium fassaite with pleochroic brown in those rims, which is average composition Wo52 containing high in over 22%CaO, 3.5-9.9%Al₂O₃ and 1-5%TiO₂. Pyroxene ranged En0-29, Fs18-50, Wo48-55. Olivine contains variable composition ranged Fo0-90 which correspond to Fe-rich rim and Mg-rich core, however most of olivine are ranged Fo57-72. Porphyritic coarse olivine grains show remarkable compositional zoning, which varied from most Mg-rich core (Fo90) to extremely Mg-poor (Fo0) immediately adjacent to the groundmass (Fig.6).

DISCUSSION: Macroscopically, LEW87051 and Asuka-881371 meteorites are clearly recognized as an individual stone for their complete fusion crust. The great distance, over 2,500 km and 6,000 km, among the three localities will strongly support the fact. It seems that the three angrites have individually been fallen on different sites and times. Therefore, the three angrites are not pair. The three angrites are unusual type for their petrographically, especially their unique mineralogy and unique chemical compositions compare with all known achondrite types. There are some differences in their texture and compositions among three angrites. Nevertheless those unique type of meteorite strongly suggested that they might be closely genetic relationship among them on the parent body.

- [1] Printz M., Keil K., Hlava P.F., Berkley J.L., Gomes C.B. and Curvello W.S.(1977) *Earth Planet. Sci. Lett.*, **35**, 317-330.
 [2] Mason B.(1989) *Antarctic Meteorite NEWSLETTER* 12, No.1, 15.

Comparison of shock induced carbonaceous matter from C_{60/70} fullerene with kerogen-like organic matter in carbonaceous chondrites

Tatsushi Murae,

Department of Earth and Planetary Sciences, Faculty of Science, Kyushu University,
Hakozaki Fukuoka 812

Akira Yamori, and Nobuki Kawashima

The Institute of Space and Astronautical Science, Yoshinodai, Sagamihara, Kanagawa
229

Wide varieties of studies on C₆₀ molecule, buckminsterfullerene have been done after Kroto's report¹⁾ that a closed, hollow, spheroidal, carbon cage structure with the symmetry of a European football can readily explain the remarkable stability observed for the C₆₀ molecule. The findings of practical preparation methods²⁾ of the molecule have prompted a large number of chemical studies on the C₆₀ molecule and its derivatives.

Most important is the discovery that C₆₀ appears to form spontaneously, and this has particularly important implications for particle formation in combustion and in space as well as for the chemistry of polyaromatic compounds (Kroto). The fullerene may have been synthesized in space. However, no report has shown the presence of the C₆₀ fullerene in meteorites. Shock on accretion of parent body of meteorites or irradiation of ultraviolet and cosmic rays might destroy the molecule. Therefore, we examined the structural alteration of C_{60/70} fullerene on shock, and compared the product with the carbonaceous matter in carbonaceous chondrites.

Tightly packed commercial C_{60/70} fullerene (Mer Corporation, U.S.A.) in a steel capsule having a copper seal was set up as a target of a high-speed rail-gun system of the institute of space and astronautical science. A polycarbonate projectile with velocity of ca. 7 km/sec hit the capsule to make a Carter in target face. The carbonaceous matter in the steel capsule was taken out by careful shaving of the vessel. The products were examined by HPLC and microscopic FT-IR³⁾.

Although the C_{60/70} fullerene is soluble in benzene, most of the products are insoluble in that solvent. The HPLC examination of the soluble part of the products using an ODS as a column and hexane as an effluent indicated the presence of the very small amount of the starting material (Fig. 1). Figure 2 indicates IR spectra of (a) the commercial C_{60/70}, (b) the products, and (c) the kerogen-like organic matter in Murchison. The spectra indicate that the molecular structure completely changed by the shock. Although the IR feature of the products is similar to that of kerogen-like organic

matters in carbonaceous chondrites,³⁾ the relative intensity of the peaks is apparently different. This fact may be interpreted by the similarity of chemical structure and difference of molecular size. The molecular size derived from fullerene is smaller than that of meteoritic kerogen-like organic matters.

References

- [1] H. Kroto (1988), *Science*, **242**, 1139.
 [2] W. Kratschmer, L.D.Lamb, K.Fostiropoulos, and D. R. Huffman (1990), *Nature*, **347**, 354.
 [3] T. Murae (1994), *Proc. NIPR Symp. Antarct. Meteorites*, **7**, 262.

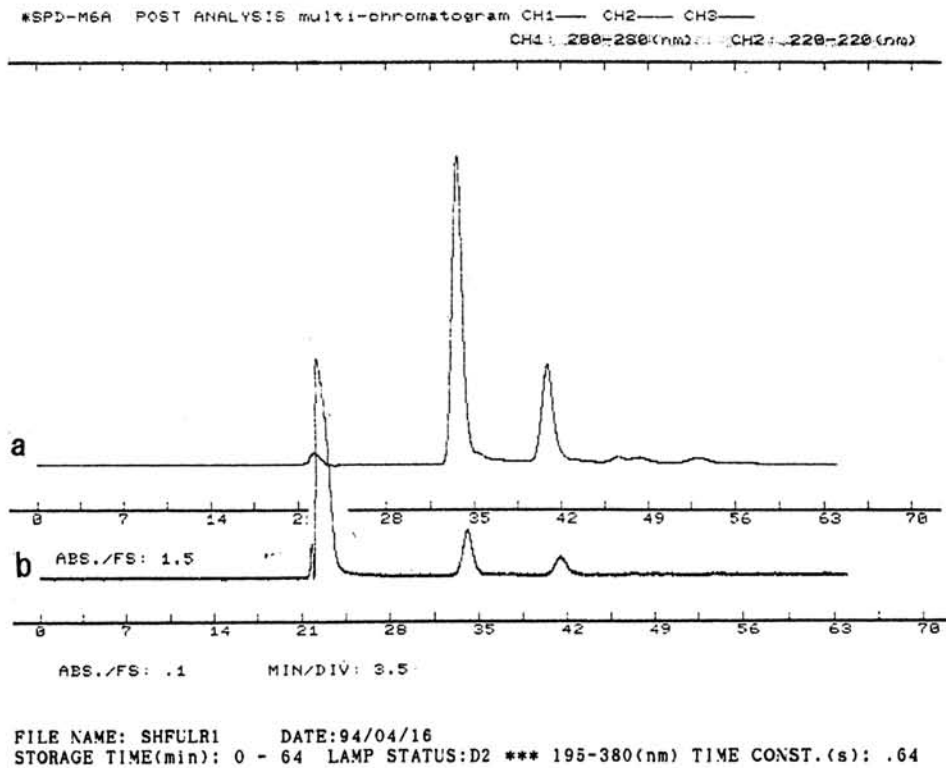


Fig. 1. HPLC chromatograms of (a) commercial C_{60/70} fullerene (absorption/full scale: 1.5) and (b) benzene soluble part of the products yielded on the shock experiment (absorption/full scale: 0.1)

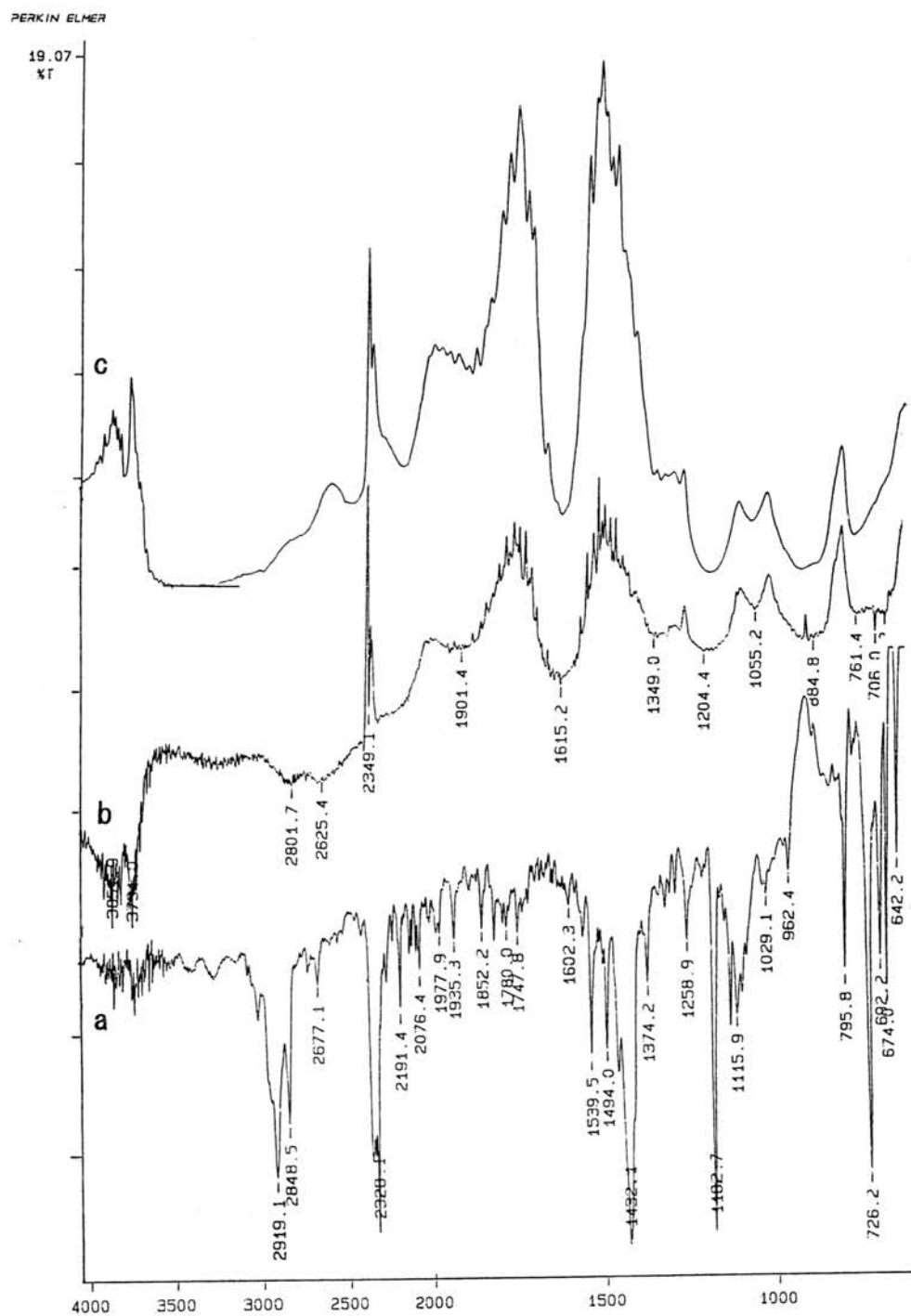


Fig. 2. FT-IR spectra of (a) commercial $C_{60/70}$ fullerene, (b) the shock products, and (c) the kerogen-like organic matter in Murchison.

A FELDSPAR-NEPHELINE ACHONDRITE CLAST IN PARNALLEE WITH POSSIBLE LINKS TO UREILITES. J.C. Bridges¹, I.A. Franchi², R. Hutchison¹, C. M. O'D. Alexander³, C.T. Pillinger²

¹ Department of Mineralogy, Natural History Museum, Cromwell Road, London SW7 5BD, UK. ² Department of Earth Sciences, Open University, Milton Keynes MK7 6AA, UK. ³ McDonnell Center for the Space Sciences, Washington University, St Louis, MO 63130, USA.

Introduction

Ordinary chondrites are known to contain exotic xenoliths or clasts. Mixing of material from different iron groups in ordinary chondrites is well documented on the evidence of oxygen isotopes [1] and a carbonaceous chondrite xenolith has also been located in Plainview H5 [2]. A micro-gabbro clast in Parnallee is believed to be a product of planetary differentiation [3]. Here we report on the finding of a feldspar-nepheline clast (FELINE) in Parnallee (LL3.6) which appears to be achondritic in origin.

Feldspar-nepheline clast (FELINE)

FELINE is a 3mm diameter subrounded feldspar-nepheline clast (Fig. 1). The clast is 88 modal% plagioclase and 12 modal% nepheline. Nepheline is located towards the margin of the sample (Fig. 2). There is no mesostasis and the only other minor phase identified is troilite which is found as veins in a fractured area. FELINE has undergone post-accretion fracturing in the Parnallee parent body. Prior to this late event the plagioclase appears to have consisted of only a few individual grains. The clast does not have any chondrule-like fine-grained outer rim and may be a fragment of a larger body.

Mineral compositions and REE abundances

Plagioclase is An₇₅₋₈₇, Ab₂₅₋₁₃ (Table 1). Nepheline contains from 0.24-3.12wt% Cl. The bulk composition of FELINE (Table 1) has been calculated using the average compositions of the plagioclase and nepheline. This mildly alkaline composition (close to that of the plagioclase) is distinct from Al-rich chondrules [4], having lower MgO and FeO contents. It is also too Na₂O- and Cl-rich for CAI-like compositions.

Trace and REE element contents have been measured using a Cameca IMS 3f ion microprobe (Fig. 3). The plagioclase has a negative chondrite-normalised slope with a pronounced positive Eu anomaly. Such a REE signature is characteristic of crystallisation from melts and is consistent with an igneous origin for FELINE.

Oxygen isotopes

The oxygen isotope composition of FELINE is $\delta^{17}\text{O}$ 4.5, $\delta^{18}\text{O}$ 8.9. FELINE lies away from the ordinary chondrite field on the three isotope plot (Fig. 4) showing its exotic origin relative to most of the chondrules and clasts in Parnallee. It plots just below the intersection of the Carbonaceous Chondrite Anhydrous Minerals Line (CCAM) with the terrestrial fractionation line (TFL). Notably the ureilite group of achondrites [5] also plot along CCAM. FELINE lies on an extension of the currently known ureilite field. A plagioclase-rich clast from the Nilpena ureilite breccia [5] lies within the ureilite field (Fig. 4).

Possible links with ureilites

The genesis of ureilites is still under considerable discussion with both igneous models requiring extensive planetary differentiation or primitive models involving relatively limited reworking and melting of primitive precursors [6, 7]. It is clear that the ureilites are derived from carbonaceous chondrite-like material because of their position near CCAM on the oxygen three isotope plot [5]. Another factor common to all models of ureilite genesis is the requirement for the loss of a Ca-, Al-rich, basaltic melt as the meteorites are predominantly composed of olivine and pigeonite [6]. Plagioclase-rich clasts in ureilite breccias have been identified [5, 8] and may be the products of this lost fraction. FELINE might also be a product of the missing Ca-, Al-rich melt though nepheline has not been reported in the ureilite breccias.

Conclusions

The mildly alkaline bulk composition and fractionated REE profile of FELINE suggests that it crystallised from a differentiated planetary melt. The oxygen isotopic signature provides a possible link with ureilites and FELINE could be part of the missing Ca-Al-rich fraction from that group of meteorites. It is however, markedly less ^{16}O -rich than a plagioclase-rich clast from a ureilite breccia (Nilpena) so this link remains tentative. Whether FELINE is related to ureilite genesis or not, it provides strong evidence that achondritic planetary differentiate clasts are one of the components in ordinary chondrites such as Parnallee.

References

- [1] Clayton R.N., Mayeda T.K., Goswami J.N. and Olsen E.J. (1991) *GCA* **55**, 2317-2337. [2] Wilkening L.L. and Clayton R.N. (1974) *GCA* **38**, 937-945. [3] Kennedy A.K., Hutchison R., Hutcheon I.D. and Agrell S.O. (1992) *EPSL* **113**, 191-205. [4] Biscoff A. and Keil K. (1984) *GCA* **48**, 693-709. [5] Clayton R.N. and Mayeda, T.K. (1988) *GCA* **52**, 1313-1318. [6] Goodrich C.A. (1992) *Meteoritics* **27**, 327-352. [7] Takeda H., Mori H. and Ogata H. (1988) *Proc. NIPR Symp. Antarct. Meteorites* **1**, 145-172. [8] Prinz M., Weisberg M.K. and Nehru C.E. (1988) *LPS* **19**, 947-948.

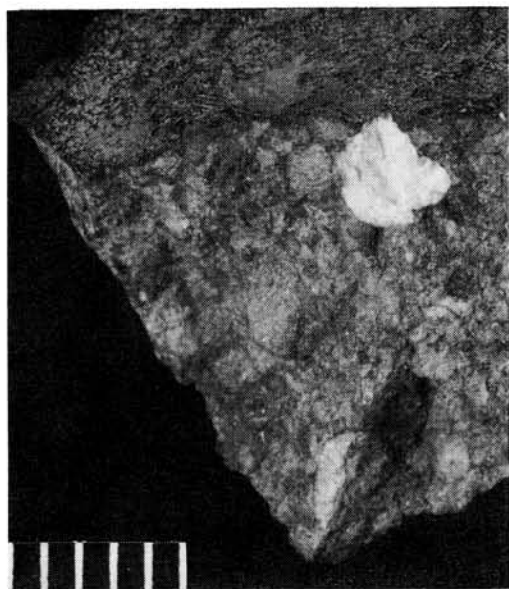


Fig. 1 FELINE on broken Parnallee surface, mm scale

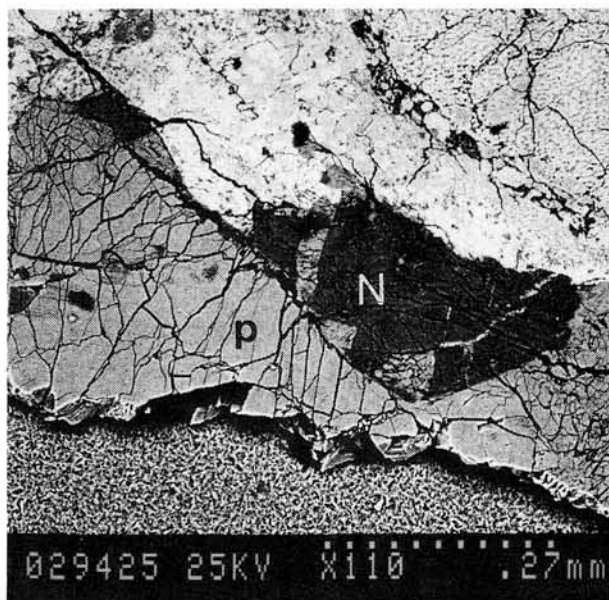


Fig. 2 Back scattered electron image of FELINE
P plagioclase, N nepheline

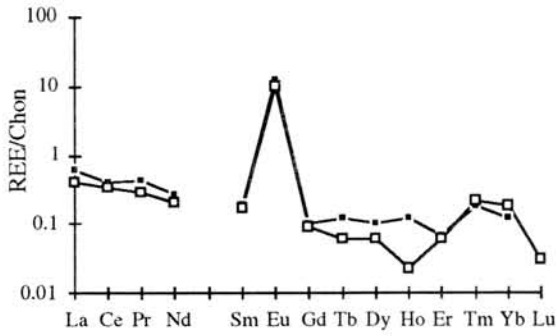


Fig. 3 Plagioclase REE

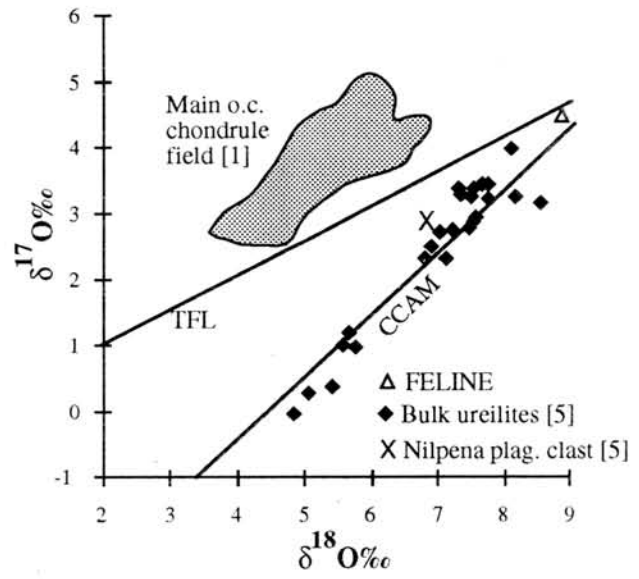


Fig. 4 Oxygen isotope plot

	SiO ₂	Al ₂ O ₃	TiO ₂	FeO	K ₂ O	CaO	Na ₂ O	Cl	Total	%An	%Ab	%Or
Plagioclase	45.71	33.33	0.05	0.11		17.66	1.67		98.52	0.85	0.15	0.00
	45.14	33.26	0.01	0.08	0.02	17.81	1.43	0.01	97.76	0.87	0.13	0.00
Average	45.06	32.97	0.03	0.06	0.01	17.48	1.61	0.02	97.23	0.85	0.15	0.00
Nepheline	44.56	33.43	0.04	0.18	0.01	0.24	21.00	0.27	99.73			
	44.92	33.63	0.03	0.20	0.05	1.29	19.47	0.24	99.83			
Average	45.57	34.60	0.02	0.11	0.44	0.66	16.90	1.64	99.95			
Bulk	45.12	33.17	0.03	0.06	0.06	15.38	3.52	0.22	97.57			

Table 1 Mineral and Bulk compositions. Analyses performed at 20kV on Cameca SX50.

KINETICS AND GRAIN GROWTH MECHANISM FOR TROILITE FORMATION ON IRON METAL IN H₂-H₂S GAS MIXTURES, D. S. Lauretta¹ and B. Fegley, Jr.^{1,2} (1) Dept. of Earth & Planetary Sciences, and (2) McDonnell Center for the Space Sciences, Washington University, St. Louis, MO 63130-4899 USA.

Introduction. Troilite formation via the net thermochemical reaction $\text{Fe(s)} + \text{H}_2\text{S(g)} = \text{FeS(s)} + \text{H}_2\text{(g)}$ is the major mechanism by which sulfur was retained in solid material in the solar nebula. Thermodynamic calculations predict that troilite is the only iron sulfide phase to condense from a solar composition gas [1-3]. However, to date the kinetics and growth mechanism of iron sulfide formation have only been studied by materials scientists working at pressure, temperature, and composition conditions that are not relevant to the solar nebula. The study of this reaction is important for understanding FeS accretion by the terrestrial planets, the origin of troilite in meteorites, and gas-grain chemistry in protostellar accretion disks. Here we present the results of an experimental study on the kinetics and growth of troilite crystals on iron metal at temperature and composition conditions similar to those accepted for the solar nebula.

Experimental Methods. Troilite formation was studied by suspending iron foil (Johnson Mathey Puratronic grade, 99.9975%), of known weight and surface area in a Deltech vertical tube furnace. The samples were first annealed in a stream of pure hydrogen gas at high temperature (750 °C). The samples were then cooled to the temperature of interest while still in hydrogen gas. When the desired temperature was reached the furnace was flooded with a hydrogen sulfide-hydrogen gas mixture of known concentration (50, 100 or 1000 ppm H₂S) and samples were reacted for a specific time period. Standard techniques were used to control gas flow rates and temperature. At the end of the reaction the samples were rapidly quenched, removed from the furnace and weighed. The composition of the newly formed layer was verified by X-ray diffraction. The samples were then cross-sectioned and polished and the thickness of the unreacted iron was measured with an optical microscope. Both the weight change and the thickness change of the sample were used to analyze the kinetic behavior of the system.

Results. Figure 1 plots the fraction of iron reacted (based on weight gain due to formation of stoichiometric FeS) vs. the time of reaction for the four isotherms (450, 505, 575 and 650 °C) studied to date. It can be seen from this graph that the weight change per unit area for the lower isotherms varies as the square root of time while the rate along the 650 °C isotherm varies

linearly with time. The growth behavior along the lower isotherms is consistent with a diffusion controlled reaction. This behavior was also noted by previous investigators though [4] suggests sulfide diffusion to the metal-sulfide interface and [5] suggests Fe^{2+} diffusion to the sulfide-gas interface. The behavior of the highest isotherm cannot readily be explained by any single rate limiting mechanism, though it appears to be an interface controlled reaction. The change in the thickness of the unreacted iron vs. time is shown in Figure 2. In both Figure 1 and Figure 2 it can be seen that the growth along the 650 °C isotherm is initially slower than that of the lower temperature ones but for extended time periods the reaction rate for the higher isotherm overtakes that of the lower ones.

Reacted Samples. Figure 3 shows several photomicrographs of the polished cross sections of samples reacted at 575 and 650 °C. Figure 3a-c are samples reacted at 575 °C for 10 hours (3a), 35 hours (3b) and 96 hours (3c). Figures 3d-f are samples reacted at 650 °C. The sample in Figure 3d reacted for 10 hours, 3e for 45 hours and 3f for 96 hours. The reacted layer in Figure 3a consists of intergrowths of troilite (identified by XRD and electron microprobe) into the pure iron metal. The layer also contains a large amount of pore space that extends into the unreacted iron. Figure 3d shows the equivalent sample for 650 °C. The structure of the reacted layer is similar to that of the layer in Figure 3a with several notable exceptions. First, the layer is less than 1/3 the thickness of the layer formed at 575 °C. Also, there is a layer of pure troilite crystals beginning to form at the very top of the intergrowth layer. The differences between these two samples suggest that the nucleation rate is slower at 650 °C than at 575 °C. This is consistent with the initially slower growth observed for the 650 °C isotherm in Figures 1 and 2.

In Figure 3b the intergrowth layer is no longer present. Instead, there are two layers of troilite crystals. The first one is in contact with the iron metal and consists of small randomly oriented crystals with a large amount of open pore space between them. The outermost layer of the sample contains relatively large crystals that appear to be oriented in the same direction to each other. Similar observations were reported by materials scientists studying sulfide scale formation on iron alloys [4,5]. It was suggested in [4] that the second layer is a recrystallization product formed at the expense of the first layer, which is a remnant of the intergrowth layer that formed in the early stages of the reaction.

The time scales for the formation of these different layers varies with the temperature of the reaction. For the 650 °C isotherm the start of the recrystallization and grain growth process for the second layer can be seen as early as 10 hours into the reaction. The intergrowth layer for this isotherm is very narrow especially when compared to the equivalent time step for the 575 °C isotherm (see Figures). It appears that the nucleation of the iron sulfide phase is slower at higher temperatures but that once nucleation has taken place the rate of crystal growth increases with temperature. As these crystals form the reaction speeds up and the rate for the highest isotherm overtakes the rate of the lower one.

Summary and Implications. Our results clearly show that the formation of troilite crystals is a rapid process forming measurable growth layers on the order of hours. However, the growth of the crystals is a complicated process. The initial nucleation of the troilite appears to be inhibited at higher temperatures. Once the troilite phase has been nucleated the reaction kinetics are entirely controlled by the growth of the crystals at the interface, which is faster at higher temperatures.

Acknowledgments. This work was supported by a grant from the NASA Origins of Solar Systems Program to Washington University (B. Fegley, Jr., P.I.). We acknowledge advice from K. Lodders and K. Kelton and technical assistance from D. Kremser and R. Poli.

Figure 1.

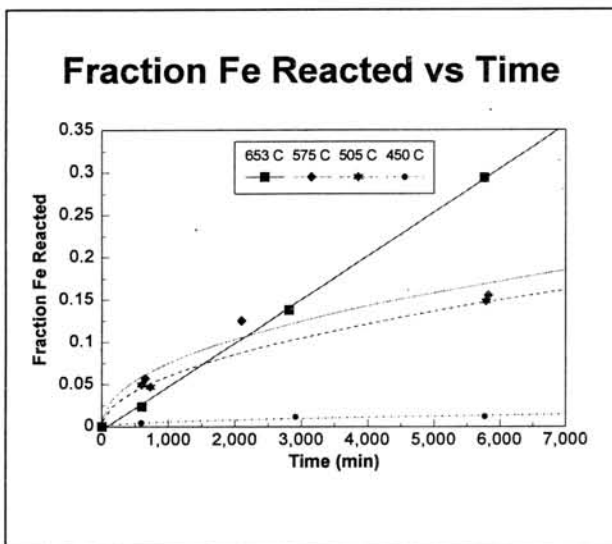
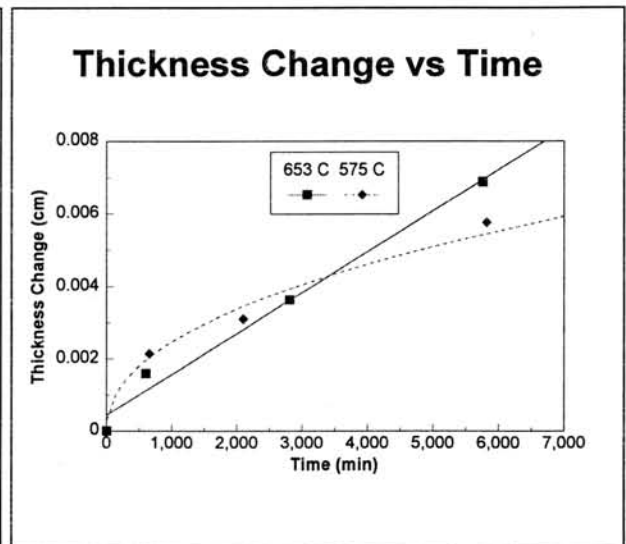
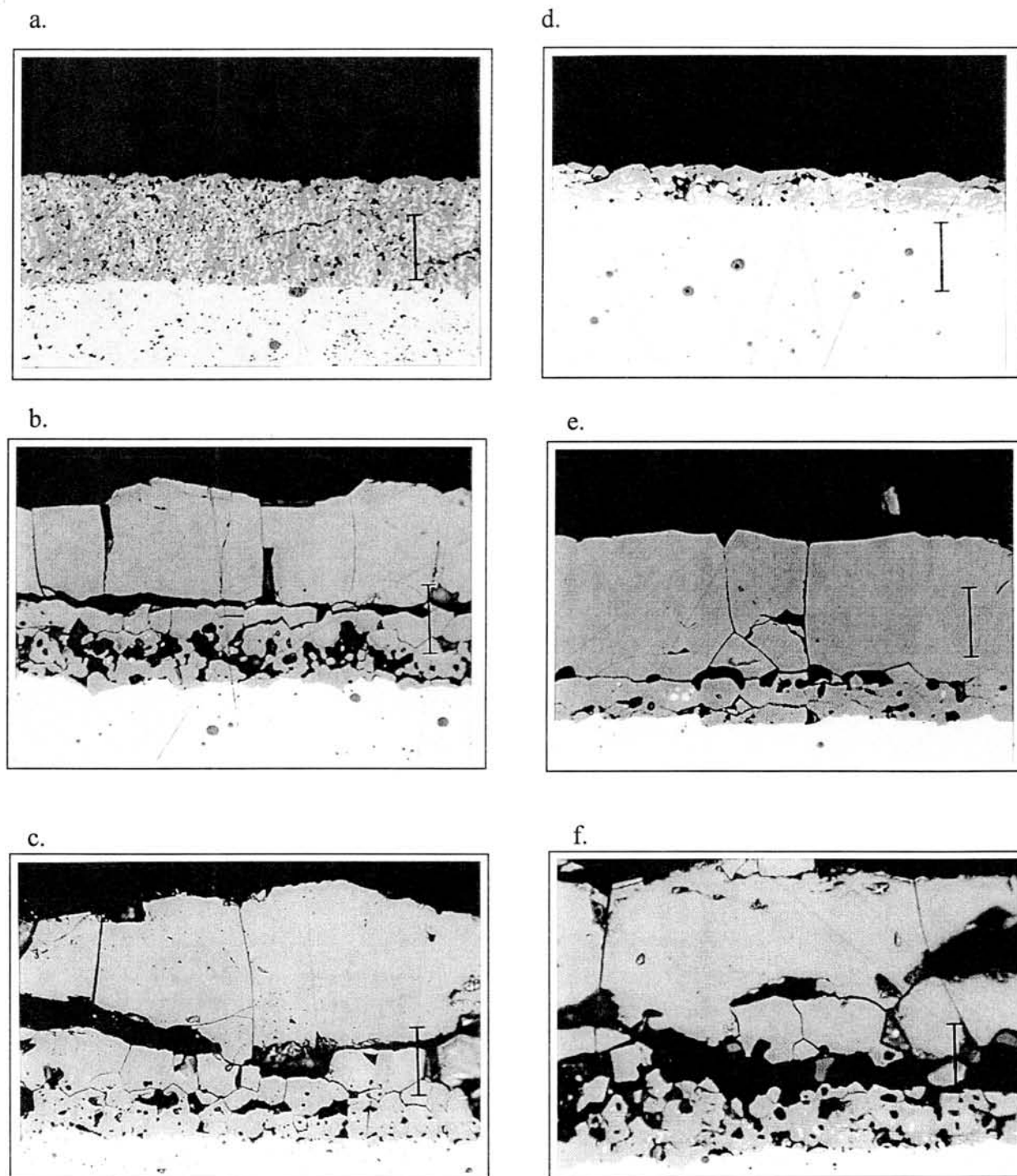


Figure 2.



References. [1] J.S. Lewis 1972 *Earth Planet. Sci. Lett.* **15**, 286-290; [2] J.W. Larimer 1967 *Geochim. Cosmochim. Acta* **31**, 1215-1238; [3] D. Lauretta and B. Fegley Jr. 1994, *Lunar Planet. Sci.* **XXV**, 773-774; [4] E. W. Haycock 1959 *J. Electrochem. Soc.* **106**, 764-771; [5] W. L. Worrel and E. T. Turkdogan 1968 *Trans. Metal. Soc. of AIME* **242**, 1673-1678.

Figure 3: Reacted Samples: a,b,d, and e are at 80x magnification, scale bar = 20 microns. c and f are at 50x magnification, scale bar = 32 microns.



Troilite formation reaction between metallic grain and S-rich gas in chondrites

Naoya Imae and Masao Kitamura

Department of Geology and Mineralogy, Kyoto University, Kyoto 606, JAPAN.

Troilite has been found with various paragenesis in chondrites: chondrule rim, metal-troilite eutectic texture, troilite-rich fragment, and troilite rim around metallic grain. Mastunami (1985) reported that troilite rim around metallic grain in ALH-764 has been interpreted to be formed by the reaction between metal and sulfur gas, and he also discussed the cooling conditions of the gas. In the present study, we found the characteristic texture in the troilite rims, which gives clear evidence of the solid-gas reaction. Furthermore, we estimated the cooling conditions of the gas from the thickness of the rims using properly the reaction rates of the solid and gas, while Mastunami (1985) estimated those by ~~possible~~ ^{forced} assumptions.

Lots of troilite rims surrounding metallic grains were ~~observed~~ ^{forced} in Y-79019 (LL, fine grained fragment), ALH-764 (LL3) and Y-791717 (CO3). The thicknesses of the troilite rim measured under an scanning electron microscope are about a few μm - a few tens μm in Y-790519, a few μm - one hundred and a few tens μm in ALH-764, and a few tens μm in Y-791717 (Fig. 1). In ALH-764 and Y-791717, fractures which divide troilite rims into inner and outer layers were often found (Fig. 1a). In the field of metallurgy, this type of the fractures has been considered to be formed by the difference of the growth mechanism due to the growth stress of the rim, when the sulfide formation reaction between metal and sulfur gas happens. Therefore, the texture in these chondrites must have been formed by the solid and gas reaction.

Troilite in the present case appears as rims of metallic grains. Based on the texture, the troilite formation reaction in the chondrites is assumed to have not completed and sulfur have left in the gas phase in chondrite formation. This means that the rim was formed as pyrrhotite by the reaction and then changed the composition to troilite by equilibration with metallic iron after the reaction. Therefore the thickness of troilite can be an indicator to know the cooling conditions in chondrite formation when the rate constant to form sulfide k can be known.

We assume that the relative abundance of iron and sulfur in the chondrite formation is the same as the solar abundance. The formation rate of iron-sulfide in the solar nebula condition has been derived by Imae et al. (1993) making use of the corrosion rate of metallic iron with H_2S gas. From the treatment, the rate k can be expressed as a function of $A(\text{S})/A(\text{H})$ and T ,

$$k = \frac{A(\text{S})}{A(\text{H})} 843.33 \exp(-32438.4 / RT)$$

where $A(S)$ and $A(H)$ are an elemental abundance of sulfur and hydrogen, respectively, and T temperature. The thickness of troilite in the cooling nebula is given as a function of the cooling time scale by

$$d = \sqrt{\frac{k(T_e)RT_e\tau}{32438.43}},$$

where T_e is the reaction starting temperature, R gas constant, 1.987 cal/mol K and τ cooling time scale of the gas. On the other hand, the relation between T_e and $A(S)/A(H)$ is given by

$$\frac{A(S)}{A(H)} = 10^{0.4-3610/T_e}$$

Therefore, d is only a function of T_e and τ (Fig. 2). Using this relation, the restricted condition of τ and T_e can be obtained when the troilite rim formed by the solid-gas reaction can be found.

When the reaction starting temperature is about 700 K as same as the one of the solar nebula, it is estimated that the cooling time scale is about 10^6 s from the average thickness of troilite. This time is too late compared with the cooling time of chondrule (e. g., Tsuchiyama et al., 1980), which is estimated to be 10^2 - 10^3 s, if it is assumed that the reaction rim is formed at the time of chondrule formation. Then the reaction starting temperature and $A(S)/A(H)$ must be about 900-1000 K and 2×10^{-4} - 6×10^{-4} , respectively, using the time scale. This implies that the formation of chondrules have occurred in such a hydrogen depleted condition with the solar gas.

References:

- Imae N. and Kitamura M. (1993): Proc. of the 25th ISAS Lun. and Planet. Symp., 120-123.
 Mastunami, S. (1985): Grain Formation Work Shop.
 Tsuchiyama, A., Nagahara, H. and Kushiro, I. (1980): Earth and Planet. Sci. Lett., 48, 155-165.

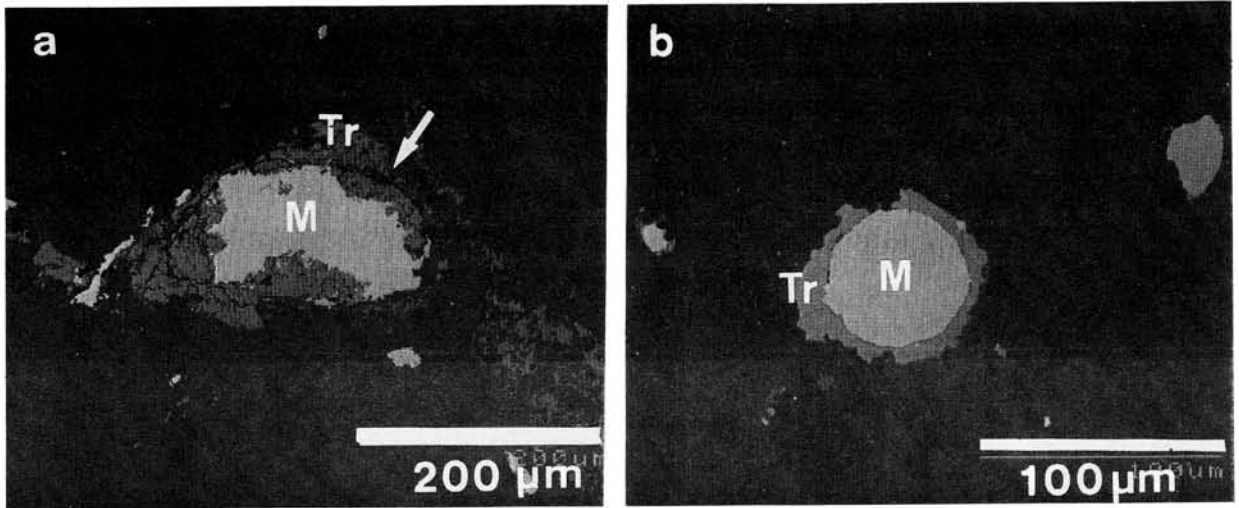


Fig. 1. Troilite rim surrounding metallic grain. Tr=troilite, M=Fe-Ni alloy. (a) ALH-764. The characteristic texture showing solid-gas reaction is indicated by an arrow. (b) Y-790519.

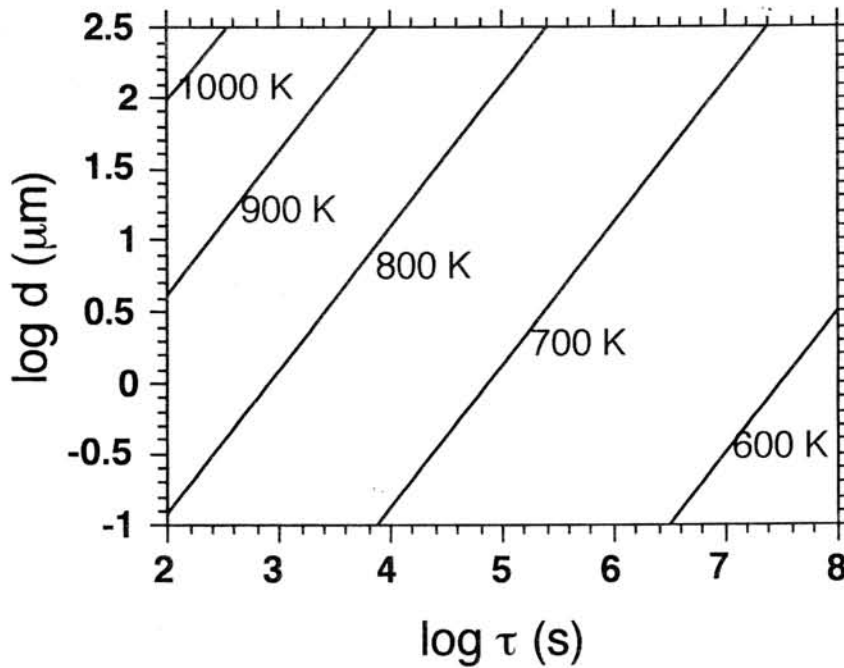


Fig. 2. The relation of the thickness of troilite reaction rim d , cooling time scale τ and reaction starting temperature T_e .

Tuesday, May 31, 1994

0930 - 1615 Symposium, Auditorium

1615 - 1715 Special Lecture (I)

Dr. M. Weisberg

*American Museum Natural History
New York, U.S.A.*

*1730 - 1930 Reception, Lecture Room,
2nd Floor*

Evaporation experiments of metallic iron into vacuum.

TSUCHIYAMA Akira, FUJIMOTO Kiyoshi and UYEDA Chiaki

Department of Earth and Space Science, Osaka University, Toyonaka 560, JAPAN

Introduction. It is considered that evaporation and condensation of minerals occurred in the primary solar nebula were responsible for elemental and isotopic fractionations observed in the planets and meteorites. Especially, in recent cold nebula models, evaporation process is important. In this study, evaporation experiments of metallic iron, one of the important materials forming the terrestrial planets and meteorites, were carried out under vacuum to obtain the evaporation kinetics, such as mode and rates.

Experiments. Plates of polycrystalline metallic iron of 99.99% purity were used in the present experiments. They were cut into platelets (about 0.5 mm thick and about 5 x 9 mm² in surface area), and the surfaces were polished. The samples were heated in an gold image furnace at temperatures ranging from 1075 to 1312°C under vacuum for 0.5 to 96 hrs. The vacuum was obtained by an oil diffusion pump, and the pressure was ranging from 10⁻⁵ to 10⁻⁶ Torr.

Results. Mass loss of an experimental charge by each run per unit area, ΔM , is plotted against time, t (Fig.1). The mass loss is roughly proportional to time at constant temperatures although some scatters are present. The evaporation rates, j , were calculated from the ΔM - t slopes. The evaporation rates shows Arrhenius relation, $\ln j = 9.946 \pm 0.993$ [mol m⁻² sec⁻¹] - 390.6 \pm 29.2 [kJ mol⁻¹] /RT (Fig.2). The surfaces of the charges were observed under an SEM. Networks of grooves were observed on the surfaces irrespective

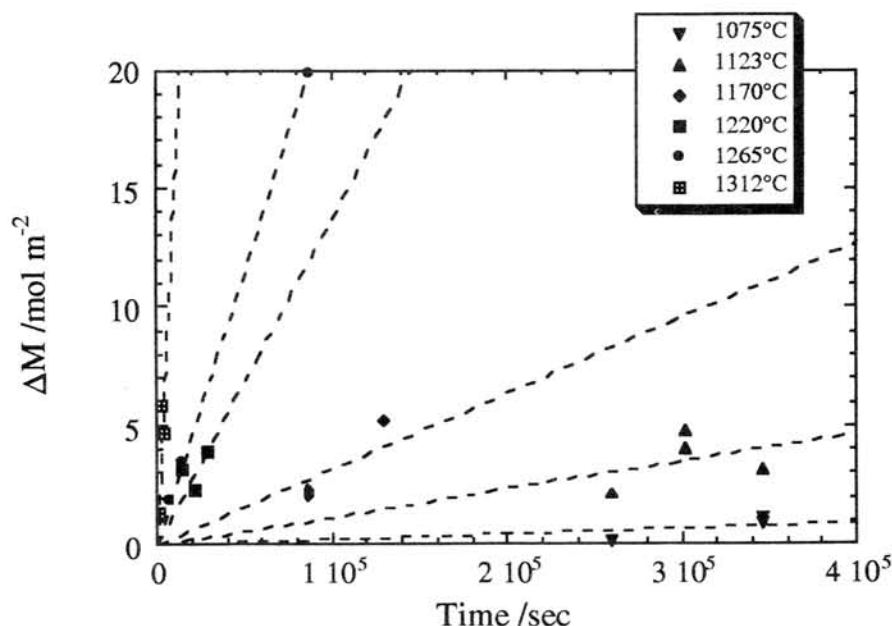


Figure 1. Mass loss of experimental charges per unit area, ΔM , as a function of time by evaporation of metallic iron at different constant temperatures into vacuum. of the temperatures (Fig.3a). These grooves are considered to correspond to grain

boundaries of polycrystalline iron. The size of each single crystal is ranging from a few tens to a few hundreds μm . Evaporation steps were observed in single crystal domains (Fig.3a). Because crystallographic directions are different for different single crystal domains, steps with different spacings and probably different heights were observed. Euhedral crystals of about $10\ \mu\text{m}$ size are always attached to the stepped surfaces. Occasionally, the crystals show a beautiful pyramidal shape, which is the half of octahedron (Fig.3b). These crystals cover the surfaces by up to a few tens % or more. The powder X-ray diffraction pattern showed that they are wüstite. Under the vacuum in the experiments (about 10^{-5} to 10^{-6} Torr), partial pressure of oxygen should be about 10^{-9} atm (3×10^{-9} to 3×10^{-10} atm) if residual gas is assumed to be composed of air. Under the oxygen partial pressure range wüstite and magnetite are stable at high and low temperatures of the experiment, respectively. Accordingly, wüstite was formed by oxidation of metallic iron even under vacuum. Magnetite was not detected.

Discussion. It is shown from the surface observations that the evaporation of metallic iron in the present experiments occurs by forming evaporation steps. It is reasonable to imagine that the evaporation proceeds by going back of the steps which were formed at screw dislocations and grain boundaries [1]. The evaporation rates of metallic iron can be calculated from Hertz-Knudsen equation (e.g., [1]) if we assume that monomolecules of iron are formed by the evaporation;

$$j_{calc} = \frac{\alpha_v P_{Fe}}{\sqrt{2\pi m_{Fe} kT}}, \quad (1)$$

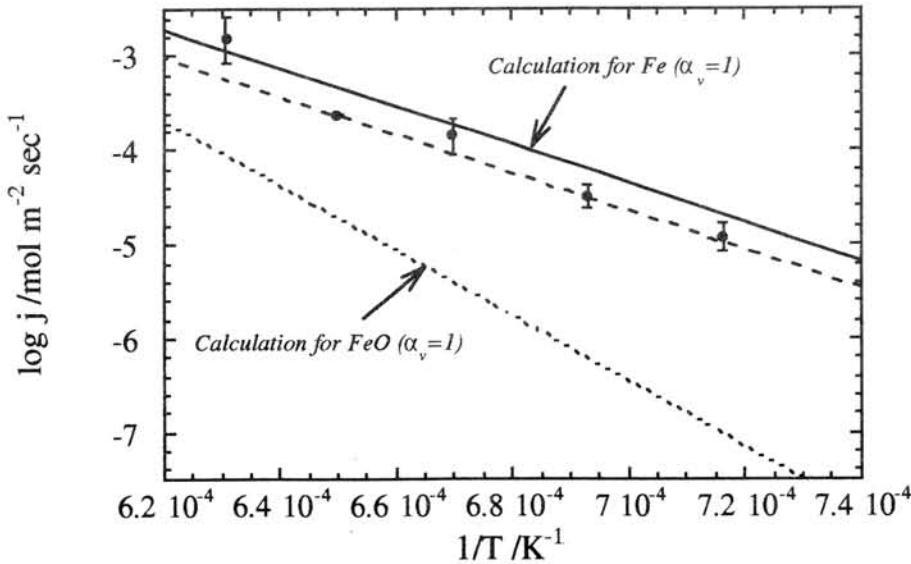


Figure 2. Arrhenius relation of the evaporation rates of metallic iron obtained from the slopes of ΔM - t relation in the experiments. Calculated rate with $\alpha_v = 1$, and that for FeO at oxygen partial pressure of 10^{-9} atm are also shown.

where α_v is the evaporation coefficient, p_{Fe} the equilibrium pressure of Fe gas molecules, m_{Fe} the mass of the molecule, k the Boltzmann constant, and T the temperature. The value of the evaporation coefficient is between zero to unity, depending on the evaporation kinetics. If any kinetic constraint is absent, it becomes unity and becomes the maximum. The evaporation rates were calculated by using thermochemical data [2] for obtaining p_{Fe} . The calculated rates are also shown in Fig.2. The evaporation rates obtained in the present experiments are slightly smaller than the calculated rates, and α_v is about 0.5. However, the presence of the wüstite crystals disturbs the evaporation rates as follows. (1) Based on the evaporation theory with thermochemical data, the calculated evaporation rate of FeO is lower than that of metallic iron by order of one or more (Fig.2), that is, wüstite is more refractory than metallic iron. Accordingly, the evaporation surface of metallic iron was reduced. (2) Effects of wüstite were not considered when the evaporation rates were obtained from the mass loss in the experiments. Both effects, (1) and (2), cause increase of α_v . Therefore, it is concluded that α_v in the present experiments should be close to unity although any quantitative correction for the wüstite effects was not made.

Summary. Metallic iron was evaporated into vacuum by forming evaporation steps. The evaporation coefficient is close to unity if partial oxidation effects to form wüstite were taken into consideration. The present results can be useful for discussing chemical evolution of the primary solar nebula.

References: [1] Hirth and Pound (1963) Condensation and nucleation; nucleation and growth kinetics. Pergamon Press, pp.191. [2] JANAF Thermochemical Tables (1991) 2nd. Ed., pp.141, NBS, USA, NSRDS-NBS37.

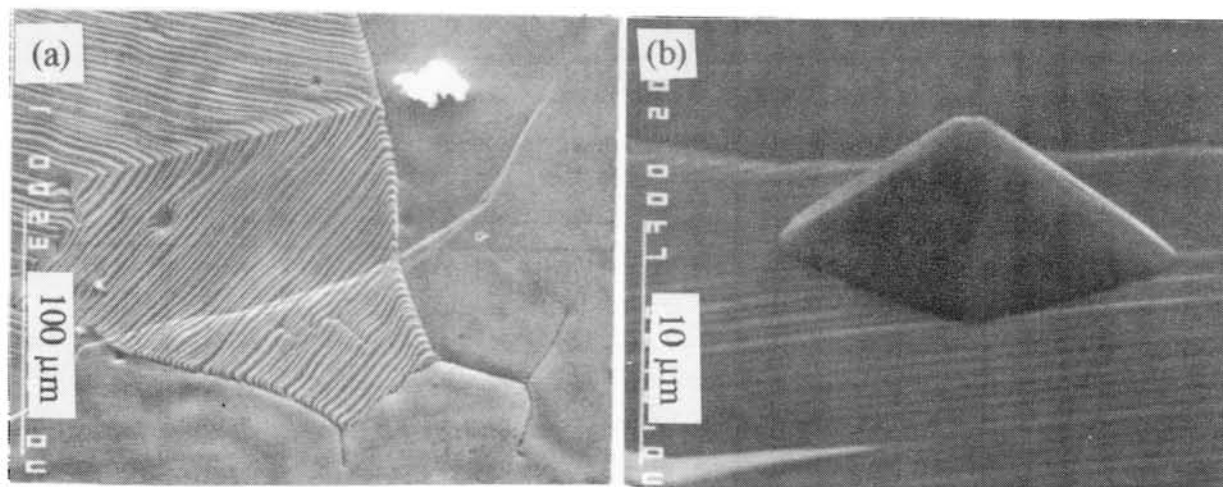


Figure 3. SEM micrographs of the surfaces of run products. (a) Grain boundaries and evaporation steps at 1170°C for 24 hrs. Coarse or fine (sometimes very fine) steps are observed in each single crystal region. (b) A wüstite crystal with a pyramidal shape attached on a stepped surface. The micrograph was taken from an oblique angle.

MAGNESIUM ISOTOPIC FRACTIONATION IN THE OLIVINES FROM ALLENDE CHONDRULES AND ISOLATED GRAINS CAUSED BY EVAPORATION IN THE SOLID STATE: Akinori KOGA and Hiroko NAGAHARA, Geol. Inst., Univ. Tokyo, Hongo, Tokyo 113, Japan.

Koga *et al.* [1] showed that Mg isotopes in some isolated olivines and forsteritic olivines in chondrules from Allende are fractionated to be heavy by 5 to 7 per mil. It was not clear whether the fractionation was formed in the liquid state during chondrule formation or was achieved in the state of solid before chondrule formation. In order to answer this question, vaporization rates of forsterite in various hydrogen gas pressures and elemental diffusion rates of Mg, Si, and O in forsterite and in liquid were compared. If the diffusion rate of an element is larger than evaporation rate of the material, the element can isotopically fractionate where heavy isotope(s) concentrate in the evaporation residue. On the other hand, if the vaporization rate is larger than the diffusion rate, the interior of the material can not isotopically fractionate.

By using the experimentally obtained vaporization rates of forsterite in vacuum and various hydrogen pressures [2], we have compared the vaporization rates and diffusion rates of elements in solid forsterite and silicate liquid in a simple one dimensional semi-infinite slab. The temperature dependence of the forsterite vaporization rate was estimated by using the activation energy of forsterite evaporation rate obtained by Hashimoto [3] for both vacuum and under the presence of hydrogen gas. The data source for elemental diffusion rates in forsterite are Morioka [4] for Mg, Gerald and Jaoul [6] and Ryerson *et al.* [6] for O, and Jaoul *et al.* [7] for Si. The elemental diffusion rates in a liquid with chondrule compositions are not known, and therefore those for basaltic liquid [8] were tentatively used. The diffusion rates can be larger in the presence of hydrogen gas and the elemental diffusion rates in chondrule liquid can be larger than those in basaltic melt because of highly MgO-rich and SiO₂-poor nature of chondrule liquid. These effects were, however, not taken into consideration in the present study.

The results are shown in Fig. 1, where diffusion rates of elements in forsterite and basaltic melt are shown by broken lines and evaporation rate of forsterite by solid lines. As shown in a companion paper [2], vaporization rate of forsterite is not a linear function of P_{H_2} . At pressures below 10^{-6} bar including vacuum, the reaction is governed by evaporation of forsterite into gas which does not have dependence on the gas pressure. At pressures between 10^{-6} bar to 10^{-5} bar, the reaction between solid forsterite and hydrogen on the surface of forsterite controls the reaction rates, which has dependence on hydrogen pressure. At pressures above 10^{-5} bar, the rate tends to become independent of hydrogen pressure because the reaction is limited by the defect density on the surface of forsterite. In spite of the P_{H_2} dependence, the rate of vaporization is confined within two orders of magnitude, which can be shown by the fairly narrow range between two thick lines. At 1700°C, Mg diffusion

distance in forsterite is larger than the evaporation distance at pressures below 10^{-5} bar. In other conditions, diffusion distance of Mg is smaller than the evaporation distance, which means that isotopic fractionation could not take place. Oxygen and silicon isotopes can never fractionate because of much smaller diffusion rates. Because the temperature dependence of evaporation and vaporization is larger than that of diffusion, the conditions where the Mg diffusion distance is larger than the vaporization distance becomes larger at lower temperatures. However in that case, the absolute reaction distance becomes smaller. It will be thus difficult for us to observe the isotopic fractionation in vaporization residue.

The present calculation gives the maximum distance of evaporation. In the experiments, the generated gas is evacuated away and the solid and generated gas never get equilibrium. However, in the solar nebula, the generated gas tended to get equilibrium with residual solid; that is, the evaporation rate should have become smaller with the progress of vaporization.

The elemental diffusion rates in basaltic melt is large compared to those in solid. In the figure, the diffusion rates of elements in basaltic melt is shown [9]. In silicate melts, the difference in diffusion rates among elements is small, which is generally within 1.5 orders of magnitude [10]. These relationships predict that isotopes can fractionate for every element. Previous isotopic studies on chondrules show that there is no significant isotopic fractionation for O and Si in chondrules [11]. If these observations are the case in the scale of micrometers, although there is no systematic SIMS work for the possibilities of isotopic fractionation of Si and O, Mg is the only element that shows isotopic fractionation. The heavy Mg enrichment in chondrule forsterites and isolated olivines in Allende should have thus formed in the solid state before chondrule formation which survived heating during chondrule formation.

References: [1] Koga, A. *et al.* (1994) Abstract paper presented at the 1994 joint meeting of Earth and Planetary Science Societies, [2] Nagahara, H. and Ozawa, K. (1994) this volume, [3] Hashimoto, A. (1990) *Nature* **347**, 53, [4] Morioka, M. (1981) *GCA* **45**, 1573, [5] Gerald, O. and Jaoul, O. (1989) *JGR* **94**, 4119, [6] Rhyerson, F. J. *et al.* (1980) *JGR* **94**, 4105, [7] Jaoul, O. *et al.* (1980) *EPSL* **47**, 391, [8] Dunn, T. (1982) *GCA* **46**, 2293. [9] Watson, E.B. and Baker, D. (1991) in Physical Properties of Magmas, 120-151, Springer-Verlag, [10] Chekhmir, A. S. and Epel'baum (1991) in Diffusion, Atomic Ordering, and Mass Transport, Springer-Verlag.

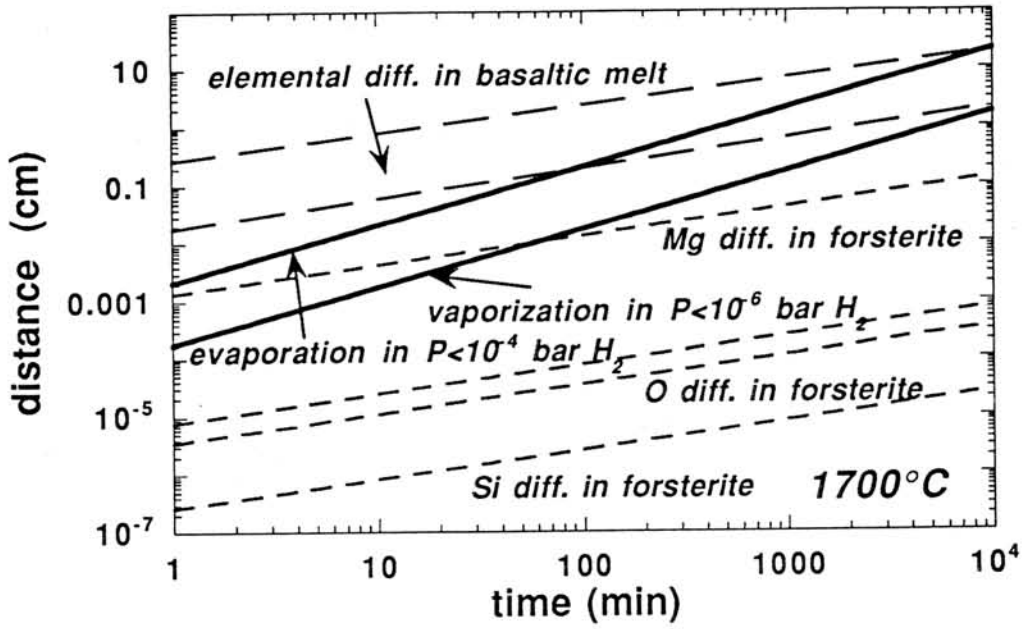


Fig. 1 Comparison of evaporation-vaporization rates and diffusion rates in solid forsterite and basaltic liquid.

KINETICS OF EVAPORATION AND REACTION WITH HYDROGEN OF FORSTERITE

Hiroko NAGAHARA AND Kazuhito OZAWA, Geol. Inst., Univ. Tokyo, Hongo, Tokyo 113, Japan

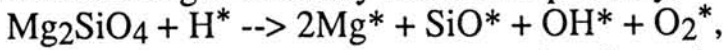
Nagahara et al. [1, 2] experimentally showed that vaporization rate of SiO_2 in a hydrogen gas flow of 10^{-5} bar is larger than that in vacuum by ~ 1 order of magnitude. Contrary to the vaporization rate, the degree of oxygen isotopic fractionation is larger in vacuum than in hydrogen gas. This is because the vaporization rate is larger than the diffusion rate of oxygen in the solid SiO_2 at the experimental conditions, which results in non-fractionated composition at the surface of solid through the vaporization. The results gave an important insight into the isotopic signature of CAIs and chondrules formed in the solar nebula. In order to know the more realistic conditions for chondrule and CAI formation in the solar nebula, vaporization rates of single crystal of forsterite by free evaporation and reaction with hydrogen at various gas pressures was experimentally studied.

The starting material is a single crystal of forsterite made by Takei with the Czochralski pulling technique. About 30 mg of crystal which was cut into a rectangular parallelepiped along the a-axis was used for each experiment. They were kept in a graphite capsule without a lid. Sample weight before and after experiment was precisely measured. Experimental temperature was 1700°C and the hydrogen gas pressure ranged from 10^{-7} to $\sim 10^{-3}$ bar. The pressures above 2×10^{-5} bar are not precise because they were not measured with an ionic gauge attached close to the furnace. The base gas pressure of the vacuum chamber was 10^{-11} - 10^{-9} bar. Experimental duration for each run ranged from 2 min. to 28 hours. Evaporation rate per a unit area and a unit time was obtained by assuming that evaporation took place at a constant rate from every surface.

The results are shown in Fig. 1. The P_{H_2} - J (vaporization flux of the forsterite in $\text{gram}\cdot\text{cm}^{-2}\cdot\text{sec}^{-1}$) relationship can be divided into three ranges. At pressures below 10^{-6} bar, J is independent of P_{H_2} , and the flux is nearly the same as that for the constant evacuation without hydrogen gas. Thus the vaporization of forsterite at low pressures is basically governed by free evaporation.

At pressures between 10^{-6} to 10^{-5} bar, J is a function of P_{H_2} , which suggests that the vaporization is controlled by a reaction of forsterite with hydrogen gas. Since the dependence is power of $\sim 1/2$, the rate-controlling elementary reaction should contain $1/2\text{H}_2$. The vacuum chamber is in the molecular condition at the experimental conditions, and gas reaction may not be so important. Therefore, the critical reaction should take place on the surface of forsterite. The most plausible process is dissociation of hydrogen molecules on

the surface of forsterite when they were adsorbed and that the adsorbed hydrogen atom reacts with a forsterite molecule. At the experimental conditions, most abundant gas species of Mg and Si would be Mg and SiO. If we assume that these species are also dominant ones adsorbed on the crystal surface, then the rate-controlling elementary reaction is possibly,



where asterisk indicates atoms or molecules adsorbed on the surface of forsterite.

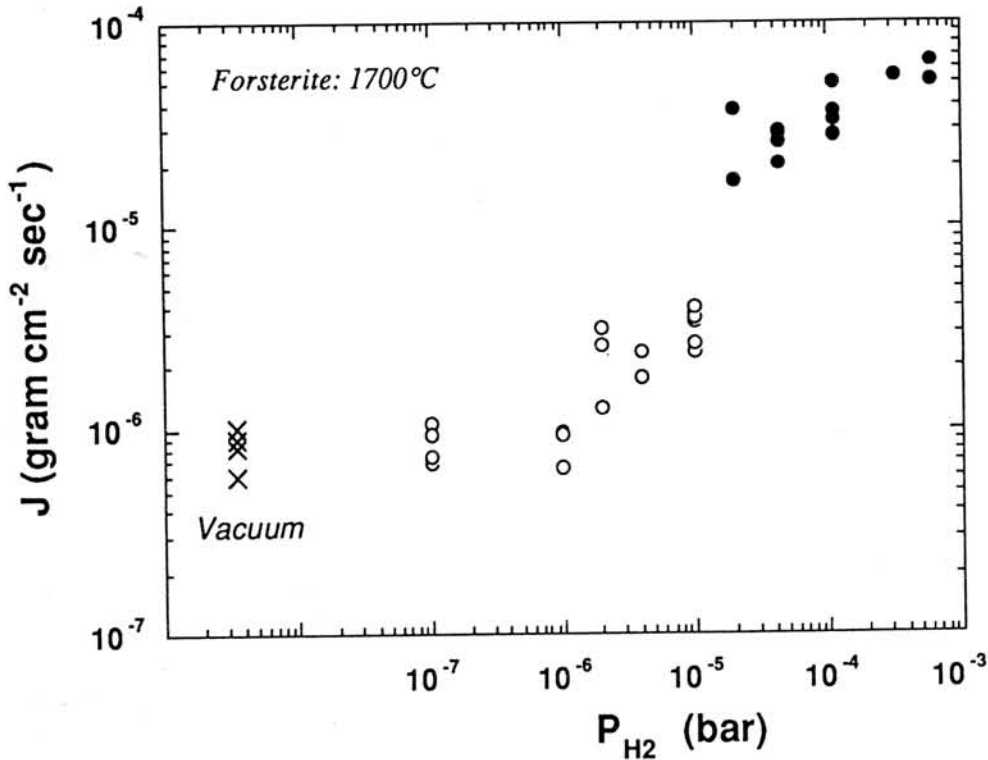


Fig. 1: Vaporization flux of forsterite ($\text{gram cm}^{-2} \text{sec}^{-1}$) plotted against P_{H_2} . Crosses are for evaporation flux in vacuum experiments. Open circles indicate runs for which gas pressure was measured by an ionic gauge attached close to the furnace, and filled circles indicate runs without precise determination of pressure by the gauge. In the latter case, a penning gauge was used to roughly estimate the pressure by extrapolating the calibration with ionic gauge in lower pressures.

At pressures higher than 10^{-5} bar, the dependence of the reaction rate on the hydrogen pressure is much smaller. It suggests that the reaction mechanism is different from that at lower pressures. SEM observation on the surface of the products shows an extremely rough surface morphology, suggesting a possibility that in the higher P_{H_2} conditions the reaction is controlled by the amount of dislocations available.

The results are applied to estimate the upper limit of vaporization time scale of forsterite grains in the solar nebula. The time required for total vaporization of a spherical forsterite with radius of $0.1\mu\text{m}$ to 1cm at 1700°C was calculated. Within the plausible range of hydrogen pressure in the solar nebula, forsterite vaporizes very quickly (Fig. 2). Even a grain with 1mm radius completely vaporizes in a several days at 1700°C . If the activation energy for the reaction is similar to that of evaporation of forsterite determined by Hashimoto [3], the grain completely vaporized in a month at 1600°C . Because the experiments were made in molecular flow of hydrogen gas that is continuously evacuated, the estimated vaporization time gives probably the upper limit.

REFERENCES: [1] Nagahara, H. *et al.* (1993) *Meteoritics* **28**, 406-407, [2] Nagahara, H. (1994) *LPSC XXV*. [3] Hashimoto, A. (1990) *Nature* **347**, 53-55.

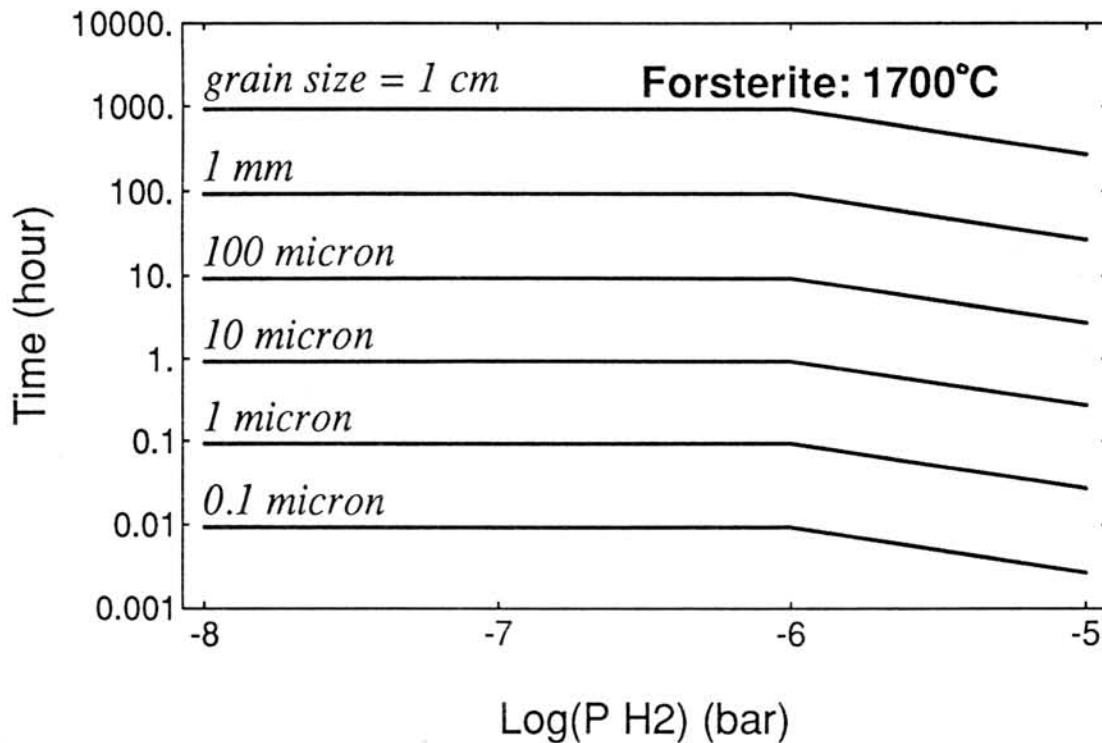


Fig. 2: Time required to completely vaporize a spherical grain of forsterite plotted against logarithm of gas pressure (P_{H_2}) at 1700°C . Because the gas pressure for the experiments under higher pressure is not precise, the vaporization time is estimated only up to $P_{\text{H}_2} = 10^{-5}$.

Heating During Solar Nebula Formation and Mg Isotopic Fractionation in CAI

Sho Sasaki¹, Hiroko Nagahara¹, Kyoko Kitagami^{2,*}, and Yoshi Nakagawa^{2,#}

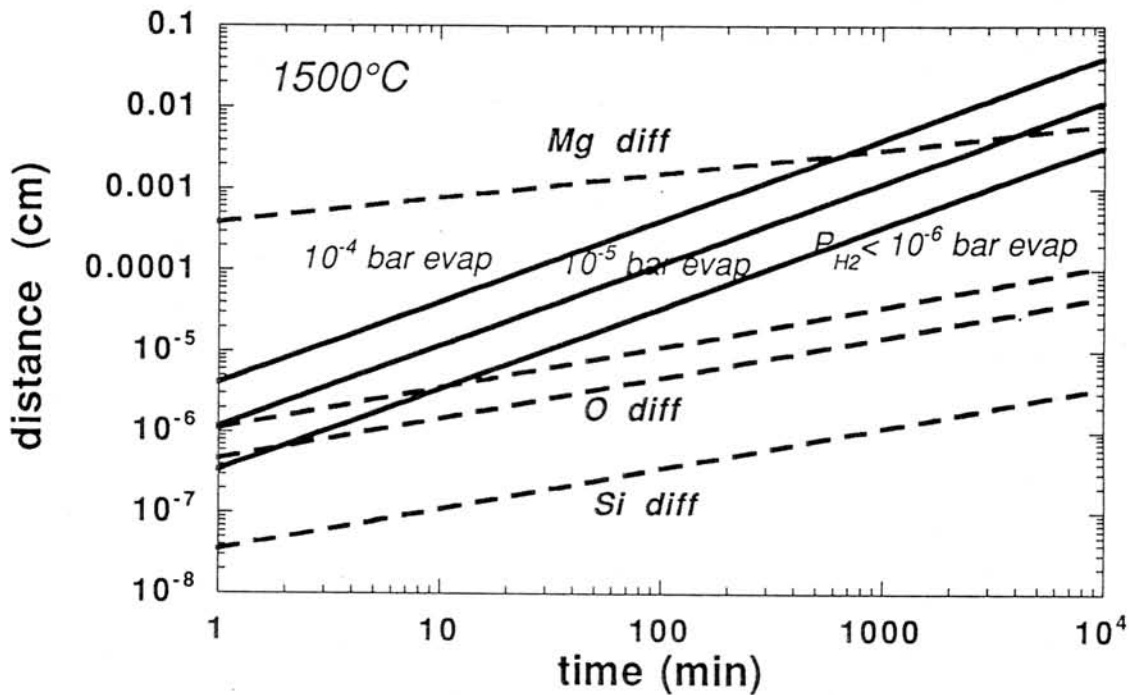
¹Geological Institute, School of Science, Univ. Tokyo, Tokyo 113, JAPAN,

²Dept. Earth and Planetary Physics, School of Science, Univ. Tokyo, Tokyo 113, JAPAN, *Now at Dept. Earth and Planetary Sci., Tokyo Inst. Technology, Tokyo 152, JAPAN, #Now at Dept. Earth and Planetary Sci., Kobe Univ., Kobe 657, JAPAN

Mass-dependent isotopic fractionations of most abundant rock-forming elements Mg, Si, O are observed in CAIs. Of these, magnitudes of Mg and Si isotopic fractionations are much larger than those by igneous processes and they are ascribed to cosmochemical processes such as evaporation and condensation (Clayton et al., 1985). However, environment (P - T condition) of isotopic fractionation has not been discussed in detail.

Nagahara (1994) conducted evaporation experiments of forsterite (Mg_2SiO_3) at various P_{H_2} conditions. Similar to the previous experiments of SiO_2 evaporation (Nagahara et al. (1993)), the evaporation at $P_{\text{H}_2} > 10^{-5}$ bar proceeds much faster than at $P_{\text{H}_2} < 10^{-6}$ bar. Reducing reaction by H_2 at the surface should tantalizingly promote the evaporation at high P_{H_2} environment.

Figure shows comparison between evaporation rate and diffusion rate of Mg, Si, O in forsterite in terms of typical distance d . In this figure, these rates are calculated assuming that temperature is 1500K. Remember that $d \propto t^{1/2}$ in diffusion and $d \propto t^1$ in evaporation. When the diffusion distance is compatible or slightly higher than the evaporation distance, significant isotopic fractionation (enrichment of heavier isotopes) in evaporation residues is expected. At nearly vacuum condition ($P_{\text{H}_2} < 10^{-6}$ bar), much longer duration (or slower rate of temperature change) is sufficient and rather rapid process is unnecessary for the isotopic fractionation. At higher P_{H_2} , the evaporation rate tends to be higher than Mg diffusion rate; Mg isotopic fractionation would not take place. Typical midplane pressure of the solar nebula at the asteroidal zone is higher than 10^{-6} bar when $T = 1000\text{K}$. Evaporative fractionation of Mg isotopes should require rather thin (low-pressure) environment.



Kitagami (1994) numerically simulated the formation stage of the solar nebula following gravitational collapse of a cloud core, solving vertical gas motion and radiative transfer precisely. According to vertical (z) component of solar gravity, gas should contract toward the disk's midplane, forming a shock wave at off-disk region. Position of the shock front depends on the initial density distribution: typically at the asteroidal zone (a (heliocentric distance) = 2.8AU) the shock is first formed around $z = 0.05$ AU, compressed to be about 0.01 AU, then rapidly expand to be about 0.2-0.8 AU.

Much heat is released at and around the shock and radiated both inward and outward. When the initial density distribution is flattened ($z_0 > a$: z_0 being the position where gas density is 1/4 of the midplane density), the midplane region between shocks is heated not only by radiation from shock but also by continuous compression. Temperature is enhanced up to 1700 K at $a = 2.8$ AU. On the other hand, when the initial density distribution is concentrated ($z_0 = 0.1a$), the shock should rebound, expanding the inner zone and suppressing its temperature. The midplane zone is finally heated up by radiation from the shock. The peak temperature, although lower than that of flattened density case, is still as high as 1000 K at 2.8 AU.

Because the generated heat is also propagated outward by radiation, high temperature can be realized in low-density off-disk region. Typical gas density there is as low as 3×10^{-9} - 10^{-8} bar, which is much lower than that of

expected mid-plane density at the asteroidal zone of the solar nebula. At this low pressure environment, evaporation rate should be slow.

We find that the extent of heating depends on heliocentric distance and the assumed initial vertical distribution of gas density. In a simple approximation, the equilibrium temperature can be written by

$$T \approx \left(\frac{GM_{\odot} \dot{\Sigma}}{a \sigma_{SB}} \frac{3\kappa \Sigma_s}{8} \right)^{\frac{1}{4}}$$

where G is the gravitational constant, M_{\odot} is the solar mass, σ_{SB} is Stefan-Boltzmann constant, κ is opacity, $\Sigma_s (= 2 \int_z^{\infty} \rho dz)$ is column density, and $\dot{\Sigma}$ denotes mass accretion rate. If we use $\Sigma \propto a^{-3/2}$ from the solar nebula model and $\dot{\Sigma} \propto \Sigma / t_K \propto a^{-3}$ (t_K being Keplerian period), we have analytic relations $T \propto a^{-11/8}$, $\rho \propto a^{-37/16}$, and $P \propto a^{-59/16}$. These dependencies on a are observed in numerical results. Because of rapid decrease in temperature (T at Jovian region being about half of T at asteroidal region), evaporative fractionation would not take place in the outer region ($a > 4\text{AU}$).

Duration of the peak temperature as well as cooling rate from it can be estimated from numerical results. At the shock front of the asteroidal zone, the duration is about 70days $\sim 10^5$ min. And the initial cooling rate is 100K/(20-50days). This timescale is compatible with the typical time for isotopic fractionation at the vacuum case ($P_{\text{H}_2} < 10^{-6}$ bar) when the temperature is around 1500K.

Mg isotopic fractionation in chondrules is, if exists, much smaller than that in CAI. Here we propose explanations for the difference. One is simply because most chondrules were molten and diffusion in melt is much faster than that in solid. Compared with chondrules, fewer CAI experienced melting. Another explanation is the difference of evaporation temperature: chondrule source materials are evaporated nearly completely when CAI source materials suffers evaporative fractionation, or chondrules source materials are evaporated at later heating event at higher pressure whereas CAI source materials mostly remain solid without evaporation.

Reference

- Clayton, R. N. et al. (1985) in *Protostars and Planets II*, 755-771.
 Kitagami, K. (1994) Master dissertation, Univ. Tokyo.
 Nagahara, H. (1994) in this volume

**Trace elements of Antarctic meteorites
by INAA (I)**

Shigeko Togashi¹, Hikari Kamioka¹, Mitsuru Ebihara², Keizo Yanai³ and
Hideyasu Kojima³

- 1) Geological Survey of Japan, Higashi, 1-1-3, Tsukuba, Ibaraki 305.
2) Tokyo Metropolitan University, Minami-Ohsawa, Hachioji, Tokyo 192-03.
3) National Institute of Polar Research, Kaga 1-9-10, Itabashi, Tokyo 173.

Trace elements in twenty meteorites were determined by instrumental neutron activation analysis to characterize the Antarctic meteorites. The sample powder was magnetically separated into magnetic and nonmagnetic fractions. Small mass of the separates (5-30mg, typically 10mg) were applied for analyses. These procedures would emphasize the differences in chemical compositions of metal phases among different kinds of chemical groups and petrological types.

Samples were irradiated in S-pipe of JRR-4 reactor at Japan Atomic Energy Research Institute for 6 hours with a thermal neutron flux of $5.5 \times 10^{13} \text{cm}^{-2} \text{S}^{-1}$. Chemical standards for Os, Ir and Au and GSJ rock reference sample JB-1 for other elements were irradiated simultaneously with the samples. The abundance of elements was determined with high-purity Ge gamma-ray detector (ORTEC GEM20180) of Geological Survey of Japan (Tanaka et al., 1988).

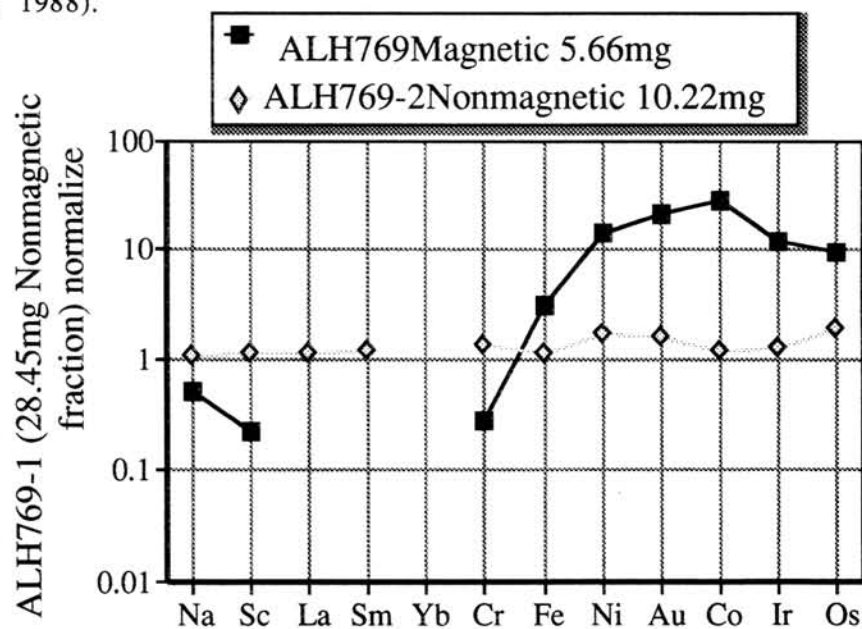


Fig.1. Normalized values to the nonmagnetic fraction of ALH769-1 (28.45mg)

There is a small difference in composition between 28.45 mg (ALH 769-1) and 10.22 mg (ALH769-2) of the nonmagnetic fractions of the powder of ALH769(L6) chondrite (Fig.1). This means that the composition of the nonmagnetic fraction is relatively homogenous even in such a small aliquot from a few g of the sample. On the other hand, the magnetic fraction shows high concentration of siderophile elements. There are small but distinct differences in the relative abundance of siderophile elements between magnetic and nonmagnetic fractions. The magnetic fraction has higher normalized values of Co than those of Ni, Ir and Os. Silicate phases could not contribute to change the relative abundance of siderophiles in bulk samples, because silicate phases have significantly low abundance of siderophiles compared with metal phases. The normalized values for a low concentrator such as silicate phases are hidden by the values of a small amount of contamination of a high concentrator. Therefore, the nonmagnetic fraction should include a small amount of metal phases with high Ir/Co, Os/Co and Ni/Co ratio compared with the magnetic fraction.

The Co-Ir diagram (Fig. 2) indicates that the data of nonmagnetic fractions of analyzed samples are plotted in lower extent of bulk compositions of ordinary chondrites (Kallemeyn et al. 1989). The nonmagnetic fractions of different LL chondrites make a cluster, which is plotted on the lower extent of the array of bulk compositions of ordinary chondrites. Most data of nonmagnetic fraction of L and H chondrite, except for H5 and L3, plotted in the left down side of the array of bulk composition of ordinary chondrites. This fact is consistent with the case of ALH 769 (Fig. 1 and Fig. 3). The data of C-chondrite lie near the array and the mean composition of C1 chondrite (Anders and Grevesse, 1989).

Although further data on chemistry and mineralogy are required, the present data suggest the presence of multiple metal phases that have enough size to be magnetically separated. The behavior of the siderophiles in chondrites is qualitatively similar to that in iron meteorite. The concentrations of refractory siderophile (Ru, Re, Os and Pt) negatively correlate with those of Ni and Au among iron meteorites in a single group (Pernicka and Wasson, 1987). Moreover, the multiple metal phases with siderophiles in chondrite have been suggested based on the absences of homogenization of Fe, Ni and Co in the metal particles even in so-called equilibrated chondrites (Smith et al, 1993).

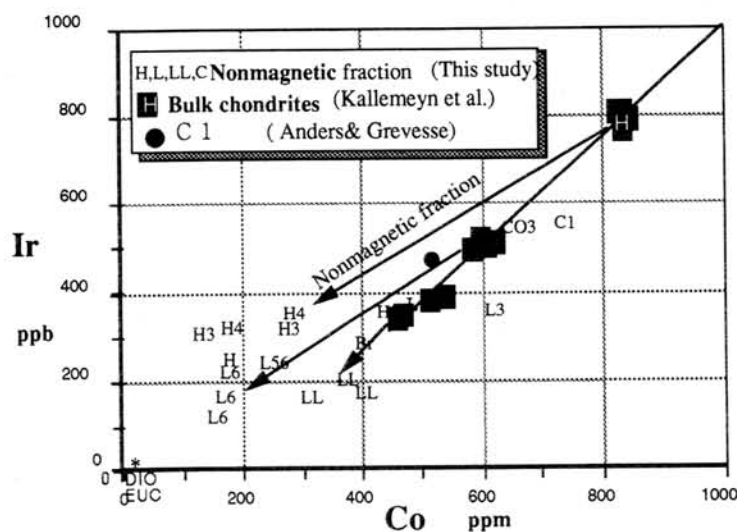
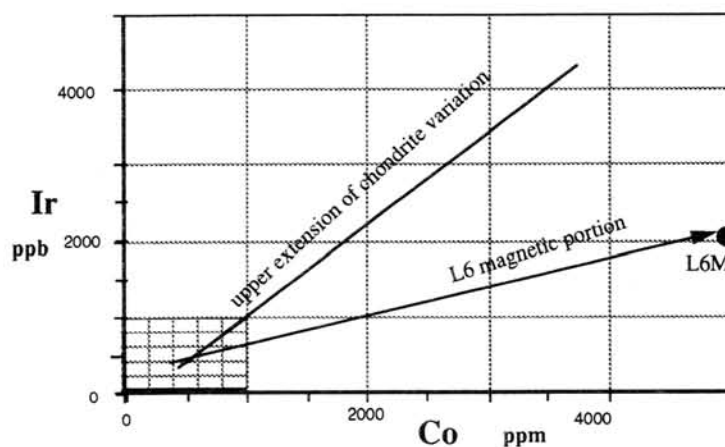


Fig 2. Ir-Co diagram for nonmagnetic fraction

Fig 3. Ir-Co diagram for magnetic fraction
L6M(magnetic fraction of ALH769)

- Anders, E and Grevesse, N. (1989) *Geochim. Cosmochim. Acta*, 53,197-214.
- Kallemeyn, G.W., Rubin, A.E., Wang, D. and Wasson, J. T. (1989) *Geochim. Cosmochim. Acta*, 53,2747-2767.
- Pernicka, E and Wasson, J.T. (1987) *Geochim. Cosmochim. Acta*, 51, 1717-1726.
- Smith, D.G.W., Miura, Y. and Launspach, S. (1993) *Earth Planet. Sci. Lett.*120, 487-498.
- Tanaka, T., Kamioka, H. and Yamanaka, K. (1988) *Bull. Geol. Surv. Japan*. 39. 537-557
- Yanai, K (1979) *Catalog of Yamato meteorites*.
- Yanai, K and Kojima, H. (1987) *Photographic catalog of the Antarctic meteorites*. NIPR, Tokyo.

LOONGANA 001 AND COOLIDGE: A NEW CARBONACEOUS CHONDRITE GROUplet. Gregory W. Kallemeyn and Alan E. Rubin, Institute of Geophysics and Planetary Physics, University of California, Los Angeles, CA 90024-1567

The Coolidge meteorite was found in Hamilton County, Kansas in 1937. Van Schmus [1] classified Coolidge as a CV4 carbonaceous chondrite based on petrographic and bulk compositional data. McSween [2] included it as a member of the 'reduced subtype' of the CV group, characterized as having more abundant metal than magnetite, and a relatively low matrix/chondrule ratio. Kallemeyn and Wasson [3] concurred with the CV4 classification, showing Coolidge to have similar nonvolatile element abundances, but lower volatile element abundances than CV3 chondrites.

Loongana 001 (hereafter referred to as Loongana) was found in 1990 in the Nullarbor region of Western Australia. An initial study by Spettel et al. [2] concluded that it was a carbonaceous chondrite, possibly related to CR chondrites or the ungrouped ALH85085 because of its low abundance of moderately volatile elements. The high matrix/chondrule modal abundance ratio in Loongana (~0.3) and the occurrence of 1-2 vol.% refractory inclusions is consistent with its classification as a carbonaceous chondrite.

Refractory lithophile abundances in Loongana and Coolidge are similar to each other and to those in CV chondrites, and distinct from those in CR (or other) carbonaceous chondrite groups (Fig. 1). They also have volatile element abundance patterns similar to each other, and similar ratios of characteristic elements such as Zn/Mn and Al/Mn (Figs. 2). Petrographically, Loongana and Coolidge have many similarities: chondrule size, abundances of coarse-grained chondrule rims, degree of oxidation, petrologic type and shock stage.

Loongana and Coolidge are not CV chondrites. Loongana and Coolidge are depleted in moderately volatile lithophiles, siderophiles and chalcophiles relative to CV chondrites. They are distinguished from CV chondrites (and all other carbonaceous chondrite groups) on a plot of Zn/Mn vs. Al/Mn (Fig. 2). Loongana and Coolidge also have smaller chondrules and far fewer coarse-grained chondrule rims than CV chondrites.

Kallemeyn and Wasson [3] previously suggested that Coolidge might have formed from open-system metamorphism of CV3 material. This seems unlikely in light of our current petrographic observations. Metamorphic temperatures necessary to cause the observed volatile element depletions in Loongana and Coolidge ($\geq 1000^\circ\text{C}$) would also cause significant petrographic changes characteristic of petrologic type ≥ 6 [5,6]. Loongana and Coolidge are only petrologic type 3.8-4, and therefore underwent only minimal metamorphic heating.

Loongana 001 and Coolidge are carbonaceous chondrites with similar compositional and petrographic characteristics. Similarities in refractory lithophile compositions suggest that they may belong to the CV chondrite clan. However, they differ significantly from the CV chondrites and any of the other established carbonaceous chondrite groups. Thus, Loongana 001 and Coolidge constitute their own carbonaceous chondrite grouplet.

REFERENCES:

- [1] Van Schmus W. R. (1969) Mineralogy, petrology, and classification of types 3 and 4 carbonaceous chondrites. In *Meteorite Research* (ed. P. M. Millman), Vol. 112, pp. 480-491. D. Reidel Publishing Company. [2] McSween H. Y. (1977) Petrographic variations among carbonaceous chondrites of the Vigarano type. *Geochim. Cosmochim. Acta* **41**, 1777-1790. [3] Kallemeyn G. W. and Wasson J. T. (1982) The compositional classification of chondrites-III. Ungrouped carbonaceous chondrites. *Geochim. Cosmochim. Acta* **46**, 2217-2228. [4] Spettel B., Palme H., Wlotzka F. and Bischoff A. (1992) Chemical composition of carbonaceous chondrites from Sahara Nullarbor Plains. *Meteoritics* **27**, 290-291. [5] Ngo H. T. and Lipschutz M. E. (1980) Thermal metamorphism of primitive meteorites - X. Additional trace elements in Allende (C3V) heated to 1400° C. *Geochim. Cosmochim. Acta* **44**, 731-739. [6] McSween H. Y., Sears D. W. G and Dodd R. T. (1988) Properties of chondrules. In *Meteorites and the Early Solar System* (eds. J. F. Kerridge and M. S. Matthews), pp. 102-113. Univ. of Arizona Press.

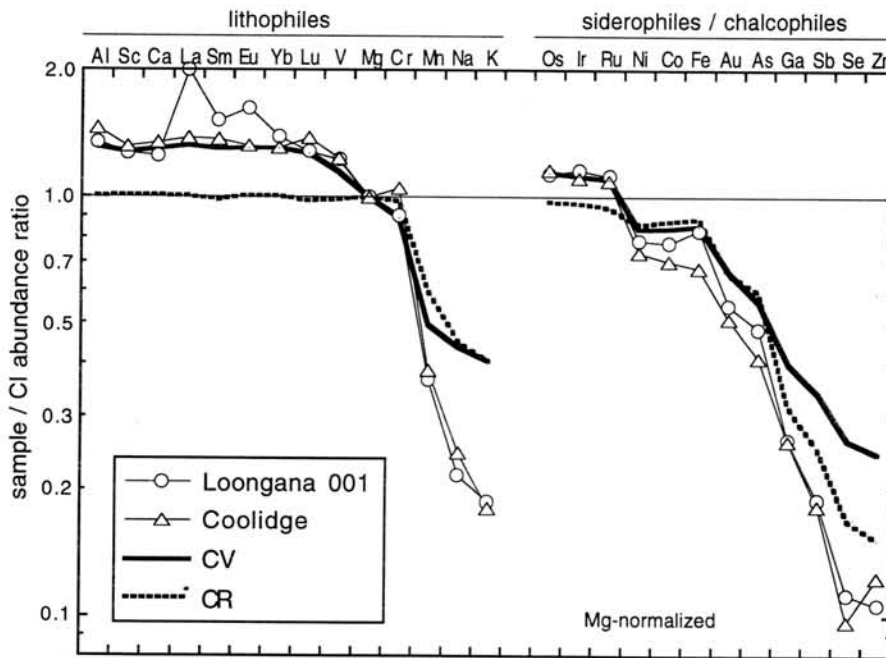


Fig. 1. CI- and Mg-normalized abundance plot.

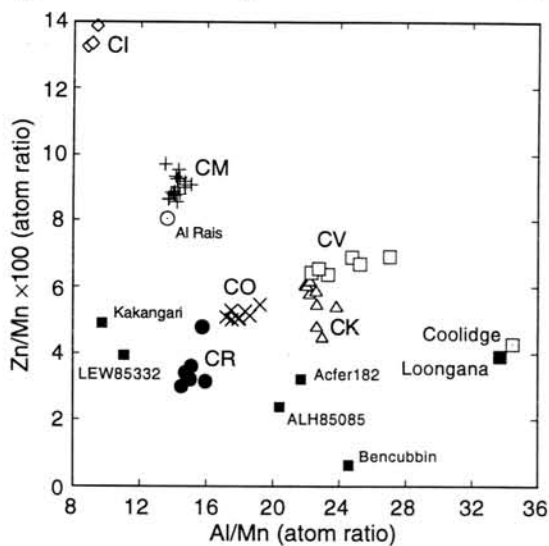


Fig. 2. Zn/Mn vs Al/Mn plot.

THE U-Th-Pb AND Sm-Nd ISOTOPIC SYSTEMATICS OF MET 78008 UREILITE. Noriko Torigoye^{1*}, Mitsunobu Tatsumoto¹, and Keizo Yanai². ¹US Geological Survey, MS 963, Box 25046, Denver, CO 80225, USA. National Institute of Polar Research, 9-10, Kaga 1-chome, Itabashi-ku, Tokyo 173.

Ureilites consist of ultramafic minerals, such as olivine and pyroxene, with minor amounts of carbon, metal, and sulfide. The incompatible trace elements are highly depleted in ureilites, which indicate ureilite formation through extensive igneous processes, either by cumulates formation from a magma or partial melting residues in the ureilite parent body(ies). However, different types of ureilites also show oxygen isotopic heterogeneities, indicating that nebular signature still remains among ureilites. The genesis of ureilites is not well known because of their complex characteristics [1].

Takahashi and Masuda [2] investigated the Rb-Sr and Sm-Nd systematics of MET 78008 ureilite. They obtained a Rb-Sr internal isochron age of 3.97 ± 0.07 Ga using mineral separates. Their Sm-Nd results yield a line using 6N HCl leachate and residue data, that corresponds to an age of 4.09 ± 0.08 Ga, consistent with the Rb -Sr age. Goodrich and her co-workers further obtained Sm-Nd ages of ureilites which are significantly younger than the so-called "4.55 Ga canonical age of meteorites"; 3.74 Ga for Kenna [3] and 4.23 Ga for PCA 82506 [4]. Therefore, some recent ureilite formation models include secondary event such as metasomatism in order to explain these younger ages [3]. However, Torigoye et al. [5, 6] presented U-Th-Pb analyses of Goalpara and MET 78008 ureilites, which indicated a formation age as old as 4.55 Ga. Here, the U-Th-Pb and Sm-Nd systematics of MET 78008 are reported to confirm the old formation ages for ureilites.

Several small chips of MET 78008, allocated to us from NIPR, weighed 4.5g. One of the pieces with dark green color (GR) looked different from the others, so it was measured separately. The other pieces were gently crushed and sieved into three fractions; 300-150 μm , 63-150 μm , and <63 μm . The olivine and augite grains were hand-picked from the coarse grain fraction, several magnetic separates were obtained using a Frantz isodynamic separator (M1~ M4), and a fine fraction was used to represent the whole rock (WR). In order to remove terrestrial Pb contamination, a leaching procedure was applied to all these samples. They were washed by ethanol and acetone, and then leached successively by 0.1N HBr, 1N HNO₃, and 7N HNO₃, and the final residues were dissolved by using an HF-HNO₃ mixture.

*Present Address: Geological Survey of Japan, 1-1-3 Higashi, Tsukuba, Ibaraki 305.

U-Th-Pb system: The Pb-Pb isotopic compositions of residues and leachates are shown in Fig. 1. The leachates plot along a mixing line between the Pb isotopic composition of primordial meteoritic Pb (CDT) and that of modern terrestrial Pb (MT), indicating leachates contain terrestrial contamination. The residues plot well above this mixing line and three of them (GR, AG, M1) show a good linear trend which corresponds to the Pb-Pb age of 4.563 ± 21 Ma. In Fig. 2, these data plot close to the U-Pb concordia curve, while other data plot out side of the concordia curve, indicating the addition of terrestrial Pb to the samples. Three points corresponding to 4.56-Ga Pb-Pb ages plot slightly inside the concordia curve. If some radiogenic Pb were lost during the extensive leaching procedure, the U-Pb concordia age of 4.572 ± 6 Ga is obtained as the average of $^{207}\text{Pb}^*/^{206}\text{Pb}^*$ of these three points. Both Pb-Pb and U-Pb ages are consistent each other.

Sm-Nd system: As shown in Fig. 3, our Sm-Nd data of MET 78008 plot near the 4.55-Ga chondritic isochron, though they are scattered and only a few data plot exactly on the line. In our previous work, we found that the Sm-Nd data of the Goalpara ureilite plot on the terrestrial contamination mixing line, which goes through the highly depleted ureilitic composition and an average terrestrial crustal Sm-Nd composition [5]. It seems like some of our MET 78008 data are also shifted towards the contamination mixing line, indicating terrestrial contamination may be one of the reasons for the data scatter. Because of this scattering and smaller variations in $^{147}\text{Sm}/^{144}\text{Nd}$ ratios, we could not obtain a precise Sm-Nd age for the meteorite. However, it should be mentioned that our most precise data from augite separates with high Sm and Nd concentrations plot well above the 4.1-Ga isochron age obtained from the leaches of MET 78008 by Takahashi and Masuda [2].

During the Nd isotopic analysis, $^{142}\text{Nd}/^{144}\text{Nd}$ isotopic ratios were also measured. The results (Fig. 4) indicate a positive ^{142}Nd anomaly from in-situ decay of ^{146}Sm (half-life of 100 Ma). The presence of a ^{142}Nd anomaly supports for an old formation age of MET 78008 close to 4.55 Ga. It is now very likely that formation ages of ureilites are consistent with so-called "4.55-Ga canonical age of meteorites". The younger internal isochron ages obtained previously should be evaluated more strictly for possible contamination effects that may have disturbed all of the isotopic systematics of the trace elements which are highly depleted in ureilitic meteorites.

References: [1] Goodrich (1992) *Meteoritics*, 27, 327. [2] Takahashi and Masuda (1990), *Meteoritics*, 25, 413. [3] Goodrich et al. (1991) *Geochim. Cosmochim. Acta*, 55, 829. [4] Goodrich and Lugmair (1993), *LPSC XXIV*, 547. [5] Torigoye et al. (1993) *Meteoritics*, 28, 450. [6] Torigoye et al. (1994) *LPSC XXV*, 1409.

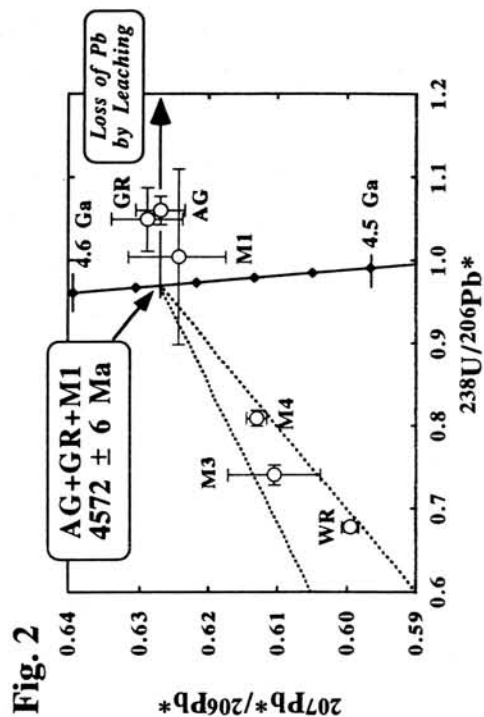


Fig. 2

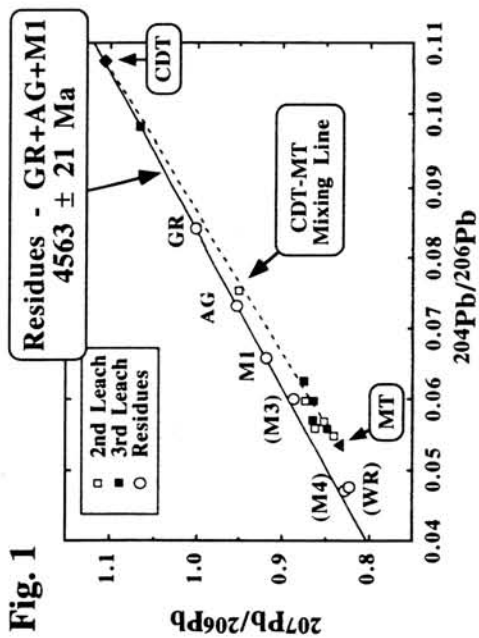


Fig. 1

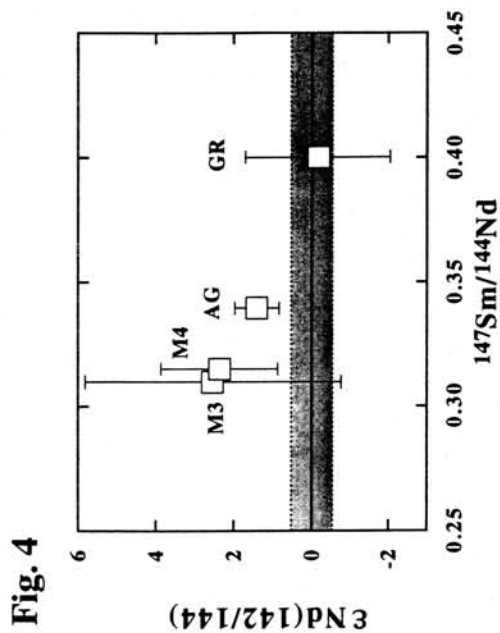


Fig. 4

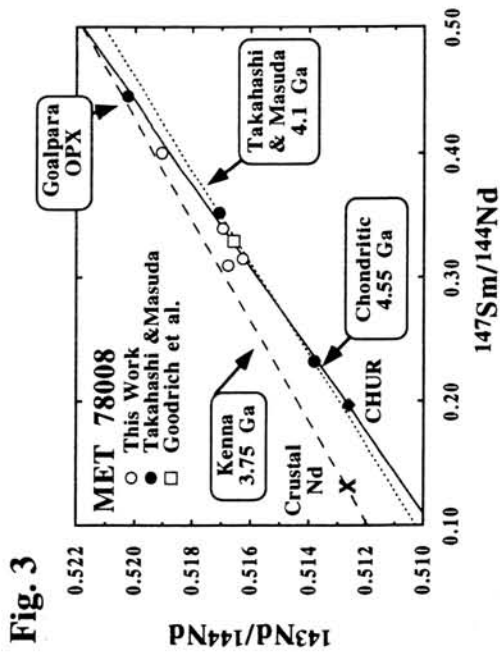


Fig. 3

CHEMICALLY DIFFERENT POPULATIONS OF HIBONITES AND PEROVSKITES IN A CAI FROM Y-791601: EVIDENCE FOR AN EXTRANEEOUS ORIGIN: Hideyasu Kojima¹, Ahmed El Goresy² and Keizo Yanai¹; ¹National Institute of Polar Research, Tokyo 173, Japan; ²Max-Planck-Institut für Kernphysik, P.O.Box 103980, D-69029 Heidelberg, Germany

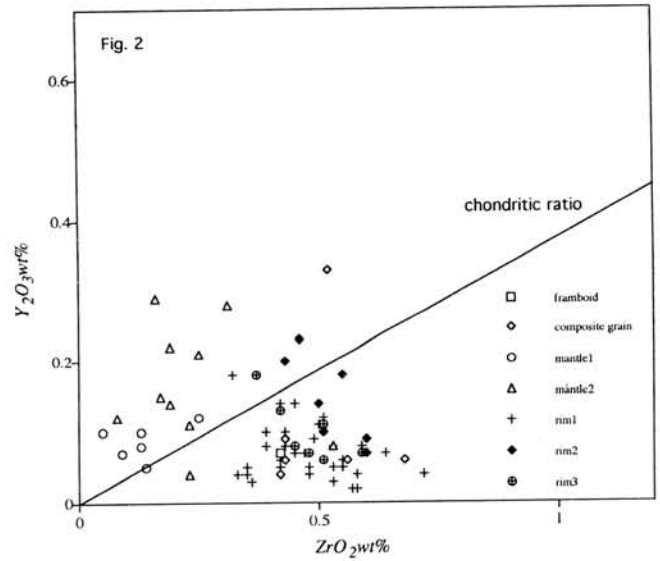
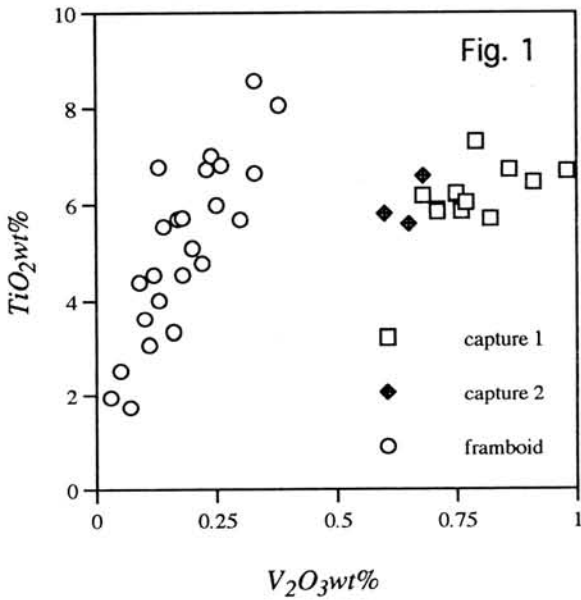
A petrographic and EPMA study revealed the presence of different populations of perovskites and hibonites in CAI from the Y-791601 CV3 chondrite. Some of them probably are of extraneous origin. This CAI(YM1) is very large (2 cm in length) and has a core-mantle structure. The core consists mainly of loosely packed coarse spinels with anorthite, fassaite, diopside and grossular in their interstices. The mantle consists of melilite (Ak₉) with minor spinel, hibonite and perovskite. A few euhedral grains of corundum, several μm in size, are found in the melilite mantle. The narrow rims are developed as successive layers on the outermost mantle. In thin section YM1 (Y-791601, 51-1) is quadrilateral in shape and lacks mantle and rim in both elongated sides. It seems that the spinel core lies between the two mantles (mantle 1 and mantle 2). The mineral assemblage resembles type A CAI (CTA), however, the abundance of spinel and melilite and the textural features differ from type A.

Three distinct populations of hibonites were encountered: a) in the rim sequence, b) in spinel framboids, and c) in captured multiphase fragments. Two type C assemblages consisting of hibonite and spinel occur along with a spinel framboid in mantle 1. Hibonites in captured fragments are rich in V_2O_3 (0.6 - 1.0%). In contrast, hibonites in spinel framboids are depleted in V_2O_3 ($\leq 0.4\%$). These hibonites display a positive correlation between V_2O_3 - and TiO_2 - contents (Fig. 1). This results suggests that the hibonite populations originated from different sources.

There are three categories of perovskites: a) in the rim sequence, b) as a composite grain, and c) subhedral grains in the melilite mantle. Perovskites forming the innermost rim with spinel and hibonite are heterogeneously distributed. Here, three domains enriched in perovskite are encountered: rim 1 consisting of perovskite and spinel, rim 2 and 3 consisting of perovskite, hibonite, and spinel. The composite grain is amoeboid in shape and consists of a bright and a dark portion on BEI image. Two chemically different perovskite types were found: (1) perovskite with higher than chondritic

ZrO₂/Y₂O₃ ratios, (2) perovskite with lower than chondritic ZrO₂/Y₂O₃ ratios (Fig. 2). Type 1 perovskites either condensed from a reservoir with non chondritic ZrO₂/Y₂O₃ ratio or were formed by fractional condensation[1]. Perovskites in the rims show negative relationship between Y₂O₃ and ZrO₂ and mainly belong to type 1. This indicates that the perovskites in rims did not crystallize from the host CAI liquid and are probably condensates and extraneous to CAI. The composite grain also belongs to type 1. The bright portion is higher in ZrO₂ than the dark one. These results are indicative of a very complex formation history of the composite grain. Single grains and aggregates of perovskite in the mantle belong to type 2. Type 2 perovskites have Y₂O₃/ZrO₂ ratios similar to those obtained from crystal/liquid fractionation experiments[2]. In these perovskites the abundance of Sc₂O₃ is positively correlated with both ZrO₂ and Al₂O₃.

[1] Zinner, E. and El Goresy, A.(1994): LPS XXV, 1557-1558. [2] Simon S. B. et al.(1994): GCA 58, 1525-1536



Chemical Fractionations of Primitive Achondrites and their Implications for Melting Processes.

Noritoshi Morikawa¹ and Noboru Nakamura^{1,2}, ¹Department of Nature of the Earth, Graduate School of Science and Technology, ²Department of Earth and Planetary Sciences, Kobe University, Nada, Kobe 657, Japan

Primitive achondrites have approximately chondritic bulk chemical compositions and mineralogies, but achondritic textures. They are thought to have been heated at high temperature. Several authors argued about thermal history of these meteorite groups, and suggest that acapulcoites experienced partial melting at the Fe,Ni-FeS eutectic and lodranites experienced partial melting of silicates (1). Winonaites also experienced thermal metamorphism at high temperature.

We reported results of analyses of lithophile trace elements together with some major and minor elements, and found fractionated abundance pattern of trace elements, typically alkalis and REE, for all these meteorite groups (2,3). Some authors suggest that chemical compositions of acapulcoites and winonaites are not fractionated, and that acapulcoites were not subjected to partial melting of silicate phase. However, it is noted that the depletion of alkali elements and fractionated REE patterns in Acapulco and other acapulcoites are significant, suggesting that silicates in acapulcoite also caused partial melting to a certain extent. Similar chemical fractionations are also noted in winonaite. Lodranites are believed to have experienced partial melting and lost feldspathic melt.

In this work, in order to understand more quantitative melting processes of these meteorites, we performed model calculations based on two different kinds of partial melting modes for lithophile trace elements. As shown in Fig.1, data points of acapulcoite and winonaite plot on near the trend of fractional melting residue, while lodranites are close to the fractionation line of batch melting residue. Therefore, alkali/REE fractionation between acapulcoites and lodranites are remarkably different and may indicate the difference in melting mechanism of two meteorite groups. The degree of melting in silicate portion is less than a few % for acapulcoites and winonaites (Fig.2-a) and larger than ten % for lodranites (Fig.2-b). Some meteorites show unusual REE patterns. It is impossible to account for the observed trace element fractionations by single stage partial melting. LREE enrichment of Acapulco may be considered to due to apatite. In order to account for both the high degree of LREE enrichment and alkali metal depletion (especially Rb), igneous apatite with low alkali abundance should be introduced to Acapulco source.

References

- (1) McCoy, T.J. et al. (1992) *Lunar Planet. Sci.* **XXIII**, 871-872. (2) Torigoye, N. et al. (1993) *Proc. NIPR Symp. Antarct. Meteorites* **6**, 100-119. (3) Morikawa, N. and Nakamura, N. (1993) Papers presented to the 18th Symp. on Antarct. Meteorites, 38-40.

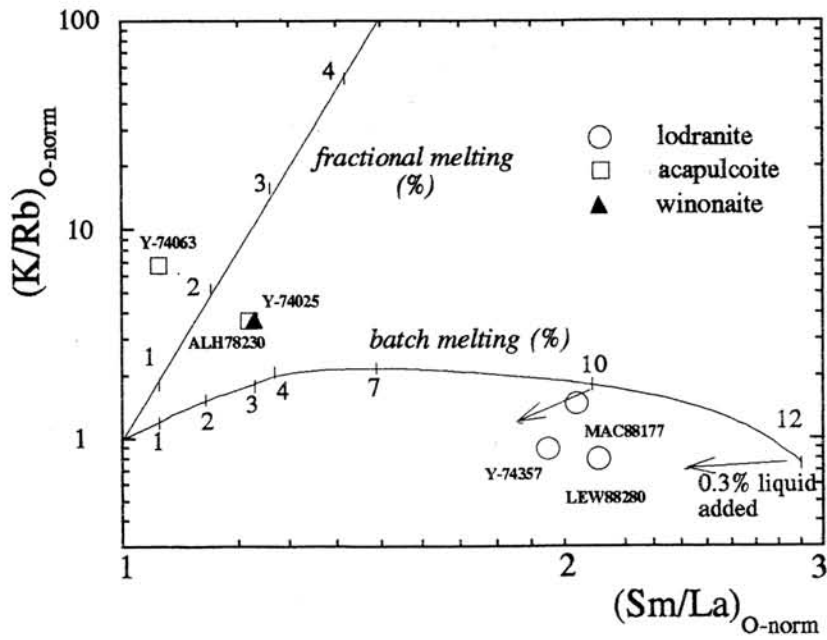


Fig.1 Correlated REE and K/Rb fractionation for the partial melting residue. The data of primitive achondrites are also plotted.

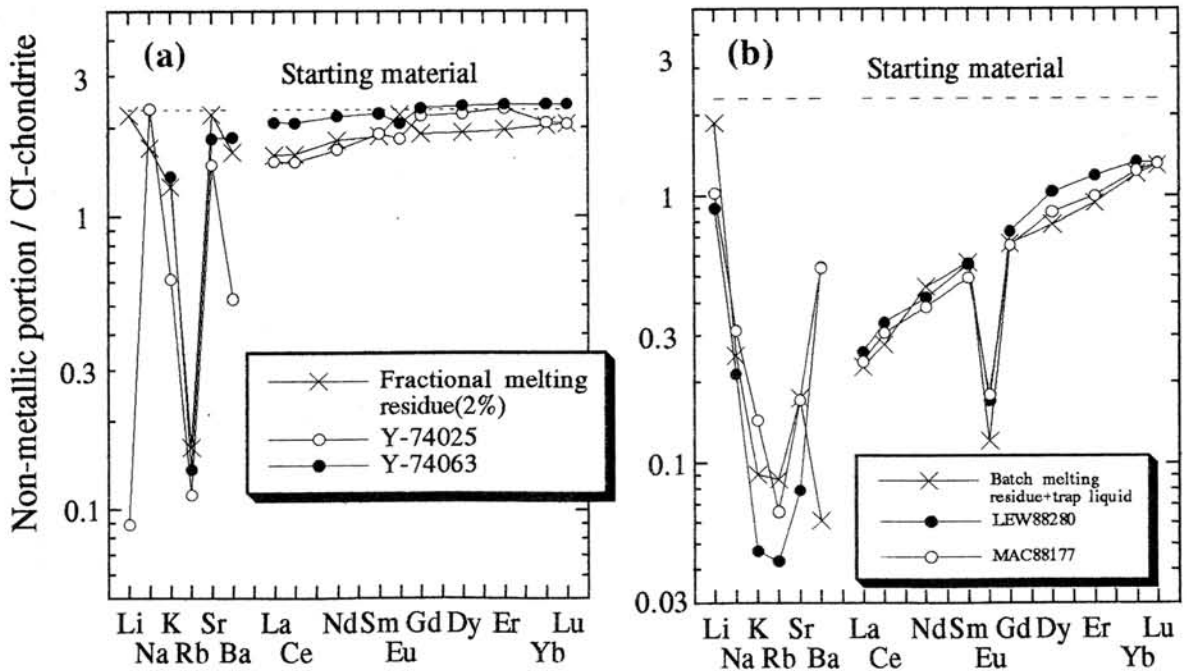


Fig2 Calculated trace element patterns (x) compared with measured patterns (o, •). (a) Fractional melting for acapulcoite and winonaite. (b) Batch melting for lodranite.

SHOCK-INDUCED MELT MIXING OF L AND LL MATERIALS IN Y-793533.

Osamu Okano and Hiroko Katayama

Department of Earth Sciences, Okayama University, Okayama 700, Japan

Introduction Shock processes are essentially the main phenomena in asteroidal objects during and after their formation. A study of shocked meteorites is, therefore, of great importance in understanding the evolutionary history of the solar system. The physicochemical features caused by shock, however, are not well understood partly because of difficulties in distinguishing genuine shock features from other features caused by "metamorphism", both of which, in many cases, are recorded in the meteorites. The shock-melted Y-79 LL-chondrite samples are regolith breccias which experienced intense shock-melting on the parent body 1.2 Ga ago[1-3], and are presumably the best samples for a study of asteroidal shock processes because they might have preserved the shock features without any serious disturbances after the young collisional event. Y-793533 is a porous dark stone classified as an LL6 chondrite[1]. The appearance of Y-793533 is quite similar to those common in the shock-melted Y-79 LL-chondrites, suggesting that they could have fallen as a single meteorite shower. A dark area of ovoid shape (6x4 mm) was recognized on a cut surface of the specimen provided for this study (Y-793533,67). This part appears darker and more intensely melted and has more abundant vesicles of irregular shapes compared to the surrounding main part. To investigate their shock features and genetic relations between the two different lithologies, we carried out petrological and Rb-Sr isotopic investigations on both portions.

Experimental The dark portion(219 mg) was first taken out from the mass(1.5g). Each of the dark and the remaining (main) portions was ground and subjected to size- and density-separations after metal-rich grains were removed using a hand magnet. Twenty-one fractions were obtained in this together with a whole rock sample(66mg) from the main part. A portion of each was mounted in epoxy resin and a polished thin section made for EPMA analyses on constituent minerals and glasses. The remaining portions of each fraction and whole rock were then used for Rb-Sr isotopic measurements by thermal ionization mass spectrometry. The latter was done on an MAT261 mass spectrometer at the Institute for Study of Earth's Interior, Tottori.

Results and discussion EPMA analyses (Fig.1) indicates that Fe/(Fe+Mg) ratios in olivines and Ca-poor pyroxenes are slightly different in the two portions. While Fa contents of olivines in the main part are mostly in the equilibrated L-chondrite range, those of the dark part are more Fe-rich, being partly in the equilibrated LL-range. A similar tendency is also recognized in the case of Ca-poor pyroxenes. The ratio is considerably dispersed for equilibrated chondrites. Although this might, in part, be due to the small grain sizes of recrystallized olivines and pyroxenes (many of them are in several μm -size), a shock-melting process is a possible cause of the dispersion, considering a similar case reported for the shock-melted LL6-chondrite, Y-790964[4]. The data points in the Rb-Sr evolution diagram(Fig.2) do not, as a whole, fall on a line but are widely scattered. Most of the fractions from the main part and whole rock, however, plot in an area along the 4.5 Ga-line. In contrast to those from the main part, fractions from the dark part remarkably shift upwards off the line, indicating a possibility of more or less Rb-loss by shock processes. Okano et al.[4] suggested that some amounts of alkali-rich fragments had been included in the shock-melted LL-chondrite Y-790964 prior to the 1.2 Ga shock event and significant Rb-loss from such materials had occurred through the shock processes. Considering the common characteristic features of Y-793533 and Y-790964, it is possible to assume that the dark portion in the Y-793533 had contained such alkali-rich LL components. It should also be noted that several fractions from the dark part plot around the 1.2 Ga-line. This suggests partial (incomplete) equilibrium in the Rb-Sr system at the 1.2 Ga (?) shock event. These fractions consist mainly of recrystallized small grains of olivines and pyroxenes and interstitial glassy materials, while two fractions with the highest $^{87}\text{Sr}/^{86}\text{Sr}$ ratios contain greater amounts of remnant mineral grains. We, therefore, consider that the dark portion was formed possibly by the 1.2 Ga shock event as a shock-melted mixture of L-chondritic and lesser amounts of alkali-rich LL-chondritic materials.

It is envisaged that a part of the Rb was lost from the LL materials whereas some of the LL constituents had survived without complete melting. This model is also supported by the results of the chemical compositions in olivine and Ca-poor pyroxene mentioned above and indicated in Fig.1.

References [1] Yanai K. and Kojima H. (1987) *Photographic Catalog of the Antarctic Meteorites*, NIPR. [2] Nakamura N. and Okano O. (1985) *Nature* 315, 563-566. [3] Takigami Y. and Kaneoka I. (1986) *Mem. Natl. Inst. Polar Res., Spec. Iss.* 46, 133-143. [4] Okano O., Nakamura N. and Nagao K. (1990) *GCA* 54, 3509-3523.

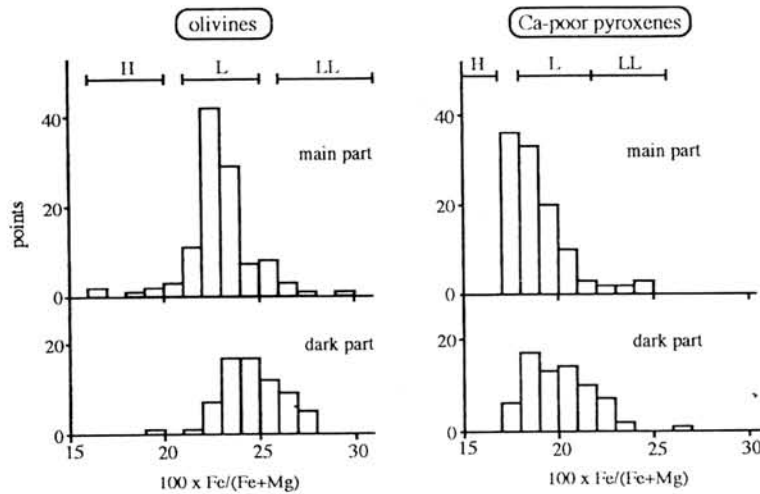


Fig.1. Frequency histograms comparing 100xFe/(Fe+Mg) in fractions separated from Y-793533,67.

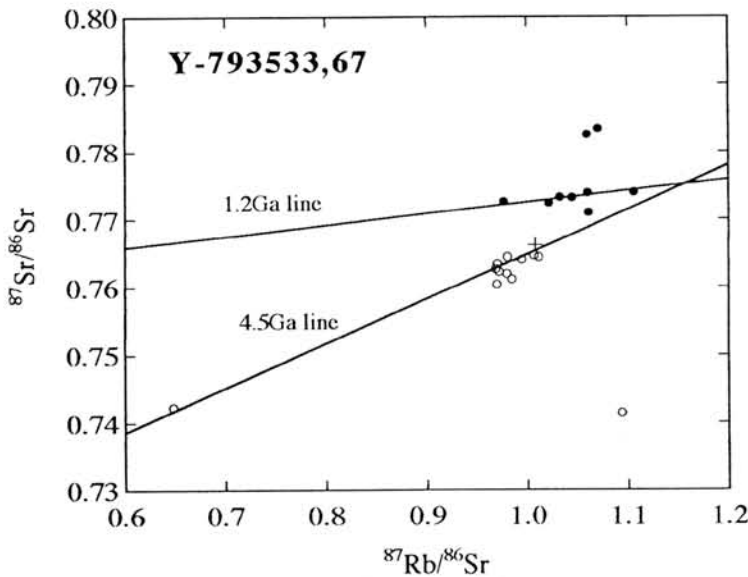


Fig.2. Rb-Sr evolution diagram for separated fractions and a whole rock from Y-793533,67. Open and filled circles represent fractions from the main and the dark part, respectively. Cross: a whole rock from the main part.

MELTED NATURE OF ORDINARY CHONDRITES: EXPERIMENTAL DATA AND STRUCTURAL-PETROLOGICAL EVIDENCE OF LIQUID IMMISCIBILITY PROCESS DURING CHONDRULE FORMATION

N.G.Zinovieva, O.B.Mitreikina and L.B.Granovsky

Department of Petrology, Faculty of Geology, Moscow State University, Lenin Gory, Moscow, 119899, Russia.

Process of the liquid immiscibility of silicate, metallic and sulphide melts is well known [3; 6; et al.]. The experimental research on the melting of the ordinary chondrite Tsarev (L5), run at water-hydrogen fluid pressure [1], showed that there was liquid immiscibility of the chondrite melt into silicate, metallic and sulphide melts. The liquid immiscibility of the silicate part of the chondrite melt is less studied, however examples of the basic - ultrabasic separation into layers in the earth rocks are well known [2].

Detailed petrological research on the partially melted (by microwave-heating, run at vacuum, $T=1400\pm 100^{\circ}\text{C}$, $t=20$ min. [8]) ordinary chondrite Tsarev (L5) carried out by SEM and microprobe study has demonstrated that the chondrite matter tends to separate into silicate and sulphide-metallic melts during the melting. This fact is in agreement with experimental research on the melting of a Yamato L3 (Y-74191) chondrite being studied at the pressure range 6-30 kbar [7].

Earlier we showed [9; 10] that there were two distinct types of the silicate areas situated in the melted part of the sample of the ordinary chondrite Tsarev being different in texture (porphyritic and intersertal), in crystallization temperature as well as in their chemical compositions. We found that the boundary between these melts was well-defined and there were two types of the silicate melt separations: layer-like and drop-like. These facts all together lead us to conclude that the silicate melt separated into two immiscible silicate melts later.

Troilite and Fe-Ni metal form only drops (from some μm to some mm-size) in the both silicate melts. It's well known that there is no stable two-liquid field in Fe-Ni-rich area (sulphide and metallic melts) of phase diagrams of Fe-Ni-S system. However, the liquid immiscibility took place in the Fe-Ni-rich area of this system in the experimental melted ordinary chondrite Tsarev. As indicated in fig. 1, there are drops of metal in the sulphide melt. This fact as well as the existence of the liquid boundary of two melts (Fig. 2) being different in S and Fe-Ni contents and the same in compositions of the crystallizing phases of the both melts can be explained by the influence of a small amount of additional components (for example P in Fe-Ni metal) in the real Fe-Ni-S system in contrast to phase diagrams.

Thus, the petrological research on the experimental melted ordinary chondrite Tsarev has showed that there existed not only liquid immiscibility of silicate and sulphide-metallic melts but also their later separation: the silicate melt separated into

two coexisting silicate melts and the sulphide-metallic melt separated into sulphide and metallic melts.

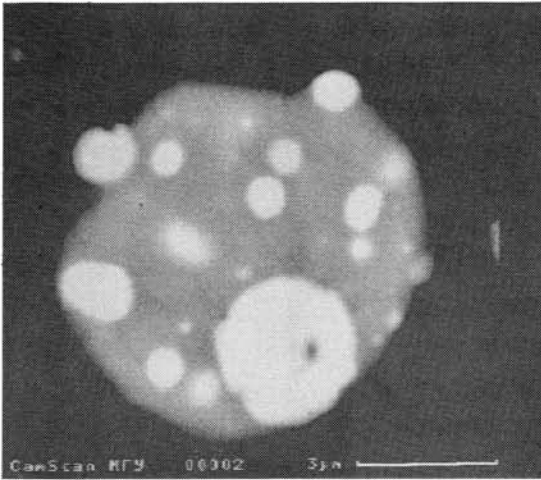


Fig. 1. Experimental melted chondrite Tsarev (L5): Drops of the metallic melt (white) in the sulphide melt (gray).

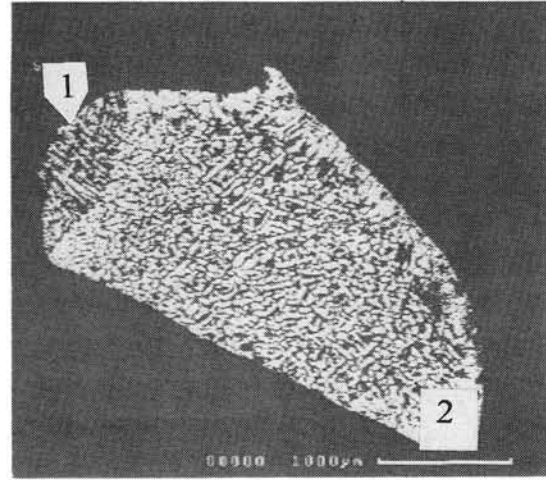


Fig. 2. Experimental melted chondrite Tsarev (L5): The liquid boundary of two melts (1 and 2) being different in S and Fe-Ni contents. Compositions of FeS (dark gray) and Fe-Ni metal (white) are the same in the both melts.

A comparison between compositions of experimental silicate melts and chondrules of ordinary chondrites on the one hand and between experimental sulphide-metal drops and sulphide-metal matrix of the ordinary chondrites on the other hand demonstrated that the products of the experiment were similar to those in nature. It's necessary to note that the silicate-metallic separation presents as in the matrix as in the chondrules of the ordinary chondrites. The sulphide-metal drops occur as inside silicate crystals as in the interstices between them being pushed either to the central or to the border parts of the chondrules.

Earlier we presented [4] the evidences of liquid immiscibility genesis of chondrites: 1) the drop-like chondrule structure often slightly extended according to the fluidal structure; 2) the existence of the complicated chondrules forming dumb-bell shaped clusters of two or three drops and 3) the existence of the sharp boundary chondrule - matrix often accompanied by the monomineral olivine rim in which we could observe the growth of the olivine crystals (directed normally to the boundary) both toward the chondrule and the matrix. Melted nature of the matrix is supported by the existence of the melted objects (without even signs of impact metamorphism) in it, the structure and paragenetic sequence of which show [11] that their crystallization followed for a decreasing temperature and solidified after the chondrules. The silicate groundmass surrounding chondrules (in the high petrological Fucbin L5 chondrite) conforms to the chondrule's outlines, and some minerals and their aggregates started to crystallize on the chondrule surface. This process indicates that the chondrule - matrix boundary did exist prior to the groundmass crystallization.

The comparison of bulk chemical compositions of the chondrules by major components demonstrates their basic-ultrabasic subdivision into the groups of dunitic and pyroxenitic composition. This separation is further validated by the character of zoning in the chondrules of the intermediate, peridotitic type. The effect is vividly demonstrated by the "chondrule-in-chondrule" structure. The coexistence, within a single chondrite, of chondrules belonging to different textural types is considered from the viewpoint of microheterogeneities in a polymerizing silicate melt. The diversity of textural types in chondrules with different silicities as well as their discrete silicity itself and the immiscible separation of chondrite melt into silicate and metal-rich constituents is controlled, within a particular meteorite, by the acid-base interaction of chemical components of a single silicate system [5]. This phenomenon is typical of all chondrites, including their high petrological types.

ACKNOWLEDGMENTS: This work was supported by International Science Foundation (ISF) and Russian Fund of Fundamental Researches (RFFI), Project 94-05-16942. We thank Prof. A.V.Vityasev for providing the experimental melted sample of the Tsarev chondrite.

REFERENCES: [1] Marakushev A.A. and Bezmen N.I. (1983) *Evolution of meteorite substance...*, Nauka Press, 184 pp. (in Russian); [2] Marakushev A.A. (1988) *Petrogenesis*, Nedra Press, 293 pp. (in Russian); [3] Marakushev A.A. et al. (1992) *Space petrology*, Moscow University Press, 325 pp. (in Russian); [4] Mitreikina O.B. et al. (1992) *Vestnik Moskovskogo Universiteta, seriya geologiya* 1, 38-48 (in Russian); [5] Mitreikina O.B. et al. (1994) *Petrology*, v.2, N 3, 311-324; [6] Ramdohr (1960) *Die Erzminerale und ihre Verwachsungen*, Akademie-Verlag, 1132 pp.; [7] Takahashi E. (1983) *Proc. 8th Symp. Antarct. Meteor., special issue*, 30, 168-180; [8] Zetser Yu.I. et al. (1993) In: *Origin of Solar System*, A.V.Vityasev ed., Nauka Press, 112-115 (in Russian); [9] Zinovieva N.G. et al. (1994) *LPS XXV*; [10] Zinovieva N.G. et al. (1994) *LPS XXV*; [11] Zinovieva N.G. et al. (1994) *19th Symp. Antarct. Meteor.*, this volume.

CHEMISTRY OF THE LITHIC INCLUSIONS IN YAMATO-75097, -793241 AND -794046 METEORITES

Fukuoka, T.

Department of Chemistry, Gakushuin University, Mejiro, Toshima-ku, Tokyo 171.

Yamato-75097 (L6), -793241 (L6) and -794046 (H4) chondritic meteorites have igneous-like inclusions (1). Yanai et al. (2) indicated the lithic inclusion of Y-75097 has unique mineral and chemical compositions, by their preliminary examination. Clayton et al. (3) assigned the lithic inclusions in Y-75097, -73241 and -794046 meteorites are H group by the oxygen isotopic compositions. Chemical studies of these inclusions and host meteorites provide possible informations of the early solar system. The mineralogical, chemical and isotopic studies have been carried out as consortium study (e.g. (1), (4), (5), (6)). We have reported part of chemical study of Y-793241 and -794046 meteorites (7).

We have analyzed more than 27 major, minor and trace elements in lithic inclusion and host samples of Y-75097 meteorite by conventional instrumental neutron activation analysis (INAA). Two aliquots of host samples of this meteorite have been analyzed. A chip of host sample of Y-794046 meteorite have also been analyzed. Preliminary analytical results are shown in Table 1 together with the results of control samples, JB-1 and Allende bulk powder. The chemical abundances of the lithic inclusions and host samples of Y-793241 and -794046 meteorites (7) were also shown in Table 1.

The analytical values of total iron contents confirm the hosts of Y-75097, -793241 and -794046 meteorites belong to the L, L and H groups, respectively. The REE patterns of hosts of Y-75097, -793241 and -794046 meteorites are basically chondritic, although one host chip of Y-794046 indicates fractionated pattern (Fig. 1). The abundances of siderophile elements in the inclusions of Y-75097, -793241 and -794046 are highly depleted, compared with their hosts (Fig. 2). This implies the inclusions suffered igneous process such as partial melting. They lost the most metal phases under the igneous process. This is consistent with the petrographical observations in (1).

The REE pattern of inclusion of Y-75097 is fractionated and has a negative Eu anomaly (Fig. 1). The REE abundances in the inclusion are enriched factor 2 to 4 compared with those of bulk chondrite. This pattern is quite different from the REE pattern (4) of inclusion of this meteorite. This imply the inclusion has extremely heterogeneous feature.

The chemical data in this study suggest the inclusions of Y-75097, Y-793241 and -794046 meteorites suffered some igneous process on the evolution of early solar system.

REFERENCES:

- (1) Yanai and Kojima (1993) Papers the 18th Symp. Antarct. Meteorites, 57.
- (2) Yanai *et al.* (1983) Mem. Natl Inst. Polar Res., Spec. Issue, 30, 29.
- (3) Clayton *et al.* (1991) Geochim. Cosmochim. Acta, 55, 2317.
- (4) Nakamura *et al.* (1993) Papers the 18th Symp. Antarct Meteorites, 61.
- (5) Sack and Lipschutz (1993) *ibid.*, 65. (6) Fujimaki *et al.* (1993) *ibid.*, 74. (7) Fukuoka (1993) *ibid.*, 71.

Table 1. Preliminary results of chemical abundances of Y-75097 and -794046 meteorites.

Wt mg	Y-75097				Y-794046				Y-793241 ¹⁾				Controls		Error* (%)	
	Host A		Host B		Host C		Host A ¹⁾ Host B ¹⁾		Wtd.mean Inclusion ¹⁾		Wtd.mean host		Inclusion	JB-1		Allende
	108, 1	108, 2	108, 1	108, 2	65, 3	65, 1	65, 1	65, 2	101	101	64	78				
Ti %	0.06	0.07	0.07	0.06	0.07	0.11	0.04	0.04	0.07	0.06	0.06	0.07	0.79	-	-	17-30 ³⁾
Al %	1.11	1.28	0.35	1.19	0.89	1.01	0.84	0.84	0.91	1.33	1.02	1.61	7.20	-	-	1-2 ⁴⁾
Fe ²⁺ %	18.4	19.0	14.5	18.7	26.9	25.0	25.5	25.5	25.7	11.4	23.2	15.2	=6.30	24.6	-	0.5
Mg %	15.1	15.2	19.1	15.1	12.2	14.2	14.0	14.0	13.5	18.5	15.1	19.5	4.66	-	-	1-3
Ca %	1.39	1.59	0.95	1.49	1.06	1.21	1.14	1.14	1.14	1.55	1.29	0.74	6.68	-	-	3-81
Na %	0.683	0.772	0.883	0.726	0.527	0.591	0.639	0.639	0.589	0.920	0.745	0.852	=2.07	0.393	-	0.5
K %	0.088	0.095	0.081	0.081	0.056	0.032	0.045	0.045	0.043	0.176	0.087	0.049	1.20	0.024	-	10-28 ⁵⁾
Mn %	0.260	0.267	0.263	0.263	0.211	0.239	0.226	0.226	0.226	0.304	0.267	0.312	0.116	-	-	0.5
Cr %	0.312	0.263	0.288	0.288	0.273	0.263	0.275	0.275	0.270	0.366	0.278	0.303	=0.0414	0.298	-	0.5
Rb %	n.d.	n.d.	7.6	n.d.	n.d.	n.d.	n.d.	n.d.	9.3	n.d.	n.d.	n.d.	=41	-	-	38 ⁶⁾
V ppm	77	67	122	72	64	82	59	59	69	87	68	79	217	-	-	2-4
Sc ppm	7.89	8.67	8.27	8.27	6.59	7.46	8.31	8.31	7.51	10.9	8.66	2.54	=28.9	12.9	-	0.5-1
La ppm	0.30	0.32	1.18	0.31	0.20	0.28	0.35	0.35	0.28	0.48	0.35	0.18	=38.8	0.54	-	9-20 ⁷⁾
Ce ppm	0.77	0.96	2.93	0.86	0.65	0.51	0.72	0.72	0.62	0.99	0.86	0.43	=63	1.02	-	11-23 ⁸⁾
Nd ppm	0.85	0.64	0.75	0.75	0.47	0.33	0.34	0.34	0.37	0.72	0.36	0.24	=27	1.69	-	20-31 ⁹⁾
Sm ppm	0.205	0.229	0.217	0.217	0.156	0.165	0.182	0.182	0.168	0.250	0.207	0.045	=5.02	0.346	-	1-2
Eu ppm	0.097	0.100	0.098	0.098	0.088	0.066	0.068	0.068	0.073	0.107	0.087	0.125	=1.59	0.150	-	12-26 ¹⁰⁾
Dy ppm	0.21	0.57	0.39	0.39	0.36	0.35	0.26	0.26	0.32	0.47	0.32	0.16	4.00	-	-	28-76 ¹¹⁾
Ho ppm	0.09	0.08	0.09	0.09	0.16	0.086	0.092	0.092	0.11	0.058	0.076	n.d.	=0.70	0.23	-	7-14
Yb ppm	0.23	0.29	0.26	0.26	0.27	0.20	0.27	0.27	0.24	0.31	0.26	0.073	=2.4	0.36	-	5-15 ¹²⁾
Lu ppm	0.042	0.048	0.045	0.045	0.040	0.035	0.033	0.033	0.036	0.051	0.039	0.014	=0.37	0.072	-	5-13
Hf ppm	0.16	0.15	0.16	0.16	0.09	0.12	0.14	0.14	0.12	0.18	0.14	0.16	3.70	0.25	-	12-22 ¹³⁾
Zn ppm	37	47	42	42	24	38	39	39	34	44	67	84	=83	104	-	2-8
As ppm	1.3	1.4	1.3	1.3	2.7	2.26	2.34	2.34	2.4	0.078	1.65	n.d.	2.48	1.94	-	5-10
Se ppm	9.9	7.9	8.9	8.9	10.3	12.1	11.8	11.8	11.5	2.3	15.8	0.37	n.d.	=11	-	5-6
Co ppm	448	501	474	474	934	775	786	786	823	33.0	651	47.5	=39.1	696	-	0.5-1
Ni %	0.961	1.16	1.06	1.06	1.89	1.78	1.84	1.84	1.83	0.0550	1.64	0.0718	=0.160	=1.55	-	0.5-3 ¹⁴⁾
Os ppb	230	227	229	229	387	377	506	506	426	n.d.	327	46	n.d.	=674	-	6-10
Ir ppb	255	250	253	253	416	491	574	574	499	17.0	402	70.9	n.d.	=853	-	0.5-2
Au ppb	114	132	123	123	240	205	210	210	217	2.13	172	2.52	n.d.	=157	-	1-2 ¹⁵⁾

* Errors for INAA are due to counting statistics.

1) Fukuoka (1993). 2) Total iron as Fe. 3) Except for JB-1(3%). 4) Except for Y-75097,109(15%). 5) Except for and JB-1(4%).

6) Except for JB-1(8%). 7) Except for Y-75097,109(4%). 8) Except for Y-75097,109(5%). 9) Except for 794046,65,3(62%).

10) Except for Y-75097,109(5%). 11) Except for JB-1(5%). 12) Except for JB-1(1%). 13) Except for JB-1(10%). 14) Except for Y-75097,109(255%).

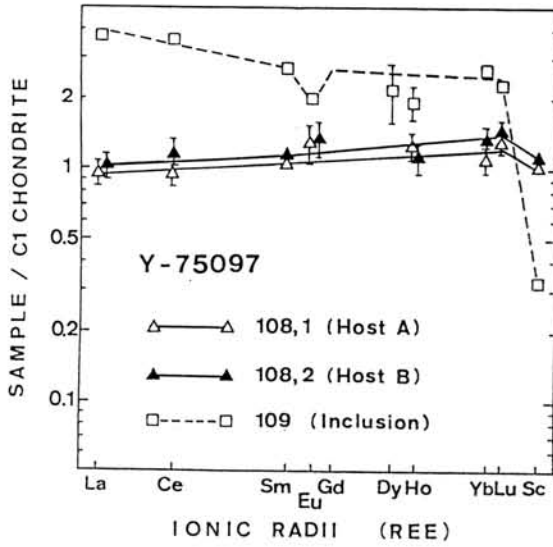


Fig. 1. C1 Chondrite (non-volatile) normalized abundance patterns of rare earth elements (REE) and Sc.

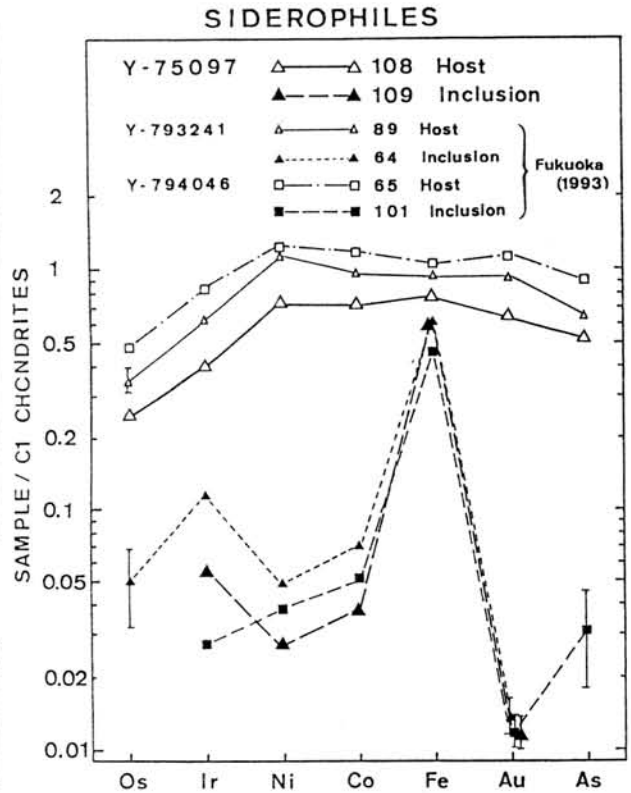
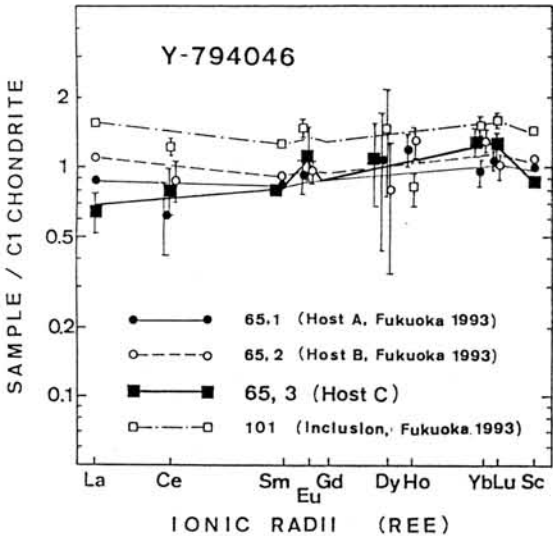
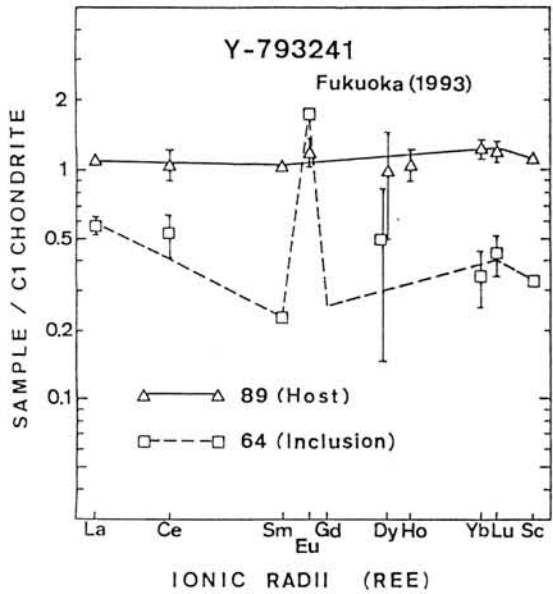


Fig. 2. Siderophile elements abundance ratios relative to C1 chondrite (non-volatile) for Y-75097, -793241 and -794046 meteorites.

ZONAL DISTRIBUTIONS OF REE IN THE Y-75097 INCLUSION AND THEIR IMPLICATIONS FOR THE EARLY FORMATION AND METAMORPHISM

Noboru Nakamura^{1,2}, Noritoshi Morikawa¹, Hideyasu Kojima³, Keiji Misawa^{1,2} and Keizo Yanai³

¹Department of Nature of the Earth, Graduate School of Science and Technology, ²Department of Earth and Planetary Sciences, Kobe University, Nada, Kobe 657

³National Institute of Polar Research, Itabashi, Tokyo 173

INTRODUCTION: In order to obtain evidence for the early melting event of chondritic materials, we have carried out comprehensive investigation into the three large (a few cm size) igneous inclusions in Yamato ordinary chondrites (Y-75097 [L6], Y-793241 [L6] and Y-794046 [H5]) and some results of consortium works have been reported elsewhere [1,2]. The previous works include analytical data for many different parts (mostly the mantle) of the inclusions and thus rather difficult to give overall chemical features of the inclusions.

In this work, we focussed more on systematic chemical (particularly REE) analyses of the inner (core) to outer (mantle) parts of the inclusion in the Y-75097 L6 chondrites. The Y-75097 inclusion has troctolitic mineralogy with uneven distributions of chlor-apatite/merrillite (~0% in the inclusion mantle and up to 10% in the core) [3] and has the oxygen isotopic composition similar to that of H-chondrites [4]. Both the inclusion and host were reheated during the early thermal metamorphism and by a 490 Ma shock event [4].

SAMPLES: The specimen Yamato-75097,52 is a cut slice containing the inclusion and the host (Fig. 1). A part of the slice (sub No ,105) was carefully sawed at NIPR. As seen in Fig 1, the sub-sample (0.516g) was taken from near the center to the surface of inclusion and the contact of host. The sample was further divided into six splits (A-F). A few fragments of each split were set aside for petrographic descriptions. The major parts (~50 mg) were grounded coarsely and aliquots were subjected to trace element analyses by isotope dilution (present study) and RNAA/INAA analyses (Lipschutz group).

RESULTS AND DISCUSSION: A preliminary result of petrographical examination is presented in Table 1. The sub-samples A and B are coarse grained and contain abundant phosphates and thus probably represent the core of inclusion as mentioned in Yanai et al. (1983)[1]. On the other hand, no phosphate nor pyroxene were identified in the sections of the mantle specimens (D and E). The section of specimen F consists mainly of the host meteorite but contains a very minor amount of the inclusion which contacts with the host. It is clear that the composition of olivine is perfectly homogeneous in the inclusion and the host. The mean composition of plagioclases is also mostly homogeneous, while plagioclases with low An (An=13%) and high An (up to An=21%) occurred occasionally in the sections with no systematic trend.

We suggest that the inclusion was mostly equilibrated with the host meteorite during the early thermal metamorphism and the late shock-reheating. Nevertheless, oxygen and minor parts of plagioclase were not in equilibrium between the host and the inclusion.

The results of isotope dilution analyses were shown in Fig. 2. The specimens A and B show the highest and slightly light-REE enriched pattern (A:20-10 times O-chondrite) and a large negative Eu anomaly. The patterns indicate characteristic features of phosphates and is complimentary to those of phosphate-poor and plagioclase-rich natures of samples D and E which have a large positive Eu anomaly. The specimen C taken from middle part of inclusion shows less fractionated pattern. The specimen D has the extreme middle REE depletion and the largest Eu anomaly (144 times chondritic). The degree of Eu anomaly is even larger than those previously reported [3,5]. Therefore, it was found that REE abundances are zoned from the outer parts to the inner core, but the abundances and fractionations are most extreme in middle parts of mantle at portion D. Assuming that the sub-sample (,105) represents whole spherical inclusion, the bulk concentration (weighted mean concentration) of REE were calculated. As shown in Fig. 2, the bulk REE abundances (dotted line) in the inclusion are grossly unfractionated and ordinary chondritic in absolute abundance (1.3-2.0 times ordinary chondrites). It is suggested that the bulk inclusion was formed from ordinary chondritic material and has been grossly in closed system in terms of REE abundance in silicate. This implies that the equilibrium solid/liquid fractionation did not occur during the early igneous formation [3]. One of the possibilities is that the inclusion represents a "giant olivine chondrule" formed in closed system by melting (probably in space) and the zonal structure of minerals was established during the melting and solidification without separation of solid from melt.

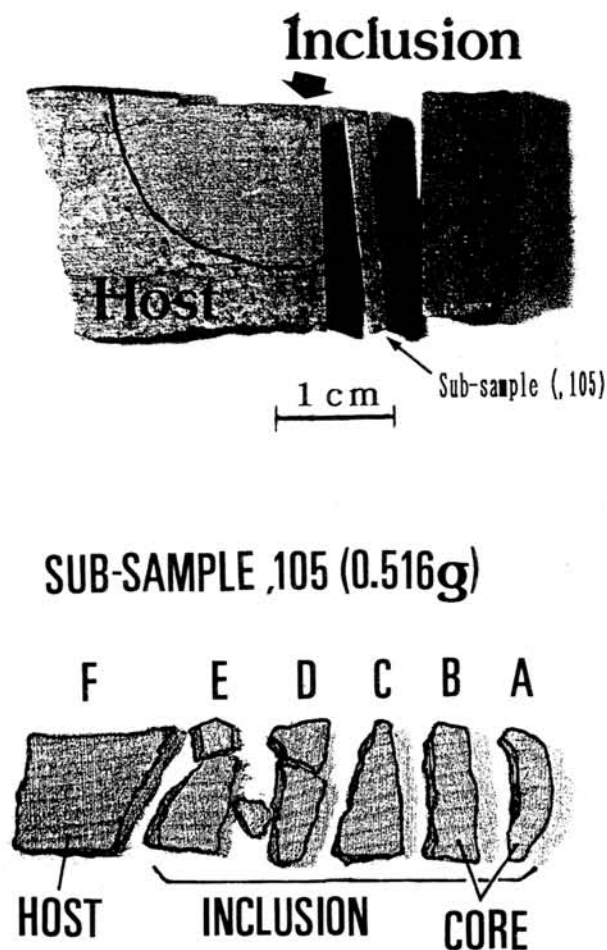
On the other hand, close inspection of the estimated bulk REE abundances in Fig. 2 indicates that the pattern is somewhat fractionated (light-REE enriched). Then it is considered that REEs were not sufficiently in closed system in the inclusion during the igneous formation and/or the later thermal metamorphism. In order to clarify this problem, further detailed petrographic investigations and chemical analyses are in progress. We thank Miss T. Kani for preparation of thin section.

References: [1] Yanai K. et al. (1983), Mem. natl. Inst. Polar Res. Spec. Issue No. 30, 29-35. [2] Nakamura N. et al. (1993) Papers 18th Symp. Antarct. Meteorites 234-235; see Proc. NIPR Symp. Antarct. Meteorites No. 7. [3] Nakamura N. et al. (1994) Proc. NIPR Symp. Antarct. Meteorites No.7, 125-144. [4] Mayeda T.K. et al. (1987), Mem. Natl. Inst. Polar Res. Spec. Issue 46, 144-150. [5] Warren P.H. and Kallemeyn G.W. (1988), Proc. Lunar Planet. Sci. Conf. 19th 475-486.

Table 1 Composition of the constituent minerals of Y-75097,52

Specimen	Olivine	Plagioclase		Phosphate	
	Fa(%)	Ab(%)	An(%)	Pyroxene	
Inclusion					
A	24.6 ± 0.4	76.2 ± 1.3	16.6 ± 1.6	+++++	(-)
B	25.2 ± 0.6	75.7 ± 2.0	16.1 ± 1.2	+++++	(-)
C	25.3 ± 0.4	75.0 ± 0.5	18.1 ± 0.6	+++	(-)
D	25.4 ± 0.6	72.9 ± 4.8	17.3 ± 1.2	(-)	(-)
E	25.3 ± 0.4	74.7 ± 0.6	19.2 ± 1.2	(-)	(-)
F	25.4 ± 0.8	73.7 ± 1.3	16.8 ± 1.5	(-)	(-)
Host F	24.5 ± 0.5	75.5 ± 1.0	16.5 ± 0.9	(-)	En=78.0 Fs=19.6

Fig. 1 Illustration of a slice sample of Yamato-75097,52 and sub-sample (,105) analyzed in this work.



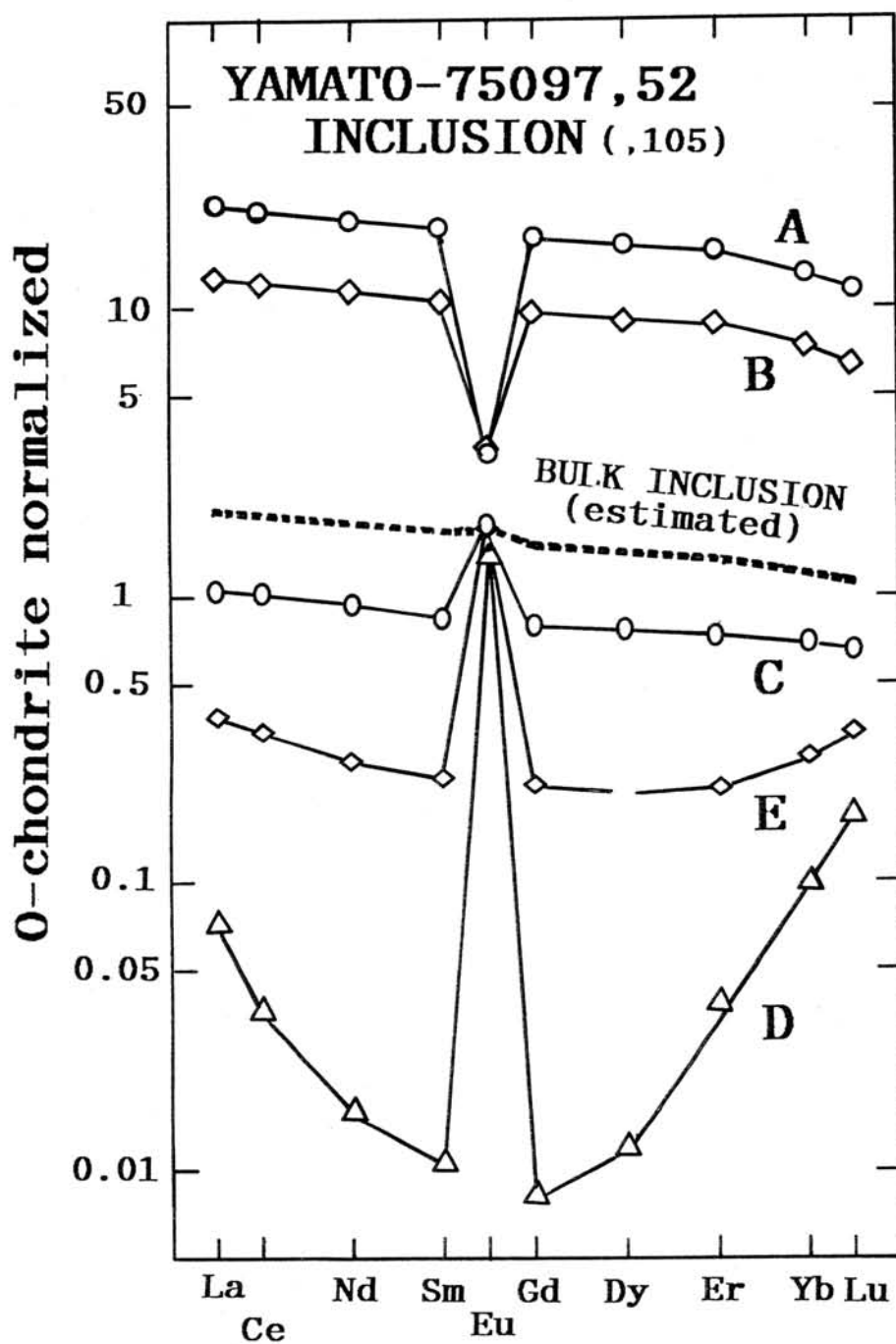


Fig. 2 The ordinary-chondrite normalized REE patterns for the different parts (inner part: A to outer part: E) of the inclusion of Y-75097. "Bulk inclusion" is bulk REE abundances calculated for weighted fractions of the sub-sample (,105).

NOBLE GAS ISOTOPIC COMPOSITIONS IN THE YAMATO-75097 INCLUSION REVEALED BY STEPWISE HEATING EXPERIMENT

Keisuke NAGAO¹⁾ and Yayoi MIURA²⁾

1) Institute for Study of the Earth's Interior, Okayama University, Misasa, Tottori-ken 682-01, Japan.

2) Department of Earth and Planetary Physics, University of Tokyo, Yayoi, Bunkyo, Tokyo 113, Japan.

Yamato-75097(L6) chondrite contains a dunitic inclusion which is similar to the Brachina meteorite in mineral assemblage and texture (Yanai et al., 1983). The inclusion showed characteristic noble gas compositions i.e., 1) very low concentrations of trapped noble gases with elemental ratios similar to subsolar or Ar-rich component (Crabb and Anders, 1981), 2) high concentrations of radiogenic ^{129}Xe and ^{244}Pu -derived fission Xe isotopes, and 3) presence of neutron induced ^{80}Kr , ^{82}Kr and ^{128}Xe (Nagao, 1993,1994; Ott et al., 1993). The noble gas signature resembles those of the brachinites, Brachina and ALH84025 (Ott et al., 1993). The results obtained by the total melt experiment (Nagao, 1994) indicate that the heating event which produced the brachina-like igneous materials occurred in the early solar system, ca. $\geq 4.55\text{Ga}$. An impact heating event at about 0.5Ga ago, which involved many L chondrites, is suggested by the concordant K-Ar ages for the host and the inclusion. This meteorite has been ejected from its parent body 21Ma ago.

For better understanding, we measured noble gases of the inclusion of Y-75097 in combination with a stepwise heating experiment. The temperatures employed in this work are shown in Tables 1 and 2. Gently crushed material weighing 33.0 mg was used in this analysis. Isotopic compositions of noble gases are summarized in Table 1 along with the published ones (Nagao, 1994). Trapped Ne component could not be observed in all temperature steps due to overwhelming abundance of cosmogenic Ne. $^{40}\text{Ar}/^{36}\text{Ar}$ ratio decreased from 430 to 100 as the increase of temperature. Concentrations of cosmogenic, radiogenic, fissionogenic and trapped noble gases are listed in Table 2. The concentrations of cosmogenic ^3He and ^{21}Ne agree with those obtained by the total melt experiment using 56.5 mg. Whereas, the concentration of cosmogenic ^{38}Ar is twice the previous value, suggesting higher concentration of Ca in our sample compared with that of the previous one. Discordances between the two analyses are also observed in the concentrations of radiogenic, fissionogenic and trapped gases. The radiogenic ^{129}Xe concentration is 1/3 of the previous one, while the fission-derived ^{136}Xe concentration is about 7 times higher. Trapped ^{36}Ar concentration is much higher than the previous value. Accordingly, the trapped $^{36}\text{Ar}/^{132}\text{Xe}$ ratios are much higher than the chondritic values and in or even more higher than the range for E chondrites and brachinites with the subsolar component. The total values of 2560 and 5.85 for $^{36}\text{Ar}/^{132}\text{Xe}$ and $^{84}\text{Kr}/^{132}\text{Xe}$, respectively, are identical with those of the South Oman E chondrite, which are the highest ratios so far observed in E chondrite group (Crabb and Anders, 1981). The maximum release of the component is 1000-1200 °C. These results indicate heterogeneous distribution of noble gases as well as the parent nuclides such as Pu, I and K in the inclusion.

References: Crabb, J and Anders, E. (1981) G.C.A. 45, 2443-2464; Nagao, K. (1993) Papers 18th Symp. Antarct. Meteorites, 234-235; Nagao, K. (1994) Proc. NIPR Symp. Antarct. Meteorites 7, 197-216; Ott, U., Löhr, H.P. and Begemann, F. (1993) Papers 18th Symp. Antarct. Meteorites 236-239; Yanai, K., Matsumoto, Y. and Kojima, H. (1983) Mem. Natl Inst. Polar Res. Spec. Issue 30, 29-35.

Table 1. Noble gas isotopic compositions of Y-75097 inclusion.

Temp. (°C)	$^4\text{He}^{1)}$	$^3\text{He}/^4\text{He}$ (10^{-4})	$^{20}\text{Ne}^{1)}$	$\frac{^{20}\text{Ne}}{^{22}\text{Ne}}$	$\frac{^{21}\text{Ne}}{^{22}\text{Ne}}$	$^{36}\text{Ar}^{1)}$	$^{40}\text{Ar}^{1)}$	$\frac{^{38}\text{Ar}}{^{36}\text{Ar}}$	$\frac{^{40}\text{Ar}}{^{36}\text{Ar}}$	$^{84}\text{Kr}^{2)}$	$^{132}\text{Xe}^{2)}$	$\frac{^{129}\text{Xe}}{^{132}\text{Xe}}$
600	188	369 ± 1	0.205	0.846 $\pm .012$	0.858 $\pm .004$	0.0633	27.3	0.6029 $\pm .0066$	430.3 ± 2.0	5.46	1.07	1.27
800	215	775 ± 3	1.34	0.811 $\pm .003$	0.894 $\pm .003$	0.183	84.9	0.7253 $\pm .0026$	464.1 $\pm .9$	6.06	0.662	1.75
1000	106	916 ± 4	0.919	0.802 $\pm .003$	0.896 $\pm .003$	0.590	91.4	0.5246 $\pm .0008$	154.9 $\pm .2$	7.76	3.25	5.05
1200	24.6	557 ± 11	2.42	0.830 $\pm .001$	0.928 $\pm .003$	1.11	150	0.6666 $\pm .0009$	134.3 $\pm .2$	19.3	12.9	30.9
1400	0.94	300 ± 150	2.76	0.845 $\pm .002$	0.937 $\pm .003$	0.384	38.1	0.6963 $\pm .0029$	99.3 ± 1.0	5.65	6.38	50.8
1600	0.05	n.d.	0.718	0.844 $\pm .003$	0.944 $\pm .003$	0.0331	4.26	0.993 $\pm .095$	129 ± 19	1.41	0.66	14.7
1800	0.10	n.d.	0.184	0.871 $\pm .026$	0.929 $\pm .005$	0.0391	7.02	0.64 $\pm .21$	179 ± 55	3.2	n.d.	n.d.
Total	535	650	8.55	0.830	0.920	2.40	403	0.646	168	48.8	24.9	
Nagao(1994)271		1407	9.43	0.844	0.943	0.645	205	1.018	317.7	16.2	7.5	49.7

1) $10^{-8}\text{cm}^3\text{STP/g}$, 2) $10^{-12}\text{cm}^3\text{STP/g}$.

$^{129}\text{Xe}/^{132}\text{Xe}$ ratios were calculated by subtracting cosmogenic and fissionogenic isotopes.

Weight of the sample used in this work was 33.0 mg.

Table 2. Concentrations of cosmogenic, radiogenic, fissionogenic and trapped noble gases.

Temp. (°C)	Cosmogenic			Radiogenic			Fissionogenic	Trapped				
	^3He	^{21}Ne	^{38}Ar	^4He	^{40}Ar	^{129}Xe	^{136}Xe	^{36}Ar	^{84}Kr	^{132}Xe	$\frac{^{36}\text{Ar}}{^{132}\text{Xe}}$	$\frac{^{84}\text{Kr}}{^{132}\text{Xe}}$
600	6.94	0.208	0.0299	152	27.3	0.206	0.071	0.044	5.36	0.908	485	5.90
800	16.7	1.48	0.112	128	84.9	0.448	0.063	0.111	5.79	0.599	1850	9.67
1000	9.72	1.03	0.226	55	91.4	6.39	1.67	0.444	6.29	1.59	2790	3.95
1200	1.37	2.71	0.606	17	150	54.7	10.9	0.720	14.3	1.84	3920	7.79
1400	0.029	3.06	0.223	0.8	38.1	46.3	5.23	0.241	3.48	0.930	2590	3.74
1600	n.d.	0.803	0.0304	n.d.	4.26	5.07	0.28	0.014	1.32	0.370	365	3.57
1800	n.d.	0.196	0.0201	n.d.	7.02	n.d.	n.d.	0.026				
Total	34.8	9.48	1.25	353	403	113	18.2	1.60	36.5	6.24	2560	5.85
Nagao(1994)	38.1	10.55	0.610	73	205	367	2.63	0.252	15	5.05	499	2.9

Concentrations of He, Ne and Ar are given in unit of $10^{-8}\text{cm}^3\text{STP/g}$, and those of Kr and Xe are in $10^{-12}\text{cm}^3\text{STP/g}$.

REE Abundances and Mg Isotopic Compositions of Allende Barred Olivine Chondrules

K. Misawa¹, N. Nakamura¹, T. Fujita², M. Kitamura² & H. Yurimoto³

¹ Dept. of Earth & Planet. Sci., Faculty of Science, Kobe Univ., Nada, Kobe 657, Japan

² Dept. of Geology & Mineralogy, Faculty of Science, Kyoto Univ., Sakyo, Kyoto 606-01, Japan

³ Inst. of Geoscience, Univ. of Tsukuba, Ibaraki 305, Japan

Barred olivine (BO) chondrules are mainly intermediate in major element composition between the abundant ferromagnesian chondrules and the rare Al-rich chondrules [1,2], and sometimes show fractionated REE patterns [3]. These chemical characteristics suggest that refractory precursor materials of BO chondrules could be related some type of CAIs. We have continued the combined chemical and Mg isotopic studies on BO chondrules to search for possible relationship between ferromagnesian chondrules and CAIs.

Allende BO chondrule R-11 is the first observed case that a ferromagnesian chondrule and a CAI (mainly Mg-Al spinel) joined together [4]. The REE pattern of R-11, excluding the spinel grain, shows a fractionated, HREE-depleted pattern (normalized La/Lu = 1.6) with a 30% positive Yb anomaly, indicating that the refractory lithophile precursor component of R-11 could be a condensate from the nebular gas and related to Group II CAIs (Fig. 1). The LREE (La - Eu) fractionation of R-11 is complementary to that of Allende chondrule No. 9 studied previously [3].

Mg isotopic compositions of spinel and plagioclase were measured by using the CAMECA IMS-3f ion microprobe at the Univ. of Tsukuba. The results are shown in Table 1. Unfortunately, we cannot obtain good data on Mg mass fractionations of plagioclase, mainly due to matrix effects and small grain size. The spinel exhibits enrichment of the heavier Mg isotopes, ~7‰/amu. However, there is a significant difference in Mg mass fractionation between the spinel and the host chondrule (~2.5‰/amu [5]). The spinel is enriched in heavier Mg relative to the host chondrule. The preservation of Mg isotopic heterogeneity in R-11 strongly suggests that chondrule precursor materials may have been isotopically heterogeneous. Plagioclase in the host chondrule does not show evidence for radiogenic ²⁶Mg*.

We have started direct-loading Mg isotopic analysis for small samples. The terrestrial spinel crystals were directly loaded for mass spectrometry without chemical treatment. As shown in Fig. 2, the $\Delta^{25}\text{Mg}$ of normal runs lie between -4‰ to 1‰ with a mean of ~-2‰. Comparing the range of fractionation there is ~-2‰ shift between the directly loaded sample and the chemically separated sample. Mg isotopic analysis of spinels from chondrules and from CAIs are in progress.

REFERENCES : [1] S. B. Simon & S. E. Haggerty *Proc. 11th LPSC*, 901 (1987) [2] M. K. Weisberg *Proc. 17th LPSC, JGR* 92, E663 (1987) [3] K. Misawa & N. Nakamura *GCA* 52, 1669 (1988) [4] K. Misawa & T. Fujita, *Nature* 368 (1994) [5] K. Misawa *et al. LPSC XXIV*, 991

Table 1. Mg Analytical Results (Ion Probe Data)

	$\Delta^{25}\text{Mg}^* \pm 2\sigma_m$ (‰)	$\delta^{26}\text{Mg}^\dagger \pm 2\sigma_m$ (‰)	$^{27}\text{Al}/^{24}\text{Mg}$ $\pm 2\sigma_m$
Spinel			
terrestrial	-11.7 ± 0.9	2.1 ± 1.2	1.96 ± 0.03
	-11.3 ± 0.7	-0.3 ± 2.6	1.96 ± 0.03
R-11	-4.1 ± 1.4	5.1 ± 1.3	2.52 ± 0.07
	$F_{\text{Mg}}^\ddagger = 7.4$		
Plagioclase			
terrestrial	-3.0 ± 0.8	2.9 ± 1.5	309 ± 1
	-2.8 ± 1.2	-0.9 ± 3.0	317 ± 3
R-11	-14	-0.3 ± 9	21.3 ± 1.2

* $\Delta^{25}\text{Mg} = ((^{25}\text{Mg} + ^{24}\text{Mg}^+)_{\text{meas}} / (^{25}\text{Mg} / ^{24}\text{Mg})_{\text{ref}} - 1) \times 1000$.

† $\delta^{26}\text{Mg} = ((^{26}\text{Mg} + ^{24}\text{Mg}^+)_{\text{meas}} / (^{26}\text{Mg} / ^{24}\text{Mg})_{\text{ref}} - 1) \times 1000 - 2 \times \Delta^{25}\text{Mg}$, where $(^{25}\text{Mg} / ^{24}\text{Mg})_{\text{ref}}$ and $(^{26}\text{Mg} / ^{24}\text{Mg})_{\text{ref}}$ are assumed to 0.12663 and 0.13932, respectively (Catanzaro *et al.* 1966).

‡ $F_{\text{Mg}} = \Delta^{25}\text{Mg} - \Delta_{\text{std}}^{25}\text{Mg}$ (‰).

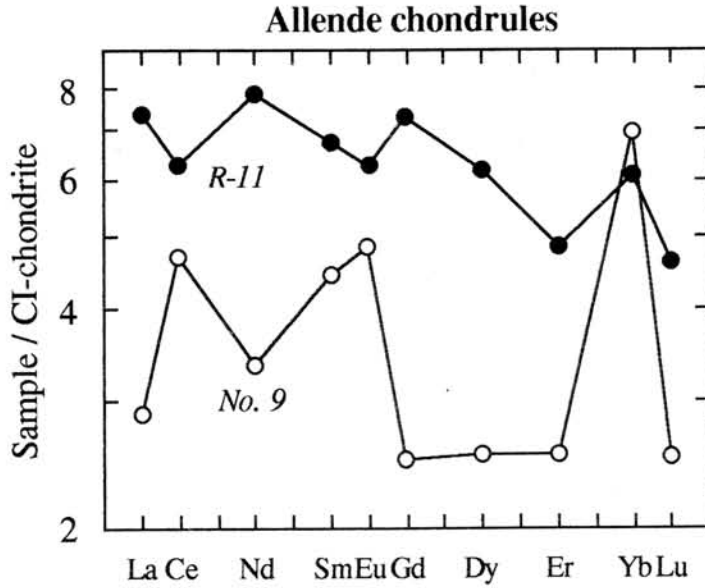


Fig. 1. The REE patterns of Allende chondrules. Data of Allende No. 9 (plagioclase bearing microporphyritic pyroxene chondrule) are from [3]. The LREE (La - Eu) fractionation is complementary in both chondrules.

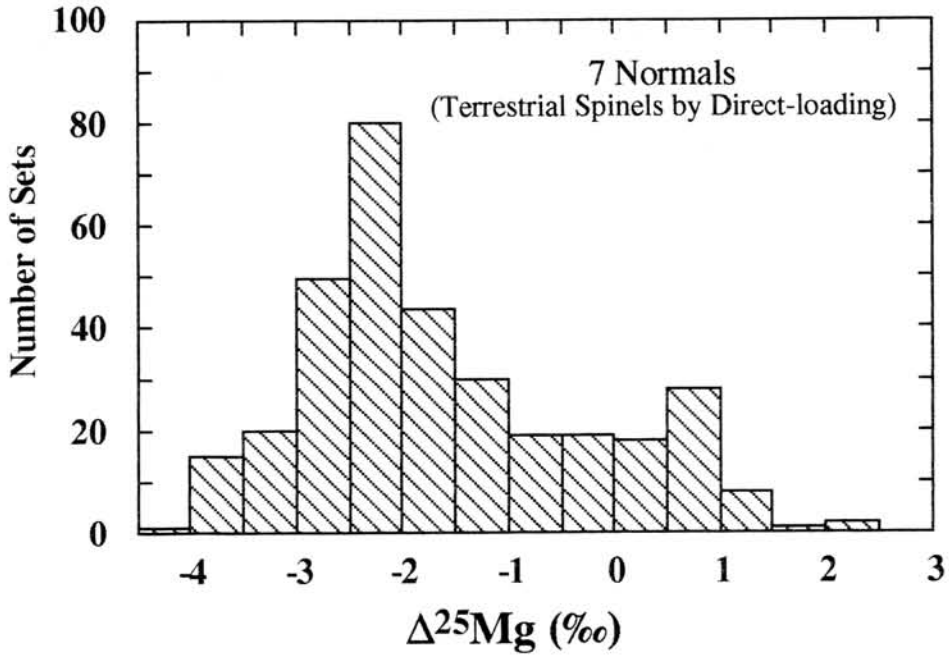


Fig. 2. Histogram of $^{25}\text{Mg}/^{24}\text{Mg}$ for terrestrial spinels. Permil deviation relative to $^{25}\text{Mg}/^{24}\text{Mg} = 0.12464$ is plotted.

ISOTOPIC, CHEMICAL AND TEXTURAL PROPERTIES OF ACID RESIDUES FROM VARIOUS METEORITES (II)

N. Kano, K. Yamakoshi and H. Matsuzaki

Institute for Cosmic Ray research, University of Tokyo, Tanashi, Tokyo 188.

Detail analysis of primitive meteorites particularly acid insoluble fractions and metal phases from them has been continued for study of the evolution of the solar system and information on processes of nucleosynthesis in the pre-solar stage. Last year we reported the analytical results of acid residues from Allende (CV3), Nuevo Mercurio (H5) and Canyon Diablo (IA) [1]. This talk deals with the chemical and textural properties of acid residues from Murchison (CM2), La Criolla (L6), Qingzhen (EH3) and Cr isotopic compositions in these meteorites measured so far. Cr isotopic analyses are performed to investigate 1) ^{54}Cr (produced by neutron-rich e-process) anomaly and 2) the effect of extinct radioactive nuclide ($^{53}\text{Mn} \rightarrow ^{53}\text{Cr}$).

Major element compositions in acid residues of Murchison, La Criolla, Qingzhen are shown in Table 1 along with the fraction of these acid residues. Representative SEM photographs with EDS spectra of the aliquants of acid residues of them are shown in Fig. 1. It is known that spinel, hibonite, chromite etc. as well as carbonaceous matter are present in Murchison residues [e.g. 2], and in our sample, EDS spectrum suggests that spinel (MgAl_2O_4) and chromite (FeCr_2O_4) may be included. But high S content indicates that it also contains much S-bearing particles and/or organic matter or something. On the other hand, acid residues of La Criolla consist of chromite for the most part judging from TEM bright field image and SAD (selected area diffraction) pattern (Fig. 2), abundant Cr and Fe contents by INAA and Cr:Fe ratios of about 2:1 in the EDS spectra. Ti and V are also much enriched (Ti: 1.51%; 35 times/CI; V: 0.445%; 79 times/CI) in La Criolla residues. In acid residues of Qingzhen, Cr content is relatively low than that of other meteoritic residues and Cr is mostly distributed in HCl/HF soluble fraction (table 2). It is consistent with the fact that enstatite chondrite contain no chromite [3]; and enstatite (MgSiO_3), oldhamite (CaS) and daubreelite (FeCr_2S_4) which are characteristics of E chondrite may be present in Qingzhen residues judging from EDS spectrum and so on. In addition, refractory siderophiles are generally enriched in acid residues for any kind of meteorites. We are going ahead with TEM/SEM-EDS analyses of these acid residues in details to identify minerals therein definitely.

The samples (HCl/HF residues) were decomposed in sealed teflon vessels by a microwave dissolution method with several mixed acids and Cr was separated by precipitation and anion exchange method [4]. In mass spectrometric techniques of Cr, the zone-refined (99.995%) outgassed V-shaped Re single filament with silica gel and boric acid was employed. Isotopic analyses were performed by a VG 354 thermal ionization mass spectrometer.

Principal Cr isotopic analytical results of some chondrite meteorites were shown

in Fig. 3. The most noticeable result is that the enrichment of $^{54}\text{Cr}/^{52}\text{Cr}$ relative to normal (Cr reagent standard) value is detected in a specimen of Qingzhen acid soluble fraction. In addition, in acid residues of Murchison, $^{54}\text{Cr}/^{52}\text{Cr}$ are also enriched relative to normal values though errors are rather large. In recent paper, Rotaru et al. [5] suggested that Cr isotopic composition of the Solar System results from the mixing of several major components with distinct isotopic compositions, and that particularly C1 and C2 chondrites keep, at least partially, the memory of their initial isotopic diversity. ^{54}Cr is synthesized in a neutron-rich nuclear statistical equilibrium; so our results suggest that such heterogenities are also present in unequilibrated EH chondrite: Qingzhen. In other words, some grains carrying exotic Cr components still remained in Qingzhen. Isotope abundance studies in primitive meteorites concentrating on more specific mineral phases by means of stepwise dissolution method, are currently underway. In addition, we are preparing to carry out Cr isotopic analyses in other unequilibrated E chondrite.

Acknowledgements-- We thank Y. Suzuki of Yamagata University for analyses of samples by TEM/SEM-EDS ; H.Mori of Tokyo University for valuable suggestions for analyzing the results of TEM images-SAD patterns and SEM-EDS spectra of these samples.

References : [1] Kano, N. et al. (1993) Abs. of 18th NIPR Symp. 170-173 [2] Alaerts, D. N. et al. (1980): GCA, **44**,189-209 [3] Srinivasan, K. et al. (1977): JGR, **82**, 762-778. [4] Lee, T. and Tera, F. (1986): GCA, **50**, 199-206. [5] Rotaru et al. (1992): Nature, **358**, 465-470.

Table 1 Major element contents in acid residues of three meteorites

Sample	Acid residues fraction (wt.%)	combustion method(%)				INAA [#] (%)					
		C*	H*	N*	S*	Cr	Fe	Ni	Al	Mg	
Murchison(CM2)	HCl/HF residue	3.12	34.6	2.10	1.48	46.5	1.14	0.694	0.240	0.958	0.943
	HCl/HF-HNO ₃ residue	1.30	29.5	1.71	2.56	27.5	1.75	3.50	0.191	1.13	2.15
La Criolla(L6)	HCl/HF residue	0.83	1.20	0.16	---	12.8	35.6	18.8	0.424	2.76	2.75
Qingzhen (E3)	HCl/HF residue	0.65	6.26	2.05	0.71	7.27	0.409	0.800	0.0216	0.673	7.92

*) We are indebted to T. Seki of Tokyo University for determining C,H,N,S.contents of samples.

#) Errors of INAA data are below 5% except Ni in Qingzhen(~10%). Neutron irradiations and use of the counter facilities were carried out at the Inst. for Atom. Energy Res. in Rikkyo University.

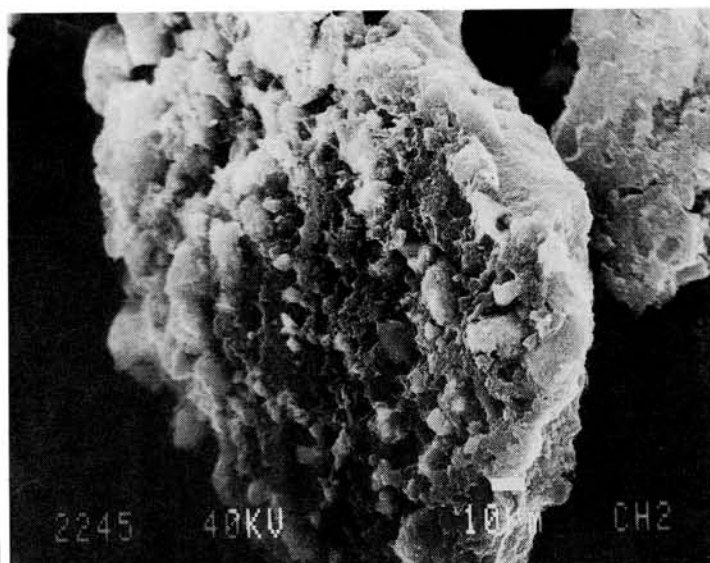
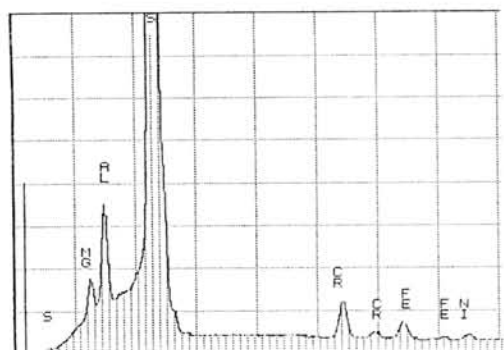
Table 2 Distribution of Cr in three meteorites (ppm) by AAS[#] and INAA[#]

	HCl/HF soluble	HCl/HF residue	HNO ₃ soluble	HNO ₃ residue	Total (Bulk)
Murchison	2480	356	109	228	3090 ^{*1)}
La Criolla	674	2955			3580
Qingzhen	2216	26.6			3100 ^{*2)}

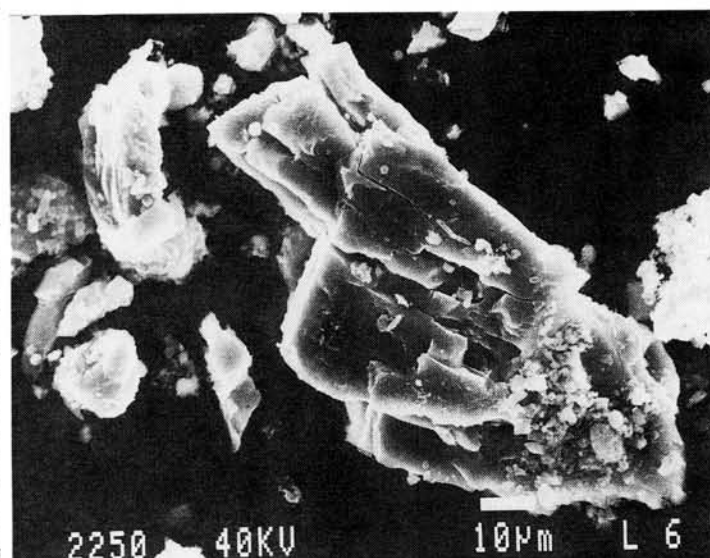
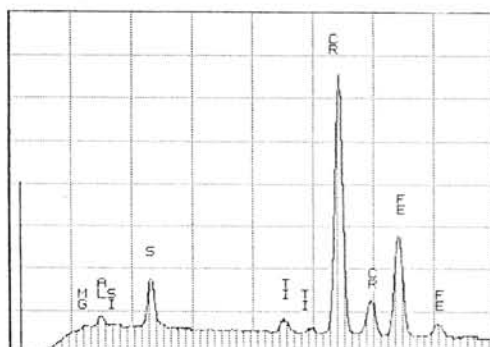
*) Data for whole meteorite of Murchison and Qingzhen are by Kallemyne and Wasson: 1)GCA(1981), **45**, 1217; 2)GCA(1986), **50**, 2153

#) Errors of data are below 5%.

(a): Murchison(CM2)



(b): La Criolla(L6)



(c): Qingzhen(E3)

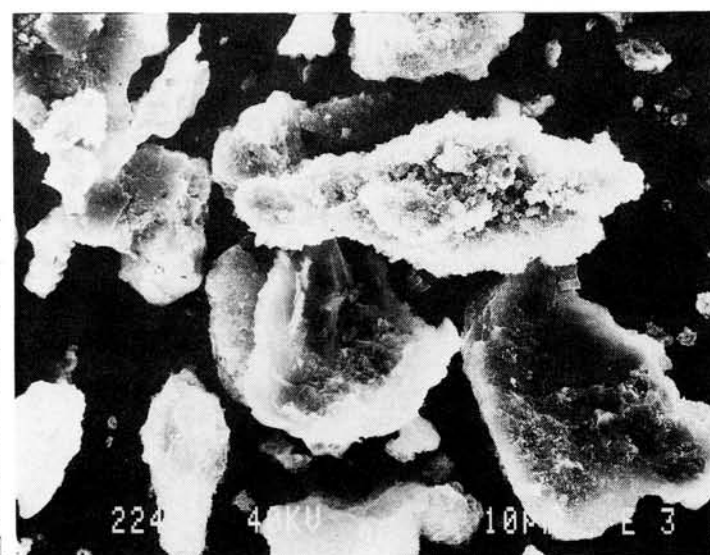
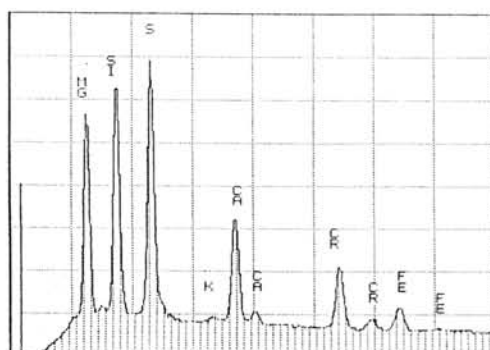


Fig. 1 Representative SEM pictures with EDS spectra of the aliquants of acid(HCl/HF) residues from three meteorites((a): Murchison(CM2), (b): La Criolla(L6), (c):Qingzhen(E3)).

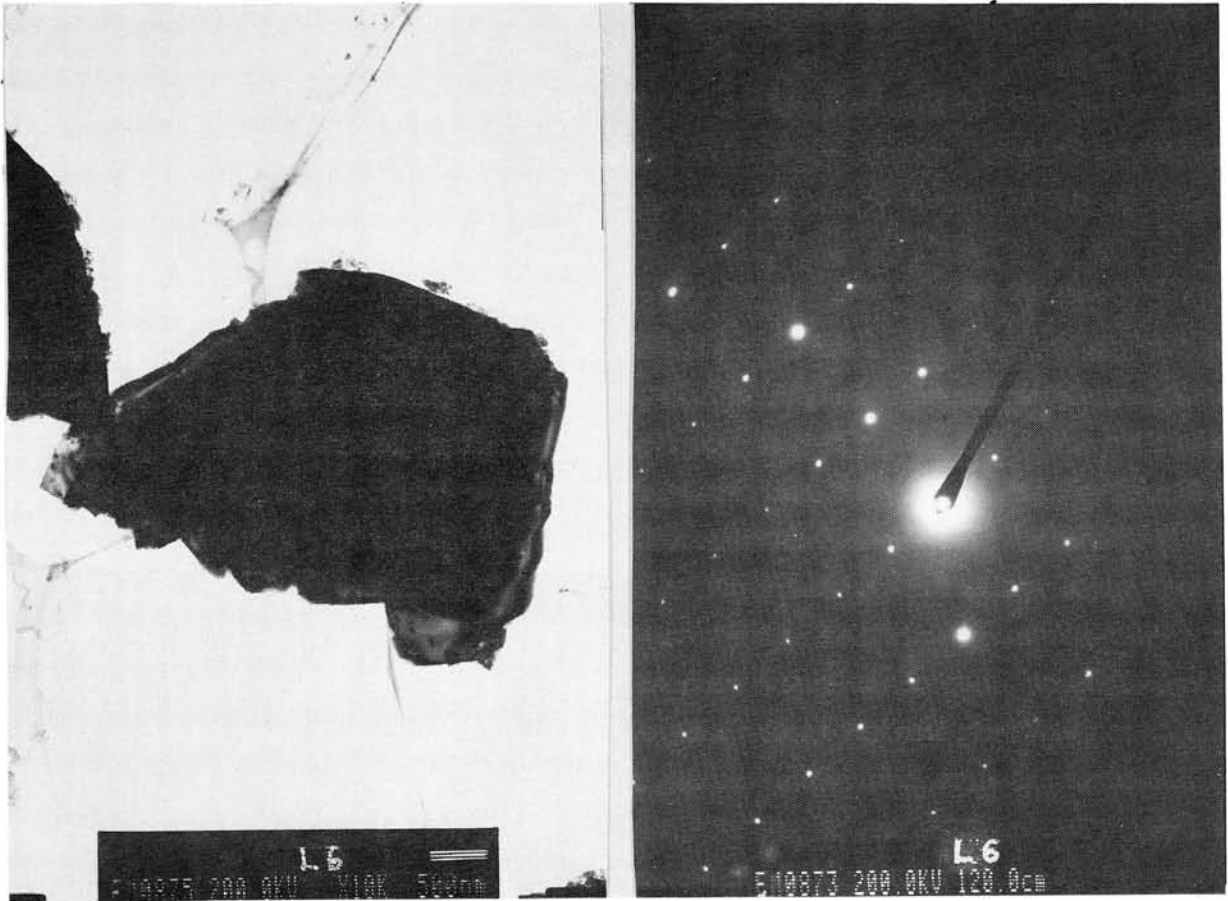
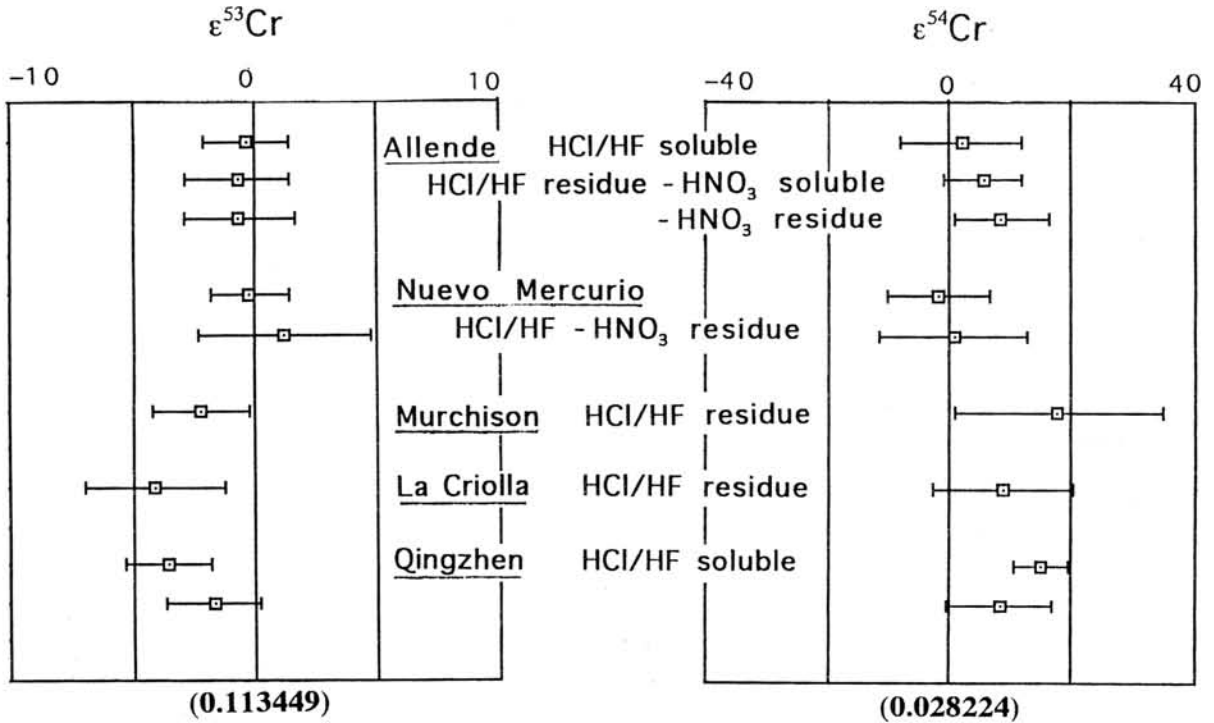


Fig.2 TEM bright field image and SAD pattern of the aliquants of acid residues from La Criolla.



All isotope ratios are normalized to $^{50}\text{Cr}/^{52}\text{Cr}=0.051859$ by exponential law. (Shields et al.1966)

Fig.3 Cr isotopic compositions in some chondrite meteorites.

RHENIUM, OSMIUM AND IRIDIUM IN ANTARCTIC UNEQUILIBRATED ORDINARY CHONDRITES

Ozaki, H. and Ebihara, M.

Department of Chemistry, Faculty of Science, Tokyo Metropolitan University,
Minami-ohsawa, Hachioji, Tokyo 192-03, Japan

Introduction

Cosmochemically, Re, Os and Ir are classified as refractory siderophile elements. According to thermodynamic calculation, these elements are scarcely unfractionated during the condensation process. However, their abundance ratios have not always agreed with each other among the meteorite classes. After a longstanding consideration about this problem, Anders and Grevesse (1989) concluded that this disagreement was due to mainly differences in laboratories or analysts and that these elements were not fractionated in chondrites. The discussion about a fractionation of these elements in ordinary chondrites (OC) has been based mainly on the data of equilibrated ordinary chondrites (EOC) because of the scarcity of the data for unequilibrated ordinary chondrites (UOC). Considering that UOC are more primitive in OC, we may use the data of UOC rather than those of EOC. Refractory siderophile elements such as Re, Os and Ir are hosted mostly in metallic phases in chondrites and are partly localized in small region such as tiny metal nuggets in primitive meteorites (e.g. Rambaldi, 1976). As their absolute contents are accordingly highly dependent on the content of such metallic phases, simultaneous determination of these elements is highly desirable for discussion about their relative abundances. In this study, we simultaneously determined Re, Os and Ir in Antarctic UOC by radiochemical neutron activation analysis (RNAA) in order to discuss the fractionation of these elements among them. In addition, weathering effect on their abundances is also discussed.

Experimental

All meteorite samples used in this study are Antarctic UOC, which were loaned by NIPR and NASA. The samples were received in chips, which were sampled from interior portions of the individual meteorites. About a few hundred mg of each sample was ground in an agate mortar and 50 to 100 mg of the powdered sample was sealed in a synthesized quartz tube. The samples were irradiated in the JRR-4 reactor of the Japan Atomic Energy Research Institute at a neutron flux of $5.0 \times 10^{13} \text{ cm}^{-2}\text{sec}^{-1}$ for 12 hours. Reference standards were prepared from chemical reagents and were simultaneously irradiated with the meteorite samples. After irradiation, the samples were cooled for 5 days and were subjected to the radiochemical purification of Re, Os and Ir. The purification procedure is described in Ozaki et. al. (1994).

Results and Discussion

Analytical results in this work are shown in Figs. 1 and 3. All data plotted are relative abundances normalized to C1 chondrite values (Anders and Grevesse, 1989). For comparison, literature values for non-Antarctic ordinary chondrites is shown in Fig. 2 and 4. Analytical uncertainties are deduced to be less than 10% for these three elements. As can be seen in Fig. 1, Os and Ir abundances in Antarctic UOC are well correlate with each other, and such a good correlation is recognized in non-Antarctic OC (Fig. 2) as well as in Antarctic UOC. On the contrary, Re and Os in Antarctic UOC (Fig. 3) are seem to be considerably fractionated from each other compared with Ir and Os (Fig. 1). Although we can not discussed about the siderophile abundances in non-Antarctic UOC because of scarcity of data, the correlation between Re and Os in non-Antarctic EOC (Fig. 4) is apparently better than that of Antarctic UOC (Fig. 3). Therefore, it is suggested that Re is fractionated from Os and Ir in Antarctic UOC. If such a fractionation is characteristic feature for Antarctic UOC, this could be extended to the discussion about the difference between Antarctic and non-Antarctic meteorite groups.

Ir/Os ratios of Antarctic UOC is nearly identical to that of C1 chondrite (Fig. 1), whereas their Re/Os ratios (especially those for H group) seem to be slightly higher than C1 value (Fig. 3). Such as disagreement can also be recognized in non-Antarctic OC. Therefore, it is suggested that Re is fractionated from Os and Ir among chondritic meteorites. Such a fractionation is thought to have been caused during condensation and/or accretion processes. Alternatively, the fractionation may have reflected the elemental heterogeneity in solar nebula.

As it has been recognized that Re was one of the mobilized elements by aqueous alteration on the meteorite parent body (Ebihara et. al., 1982), Re may have been fluctuated in Antarctic UOC by terrestrial weathering on Antarctica. In our INAA work of Antarctic UOC (Ebihara and Ozaki, 1994), it was suggested that Na and Au were slightly redistributed by terrestrial weathering on Antarctica. Considering that the fluctuation of Re in Antarctic UOC is bigger than those of Na and Au and the mobility of Re by aqueous alteration is smaller than that of Au, the fractionation of Re from Ir and Os in Antarctic UOC is inherent rather than redistributed by terrestrial weathering.

References

- Anders, E. and Grevesse, N. (1989) *Geochim. Cosmochim. Acta* **53**, 197-214.
 Rambaldi, E. (1976) *Earth Planet. Sci. Lett.* **31**, 224-238.
 Ozaki, H., Ebihara, M. and Nakahara, H. (1994) *J. Radioanal. Nucl. Chem.* (submitted).
 Ebihara, M., Wolf, R. and Anders, E. (1982) *Geochim. Cosmochim. Acta* **46**, 1849-1861.
 Ebihara, M. and Ozaki, H. (1994) *Meteoritics* (submitted)

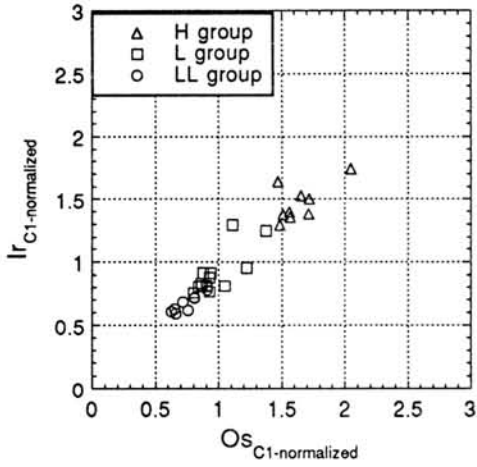


Fig. 1. Relationship between Ir and Os in Antarctic UOC.

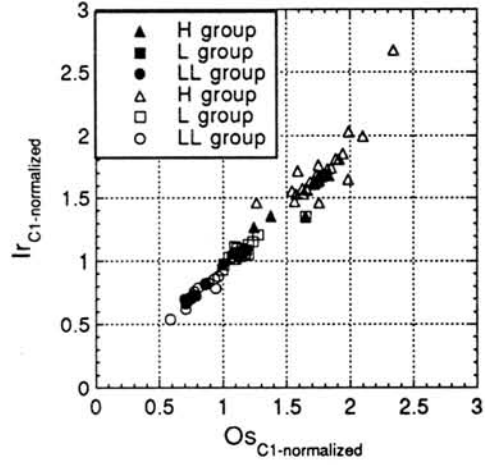


Fig. 2. Relationship between Ir and Os in non-Antarctic OC (open - EOC; filled - UOC).

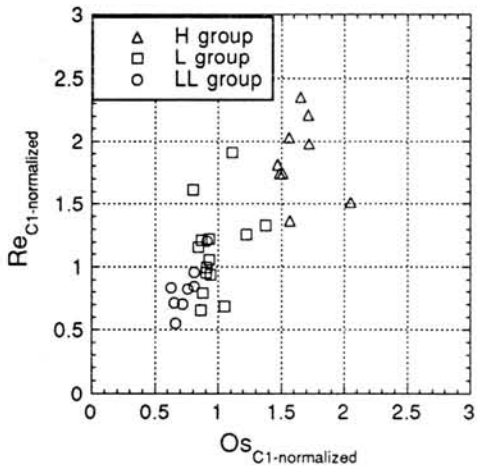


Fig. 3. Relationship between Re and Os in Antarctic UOC.

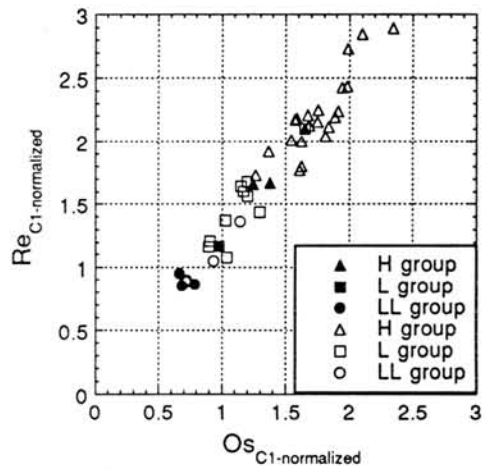


Fig. 4. Relationship between Re and Os in non-Antarctic OC (open - EOC; filled - UOC).

Preliminary study of element distribution trends in metallic fractions of an Antarctic ordinary chondrite ALH77231.51 (L6)

Ping KONG¹, Mitsuru EBIHARA¹ and Kazutoyo ENDO²

¹Department of Chemistry, Faculty of Science, Tokyo Metropolitan University, Hachioji, Tokyo 192-03, Japan

²Faculty of Pharmacy, Showa College of Pharmaceutical Sciences, Machida, Tokyo 194, Japan

Introduction

Kamacite and taenite grow with a geometric orientation parallel to each plane and form a specific crystallographic pattern during cooling processes of iron meteorites, called as WIDMANSTATTEN pattern. This fascinating pattern is believed to be an imprint of the thermal history that an iron meteorite parent body has experienced [1,2,3]. Kamacite and taenite are also major metallic phases in ordinary chondrite, but are found usually to be separated from each other, in individual grains of pure alloy [4]. WOOD[4] interpreted the concentration gradients of nickel found in two metal phases as a result of exsolution of kamacite from taenite followed by sluggish diffusion of Ni into the taenite crystals upon cooling through approximately 500°C. RAMBALDI[5,6] analyzed trace element distributions in different sizes of metal grains of ordinary chondrites and found that elements have different affinities either to fine grains corresponding to taenite or coarse grains corresponding to kamacite. In this paper, we separated taenite from kamacite by using a selective chemical dissolution method and then evaluated the distributions of various elements between taenite and kamacite. We hope we can get some messages of thermal histories which ordinary chondrite parent bodies have experienced by comparing element distribution patterns among different petrographic chondrites. We report here the preliminary results obtained from an Antarctic L6 ordinary chondrite.

Sample and methods

767mg bulk sample of an Antarctic meteorite ALH77231.51 (L6) was first treated by hand magnetic separation. As considerable amount of silicates were found to be attached with the magnetic fraction and could not be cleanly separated physically, a chemical dissolution method was applied. We got pure metals by boiling the magnetic fraction in concd. HF acid for as short as 2 minutes [7], and then continually treated the metal fraction to get taenite. The separation scheme is shown in Fig. 1.

Results and discussions

M-1 is the least treated fraction of metal separates, corresponding to 10.4% of bulk sample. No silicates were found to be attached with this sample under microscopic observation. Mössbauer spectrum showed that M-1 composed almost of α -phase, kamacite (relative intensity: 93%). This means that our procedure is effective to remove silicates from magnetic separates but keep the metal intact. Mössbauer spectra and INAA analyses showed that M-2, M-3 and M-4 have similar compositions. This means that 5 minute boiling with concd. HF can considerably remove kamacite but taenite and tetrataenite are scarcely affected even with boiling for up to 15 minutes. So, we can accurately compare the chemical compositions of taenite and tetrataenite with those of kamacite.

Mössbauer spectroscopy

Mössbauer spectra of four metal portions (M1—M4) were obtained at room temperature by using a Co/Rh source (figure 2).

Spectrum of M-1 shows that this metal fraction composes mostly of α -phase (kamacite). After removing of kamacite, spectra of tetrataenite can be clearly seen for M-2, M-3, and M-4. Tetrataenite is an ordered taenite that can be formed in meteorites with a slow cooling rate below a critical temperature 320°C[8]. Spectra of M-2, M-3 and M-4 show similar features but the proportion of tetrataenite is slightly increased with prolonging boiling time with HF acid. On the basis of different leaching rate with concd. HF acid between kamacite and taenite (and maybe also tetrataenite), we can determine element distributions in these different fractions.

INAA results

Table 1 lists trace element contents in the metal fractions of ALH77231.51 analyzed by INAA. Contents of Ni in M-2, M-3 and M-4 show that these three metal fractions are mainly composed of taenite with a mean value of 36% for Ni content. Siderophile elements are shown to be heterogeneously distributed in these fractions. On the basis of Fe-Ni phase diagram, it is suggested that kamacite that equilibrates with taenite having 36% Ni contains 7% of Ni. So we can calculate the proportion of kamacite in M-1 to be 90%. Based on these compositions, we can calculate siderophile element contents in taenite, kamacite and their concentration ratios between taenite and kamacite (listed in the last three columns of Table 1). Our data imply the following characteristic features for the metallic phase in ALH77231 L6 chondrite:

- (1) Cu shows the highest affinity to taenite; 21 times higher than that of kamacite.
- (2) Rh, Ge and Sb along with Ni show similar distributions between taenite and kamacite.
- (3) Co and Mn are depleted in taenite and enriched in kamacite.
- (4) Arsenic is fairly distributed in kamacite and taenite.
- (5). Refractory siderophiles (Re, Os and Ir) are enriched in taenite, but are not correlated with Ni contents between taenite and kamacite.

The distribution trends of elements in taenite and kamacite should be controlled by their elemental properties, their condensation processes and thermal histories which parent bodies of meteorites have experienced (especially metamorphism temperature and cooling rate). We expect to get some information regarding these properties by comparing distribution tendencies of elements in different meteorites. Research on other meteorites is now in progress.

References

- [1]. WOOD J. A. (1964) *Icarus* 3, 429-459.
- [2]. GOLDSTEIN J. I. and OGILVIE R. E. (1965) *Geochim. Cosmochim. Acta* 29, 893-920.
- [3]. NARAYAN C. and GOLDSTEIN J. I. (1985) *Geochim. Cosmochim. Acta* 49, 397-410.
- [4]. WOOD J.A. (1967) *Icarus* 6, 1-49.
- [5]. RAMBALDI E. R. (1976) *Earth and Planetary Science Letters* 31, 224-238.
- [6]. RAMBALDI E. R. (1977) *Earth and Planetary Science Letters* 36, 347-358.
- [7]. DANON J., SCORZELLI R.B. and SOUZA AZEVEDO I. (1979) *Nature* 281, 469-471.
- [8]. CHAMBERDD A., LAUGIER J., and PENISSON J. M. (1979) *J. Magn. Magn. Mater.* 10, 139-144.

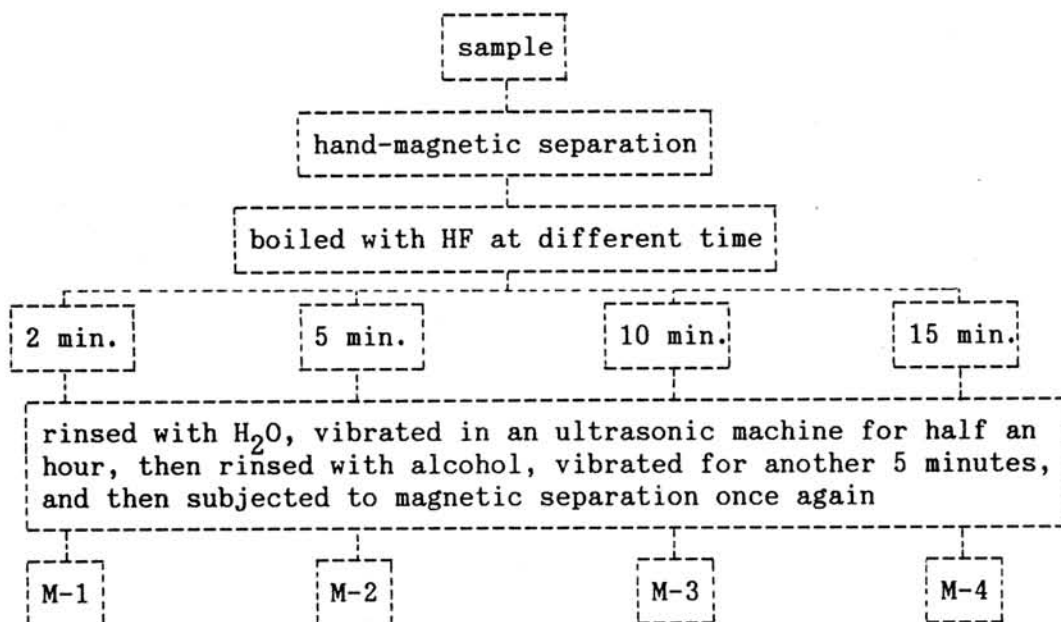


Fig. 1. A schedule of the procedure used for the separation of metal fractions from ALH77231(L6)

Table 1. Element contents (in ppm, otherwise indicated) in Antarctic ordinary chondrite ALH77231(L6) by INAA

element	Odassa	Allende this work recommended	Bulk	M-1	M-2	M-3	M-4	taenite*	kamacite	taenite/ kamacite	
As	≅12 [#] (1.3%) [@]	1.34 (4.2%)	0.8-3	1.07 (13%)	16.7 (2.2%)	15.2 (2.0%)	14.8 (3.3%)	14.8 (3.2%)	15.0	15.2	0.99
Au	1.83 (1.1%)	0.17 (2.6%)	0.15 (6.1%)	0.147 (3.9%)	1.66 (1.3%)	5.10 (0.98%)	4.26 (0.99%)	4.90 (1.0%)	4.79	1.30	3.7
Co	4205 (2.7%)	595 (1.4%)	600 (17%)	586 (0.73%)	6840 (1.0%)	2660 (1.1%)	3580 (2.0%)	2850 (1.0%)	2990	7280	0.41
Cr	51.5 (6.8%)	3580 (1.2%)	3630 (3.8%)	3930 (1.1%)	90.9 (3.6%)	218 (4.2%)	212 (4.9%)	382 (2.7%)	258	71.7	3.6
Cu	355 (3.7%)			626 (4.2%)			4010 (2.3%)	4590 (2.7%)	4280	206	21
Ge	≅285 [#] (7.6%)		11-17.9	338 (11%)	1345 (11%)	1220 (8.6%)	1030 (8.2%)	1230	236	5.2	
Ir	1.60 (2.4%)	0.833 (2.1%)	0.74 (12%)	0.512 (1.5%)	2.11 (2.0%)	6.48 (2.0%)	5.44 (2.1%)	4.99 (2.0%)	5.78	1.69	3.4
Mn	50.4 (4.2%)	1480 (4.7%)	1472 (5.2%)	2420 (2.9%)	181 (3.5%)		55.5 (5.3%)	51.5 (7.7%)	53.7	196	0.27
Ni(%)	8.04 (2.5%)	1.52 (2.4%)	1.42 (1.4%)	1.31 (2.1%)	9.98 (2.5%)	40.1 (2.5%)	30.7 (2.5%)	35.3 (2.4%)	36.0	7.00	5.1
Os	2.53 (6.8%)	0.88 (21%)	0.4-0.77	5.02 (7.2%)	14.9 (5.5%)	10.5 (9.7%)	11.1 (4.9%)	12.6	4.15	3.0	
Pt	7.22 (12%)			17.4 (18%)	37.6 (6.7%)	34.3 (6.9%)	34.9 (20%)	35.9	15.2	2.4	
Re	0.44 (6.5%)			0.675 (4.1%)	1.89 (5.1%)	1.89 (5.3%)	1.38 (11%)	1.76	0.55	3.2	
Rh	1.49 (9.5%)			0.86 (23%)		3.30 (13%)	3.40 (8.9%)	3.34	0.58	5.8	
Sb	0.564 (8.4%)			0.614 (20%)	2.00 (5.5%)	2.09 (6.1%)	2.130 (11%)	2.06	0.45	4.6	

* means of M-2, M-3 and M-4. [#] used as standard. @: errors due to counting statistics (1σ).

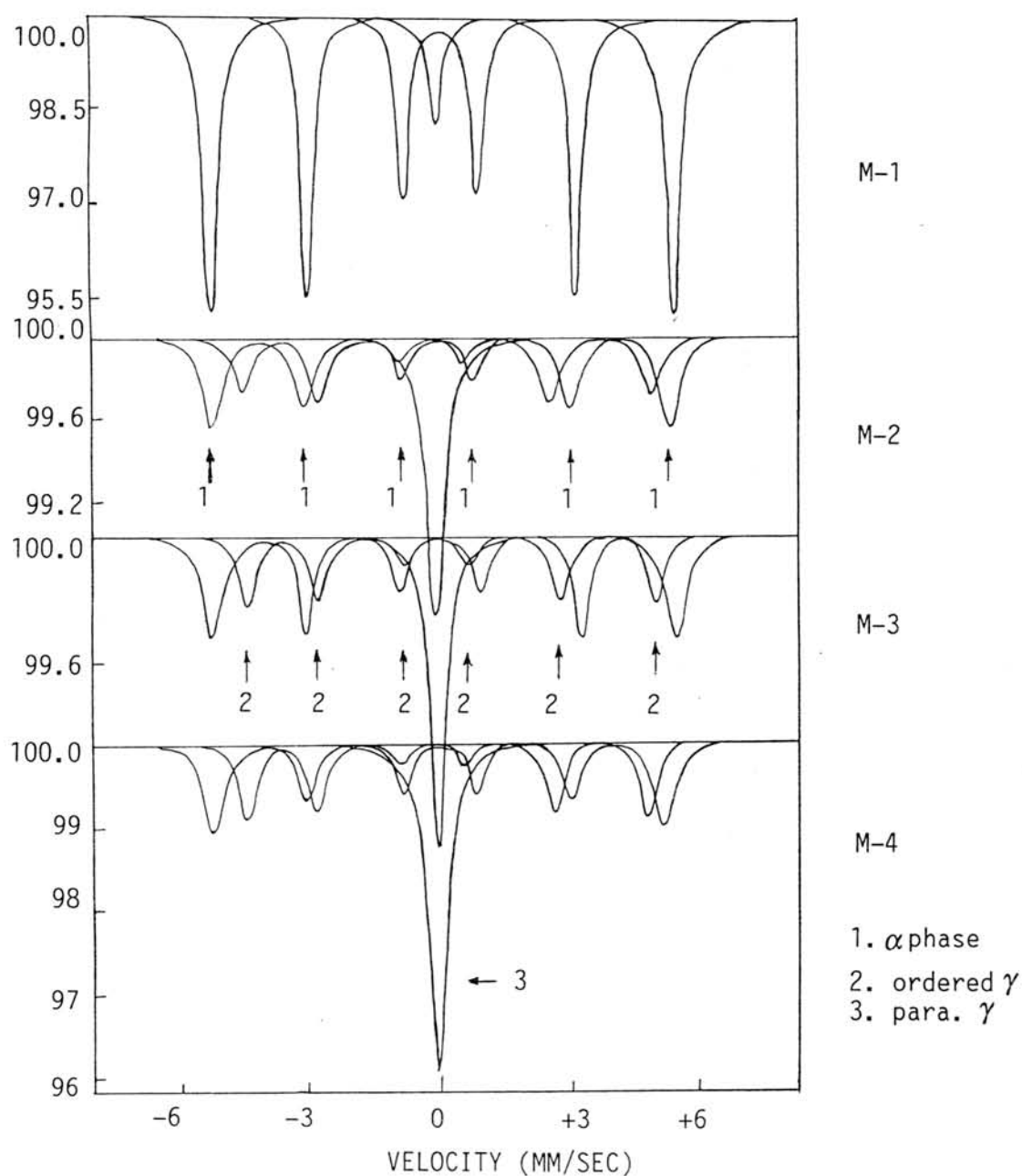


Fig. 2. Mossbauer spectra of metal fractions from ordinary chondrite ALH77231.

Table 2. Mossbauer parameters for metal fractions separated from ALH77231

parameter	M-1			M-2			M-3			M-4		
	α phase	para. γ	ordered γ	α phase	para. γ	ordered γ	α phase	para. γ	ordered γ	α phase	para. γ	ordered γ
IS(mm/s)	0.010	-0.100		0.031	-0.032	0.000	0.015	-0.060	0.000	-0.113	-0.086	0.000
ΔE_q (mm/s)	0.00	---		0.00		0.47	0.00	---	0.10	0.00	---	0.19
HF(kOe)	339	---		335		297	330	---	289	330	---	291
A (%)	93	7		47	27	26	46	26	28	38	31	31

MAGMATIC REPLACEMENT PROCESSES IN UREILITES

O.B.Mitreikina., N.G.Zinovieva and L.B.Granovsky.

Department of Petrology, Faculty of Geology, Moscow State University, Lenin Gory,
Moscow 119899, Russia.

The research on mineral parageneses of ureilites showed that an interstitial material formed by isochemical re-crystallization and partial melting of rock-forming minerals: olivine and pyroxene [5]. The existence of pyrope in the re-crystallized areas and the assemblage of new-formed Mg-rich minerals, Fe-metal, Fe - and Si - carbide, Cr-Fe - sulfides, Cr-spinellid, carbon material and diamonds let us make a conclusion that the re-crystallization of ureilites took place in high pressure conditions by the action of abyssal melts rich in hydrocarbon fluids.

A core of the planet rich in hydrocarbons, siderophile elements and noble gases could be a source of such melts. It's possible to understand the resemblance of these melts to a matrix of the carbonaceous chondrites from the point of views of the melted nature of non-differentiated chondrite bodies [2,3,4]. A primary separation of a chondrite melt into silicate chondrules and the iron-silicate matrix makes possible a gravitation separation of the carbonaceous chondrite matrix melt (rich in carbon and siderophile elements) which could form the core of the differentiated ureilites planet.

Detailed petrological research on a zonal composition of the rock-forming minerals and the interstitial material of meteorites Novo-Urei, Dyalpur, Haverro and Kenna carried out by the scanning electron microscope CamScan-4DV with energy-despersive analyzer AN 10000, let us make the following conclusions.

The reverse zonal structure of the olivine and pyroxene grains has metamorphic nature. The grains of olivine and pyroxene consist of the central parts of the grains and thin interrupted rims around them or sometimes along thin fractures inside the grains. The thickness of the alteration rim is much more in the olivine grains (up to 150 - 300 μm) than in the pyroxene (up to 30 - 50 μm) grains (Fig. 1).

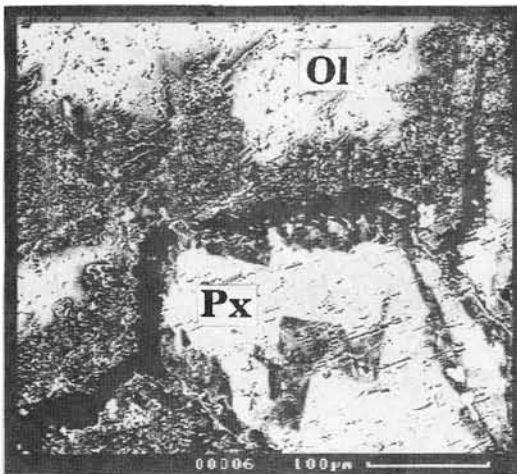


Fig. 1. Meteorite Novo-Urei. Texture of the re-crystallization of primary olivine and pyroxene.

Fractures between olivine and pyroxene grains and veins crossing these grains are filled with carbon material, Fe-Ni metal, carbides and sulfides. There are fine crystals of diamonds in these fractures. The distribution of the veins substance is

determined by the volatility of its components. Kamacite fills in the central parts of the veins, cohenite and muassanite occur both in the center of the veins and along their contacts, sulfides are in the contact part of the veins and carbon matter occurs as in the center parts as around the veins.

The outer parts of the olivine grains (rims) are re-crystallized into the aggregate of Mg-olivine, orthopyroxene and Fe-metal nearby the veins. We found that this rim had a zonal structure. There exist the following zones from the C-Me-vein to the center of the olivine grains: a - orthopyroxene + carbides and carbon matter + sulphide of Fe and Cr and Cr-spinellid + rare grains of SiO_2 ; b - orthopyroxene + olivine (Fa 2-3) + Fe-metal + carbon matter and fine chromite grains; c - olivine (Fa 5-6) + fine Fe-metal grains and carbon matter; d - olivine (Fa 10) + fine Fe-metal grains. Fe-content of the olivine grains sharply increases from the rim to the center and the centers of the grains have a constant (Fa 17-20) composition without fine grains of Fe-metal. Unlike the Fe-Ni metal of the veins, fine Fe-metal grains in olivine never contain nickel. It's necessary to note that olivine (with fine grains of Fe-metal) has the deficiency of ferrous iron as the result of reducing Fe^{2+} to Fe^0 and forming Fe-metal. Bulk composition of completely re-crystallized parts of the rim is practically the same with the composition of olivine with deficiency of ferrous iron. The re-crystallized phases are poor in Fe, and rich in Cr and have a good stehiometry. Small grains of primary olivine are completely re-crystallized. The compositions of new-formed olivine and pyroxene have similar value $X_{\text{mg}} = \text{MgO}/\text{MgO} + \text{FeO}$ ($X_{\text{mg}}^{\text{ol-2}} = X_{\text{mg}}^{\text{opx}} = 0.90-0.96$) and this value X_{mg} is much higher than the value X_{mg} of the primary olivine ($X_{\text{mg}}^{\text{ol-1}} = 0.69-0.75$) (Fig. 2, 3).

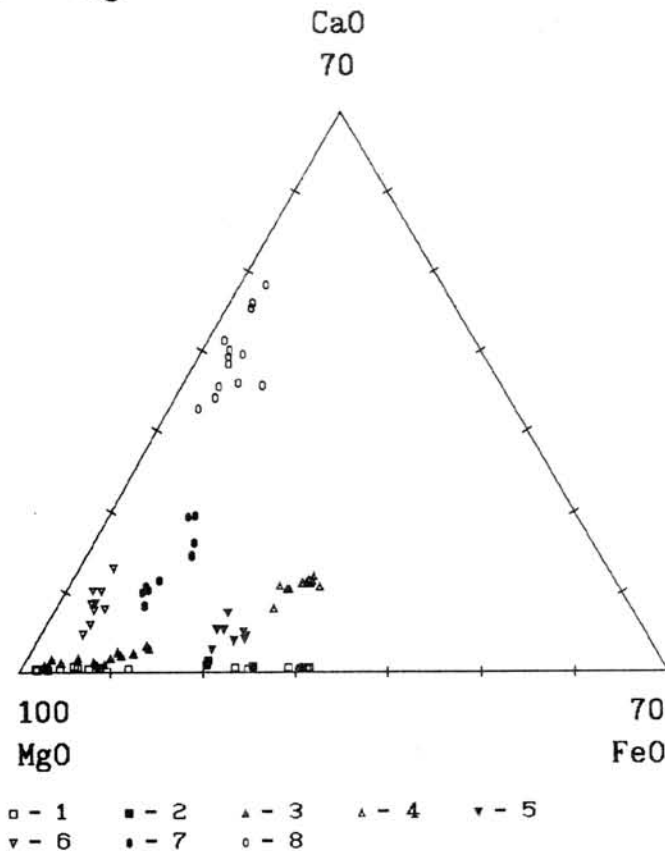
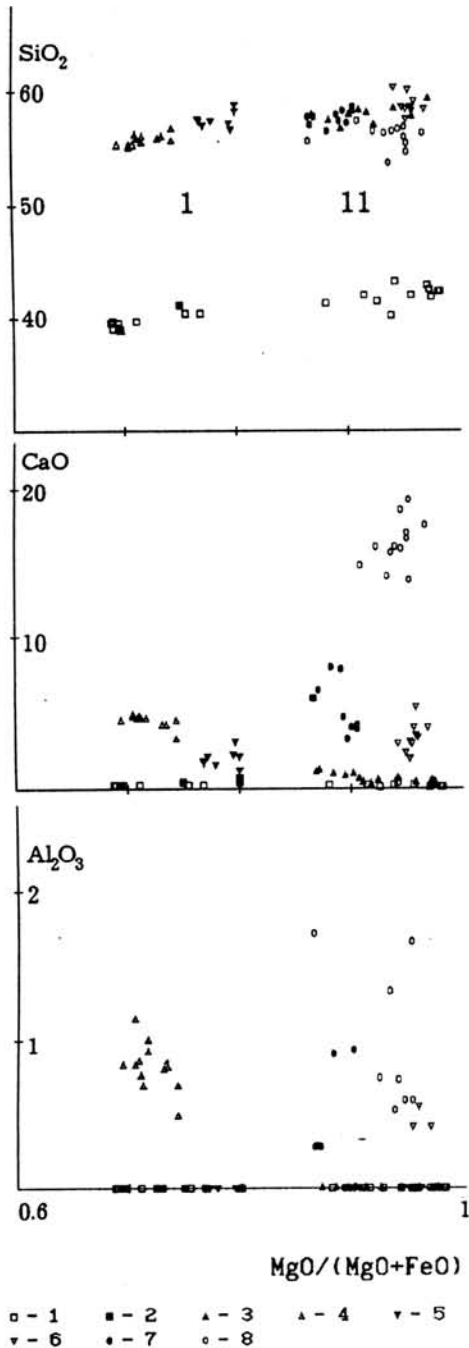


Fig. 2. Meteorite Novo-Urei. MgO-CaO-FeO diagram of olivine and pyroxene compositions: 1 - the core of the primary olivine; 2 - olivine of the re-crystallization zone; 3 - orthopyroxene of the re-crystallization zone; 4 - primary pigeonite; 5 - weak-altered pyroxene (zone 1); 6, 7 - low-Ca pyroxene (zone 2); 8 - augite (zone 2).

Thus, the zonal structure of olivine grains is formed by the reduction of ferrous iron and by the re-crystallization of olivine.

Change of parageneses of re-crystallized aggregate is discrete-gradual and shows the increase of the reduction potential from the centers of the olivine grains to the fractures into which the reduced carbon-rich melt intrudes.



The outer parts of the pigeonite grains (rims) are re-crystallized nearby the fractures, but these rims are very thin and discontinuous. The re-crystallization of pigeonite has a zonal structure as well. Zone 1 (zone of the re-crystallization) - a weak alternation of pyroxene is caused by the partial reducing of ferrous and formation of fine Fe-metal grains. Alternated pyroxene is poor in Ca and lost Al completely in comparison with pigeonite core. The thin rim of low-Ca orthopyroxene forms as a result of this process. Ca and Al are concentrated in the central part of the altered area. Zone 2 (zone of the melting) - the mineral composition of the active re-crystallized zones of pyroxene consist of low-Ca pyroxene, augite and silicate glass with variable content of Al_2O_3 and alkalis. The texture of this zone has a magmatic nature.

The bulk composition of the re-crystallized areas of pigeonite is the same with the composition of the primary pigeonite. It's necessary to note that the value X_{mg} (0.69-0.72) of primary pigeonite is equal to that of olivine cores and the value X_{mg} (0.90-0.96) of mineral phases of the re-crystallized areas of pigeonite is equal to the value X_{mg} of the products of the olivine re-crystallization. The increase of the

Fig. 3. Discrete-gradual alteration of the olivine and pyroxene compositions. I - zone of the weak alteration; II - zone of the active alteration. For legend see fig. 2

value X_{mg} of the silicates is discrete being connected with the change of mineral parageneses of the re-crystallized zones. Zone of melting has the normative pyroxene composition in a closed "melting area" inside the pigeonite grains only. Sometimes this melt intrudes (by the fractures) into the unaltered zones of pigeonite and even into partially re-crystallized grains of olivine. Contents of SiO_2 , Al_2O_3 and alkalis in the glass are increase in direction the "melting area" and both quartz and plagioclase appear in the interstices between the grains of new-formed pyroxene. Pyrope-garnet was found [5] in the melted area in the glass.

Comparing the parageneses of new-formed minerals replacing olivine and pyroxene we see that they formed under the equilibrium conditions. It's well known [1, 6, 7] that there is the heterogeneous distribution of Si, Ca, Al, Cr and alkalis in the interstitial material of ureilites but this heterogeneous distribution is connected with the different compositions of the primary olivine and pyroxene, and it's not necessary to have the residual, interstitial melt of the ureilites.

The re-crystallization of the ureilites has facial-isochemical nature and doesn't need any transport of the petrogenic elements. However, the discrete alteration of the ureilites primary minerals compositions are determined by penetration of metal melts rich in hydrocarbon. This alteration reflects the influence of reducing fluids (gradually neutralized by the rock) on the surrounding minerals. Fluid hydrocarbon pressure is responsible for active re-crystallization olivine as well as for partial melting of pyroxene and this pressure is high enough for formation of the pyrope-diamond assemblage. The existence of the glass in the melted zones of pyroxene as well as narrow re-crystallized zones of primary ureilite matter testify to high speed of neutralization of reducing fluids in relatively oxidizing environment.

ACKNOWLEDGMENTS - This work was supported by International Science Foundation (ISF) and Russian Found of Fundamental Researches (RFFR), Project 94-05-16942.

REFERENCES: [1] Goodrich C.A. (1992) *Meteoritics* 27, 327-352; [2] Marakushev A.A. et al. (1989) *Vestnik Moskovskogo Universiteta, seriya geologiya* 1, 3-19 (in Russian); [3] Marakushev A.A. et al. (1992) *Space petrology*, Moscow University Press, 325 pp. (in Russian); [4] Mitreikina O.B. et al. (1992) *Vestnik Moskovskogo Universiteta, seriya geologiya* 1, 38-48 (in Russian); [5] Mitreikina O.B. et al. (1994) *LPS XXV*; [6] Ogata H. et al. (1991) *Meteoritics* 26, 195-200; [7] Scott E.R.D. et al. (1992) *LPS XXIII*, 1253-1254.

SHOCKED CARBON MATERIALS WITH CVD-DIAMOND SHAPES

Yasunori MIURA

Faculty of Science, Yamaguchi University, Yoshida, Yamaguchi 753, Japan.

1. Introduction

Fine-grained diamond reported in the meteorites is almost based on electron microscopic data of small area, though main carbon phases are discussed by X-ray powder diffraction data of large sample as standard procedure. This is main reason why there are many carbon materials of meteorites and shocked materials observed by electron micrograph which cannot be checked by X-ray powder diffraction data as large carbon phases. In this sense, it is inevitable to obtain X-ray powder or single diffraction data by large grains of shocked carbon materials. The large blocks at the Barringer meteorite crater, U.S.A., are good candidates to check shocked carbon (diamond, chaoite or graphite) (cf. Miura et al., 1992, 1993).

High-pressure type carbon and silica minerals have been formed artificially by solid-solid transformation under static high-pressure. The high-pressure types of coesite, stishovite and diamond have been reported to be found at the Barringer impact craters as production by high-pressure condition of impact. But there are not reports on the detailed discussion of formation of high-pressure type materials. Miura (1991, 1993, 1994) reported that shocked quartz aggregates of various impact craters, meteorites and the Cretaceous-Tertiary (K/T) boundary samples are formed by quenched accretion of various aggregates from gas to solid states. Thus shocked carbon in the Barringer crater can be explained by dynamic formation from gas states, as suggested by Miura et al. (1994).

The main purpose of the present study is to describe shocked diamond-like carbon and shocked graphite with iron from compositional, structural and textural data.

I. New shocked graphites from the Barringer crater

Diamond has been reported from the Barringer crater as cliftonite (Foote, 1891) and hexagonal diamond (lonsdaleite, by Hannemann et al., 1967), though these data are based mainly on optical or powder (camera) data as solid-solid reaction. Recently shocked quartz and shocked graphite (with fine size, high density, and mixture with fine amorphous glasses) are reported from the Barringer crater (cf. Miura, 1991, Miura et al. 1993). The detailed characterization of shocked materials is also required to explain shocked carbon materials under dynamic formation processes.

I-1. Samples:

Graphite block sample of the Barringer crater used in this study is considered to be one of the evaporated sample collected at 4km west from rim of the impact crater. The samples are compared with large graphite standard samples from Korea and Madagascar, and artificial impact graphites.

I-2. Experimental methods:

X-ray calculated density has been determined by X-ray diffractometer as following equation: $\Delta \rho (\%) = 100 \cdot \{ (\rho - \rho_0) / \rho_0 \}$, where standard density ρ_0 is 2.255 g/cm³ in Korean graphite. Single sample data are checked from the strongest X-ray peaks by micro X-ray diffractometer and 4-axes X-ray diffractometer. Chemical compositions of shocked materials have been obtained by the EPMA and analytical-electron microscopy (AEM) of Yamaguchi University.

I-3. Optical observation:

There are four different mineral-aggregates of the Barringer graphite block sample.

- (a) Fine-grained shocked graphite-1 (with fine Fe) in the matrix.
- (b) Shocked graphite-2 (with chaoite-like carbon with diamond shape) surrounded by iron.
- (c) Shocked quartz-1 (with kamacite) in the rim, and
- (d) calcite from Kaibab limestone in the rim of the graphite block.

These shocked aggregates indicate dynamic accretion process of three different aggregates.

I-4. X-ray diffraction data:

X-ray diffraction peaks of shocked graphites reveal that

- (a) low X-ray intensity (i.e. abrupt stopping of reaction),
- (b) high Bragg-angle shift of X-ray diffraction peak (i.e. high X-ray density), and
- (c) multiple splitting of X-ray diffraction peaks (i.e. aggregates of quenched materials).

I-5. X-ray density data:

High density values of shocked graphite are obtained in the Barringer graphite ($\Delta\rho = +1.1 \pm 0.4\%$ and $+0.6 \pm 0.1\%$). Shocked chaoite of high-temperature type carbon shows high value of $\Delta\rho = +0.6 \pm 0.9\%$.

I-6. Compositions of two shocked graphites:

AEM data reveal the four different aggregates of the graphite block samples as follows (cf. Fig.1):

- (a) Shocked graphite-1 in the matrix: Black shocked graphites contain uniformly fine-grained Fe (from kamacite) and trace of Ca (from Kaibab limestone) which are formed under mixed gas state. Shocked graphite with fine Fe particles (up to 25 vol. %) are easily misidentified as diamond at measured density data.
- (b) Shocked graphite-2 in vein metal: Various shapes of shocked graphites and shocked chaoite-like carbon (with clear shapes) are surrounded by kamacite-rich metal under gas states of various compositions mixed from iron meteorite, sandstones and limestone. Aggregates with minor chlorine or sulfur are coexisted with the kamacite-like vein, though these elements has no more mineral state due to the evaporation and quenching by impact mixing.
- (c) Shocked quartz-1 and kamacite in the rim: Kamacite-rich metal contains Ca elements from Kaibab limestone, and shocked quartz (mainly from Coconino sandstone). Shocked quartz-1 grains with high density contain Fe and Ca, which are completely different with clear shocked quartz -2 with pure silica formed at the later stage impact from the Coconino sandstone reported by Miura (1993).
- (d) Limestone in the rim: Calcites from Kaibab limestone are only fixed without melt after hitting to the surface from the original graphite aggregates.

I-7. Scanning electron micrograph:

Scanning electron micrograph (SEM) data of shocked graphite and chaoite-like carbon are shown in Fig. 1. Chaoite-like carbon (by X-ray main peaks) shows clear outer form of cube-octahedron (i.e. 6-planes of (100) and 8-planes of (111)) which is the same diamond crystal shape of CVD plasma condition (Inuzuka et al., 1992). This indicates that first formation of CVD diamond crystal has been transformed to chaoite or graphite (with shocked structure due to quenching) during cooling process. Clear morphology of diamond is considered to be kept by surrounding by mixed iron and nickel materials of lower melting points.

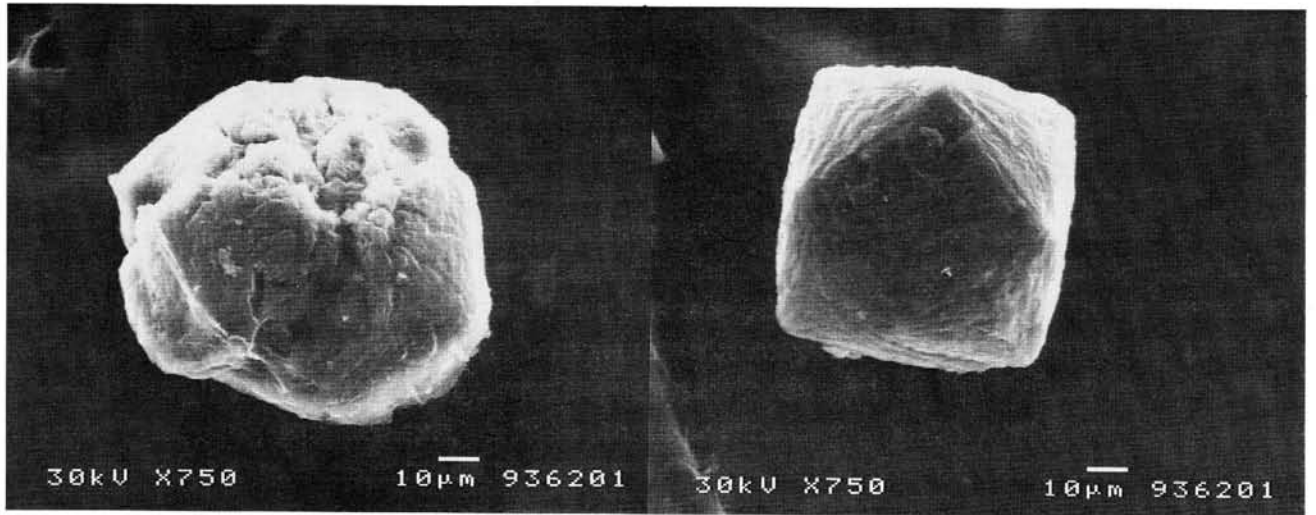
There are no other shapes of diamond (ex. cubohedron or octahedron, or twinned), though there are also various shapes with diffuse outer-form (cf. Fig.1).

II. Shocked graphites formed by impact experiments

Shocked graphites formed by artificial impact experiments (2.9km/s and 1.3g; 7km/s) at the ISAS show fine-grained and high-density ($\Delta\rho = +0.7\%$), which are easily checked by high Bragg-angle shift. It is found that high density of shocked graphites at the Barringer crater is the same of that in artificial impact experiment.

III. Dynamic formation process of shocked graphites

Shocked graphites and CVD diamond shape (chaoite-like) carbon have been found in this study. The compositions of two type shocked graphites indicate that there are two major formation stages (Cf. Gault et al., 1968; Melosh, 1989) of shocked carbon materials.



(a)

(b)

Fig. 2. Electron micrographs of (a) shocked graphite with diffuse shapes in outer vein, and (b) shocked chaoite-like carbon with morphology of CVD-diamond of cubo-octahedron (100) and (111) found at inner part of the Fe-rich vein. Carbon source is from the Kaibab limestone. These data suggest terrestrial impact origin.

- (a) First explosion by super-heating: The first shocked graphite aggregates-1 has been formed from vapor plume with *gas*-state of Fe (from iron meteorite), C (from Kaibab limestone), and Ca (from sandstone) to form graphite block under ultra-high temperature condition from meteoritic kinetic energy to chemical heat energy.
- (b) Second destruction by shock wave: The second shocked graphite aggregates-2 has been formed from huge destruction by shock wave which makes *gas-melt* states of Fe, Ni, Ca, C and Si to form Fe-rich vein. The shocked graphites in the vein were formed by relatively rapid cooling which were found outer region of the block. The CVD diamond in the inner vein was formed at first (by relatively slow cooling).

Origin of carbon of shocked graphites is considered to be Kaibab limestone in this study. This is mainly because (i) shocked graphites contain **chemical inclusions** from the target rocks of Kaibab limestone and Coconino sandstone which cannot be obtained in fine graphite of original meteorite, and (ii) shapes of shocked graphites in the shocked vein are **different at the inner and outer** regions of the graphite block which was formed **after** collision against the terrestrial target rocks (not collisions on the asteroids or in the space before entering to the atmosphere).

The present result to form CVD diamond in the impact craters can be applied to the other formations of diamond-like carbon. If there are few foreign co-existed materials of low-melting (or evaporation) points or amorphous glass (maybe from gas state), the high-pressure type of carbon or silica cannot survive after impact. The many reports on diamonds or cliftonite on the Barringer impact crater are different 2D-image planes of (100) and (111) of 3D image of cubo-octahedron which is the remnant of high-temperature gas state (not static high-pressure condition).

Table 1. Formation stages with shocked carbon and silica in the Barringer crater.

Shock stage	Impact condition	Mineral assemblages
【Shocked carbon materials】		
a) Compression-1 (with jetting)	Vapor state (vapor plume) (with Fe)	Fine shocked graphite-1 (+Fe, Ca) (in the major Carbon matrix)
b) Compression-2	Melt-solid state (mixed) (without Fe; surrounded by Fe)	Coarse CVD diamond (+Fe), to Chaoite-like carbon (inner vein) Shocked graphite-2 (+Fe) (outer)
【Shocked silica materials】		
c) Compression-3 (with jetting)	Melt-solid state (mixed) (with Fe)	Shocked quartz-1 (+Fe) in the rim
d) Compression-4 (with jetting)	Solid-melt state (mixed) (only pure silica)	Shocked quartz-2 (+stishovite, coesite)

IV. Summary

The present results are summarized as follows:

- Graphite block of the Barringer crater consists of two types of carbon materials, shocked graphite-1 and chaoite-like carbon with CVD diamond shape.
- Fine-grained graphite shows major amorphous carbon with crystalline graphites with high density and multiple aggregates.
- Shocked graphites formed by artificial impact crater experiment show similar high density (density-deviation=+0.7%) to that of natural Barringer meteorite crater.
- Shocked chaoite-like carbon with high density shows the same morphology of cubo-octahedron CVD diamond, which is not the high-pressure type carbon of diamond.
- It is considered that shocked graphite, shocked chaoite-like carbon with CVD diamond and shocked quartz with Fe-rich materials are formed under dynamic process (of gas-melt-solid state) and quenching process.
- Main carbon source of shocked graphites and CVD diamond-chaoite carbon is Kaibab limestone, because (i) chemical contamination from terrestrial target rocks, and (ii) different shapes of graphite-diamond-chaoite carbon materials in the small graphite blocks formed after impact on the Earth (not before the atmosphere).

Acknowledgements

The present research is supported by the Grant-in-Aid for Scientific Researches of the Japanese Ministry of Education and Science 1990-1993.

References

- Foote A.E. (1891): *Am. J. Sci.*, 42, 413-417.
 Gault D.E. et al. (1968): *Shock Metamorphism of Natural Materials* (ed. by French and Short), p.87-100.
 Hannemann R.E. et al. (1967): *Science*, 155, 995-997.
 Inuzuka T. et al. (1992): *Diamond and Related Materials* (Elsevier Sci.), 1, 175-179.
 Miura Y. (1991): *Shock Waves*, 1, 135-141.
 Miura Y. et al. (1992): *Shock Waves* (Springer-Verlag), 18, 403-408.
 Miura Y. et al. (1992): *Celestial Mechanics*, 54, 249-253.
 Miura Y. et al. (1993): *Meteoritics*, 28 (3), 402.
 Miura Y. (1993): *Proc. ISAS Lunar & Planet. Sci.* (ISAS, Japan), 26, 98-101.
 Miura Y. (1994): *LPSC XXV* (LPI, USA), 25, 913-914.
 Miura Y. et al. (1994): (in press).
 Melosh H. (1989) *Impact cratering* (Oxford University Press), 245pp.

Enrichment and fractionation of noble gases in bubbles

Nobuo Takaoka

Department of Earth and Planetary Sciences, Faculty of Science, Kyushu University, Fukuoka 812, Japan

An acapulcoite Yamato-74063 contains enormous amounts of trapped Ar, Kr and Xe. The Xe concentration for the bulk meteorite is even higher than that for most ureilites (Takaoka and Yoshida, 1991). According to Takaoka et al. (1993a), the isotopic composition of Xe, including ^{129}Xe , is homogeneous among bulk, silicate and metal fractions, and identical to that of Q-Xe isolated from carbonaceous (C) chondrites (Lewis et al., 1975; Wieler et al., 1992), suggesting a C-chondrite-like precursor. The homogeneous ^{129}Xe isotopic composition indicates that the gases were acquired from a single gas reservoir after most ^{129}I had decayed to ^{129}Xe . On the contrary, the $^{36}\text{Ar}/^{132}\text{Xe}$ ratio is quite variable. It is 22, 17 and 72 for the bulk, silicate and metal fractions, respectively. Because the $^{36}\text{Ar}/^{132}\text{Xe}$ ratio for the metal fraction is equal to that of the planetary gas, these observations indicate that heavy elemental fractionation took place at or after noble gases trapping in the silicate fraction and the silicate was enriched in Xe relative to Ar.

What processes caused such enormous enrichment of heavy trapped gases and large elemental fractionation? Orthopyroxene (opx) minerals containing tiny metal spherules contain many voids as well as large amounts of trapped gases (Takaoka et al., 1993b, 1994). The highest Xe abundance released by a laser shot from such an opx grain amounts to $8.5 \times 10^{-7} \text{ cm}^3 \text{ }^{132}\text{Xe/g}$ with $^{36}\text{Ar}/^{132}\text{Xe} = 11$. The voids range in size from one to several μm . Originally these voids should be filled with gases or/and fluids. Takaoka et al (1993b, 1994) have proposed a hypothesis that the large amounts of trapped gases reside in bubbles. Kim and Marti (1993) have independently given a proposal that heavy noble gases in Acapulco may have been trapped in inclusions in addition to metal blebs in opx or in micro bubbles in opx.

Here I present a model calculation to interpret the great enrichment of Xe and the low Ar/Xe ratio with the bubble hypothesis. For simplicity, we assume that all noble gases were trapped through solution in silicates (Henry's law) and

occlusion in micro bubbles. With the solubility (or Henry's constant) S_G and the gas pressure P_G in bubbles at the closure temperature T_G for gas species G ($G=Ar$ and Xe in the present case), the contents of Ar and Xe are given by

$$C(G) = P_G S_G + P_G V T_0 / P_0 T_G \quad (G=Ar \text{ and } Xe), \quad (1)$$

where V , P_0 and T_0 are the bubble density (i.e., the volume of bubbles per gram), the standard temperature (273K) and pressure (1 bar), respectively. From Eqn. (1), the Ar/Xe ratio (R) for a bulk sample is given by

$$R = C(Ar)/C(Xe). \quad (2)$$

The Ar/Xe ratio (R_b) in bubbles is given by,

$$R_b = (P_{Ar} T_{Xe}) / (P_{Xe} T_{Ar}). \quad (3)$$

For a low bubble density, in which case most noble gases were trapped through solution in silicates,

$$S_G \gg V T_0 / T_G \quad (G= Ar \text{ and } Xe). \quad (4)$$

From Eqns. (1) and (4), the gas pressure in bubbles equilibrated with the gas content dissolved in silicates can be approximated by

$$P_G = C(G) / S_G \quad (G=Ar \text{ and } Xe). \quad (5)$$

In a noble gas analysis such as laser micro-probe mass spectrometry, a very small amount of sample is probed, and the local bubble density in the sample is not constant but highly variable spot by spot. The local gas abundance $C(G)_L$ in the sample probed by laser pulse(s) is given by

$$C(G)_L = P_G S_G + (P_G T_0 / T_G) (v_L / w) \quad (G=Ar \text{ and } Xe), \quad (6)$$

where w and v_L are the sample weight fused by laser shot(s) and the volume of bubbles contained in it, respectively. Using Eqns. (5) and (6), we have

$$C(G)_L = C(G) [1 + (T_0 / T_G S_G) (v_L / w)] \quad (G=Ar \text{ and } Xe). \quad (7)$$

From Eqn. (7), the local Ar/Xe ratio (R_L) is:

$$R_L = R [1 + (T_0 / S_{Ar} T_{Ar}) (v_L / w)] / [1 + (T_0 / S_{Xe} T_{Xe}) (v_L / w)]. \quad (8)$$

As indicated by Eqns. (7) and (8), the local gas abundance and the local elemental ratio depend on the solubility, the closure temperature and the local bubble density. Because of no solubility data available for the opx crystal, we tentatively use the Ar solubility data for enstatite melt (Kirsten, 1968), in which the Xe solubility was not measured. Recently, Carroll and Stolper

(1993) have presented the relationship between solubility and ionic porosity for a wide range of silicate melt composition. According to them, the larger gas atoms are more sensitive to changes in the melt composition than the smaller ones: The ultramafic melt of low ionic porosity decreases in the Xe solubility more than in the Ar solubility, compared with silica-rich melts of high ionic porosity. Consequently the S_{Xe}/S_{Ar} ratio is systematically lower for the ultramafic melt than that for the silica-rich melt.

The temperature dependence of solubility for silicate melts is not available for opx. The closure temperature is available for Ar in some minerals that are used for K-Ar dating but not for opx. The closure temperatures of radiogenic ^{40}Ar are, for example, 490 to 578 °C for hornblende (Harrison, 1981). For Xe, no closure temperature is available. Presumably the Ar closure temperature for pyroxene is not higher than the Xe closure temperature and is similar to or higher than that for hornblende. We tentatively employ 873K (or 600°C) for T_{Ar} , and 873K and 1135K (or 862°C) for T_{Xe} .

Figure 1 shows plots of the local Xe abundance and the local Ar/Xe ratio against the local bubble density (v_L/w). The local Xe abundance increases in proportion to the local bubble density. The local Ar/Xe ratio decreases very rapidly with the increasing local bubble density and approaches to the Ar/Xe ratio in bubbles. With the Ar solubility for enstatite (Kirsten, 1968), the Xe solubility inferred from the relationship between the ionic porosity and the S_{Xe}/S_{Ar} ratio (Carroll and Stolper, 1933) and the closure temperatures given above, the local Xe abundance is given by $C(\text{Xe})(1 + 1 \times 10^5 v_L/w)$ and $C(\text{Xe})(1 + 8 \times 10^4 v_L/w)$ for $T_{Xe}=873$ and 1135K, respectively. One micro bubble of 10 μm across in 0.5 μg opx ($v_L/w=1 \times 10^{-3} \text{ cm}^3/\text{g}$) can enhance the Xe abundance 100 times and fractionate the Ar/Xe ratio 5 - 7 times with preference for Xe (Fig. 1). The ratio of the highest ^{132}Xe abundance to the lowest one determined in Y-74063 is about 200 (Takaoka et al., 1994) and agrees with the above estimation. Comparison for the Ar abundance and the Ar/Xe ratio is difficult because the lowest ^{36}Ar abundance released from melt probed by a laser shot was lower than the blank level of the analyzing system. Micro bubbles can enhance both the noble gas abundance and the elemental fractionation greatly.

References

Carroll, M. R. and Stolper, E. M. (1993) *Geochim. Cosmochim. Acta*, 57,

5039-5051.

- Harrison, T. M. (1981) *Contr. Mineral. Petrol*, 78, 324-331.
- Kim, Y. and Marti, K. (1993) *Lunar Planet. Sci.*, 24, 801-802.
- Kirsten, T. (1968) *J. Geophys. Res.*, 73., 2807-2810.
- Lewis, R. S., Srinivasan, B. and Anders, E. (1975) *Science*, 190, 1251-1262.
- Takaoka, N. and Yoshida, Y. (1991) *Proc. NIPR Symp. Antarctic meteorites*, No. 4, 178-186.
- Takaoka, N., Nagao K. and Miura, Y. (1993a) *Proc. NIPR Symp. Antarctic Meteorites*, No.6, 120-134.
- Takaoka, N., Motomura, Y., Ozaki, K. and Nagao, K. (1993b) *Papers presented to Eighteenth Symp. Antact. Meteorites*, May 31 - June 2, 1993, NIPR, Tokyo, p. 41 - 43
- Takaoka, N., Motomura, Y., Ozaki, K. and Nagao, K. (1994) *Proc. NIPR Symp. Antarctic Meteorites*, No. 7, 186-196.
- Wieler, R., Anders, E., Baur, H., Lewis R. S. and Signer, P. (1992) *Geochim. Cosmochim. Acta*, 56, 2907-2921.

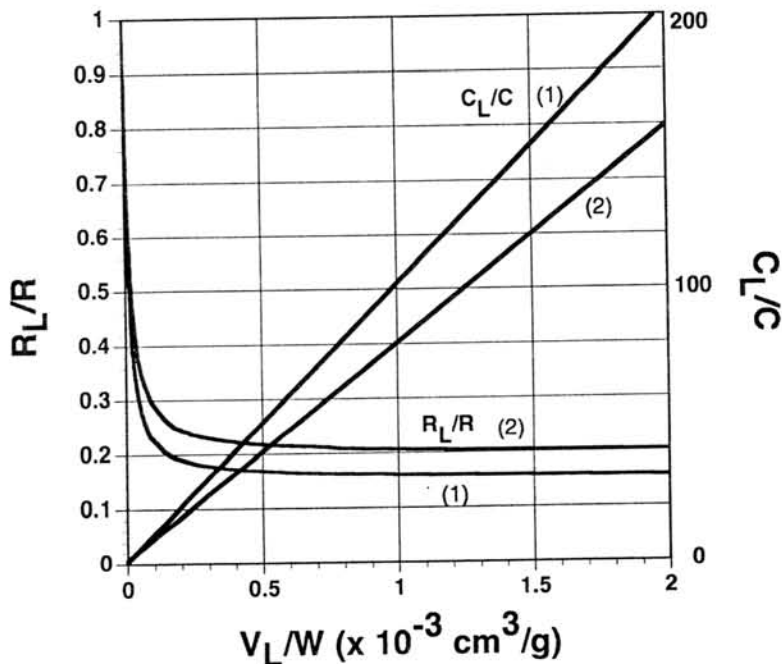


Fig. 1. The local Ar/Xe ratio (R_L) and the local Xe content (C_L) are plotted against the local bubble density (v_L/w), in comparison with the bulk ratio and content, respectively. $S_{Ar}=2 \times 10^{-5} \text{ cm}^3/\text{g bar}$ (Kirsten, 1968) and $S_{Xe}/S_{Ar}=0.15$ were used. Lines marked as (1) and (2) were calculated on $T_{Ar}=T_{Xe}=873\text{K}$, and $T_{Ar}=873\text{K}$ and $T_{Xe}=1135\text{K}$, respectively.

NITROGEN ISOTOPE MEASUREMENT OF UOCS BY A LASER PROBE METHOD

Kiyota, K and Sugiura, N

Department of Earth and Planetary Physics, Univ. of Tokyo, Japan

Introduction

Isotope anomalies of nitrogen have been found in UOCs using stepwise combustion method. For example, ALHA77214 and ALHA81251 contain isotopically light nitrogen which are not due to presolar diamond nor SiC. We have treated samples chemically and physically to concentrate and isolate the carriers of isotopically anomalous nitrogen. Though some characters about carriers are found, we have not identified the carriers, yet. Some UOCs seem to have carriers of isotopically anomalous nitrogen heterogeneously in mm scale. Therefore, we have tried to measure nitrogen and noble gases in UOCs by a laser probe method to investigate where the carriers are located.

Measurement

Samples were cut from chunks of UOCs by a diamond saw. One face of each thin sample was polished. Samples were washed with water and acetone in an ultra sonic bath and heated in a vacuum system for an hour to remove terrestrial contamination. They were installed into a sample chamber, and baked about 250°C overnight. The polished face was heated by a CW Nd:YAG laser, and extracted gases were measured with a static QMS.

Results

Mezo Madaras (LL3.4/3.7) and ALHA77214 (L3.4) were used for the preliminary measurement. The former released $\delta^{15}\text{N} > 230\text{permil}$ and $\delta^{15}\text{N} < -70\text{permil}$ nitrogen and the latter released $\delta^{15}\text{N} < -200\text{permil}$ nitrogen by the stepwise combustion method. Diameter and depth of focused laser pits are about 0.2mm and 0.1mm. Isotopically heavy nitrogen (0.6ng, $\delta^{15}\text{N} = 54\text{permil}$) was found from some pits of Mezo Madaras. ALHA77214 was heated by the laser without using a lens at about 700°C to remove contamination and adsorption, then melted by focused laser shots. Isotopically light nitrogen (0.15ng $\delta^{15}\text{N} = -50\text{permil}$) nitrogen was detected from some pits of ALHA77214. Since these isotopic anomalies are not as large as expected from stepwise combustion method, we will analyze N in smaller regions in the near future.

Special Lecture (I)

Dr. M. Weisberg

THE CR CHONDRITE CLAN. Michael K. Weisberg and Martin Prinz. Dept. Mineral Sciences, American Museum of Natural History, New York, NY 10024, USA.

The CR clan consists of five kinds of chondrites which are petrographically dissimilar, but have geochemical and mineralogical similarities that strongly suggest their kinship. The five kinds of chondrites are: (1) CR chondrites, (2) ALH 85085 (A85)-like chondrites, (3) Acfer 182 (and paired samples 207 and 214) chondrite, (4) LEW 85332 chondrite, and (5) the Bencubbin and Weatherford (Ben-W'ford) chondritic breccias. The Kaidun chondrite breccia appears to be mainly CR chondrite, as suggested by oxygen isotope data [1]. Here we bring together the petrologic, bulk chemical, and oxygen and nitrogen isotopic characteristics of the CR clan.

Petrologically the CR clan chondrites exhibit a wide range of characteristics: (1) CR chondrites (a group of nine) [2,3] are characterized by large (average diameter \approx 0.8 μ m, maximum \approx 1cm) multilayered, metal-rich chondrules and abundant (30-50 vol.%) matrix+dark inclusions (DI's). The matrix+DI's's consist of hydrous phyllosilicates, carbonates, and magnetite framboids and platelets; anhydrous silicates are minor in the matrix. Chondrules range from completely anhydrous, to having hydrated mesostases with anhydrous phenocrysts (olivine and pyroxene), to completely hydrous. Metal averages \sim 7 vol.%, and is mostly within the chondrules and their rims. (2) LEW 85332 [4,5] is a single meteorite with much smaller chondrules (avg. diam. \approx 170 μ m) and about 30% matrix+DI's. The chondrules are anhydrous whereas the matrix is hydrous with petrographic characteristics similar to those of CR matrix. Metal makes up \sim 7%. (3) Acfer 182 [6,7] is a single meteorite with even smaller chondrules (avg. diam. \approx 90 μ m) and \sim 30% matrix+DI's. Metal constitutes \sim 9%. (4) A85-like chondrites [8-12] are five meteorites-ALH 85085, PAT 91546, PCA 91328, PCA 91452, and PCA 91467 (some or all of which may be paired)-having the smallest chondrules in any chondrite (avg. diam. \approx 20 μ m) and which are also unusual in that cryptocrystalline is the dominant chondrule type. Matrix+DI's make up only \sim 5% and metal constitutes \sim 22%, making it more metal-rich than any chondrite. (5) Ben-W'ford [13-18] are chondritic breccias with similar characteristics; they are perhaps the most dissimilar to all other clan members. They consist of cm-sized metal (\sim 60%) and silicate clasts (\sim 40%). The silicate clasts are texturally and compositionally barred olivine chondrules or chondrule fragments with textures ranging from coarse-barrd to cryptocrystalline. No hydrous matrix or DI's are found in these chondrites, but they contain a variety of minor ordinary chondrite and R chondrite clasts and an anhydrous olivine-rich DI. Despite the differences in the petrographic characteristics of the five CR clan members, there are important mineralogic characteristics distinctive of this clan that indicate their kinship. These include their relatively metal-rich nature, the solar Ni-Co positive correlation of their metal, their olivine and pyroxene compositions are reduced (Mg-rich), and they contain hydrous matrix and/or DI's with similar mineralogic characteristics (except for Ben-W'ford).

Bulk compositions of CR clan members have similar refractory-moderately volatile lithophile element abundances, but the more volatile lithophiles (Mn, Na, K) are lower in the A85-like, Acfer 182, and LEW 85332 chondrites than in CR chondrites, with Ben-W'ford silicates having the lowest volatiles [11,17,19,20]. This may be mainly due to matrix+DI abundances since these are the main carriers of volatiles, and the Acfer 182, LEW 85332 and A85-like chondrites have lower matrix abundances than the CRs, and matrix is absent in Ben-W'ford.

Oxygen isotopic compositions of all clan members [2,5,12,21] plot on or close to the CR mixing line of slope-0.7, in contrast to the slope-0.52 terrestrial fractionation (TF) line and slope-1 C3 mixing line, as shown in Fig. 1. Separated components (chondrules and matrix+DI's) from CR chondrites also plot on or close to this line, as do most of the chondrule and matrix+DI separates from the A85-like and LEW 85332 chondrites (Fig. 2).

Nitrogen isotopic compositions of all CR clan chondrites have remarkably high $^{15}\text{N}/^{14}\text{N}$ ratios with $\delta^{15}\text{N}$ values of $\sim 190\text{‰}$ in CR chondrites, $\sim 1000\text{‰}$ in Ben-W'ford, $\sim 1500\text{‰}$ in A85-like chondrites, and $\sim 1600\text{‰}$ in Acfer 182 [22-29]. This contrasts with other chondrite groups which range from -90 to $+50\text{‰}$. Although the occurrence of a ^{15}N -rich component is characteristic of the CR clan chondrites, the identity of the carrier(s) is unknown. The lower $\delta^{15}\text{N}$ of CR chondrites compared to other clan members may be due to lower abundances of the nitrogen carrier(s), diluting its signal. It should be noted, however, that the combustion release temperatures of the ^{15}N -rich component(s) differ among the CR clan chondrites, suggesting differences in the distribution of the heavy nitrogen component(s) in these meteorites [28]. It has also been suggested that the brecciation process may be responsible, in part, for introducing or enhancing the ^{15}N components in these meteorites [28, 29].

The CR clan includes five kinds of chondrites which are petrographically distinct, but have mineralogic, bulk chemical and isotopic similarities that distinguish them from other chondrites and link them together. Their components appear to have formed under similar oxidation conditions from common oxygen and nitrogen isotopic reservoirs in the solar nebula. Size sorting processes may have resulted in different packagings of their silicate components, accounting for some of the petrographic differences among the CR clan chondrites.

References. [1] Clayton R. N. et al. (1994) LPSC XXV, 269-270. [2] Weisberg M. K. et al. (1993) GCA 57, 1567-1586. [3] Bischoff A. et al. (1993) GCA 57, 1587-1603. [4] Rubin A. E. and Kallemeyn G. W. (1990) Meteoritics 25, 215-225. [5] Prinz M. et al. (1993) LPSC XXIV, 1185-1186. [6] Bischoff A. et al. (1993) GCA 57, 2631-2648. [7] Prinz M. and Weisberg M. K. (1992) LPSC XXIII, 1109-1110. [8] Grossman J. N. et al. (1988) EPSL 91, 33-54. [9] Scott E. R. D. (1988) EPSL 91, 1-18. [10] Weisberg M. K. et al. (1988) EPSL 91, 19-32. [11] Wasson J. T. and Kallemeyn G. W. (1990) EPSL 101, 148-161. [12] Prinz M. et al. (1994) Meteoritics 29, in press. [13] Newsom H. E. and Drake M. J. (1979) GCA 43, 698-707. [14] Weisberg M. K. et al. (1990) Meteoritics 25, 269-279. [15] Lovering J. F. (1962) Researches on Meteorites (ed. C. B. Moore), 179-197. Wiley, NY. [16] Prinz M. et al. (1993) Meteoritics 28, 419-420. [17] Kallemeyn G. W. et al. (1978) GCA 42, 507-515. [18] Mason and Nelen (1968) GCA 32, 661-664. [19] Gosselin D. C. and Laul J. C. (1990) Meteoritics 25, 81-87. [20] Kallemeyn et al. (1994) GCA, in press. [21] Clayton R. N. and Mayeda T. K. (1978) GCA 41, 1777-1790. [22] Kung C. C. and Clayton R. N. (1978) EPSL 38, 421-435. [23] Robert F. and Epstein S. (1982) GCA 46, 81-95. [24] Prombo C. A. and Clayton R. N. (1985) Science 230, 935-937. [25] Franchi I. A. et al. (1986) Nature 323, 138-140. [26] Keeling D. L. and Marti K. (1987) Meteoritics 22, 426-427. [27] Grady M. M. and Pillinger C. T. (1989) LPSC XX, 351-352. [28] Grady M. M. and Pillinger C. T. (1990) EPSL 97, 29-40. [29] Grady M. M. and Pillinger C. T. (1993) EPSL 116, 165-180.

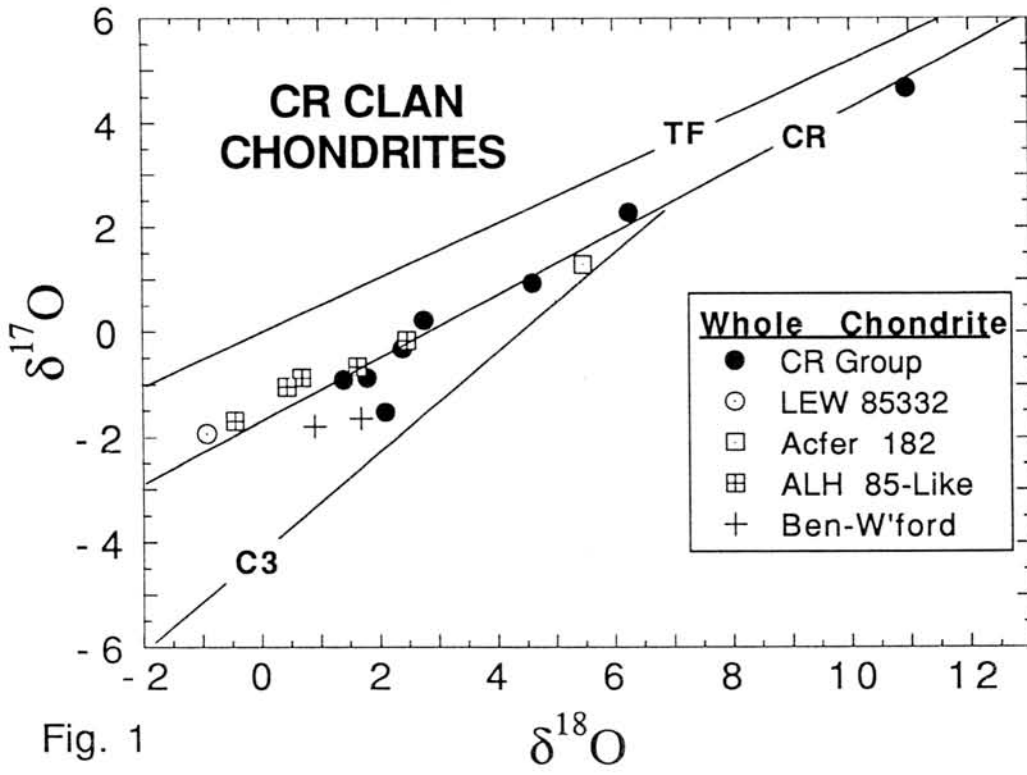


Fig. 1

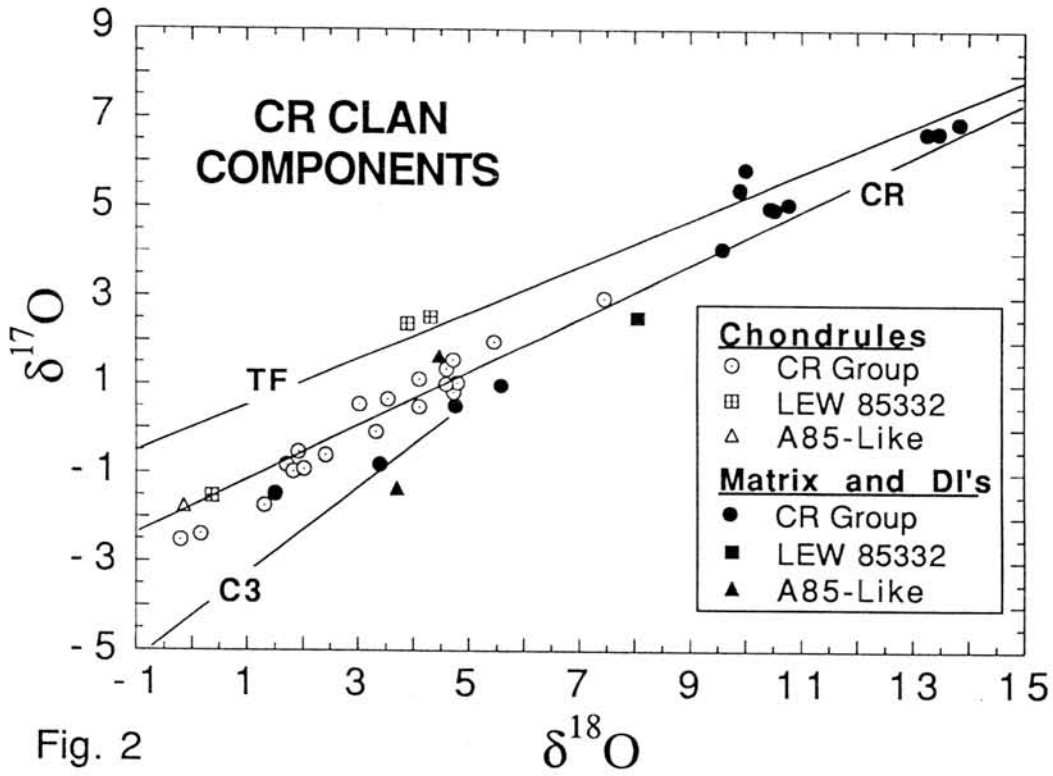


Fig. 2

Wednesday, June 1, 1994

0930 - 1440 Symposium, Auditorium

1440 - 1540 Special Lecture (II)

Dr. D. Mittlefehldt

Lockheed ESC

Houston, U.S.A.

Interrelation of parents and daughters of extinct nuclides in meteorites

Ping KONG and Mitsuru EBIHARA

Department of Chemistry, Faculty of Science, Tokyo Metropolitan University,
Hachioji, Tokyo 192-03, Japan

Introduction

Investigations on relatively short half-life radionuclides provide us very useful information to reveal the early history of our solar system. Three radionuclides, ^{26}Al , ^{107}Pd and ^{129}I with half life of 0.72 myr, 6.5 myr, and 16 myr [1], respectively, are fairly suitable for these studies, considering the formation interval of 100 myr for the solar system history. In this paper, we first try to deduce an interrelation of ^{107}Pd - ^{107}Ag nuclide pair in the metal fractions of iron meteorites, and then extend its use to ^{26}Al - ^{26}Mg nuclides in CAIs (Calcium, Aluminum-rich inclusions). In search of the mutual relation of these parent and daughter nuclides in meteorites, we attempt to give a general description about the feature of the early stage of our solar nebula.

Interrelation of parent and daughter nuclides

Because Pd and Ag have their own affinities to some specific phases in meteorites, we could draw an interrelation between Pd and Ag coexisting in those phases. Let us suppose that a meteorite parent body is homogeneous in composition, with initial concentrations for ^{108}Pd , ^{107}Pd , ^{107}Ag and ^{109}Ag being $C^0_{108}\text{Pd}$, $C^0_{107}\text{Pd}$, $C^0_{107}\text{Ag}$ and $C^0_{109}\text{Ag}$, respectively at the time of T_0 . In an interval of T , if no differentiation occurred on this body, the concentrations of these nuclides would become $C^0_{108}\text{Pd}$, $C^0_{107}\text{Pd}e^{-\lambda T}$, $C^0_{107}\text{Ag} + C^0_{107}\text{Pd}(1 - e^{-\lambda T})$ and $C^0_{109}\text{Ag}$, respectively. Because partition coefficients for Pd between metal and silicate and for Ag between sulfide and silicate, are in the order of 10^4 [2,3], which are much large than the proportion of fractionated silicate, we can neglect any change in the concentration ratio of Pd to Ag for the mixture of metal and sulfide during the segregation of silicate phases on the parent body. So fractionation of Pd from Ag will mainly be caused by the differentiation of metal from sulfide. Separation of negligible amounts of small grains compared with the total amount of metal and sulfide phases, prior to the separation of metal from sulfide, will also not change the ratio of $C_{\text{Pd}}/C_{\text{Ag}}$ for the metal-sulfide mixture. If the fractionation of metal from sulfide occurred at the time of T , then concentrations of ^{108}Pd , ^{107}Pd , ^{107}Ag and ^{109}Ag in the metal phase would be $\partial C^0_{108}\text{Pd}$, $\partial C^0_{107}\text{Pd}e^{-\lambda T}$, $\zeta(C^0_{107}\text{Ag} + C^0_{107}\text{Pd}(1 - e^{-\lambda T}))$ and $\zeta C^0_{109}\text{Ag}$, respectively, assuming that enrichment coefficients of Pd and Ag for metal (concentration in metal/initial concentration in the parent body) to be ∂ and ζ .

	^{108}Pd	^{107}Pd	^{107}Ag	^{109}Ag
T_0	$C^0_{108}\text{Pd}$	$C^0_{107}\text{Pd}$	$C^0_{107}\text{Ag}$	$C^0_{109}\text{Ag}$
T	$\partial C^0_{108}\text{Pd}$	$\partial C^0_{107}\text{Pd}e^{-\lambda T}$	$\zeta[C^0_{107}\text{Ag} + C^0_{107}\text{Pd}(1 - e^{-\lambda T})]$	$\zeta C^0_{109}\text{Ag}$

If the metal phase has not experienced any additional event causing the Ag-Pd fractionation, the present concentration of ^{107}Ag in the fractionated metal phase of meteorite, $C_{107}\text{Ag}$, will be:

$$C_{107}\text{Ag} = \partial C^0_{107}\text{Pd}e^{-\lambda T} + \zeta(C^0_{107}\text{Ag} + C^0_{107}\text{Pd}(1 - e^{-\lambda T})) \quad (1)$$

The concentrations of ^{108}Pd and ^{109}Ag , $C_{108}\text{Pd}$ and $C_{109}\text{Ag}$ in the same phase will be: $\vartheta C^0_{108}\text{Pd}$ and $\zeta C^0_{109}\text{Ag}$, respectively. So we can substitute $C_{108}\text{Pd}/C^0_{108}\text{Pd}$ and $C_{109}\text{Ag}/C^0_{109}\text{Ag}$ for ϑ and ζ , respectively in equation (1), and have the following equation:

$$C_{107}\text{Ag}/C_{109}\text{Ag} = (C_{108}\text{Pd}/C_{109}\text{Ag})(C^0_{107}\text{Pd}/C^0_{108}\text{Pd})e^{-\lambda T} + (C^0_{107}\text{Ag}/C^0_{109}\text{Ag}) + (C^0_{107}\text{Pd}/C^0_{109}\text{Ag})(1 - e^{-\lambda T}) \quad (2)$$

$C^0_{107}\text{Pd}/C^0_{108}\text{Pd}$, $C^0_{107}\text{Ag}/C^0_{109}\text{Ag}$ and $C^0_{107}\text{Pd}/C^0_{109}\text{Ag}$ are all the initial isotopic ratios for undifferentiated materials on the parent body at T_0 . Here, we substitute several simple symbols for these ratios as follows:

$A = C^0_{107}\text{Pd}/C^0_{108}\text{Pd}$, $B = C^0_{107}\text{Ag}/C^0_{109}\text{Ag}$ and $C = C^0_{107}\text{Pd}/C^0_{109}\text{Ag} = A(C^0_{108}\text{Pd}/C^0_{109}\text{Ag})$. Then we can get a general equation:

$$C_{107}\text{Ag}/C_{109}\text{Ag} - (B+C) = [A(C_{108}\text{Pd}/C_{109}\text{Ag}) - C]e^{-\lambda T} = (C_{108}\text{Pd}/C_{109}\text{Ag} - C^0_{108}\text{Pd}/C^0_{109}\text{Ag})Ae^{-\lambda T} \quad (3)$$

In this equation, $B+C = (C^0_{107}\text{Ag} + C^0_{107}\text{Pd})/C^0_{109}\text{Ag}$ is equal to the present ratio of $C_{107}\text{Ag}/C_{109}\text{Ag}$ for body where ^{107}Pd was completely decayed and Pd and Ag have not been fractionated from each other since the time of T_0 . If we plot the data from metal phases of the same group of iron meteorites on a figure of $C_{107}\text{Ag}/C_{109}\text{Ag}$ (y-axis) vs. $(C_{108}\text{Pd}/C_{109}\text{Ag} - C^0_{108}\text{Pd}/C^0_{109}\text{Ag})$ (x-axis), and if we assume these irons were parts of the metal phase from the same parent body, we could expect to get a straight line with a slope equal to $Ae^{-\lambda T}$ and intercepted at $(B+C)$ (on y-axis).

Examining the deduction process above, we can find that a similar equation could also be applied to a pair of ^{26}Al - ^{26}Mg in CAIs. CAIs are generally observed in carbonaceous chondrites and are thought to be among the earliest condensates from the gas of solar composition. So, we can expect no fractionation has occurred between Al and Mg in the solar nebula before the condensation of CAIs. Thus, we can write out an equation similar to (3) for an Al/Mg pair in CAIs of meteorites:

$$(C_{26}\text{Mg}/C_{24}\text{Mg}) - (B+C) = (C_{27}\text{Al}/C_{24}\text{Mg} - C^0_{27}\text{Al}/C^0_{24}\text{Mg})Ae^{-\lambda T}, \quad (4)$$

where $B+C = (C^0_{26}\text{Al} + C^0_{26}\text{Mg})/C^0_{24}\text{Mg}$ and $A = C^0_{26}\text{Al}/C^0_{27}\text{Al}$. If we plot $C_{26}\text{Mg}/C_{24}\text{Mg}$ vs. $(C_{27}\text{Al}/C_{24}\text{Mg} - C^0_{27}\text{Al}/C^0_{24}\text{Mg})$ on a graph for CAIs from the same meteoritic sample, and if we assume that these CAIs originated at the same time from the common reservoir with homogeneous isotopic compositions, we could also expect to get a straight line with a slope equal to $Ae^{-\lambda T}$ and intercepted at $(B+C)$.

We hesitate to extend this equation to an I/Xe pair, as the behaviors of I and Xe are obscured by the fact that the major iodine-bearing, xenon-retentive components have not been defined. If the I-bearing grains predate the agglomeration of the chondrites, then the formation intervals may be subjected to random.

Now let us examine the situation that the starting material was the nebula with the solar system composition. If we suppose a homogeneous solar nebula, then the initial values of A, B, C will remain constant for any undifferentiated meteorite parent bodies which preserve the solar system composition. For the Pd-Ag pair, the data of $C_{107}\text{Ag}/C_{109}\text{Ag}$ from terrestrial specimens could represent the value of $B+C$. Thus, we can substitute 1.0897 for $B+C$

in equation (3), obtained from a standard sample, NBS 978 [4]. Coupling the mean contents of Pd and Ag in C1 chondrites with isotopic ratios for these elements [5], we can get $C=2.46A$. So, for the meteorite parent body formed from the nebula of the solar system composition, equation (3) becomes simple as follows:

$$C_{107Ag}/C_{109Ag}-1.0897=(C_{108Pd}/C_{109Ag}-2.46)Ae^{-\lambda T} \quad (5)$$

For iron meteorites with ^{107}Ag anomaly, the data of C_{108Pd}/C_{109Ag} in metal are around 10^4 to 10^5 , so we can neglect a value of 2.46 in plotting the data on a graph of C_{107Ag}/C_{109Ag} vs. C_{108Pd}/C_{109Ag} .

For the Al-Mg pair, we can also use a value of 0.1398 from terrestrial or normal meteoritic materials to represent B+C. C_{27Al}/C_{24Mg} can be replaced with 0.098, which was calculated from the solar abundances [5]. Now equation (4) becomes:

$$(C_{26Mg}/C_{24Mg})-0.1398=(C_{27Al}/C_{24Mg}-0.098)Ae^{-\lambda T} \quad (6)$$

Values of C_{27Al}/C_{24Mg} found in CAIs with ^{26}Mg anomaly are generally larger than 100, so again we can neglect a value of C_{27Al}/C_{24Mg} (0.098) in plotting C_{26Mg}/C_{24Mg} vs. C_{27Al}/C_{24Mg} . We can expect a line with a slope of $Ae^{-\lambda T}$ intercepted at 0.1398 for the data from the same sample.

Analyses and discussions

$^{26}Al/^{26}Mg$

Intercept of the line on a graph of C_{26Mg}/C_{24Mg} vs. C_{27Al}/C_{24Mg} can imprint characters of the source material from which inclusions were formed. Most of inclusions lay a line intercepted at 0.140, so these inclusions must have been condensed directly from the nebula with solar system composition. There apparently are some inclusions with intercepts above or below 0.140 [6]; these inclusions must have either experienced secondary alterations or formed from a partly fractionated solar nebula.

We can deduce a value of $Ae^{-\lambda T}$ from the slope of a line of $^{26}Mg/^{24}Mg$ vs. $^{27}Al/^{24}Mg$ for CAIs from the same sample. Most inclusions show a typical value of $Ae^{-\lambda T}=5 \times 10^{-5}$ [7]. In order to know the time interval from the last nucleosynthesis for producing ^{26}Al to the condensation of ^{26}Al in CAIs grains, we should give a plausible production ratio of $^{26}Al/^{27}Al$ in nucleosynthesis. Several authors proposed some sources for producing a high ratio of $^{26}Al/^{27}Al$, such as red giants and novae which can steadily produce ^{26}Al [6,7,8], but none of these sources would produce ^{107}Pd and ^{129}I in an obvious fashion. Although ^{107}Pd lies on the s-process capture path, r-process contribution must be dominant [8]. ^{129}I is generally considered to be a r-process nuclide. Both red giant and nova can not provide neutron fluxes high enough to produce r-process isotopes. So, a supernova seems to be the most plausible source if we believe the three isotopes ^{26}Al , ^{107}Pd and ^{129}I were the products of one event. The production ratio of $^{26}Al/^{27}Al$ for a standard supernova is estimated to be around 10^{-3} [9,10]. So if we assume that anomalous ^{26}Al was injected by supernova explosion, at least 5% of the total ^{26}Al which was produced during the nucleosynthesis needs to have been devoted by the last event (see figure 1).

$^{107}Pd/^{107}Ag$

If the last ejection by supernova devoted the same proportion for ^{107}Pd in the solar nebula, we can calculate 'formation terms' of IVA and IVB irons

as 62.7×10^6 to 90.8×10^6 y corresponding to the proportion devoted by the last supernova explosion from 5% to 100%. Here we used 'formation terms' as the intervals between the last event of supernova explosion and the formation of iron meteorites. We predict the production ratio of $^{107}\text{Pd}_0/^{108}\text{Pd}_0$ by supernova as 0.4 by summing the isotopic distribution trends of all the even elements and this value is coincidence with that predicted by a nucleosynthesis model [8]. Thus the decay of ^{26}Al can not provide an energy source for the formation of at least some iron meteorites.

An intercept on a plot of $C_{107}\text{Ag}/C_{109}\text{Ag}$ vs. $C_{108}\text{Pd}/C_{109}$ for IVA irons [4] suggests that IVA irons have been fractionated directly from the material having solar system compositions, while IVB irons [11] must have been fractionated from a differentiated material, as inferred from a graph with an intercept of about zero. The separation of Pd from Ag was needed on the IVB iron parent body. A detail discussion of a Pd/Ag pair in iron meteorites will be appeared elsewhere.

References

- [1]. WASSON J. T. (1985) Radionuclides used to date meteoritic events. *Essays in Meteoritics*, p 243. [2]. STONE W. E., CROCKET J. H., and FLEET M. E. (1990) *Geochim. Cosmochim. Acta*, 54, 2341-2344. [3]. FLEET M. E., STONE W. E., AND CROCKET J. H. (1991) *Geochim. Cosmochim. Acta*, 55, 2545-2554. [4]. CHEN J. H., and WASSERBURG G. J. (1990) *Geochim. Cosmochim. Acta*, 54, 1729-1743. [5]. ANDERS E., and EBIHARA M. (1982) *Geochim. Cosmochim. Acta*, 46, 2363-2380. [6]. WASSERBURG G. J., and PAPANASTASSIOU D. A. (1982) Some short-lived nuclides in the early solar system—a connection with the placental ISM. In *Essays in Nuclear Astrophysics*, 77-140. [7]. LEE T., and WASSERBURG G. J. (1977) *Astrophys. j.* 211, L107-L110. [8]. BURBIDGE E. M., BURBIDGE G. R., FOWLER W. A., and HOYLE F. (1957) *Reviews of Modern Physics*, 29(4), 547-650. [9]. WOOSLEY S. E., and WEAVER T. A. (1982) Nucleosynthesis in 25M stars of different population. *Essays in Nuclear Astrophysics*, 406-426. [10]. RODNEY W. S., and WOLFS C. (1982) Hydrogen burning in massive stars. *Essays in Nuclear Astrophysics*, 193-232. [11]. KAISER T., and WASSERBURG G. J. (1983) *Geochim. Cosmochim. Acta*, 47, 43-58.

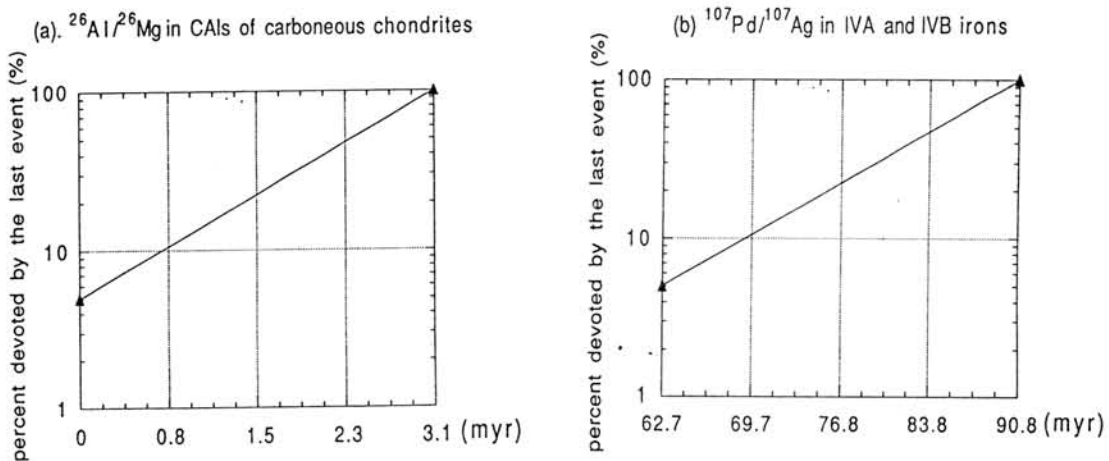


Figure 1. Formation interval after last explosion of supernova
(a) for ^{26}Al - ^{26}Mg pair; (b) for ^{107}Pd - ^{107}Ag pair.

LOW ENERGY COSMOGENIC PRODUCTS IN METEORITES

M.Honda Nihon University, College of Humanities and Sciences,
Sakura josui, Setagaya, Tokyo 156

Introduction:

Production rates of spallation products, induced by high energy particles of >50 MeV, can be systematized employing two parameters, k_2' and k_1' . These are resulted by shielding in extra-terrestrial materials against galactic cosmic ray irradiations. In general, production rate, p , of a spallation product, A and Z , in a target can be expressed by, $p(A,Z) = f \times k_1' \times (\Delta A')^{-k_2'}$, where, f and $\Delta A'$ are characterized by relations between target and product (Honda, 1985 and 1988). The equation is a simple power function as indicated from two parameter statistical relation and two variables determined by the product target relations, $\Delta A'$, reflecting hardness in reactions, and "f" a normalizing factor. The flux intensity can be expressed with k_1' and the spectra in high energy regions, or the hardness in spallation reactions, with k_2' . For small meteorites like ordinary size chondrites, k_1' can be expressed with k_2' ; that is,

$k_1' = 0.042 \times (23)^{k_2'}$, and $P(A,Z) = f \times 0.042 \times (\Delta A'/23)^{-k_2'}$ atom/min.g.
More widely, at 4π center, in a range of $k_2' = 1.7-2.8$,

$$k_1' = 0.042 \times (23)^{k_2'} \times [3.728k_2' - 2.62 - 0.931(k_2')^2]$$

According to reliable data for noble gases in irons, $^{38}\text{Ar}/^{21}\text{Ne}$ or $^3\text{He}/^4\text{He}$ can be compared with $^4\text{He}/^{21}\text{Ne}$ or $^3\text{He}/^{21}\text{Ne}$, a production ratio of lower and higher energy spallation products, or a convenient measure for shielding (Voshage and Feldmann, 1979). For multi-element targets, a composite of linear combinations of above relations will be employed. The products which are induced by low energy simple reactions, however, must be treated with modifications. The energy regions are lower than 30 MeV and very low cross-section in higher regions. In small objects and at surface of meteorites, low energy fluxes are not in equilibria with those of higher energy. Such reactions are (n,γ) , (n,p) , (n,α) , and $(n,2n)$.

(1). Cosmogenic Helium and Neon in Chondrites: (Fig.1)

Eberhardt et al (1966) pointed out that $^3\text{He}/^{21}\text{Ne}$, or simply $3/21$, and $^{22}\text{Ne}/^{21}\text{Ne}$, or $22/21$, in chondrites can be related with a linear equation (Bern line), such as, $(3/21) = 2.40 + 23.4 \times [(22/21) - 1]$. These two ratios have been used as important indexes indicating shielding. ^3He is classified into a group of high energy spallation products, and the production is more or less independent on a target and shield, whereas Ne is a lower energy product. Actually He isotope productions in iron and stones are equivalent to composites of various threshold reactions reflecting their excitation functions. Depth profiles of $22/21$ in the surface are always higher than at the center, deviating from the Bern line. In other words, even if the $3/21$ were equal, the $22/21$ at the center of smaller bodies are always lower than those at the surface of the larger objects. Therefore both data are plotted on a two dimensional plane (Loeken et al, 1992). The reason can be attributed to the behavior of ^{21}Ne . Because of this, relations between $3/21$ and

22/21 can be referred by applying the data at the center of objects. The relation at center is significantly different from that of interior or at surface of recovered materials. The center can be defined well and the sampling is reproducible.

Cosmogenic ^{21}Ne are produced by a low energy reaction, $^{24}\text{Mg}(n,\alpha)$, in addition to spallations. This is the reason why 22/21 decrease with shielding in chondrites, and a relative deficiency of low energy flux at surface causes increase in 22/21. 3/21= 5 at the center of St. Severin with 22/21 = 1.1, but at the surface 1.19 (3/21= 6) (Schultz and Signer, 1976). Various data at center, $(3/21)_c$ etc, can be collected and correlated from those of depth profiles of Knyahinya, Keyes, St. Severin, and ALH78084, and extrapolated from Chico, Bruderheim, Kokubunji, and Kiel. By a curve fitting, $(3/21)_c = 133(22/21)_c - 87 - 44(22/21)_c^2$.

The $(21/22)_{\text{spall}}$ must be the ratios of the products by spallations in Mg, Al, and Si. According to compilations of the chondrite data, samples showing cosmogenic 22/21 > 1.3 and 3/21 > 8 are rare; ALH79039, ALH77081, Narell, Thiel Mt. 82415, and Y74447, may be examples, but they never exceed 22/21:1.4. If 22/21 was close to the maximum, (n,α) must be very low, and no depth dependency was observed. $(21/22)_{\text{sp}}$ can be estimated by f and $\Delta A'$ for 21sp and 22sp. Production rate of ^{22}Ne is expressed by $0.735xk_1'x(9.5)^{-k_2'}$, whereas for that of ^{21}Ne , $\Delta A' = 9.5 + 1$ may be applied, and for the ratio of f values, a value closed to 1 can be used. The highest observed value of 22/21 \approx 1.4 in the lowest shielding will be indicating the limit. That is,

$$21_{\text{sp}}/22_{\text{sp}} = f(21)/f(22) \times (9.5/10.5)^{k_2'} = 1/1.4 .$$

Here 0.8 is used for $f(21)/f(22)$ to obtain the maximum at $k_2' = 1.5$. With shielding the spallation term of 21/22 decreases and the (n,α) term increases, resulting an overall effect of gradual decreases in 22/21 down to 1.05. After an equilibration of the flux, the decrease will cease. $(21n,\alpha / 22)$ can be estimated by a subtraction of spallation term from overall $(21/22)_{\text{chond}}$ at the center. The net n,α term at center may be expressed by a differential linear combination of two statistical relations in a range of $k_2' = 1.5 - 3.1$. It may reflect the excitation function of (n,α) reaction. (Fig. 2).

$(21n,\alpha / 22)_c = [0.022x(3.3)^{-k_2'} - 0.00012x(0.75)^{-k_2'}] / 0.735x(9.5)^{-k_2'}$,
where, $k_2' = 3.844 - 2.60x \log(^3\text{He}/^{22}\text{Ne})$ and $3/21 = 3/22 \times (22/21)$.

For profiles at the surface, a reduction factor, 0.8, can be used to suppress the n,α .

(2). Neutron Capture Products:

The contents of the lowest energy products, or neutron capture products, are very low at the surface and in small chondrites. For example, Knyahinya has an extremely low ^{36}Cl by $^{35}\text{Cl}(n,\gamma)$ at the surface relative to the central region (Nishiizumi, 1993, priv. commun.). The contribution of n,γ in the surface, depth/radius: $d/R = 0.1$, relative to the center seems to be higher by 5 or more, indicating a very steep concentration slope. On the other hand, depth profiles of Ne isotopes are quite similar to those of St. Severin, and other products have been systematized well according to their $\Delta A'$ values which have been assigned before.

High ^{60}Co contents in large chondrites were found in Jilin, Allende, Dhajala, 1976, and at much less extents in Bruderheim and St. Severin. Similar to ^{36}Cl , a very low ^{60}Co , 0.4 ± 0.3 dpm/kg chondrite at time of fall could be demonstrated in Mihonoseki, L6 (1992) (Shima et al, 1993), the 6.4 kg fragment which corresponds to a very surface sample, $d/R=0.01-0.02$, of St. Severin. Low ^{60}Co were also observed in Tahara, 1991 and near surface of Kokubunji, 1986.

(3). (n,p) Reaction Products: (Fig. 3)

In Mihonoseki, lower ^{58}Co , by $^{58}\text{Ni}(n,p)$, at $810.8 \text{ keV}\gamma$, can be shown relative to ^{56}Co a spallation product. (Shima et al, 1993), $846.8 \text{ keV}\gamma$; By a non-destructive gamma ray spectrometry, a direct comparison of the two was possible in 800-850 keV region side by side with the common 100% γ . With shielding the ratios $^{58}\text{Co} / ^{56}\text{Co}$ increase to >1 whereas in Mihonoseki it was 0.3. Similar data were reported in Innesfree, 1977 and Canon City, 1973.

Reference: Eberhardt P. et al (1966) Z. Naturf. 21a, 414-426., Eugster O. (1988) Geochim. 52, 1649-1662., Graf Th. et al (1990) Geochim. 54, 2511-2534., Honda M. (1985) EPSL, 75, 77-80; and (1988) Meteoritics 23, 3-12., Loeken Th. et al (1992) Chem. d. Erde 52, 249-259, Nagai H. et al (1993) Geochim. 57, 3705-3723., Nagao K. et al (1993) J. Massspectrom. Soc. Japan, 41, 191-209., Nishiizumi K. et al (1980) EPSL, 50, 156-170., Schultz L. and Signer P. (1976) EPSL, 30, 191-199, Schultz L. and Kruse H. (1989) Meteoritics 24, 155-172; and (1994), Shima M. et al (1993) Meteoritics. 28, 436., Voshage H. and Feldmann H. (1979) EPSL, 45, 293-308.

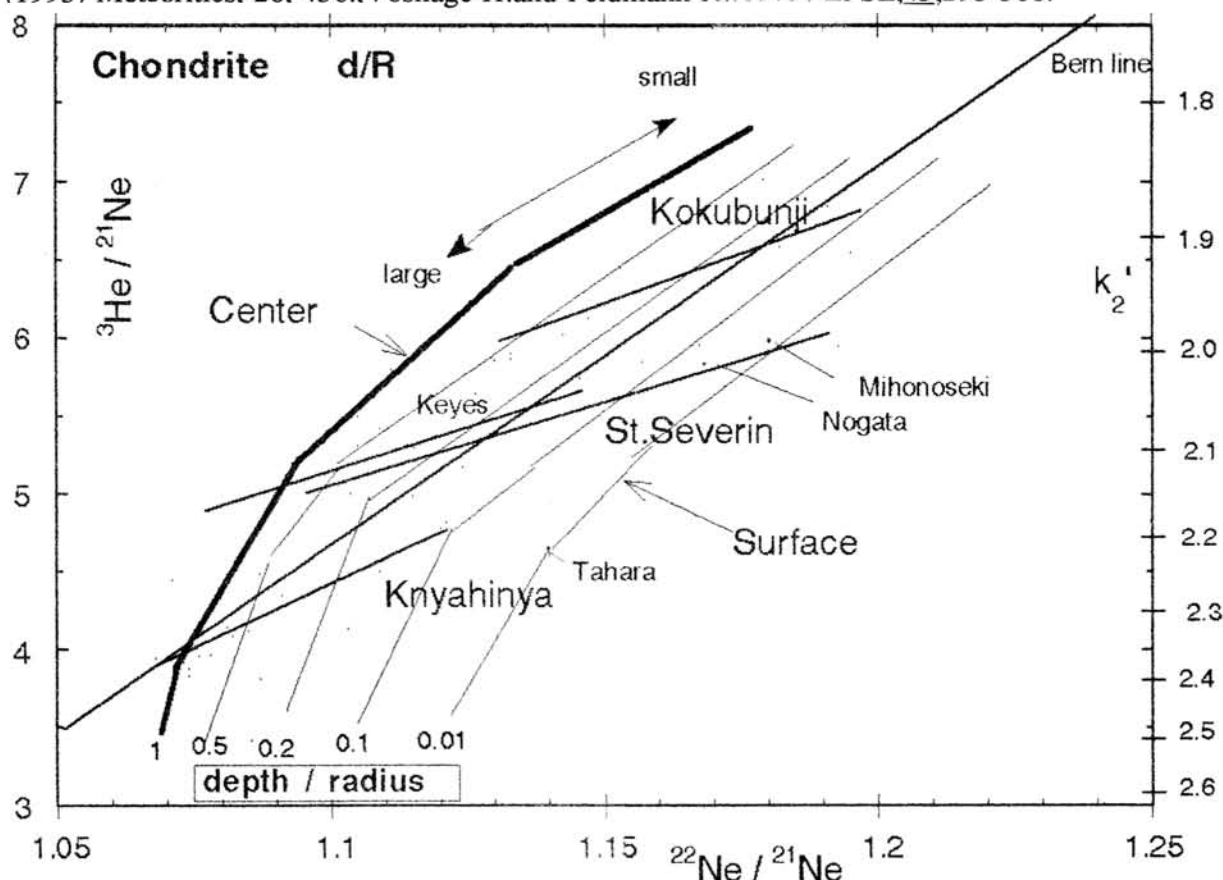


Fig.1 Relations between $^3\text{He}/^{21}\text{Ne}$ and $^{22}\text{Ne}/^{21}\text{Ne}$ in chondrites. The depth profiles observed with some chondrites. The data at center of spherical objects, $d/R = 1$, are illustrated as the reference.

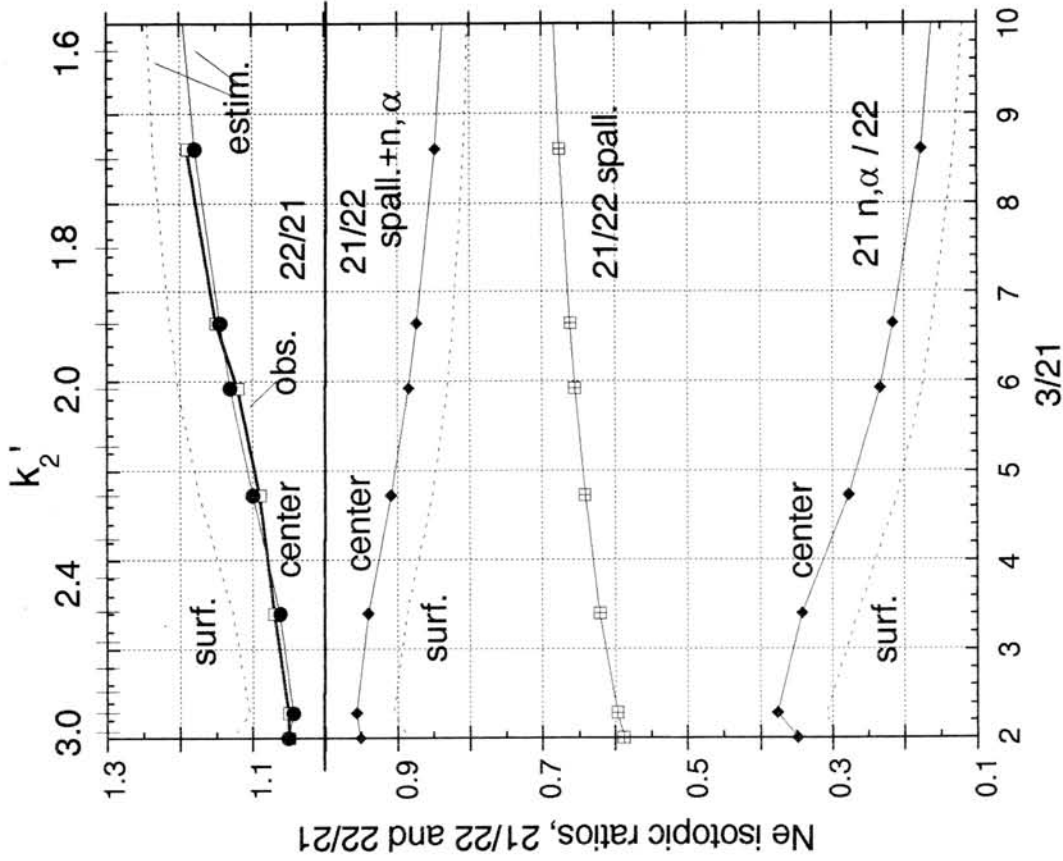


Fig.2 Two component model of ^{21}Ne productions in chondrites. $(^{21}\text{Ne}_{n,\alpha})/(^{22}\text{Ne}) = (^{21}\text{Ne}/^{22}\text{Ne})_{\text{total}} - (^{21}\text{Ne}_{\text{spallation}})/(^{22}\text{Ne})$ n,α components of ^{21}Ne can be obtained from total ^{21}Ne by subtracting the spallation components.

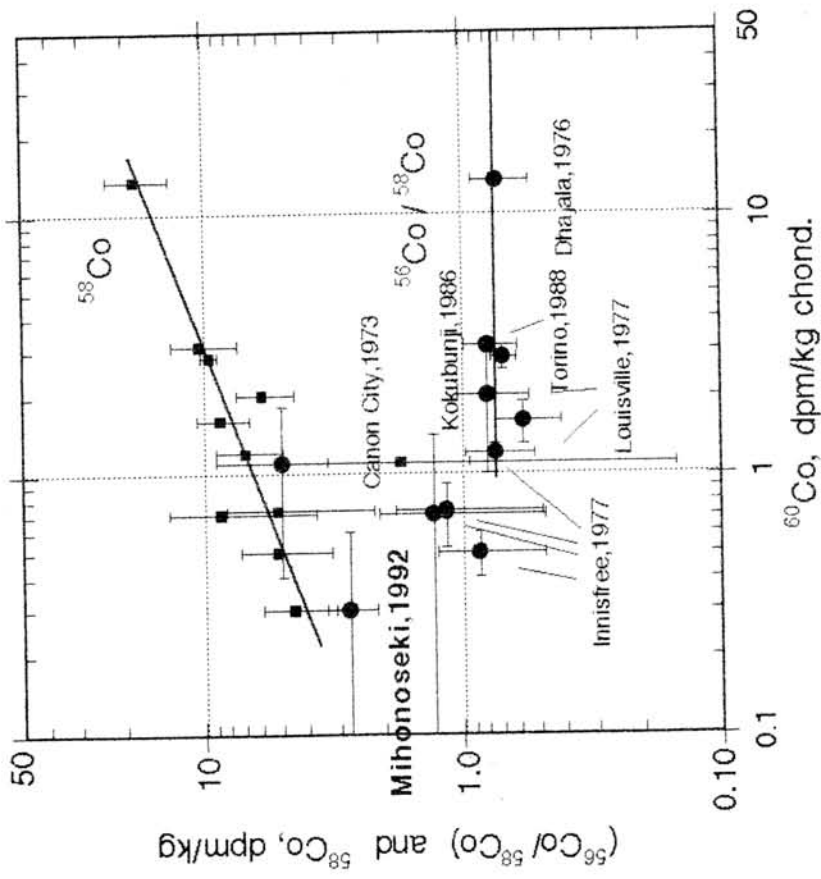


Fig.3 Co isotopes in Chondrites
Production rates of two low energy products, ^{60}Co and ^{58}Co , are extremely lower in surface and in smaller objects.

COSMIC RAY TRACKS AND COSMOGENIC ^{53}Mn IN METEORITES.

Peter A.J. Englert, Nuclear Science Facility, San Jose State University, San Jose, CA 95192-0163, USA.

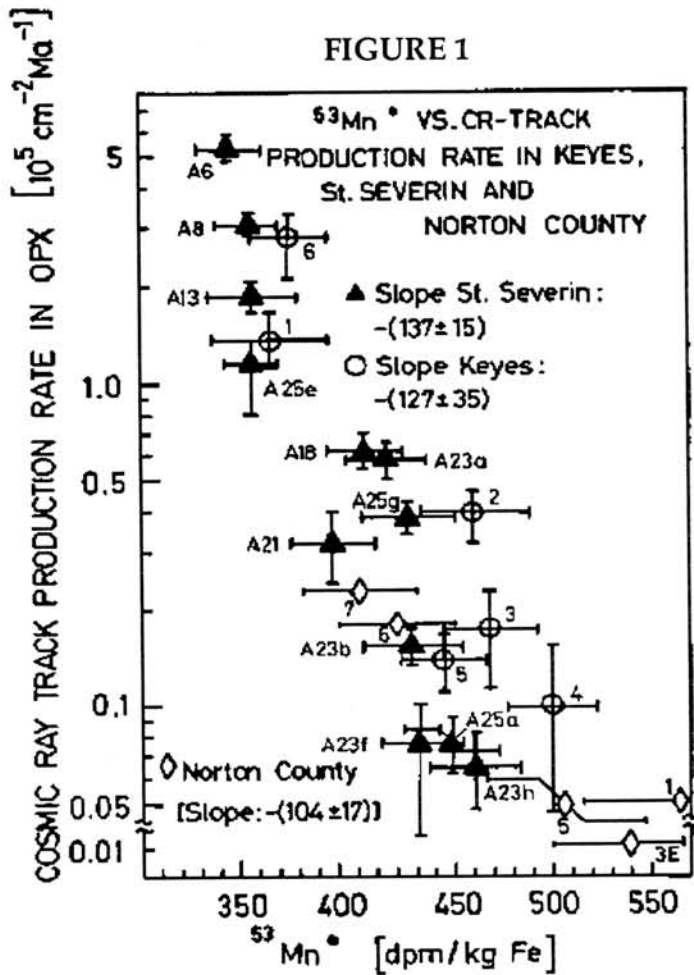
Cosmic ray tracks and long-lived cosmogenic nuclides, when measured in the same sample, are a powerful tool for assessing details of meteorite exposure histories. In this paper a sensitive method for the assessment of preatmospheric sizes of meteorites based on cosmic ray track and ^{53}Mn production rates are presented.

Stable and radioactive cosmogenic nuclides provide the basis for explaining cosmic ray history of meteorites and the cosmic radiation itself. Long-lived cosmogenic radio nuclides especially cover the last few million years of exposure ages. They are used to determine terrestrial ages, complex irradiation histories, preatmospheric sizes and shapes of meteorites, shielding depths, and the intensity of the galactic cosmic radiation.

Combining records of stable and radioactive cosmogenic nuclides for a meteorite can lead to a very detailed description of exposure and terrestrial history (Nishiizumi et al. 1989, Englert and Reedy 1986). Compilations of stable and long-lived cosmogenic nuclide data were published by Schultz and Kruse (1978, 1983) and by Nishiizumi (1987). Other useful interaction products of cosmic radiation in meteorites are cosmic ray tracks (CRTs). Bhandari et al. (1980) compiled cosmic ray track data in meteorites and used them together with stable cosmogenic nuclide data to determine shielding depths and preatmospheric sizes.

CRT density-versus-depth profiles have been measured in a number of meteorites including depth profiles in the St. Severin and Keyes chondrites (Cantelaube Y. et al. (1969), Englert P. and W. Herr (1980)). The density of cosmic ray tracks drops rapidly with depth making tracks excellent indicators of the pre atmospheric depth of the sample. Of the long-lived cosmogenic nuclides, ^{53}Mn shows the most pronounced production rate variations with shielding depth. In combining both cosmic ray records, CRT and ^{53}Mn production rates, respectively, a new tool for shielding depth and pre atmospheric size measurements becomes available. Over the last few years efforts were made to obtain as many CRT and ^{53}Mn same sample measurements of meteorite falls as possible.

Figure 1 shows the relation between the cosmic ray track production rates and the ^{53}Mn production rates for St. Severin ($T_{\text{exp}} \sim 13$ Ma), Keyes ($T_{\text{exp}} \sim 18$ Ma), and Norton County ($T_{\text{exp}} > 100$ Ma). The trend in the data is obviously determined by both depth and preatmospheric size of the meteorites. The grouping of the data points can be used to estimate preatmospheric shielding depths and sizes of meteorites when both CRTs and ^{53}Mn production rates were measured in one or, preferably, at least two samples of the meteorite.



Recently, Benoit et al. (1994) estimated the preatmospheric radius of Lost City to exceed 100 cm based on thermoluminescence depth profiles. Cosmic ray track and ^{53}Mn production rates for Lost City were measured in several samples. They are about $10^5 \text{ cm}^{-2} \text{ Ma}^{-1}$ and 400 dpm/kg Fe, respectively. This indicates that Lost City was a preatmospherically average sized meteorite, in or slightly below the range of the St. Severin and Keyes chondrites. A more careful analysis of the data suggests a preatmospheric radius of only 20 cm and a preatmospheric mass of approximately 120 kg, exceeding the preatmospheric mass estimate of 65 kg of Bhandari et al. (1980) based on CRT and noble gas measurements by a factor of two. Lost City and other examples demonstrate that CRTs in combination with ^{53}Mn provide a new and sensitive tool for preatmospheric size and shielding depth estimations for meteorite falls and finds.

REFERENCES: Nishiizumi K., et al. (1989) *Earth Planet. Sci. Lett.*, 93, 299-313; Englert P., and R.C. Reedy (1986), *Tech. Rep. 86-06*, Lunar Planet Inst., Houston, Tex.; Schultz L., and H. Kruse (1978) *Nucl. Track Detection*, 2, 65-103; Schultz L., and H. Kruse (1983) *Max Planck Institut für Chemie*, pp. 88; Nishiizumi K. (1987) *Nucl. Tracks Radiat. Meas.*, 13, 209-273; Bhandari N., et al. (1980) *Nucl. Track Detection*, 4, 213-262; Cantelaube Y. et al. (1969) In: *Meteorite Research*, P. Millman ed., 705-713; Englert P., and W. Herr (1980) *Earth Planet. Sci. Lett.*, 47, 361-369; Benoit P.H., et al. (1994) *Lunar Planet. Sci. Conf. XXV*, Abstr., 99-100.

^{40}Ar - ^{39}Ar ANALYSES OF JUVINAS FRAGMENTSIchiro Kaneoka¹, Keisuke Nagao² and Hiroshi Takeda³

1 Earthquake Research Institute, University of Tokyo, Bunkyo-ku, Tokyo 113

2 Institute for Study of the Earth's Interior, Okayama University, Misasa, Tottori-ken 682-01

3 Mineralogical Institute, Faculty of Science, University of Tokyo, Bunkyo-ku, Tokyo 113

Juvinas is an eucritic meteorite which fell near the village of Libonnes, France in 1821 and has been regarded to be a stone of over 91kg (1). About half of it has been kept in the National Museum of Natural History of Paris. For this meteorite, Rb-Sr, Pb-Pb and Sm-Nd ages were reported to be 4.50-4.56 Ga (2, 3, 4), but no ^{40}Ar - ^{39}Ar age has been reported. Generally, achondrites often show a sign of secondary disturbance(s), which is reflected in their ages, especially in ^{40}Ar - ^{39}Ar ages. For example, Pasamonte indicates Pb-Pb and Sm-Nd ages of 4.53 and 4.58Ga, respectively (5), its ^{40}Ar - ^{39}Ar age shows a secondary disturbance at about 4.1Ga(6). Furthermore, it has been revealed that Juvinas is a monomict breccia and its texture is rather heterogeneous from portion to portion. Some portions show signs of a shock and others do not. Such effect should be reflected in the apparent age. In this respect, ^{40}Ar - ^{39}Ar ages are most sensitive in identifying such an effect. In order to examine the state of Juvinas chronologically, ^{40}Ar - ^{39}Ar analyses were performed on three fragments of Juvinas which have different textures respectively.

Three fragments of Juvinas were prepared from an original block which has been kept in the National Museum of Natural History of Paris and supplied to us through the courtesy of Dr. P. Pellas. They are different in their textures. Sample 40E1(a) is a brecciated matrix, sample 40E2 a crystalline fragment and sample 40E4 a fragment with an intermediate texture between 40E1(a) and 40E2. 0.14-0.17g of fragments were wrapped in Al-foil and stacked together with the standard sample (MMhb-1, hornblende, K-Ar age; $519.5 \pm 2.5\text{Ma}$) under a vacuum in a quartz vial with Cd shielding. They were irradiated with fast neutrons in the JMTR with the total flux of about 1×10^{18} nvt/cm². Ar gas was extracted and purified at the Isotope Center, University of Tokyo and stored in collector tubes of Pyrex glass. Ar isotopes were analysed on a VG mass spectrometer at ISEI, Okayama University. Blanks and K- and Ca-derived interfering Ar isotopes were corrected. 15 temperature

fractions were taken for each sample.

The result indicates that three samples show secondary K contamination in the temperature fractions of less than 875°C. Because apparent ^{40}Ar - ^{39}Ar ages in these fractions are systematically lower of mostly less than 1000Ma and the estimated K contents calculated by the integrated ^{39}Ar in these fractions are much higher than those reported for Juvinas meteorites (230-480ppm). We applied the same procedure to prepare and analyse the present samples with the meteorites as reported before and we observed no such effects before (7). Hence, there seems to be no reason that such K contamination occurred during the experimental procedure. Hence there is a possibility that the block might have been already contaminated with K before analysis. Excluding these temperature fractions, samples 40E2 and 40E4 show similar ^{40}Ar - ^{39}Ar age spectra, where secondary disturbance ages of about 4000-4100Ma are observed in the 975-1050°C fractions with ages of about 4500Ma in the higher temperature fractions except for the 1200°C fraction. The 1200°C fraction indicates a relatively young age of less than 3500Ma. On the other hand, the sample 40E1(a) shows the ages of more than 4600Ma for the fractions of more than 1125°C. This sample shows also a rather scattered ages comparing to those of the other two fragments. This would reflect the effect of a shock on this portion and the texture of the sample. Thus, ^{40}Ar - ^{39}Ar analyses indicate a possibility that Juvinas was affected by secondary disturbance at around 4000-4100Ma, as observed for Pasamonte. This effect might have been not so intense as to cause the disturbance in the Pb-Pb and Sm-Nd systematics.

References

- (1) Graham, A. L., Bevan, A. W. R. and Hutchison, R., Catalogue of Meteorites, British Museum (Natural History), 460pp., (1985).
- (2) Allègre, C. J., Birck, J. L., Fourcade, S. and Semet, M. P., Science, 187, 436, (1975)
- (3) Manhès, G., Allegre, C. J. and Provost, A., Geochim. Cosmochim. Acta, 48, 2247, (1984).
- (4) Lugmair, G. W., Marti, K., Kurtz, J. P. and Scheinin, N. B., Proc. Lunar Sci. Conf. 7th, 2009, (1976).
- (5) Unruh, D. M., Nakamura, N. and Tatsumoto, M., Earth Planet. Sci. Lett., 37, 1, (1977).
- (6) Podosek, F. A. and Huneke, J. C., Geochim. Cosmochim. Acta, 37, 667, (1973).
- (7) e.g., Kaneoka, I. and Nagao, K., Proc. NIPR Symp. Antarct. Meteorites, 6, 88, (1993).

Nitrogen isotopic composition of CK chondrites

Naoji Sugiura and Shigeo Zashu

Department of Earth and Planetary Physics, Univ. of Tokyo, Tokyo,
Japan

Introduction

Nitrogen isotopic compositions are quite distinct for many groups of meteorites. Therefore it is useful for classification of meteorites, once it is established for each group of meteorites. Since nitrogen has only two isotopes, the classification based on nitrogen isotope is more ambiguous than that based on oxygen isotope. Also since nitrogen is a minor element, it suffers from contamination with terrestrial nitrogen more severely than oxygen-based classification. On the other hand, nitrogen isotope anomalies are much larger than those of oxygen isotopes. Also it may reveal subclassification of groups, because nitrogen isotopic composition shows some variation within ordinary chondrite groups (Hashizume, 1993)

Experiments

Here, we report nitrogen isotopic composition of three CK group chondrites (Karoonda, ALH85002 and EET92002). Previously, only Karoonda (CK4) has been studied for the nitrogen isotopic composition. Kung and Clayton (1978) reported 5 ppm of N at +2.3 permil, while Kerridge (1985) reported 18 ppm of N at +6 permil. Both measurements were, however, done by single step extraction, which is quite susceptible to contamination effect. Our measurements were made using a static mass spectrometry and the extraction was made by stepped combustion. The details on the experimental technique have been published elsewhere (Hashizume and Sugiura, 1990). Neon and Argon were also measured to estimate the contribution of cosmogenic nitrogen.

Results and discussion

The results on rare gases are summarized in Table 1 and the results on nitrogen are summarized in Table 2 and shown in Fig.1. The average delta ^{15}N value for Karoonda is somewhat lighter than but not grossly different from the literature values. It can be seen

in the figure that indigenous nitrogen in CK chondrites is isotopically light (the minimum values of $\delta^{15}\text{N}$ range from -50 to -107 permil). This variation of the minimum $\delta^{15}\text{N}$ is fairly large. Since presence of a trace amount of contamination could raise the value, lower value may be close to the true value, if the group has a single nitrogen isotopic composition. A further experiment is needed to clarify this. All CK chondrites release isotopically light nitrogen at high temperatures, while in the case of ALH85002, in addition to this high temperature component, a large amount of light nitrogen is released at low temperatures. This nitrogen is likely of organic origin, but it is not associated with primordial Ar. The ALH85002 is reported to be a typical CK4 chondrite (Kallemeyn et al, 1991) with well recrystallized matrix. Thus the presence of labile nitrogen is puzzling. Since the nitrogen isotopic compositions of the low temperature component and the high temperature component are similar, it is unlikely that these two components are totally unrelated. A possible scenario may be as follows. The light nitrogen was initially incorporated into the parent body as organic materials, and later transferred to retentive minerals by metamorphism. The organic materials were not destroyed in the cool surface region. An impact onto the surface vaporized organic materials which were transferred to the region where ALH85002 were located.

Conclusions

CK chondrites have isotopically light nitrogen. Previously, isotopically light nitrogen (about -60 permil) has been reported for E chondrites (Grady et al, 1986) and a R chondrite (Sugiura and Zashu, 1994). The lowest value for CK chondrites (-107 permil for Karoonda) is the lowest value for chondrites (excepting those presumably due to presolar grains). The nitrogen isotopic composition of chondrites now ranges from -100 permil to +200 permil, while that of more evolved meteorites (achondrites and iron) range from -150 permil (Kim and Marti, 1994) to +155 permil (Franchi et al, 1993). Our future study must solve the question how such diversity of isotopic composition evolved (or retained) in the early solar nebula.

References

- I.A.Franchi, I.P.Wright and C.T.Pillinger, Constraints on the formation conditions of iron meteorites based on concentrations and isotopic compositions of nitrogen, *Geochim. Cosmochim. Acta*, 57, 3105-3121, 1993.
- M.M.Grady, I.P.Wright, L.P.Carr and C.T.Pillinger, Compositional differences in enstatite chondrites based on carbon and nitrogen stable isotope measurements, *Geochim. Cosmochim. Acta*, 50, 2799-2813, 1986.
- K.Hashizume, Nitrogen isotopes in ordinary chondrites: a view of their parent bodies, Ph.D. Thesis, Univ. of Tokyo, 1993.
- K.Hashizume and N.Sugiura, Precise measurement of nitrogen isotopic composition using a quadrupole mass-spectrometer, *Mass Spectrosc.*, 38, 269-286, 1990.
- G.W.Kallemeyn, A.Rubin and J.T.Wasson, The compositional classification of chondrites: V. The Karoonda (CK) group of carbonaceous chondrites, *Geochim. Cosmochim. Acta*, 55, 881-892, 1991.
- J.F.Kerridge, Carbon, hydrogen and nitrogen in carbonaceous chondrites: abundances and isotopic compositions in bulk samples, *Geochim. Cosmochim. Acta*, 49, 1707-1714, 1985.
- Y.Kim and K. Marti, Genetic relationship of Acapulcoites and Lodranites? A study of nitrogen and xenon isotopic signature, *Lunar Planet. Sci.*, XXV, 703-704, 1994.
- C.-C.Kung and R.N.Clayton, Nitrogen abundances and isotopic compositions in stony meteorites, *Earth Planet. Sci. Lett.*, 38, 421-435, 1978.
- N.Sugiura and S.Zashu, Isotopic composition of nitrogen in the PCA91002 chondrite, *Lunar Planet. Sci.* XXV, 1357-1358, 1994.

Table 1. Rare gases.

sample	cosmog ²¹ Ne E-8 ccstp/g	prim. ³⁶ Ar E-8 ccstp/g	cosmog ³⁸ Ar E-8 ccstp/g	⁴⁰ Ar E-8 ccstp/g
Karoonda	11.58	2.06	1.14	1155
ALH85002	8.02	0.47	0.98	919
EET92002	9.17	0.50	1.07	742

Table 2. Nitrogen

sample	N(total) ppm	N(T>=800C) ppm	$\delta^{15}\text{N}_{\text{ave.}}$ permil	$\delta^{15}\text{N}_{\text{min.}}$ permil
Karoonda	3.62	1.63	-33.8	-106.7
ALH85002	40.67	1.46	-28.5	-50.0
EET92002	3.15	1.03	3.46	-65.4

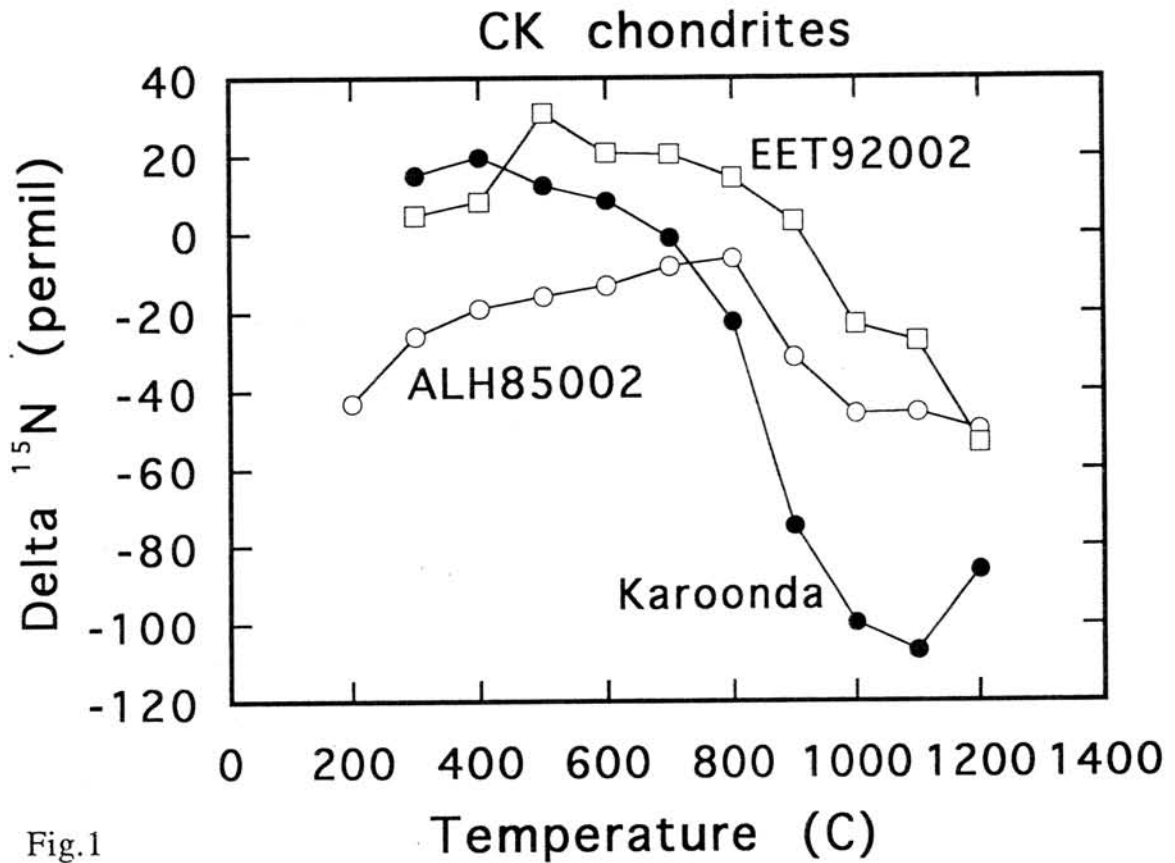


Fig.1

HEAVY NITROGEN IN A SNC ORTHOPYROXENITE ALH84001

Yayoi N. MIURA and Naoji SUGIURA

Department of Earth and Planetary Physics, University of Tokyo 113, JAPAN

INTRODUCTION

ALH84001 is a new type of SNC meteorite, SNC orthopyroxenite [1]. Mineralogical and oxygen isotopic studies confirmed that the relation between ALH84001 and SNC meteorites [1],[2]. Detailed mineralogical, petrographical and geochemical investigation by Mittlefehldt (1994) [2] has suggested that ALH84001 shows characteristic features similar to Chassigny on the one hand and also shows features similar to shergottite EETA79001 on the other. We have already reported noble gases in this meteorite [3], and found that (1)ALH84001 contains the martian atmosphere-like Xe characterized by high $^{129}\text{Xe}/^{132}\text{Xe}$. This trapped Xe is similar in isotopic composition and concentration to Xe in glass portions (lithology C) of the shergottite EETA79001. Both meteorites seem to trap noble gases of the same origin; possibly the martian atmosphere, and (2)the cosmic-ray exposure age of ALH84001 (14.4 ± 1.2 m.y.) is identical with those of Chassigny and Nakhla. These results on noble gases strongly support that ALH84001 belongs to SNC meteorite clan.

Nitrogen is also an important and useful tool for classifying the meteorite and for considering its origin. The EETA79001 lithology C shows isotopically heavy nitrogen relative to the terrestrial one, at least as high as +190 ‰ [4]. Nitrogen of the martian atmosphere observed by Viking mission is also heavy (620 ± 160 ‰ [6]). This similarity of nitrogen isotopic composition between EETA79001 and the martian atmosphere may suggest relation between them. We recently measured nitrogen isotopic composition for ALH84001, which is presented here.

EXPERIMENTAL

A crushed sample weighting 191.4mg was wrapped in Pt foil after washing with acetone. Gases were extracted by heating the sample using stepwise combustion technique [6] under an oxygen atmosphere of 0.4 - 1.2 Torr. The extraction temperatures are from 200 °C to 1200 °C with every 100 °C step. Nitrogen isotopic compositions were determined by measuring molecules of nitrogen, masses at 28, 29 and 30, using a quadruple mass spectrometer.

RESULT ON NITROGEN ABUNDANCE AND ISOTOPIC COMPOSITION

The concentrations and isotopic compositions of nitrogen are shown in Table 1 and Fig. 1, where $\delta^{15}\text{N}$ is defined as $\delta^{15}\text{N} = (^{15}\text{N}/^{14}\text{N})_{\text{sample}} / (^{15}\text{N}/^{14}\text{N})_{\text{air}} - 1 \times 1000$. Total nitrogen abundance obtained above 500 °C in ALH84001 is 0.12 ppm, which is one or a few order of magnitudes lower than those in chondrites. Since correction of blank is large at higher temperature fractions, nitrogen abundances without blank correction as well as those corrected for blanks are presented in Table 1. The corrected values will be used in the following discussion.

Nitrogen released at the temperatures lower than 400 °C is dominated by the terrestrial nitrogen. Nitrogen in 500 and 600 °C fractions, showing somewhat higher $^{15}\text{N}/^{14}\text{N}$ ratios

than the terrestrial atmosphere, seem to be mixture of the terrestrial and indigenous nitrogen. Nitrogen above 700 °C show obviously high $^{15}\text{N}/^{14}\text{N}$. The highest $^{15}\text{N}/^{14}\text{N}$ ratio of $452 \pm 37 \text{‰}$ observed in the 800 °C fraction, although cosmogenic nitrogen may be present, is higher than the highest ratio in EETA79001. Since only a small amount of cosmogenic nitrogen is released below 900 °C in general (e.g. case for eucrites [8]), the extremely high ratio observed in 800 °C of ALH84001 may be due to mainly trapped nitrogen component.

Becker and Pepin [4] proposed that compositions of nitrogen and ^{40}Ar in EETA79001 lithology C can be explained by two component mixing between the martian atmosphere and the terrestrial atmosphere. Using results on nitrogen obtained here (>700 °C) and noble gases we measured before [3], $^{40}\text{Ar}/^{14}\text{N}$ atomic ratio of ALH84001 is calculated to be ~ 0.2 . According to the two component mixing model, $^{40}\text{Ar}/^{14}\text{N}$ ratio of 0.2 expects $\delta^{15}\text{N}$ of 300- 450 ‰. This is consistent with the measured $\delta^{15}\text{N}$ value, i.e. the observed highest ratio of 452 ‰ or the bulk ratio of 315 ‰ (>700 °C).

COSMOGENIC NITROGEN

The concentration of cosmogenic ^{15}N is calculated to be 0.090 ppb if we use a production rate of ^{15}N by [7] and the exposure age of 14.4 m.y. The calculated cosmogenic ^{15}N is about 90 % of observed excess ^{15}N . The bulk nitrogen isotopic composition after correction of cosmogenic ^{15}N is, therefore, close to the terrestrial value. This is inconsistent with above interpretation. However, since the abundance of nitrogen in this meteorite is very low, correction for cosmogenic nitrogen may be serious. It is necessary to find out whether cosmogenic nitrogen is completely extracted from the sample.

Table 1 Nitrogen abundance and isotopic composition.

Temperature[°C]	Nitrogen[ppm] no blank correction	Nitrogen [ppm]	$\delta^{15}\text{N}$ [permil]
200	0.0822	0.0818	3.5 ± 2.2
300	0.0400	0.0396	-13.0 ± 2.5
400	0.0233	0.0228	-11.9 ± 3.4
500	0.0257	0.0251	39.1 ± 3.3
600	0.0195	0.0186	109 ± 5
700	0.0147	0.0135	318 ± 16
800	0.0183	0.0158	452 ± 37
900	0.0134	0.0103	311 ± 58
1000	0.0131	0.0088	352 ± 117
1100	0.0174	0.0119	248 ± 81
1200	0.0234	0.0159	200 ± 66
1200	0.0095	0.0020	364 ± 551

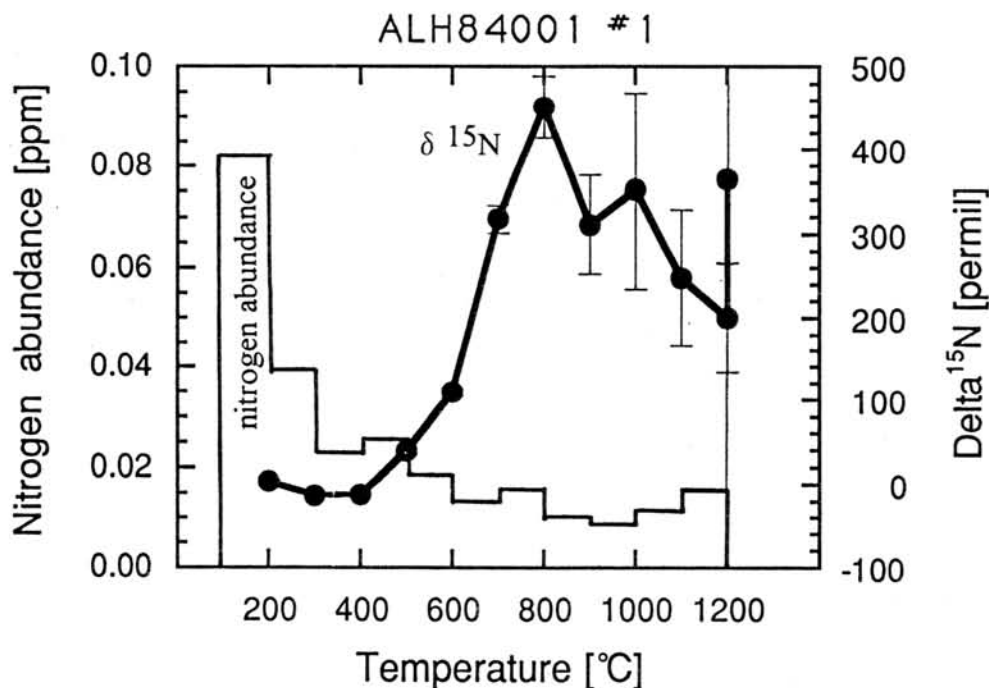


Fig. 1 Release profile of nitrogen by stepped combustion analysis.

Acknowledgment: We thank the Meteorite Working Group for providing the sample.

REFERENCES [1]Score, R. and Lindstrom, M. (1993) Antarctic meteorite Newsletter 16 (3). [2]Mittlefehldt, D.W. (1994) *Meteoritics* **20**, 214-221. [3]Miura, Y.N., Sugiura, N. and Nagao, K. (1994) *LPSC XXV*, 919-920. [4]Becker, R.H. and Pepin, R.O. (1986) *EPSL* **69**, 225-242. [5]Nier, A.O. and McElroy, M.B. (1977) *J. Geophys. Res.* **28**, 4341-4349. [6]Boyd, S.R., Wright, I.P., Franchi I.A. and Pillinger, C.T. (1988) *J. Phys. E: Sci. Instrum.* **21**, 876-885. [7]Becker, R.H., Clayton, R.N. and Mayeda, T.K. (1976) *Proc. Lunar Sci. Conf.* **7th**, 441-458. [8]Miura, Y and Sugiura, N. (1993) *Proc. NIPR Symp. Antarctic. Met.* **6**. 338-356.

Bubbles as a candidate for a noble gas trapping site : Yamato-74063

K. Ozaki ¹⁾, N. Takaoka ¹⁾, Y. Motomura ¹⁾, and K. Nagao ²⁾

¹⁾Department of Earth and Planetary Sciences, Faculty of Science, Kyushu University, Hakozaki, Fukuoka 812

²⁾Institute for Study of the Earth's Interior, Okayama University, Misasa, Tottori 682-01

Unique meteorite Yamato-74063 contains large amounts of trapped heavy noble gases. The concentration of trapped ^{36}Ar is comparable with that of E-, C-chondrites and ureilites. Trapped ^{132}Xe is also unusually abundant [1,2].

In carbonaceous chondrites and ureilites, a candidate for noble gas trapping site is carbonaceous matter [e.g., 3, 4, 5]. The concentrations of heavy noble gases in Yamato-74063 require that all the material molten by a laser shot is carbon, if carbon be the host phase of trapped gas [6, 7]. However, carbonaceous matters have not been reported for this meteorite.

For identification of a noble gas trapping site, we extracted noble gases *in situ* using laser microprobe and measured them by a high sensitivity noble gas mass spectrometer [2, 6, 7]. (See [8] for details of experimental methods) In those studies, we detected huge amounts of trapped ^{36}Ar , ^{84}Kr , ^{132}Xe in orthopyroxene containing tiny metal inclusions. Inspecting with an optical microscope and an electron probe microanalyser (EPMA), we discovered bubbles in the orthopyroxene of other polished thin sections that were prepared from the same chip as analysed in the laser experiment [6]. Consequently we proposed the bubble hypothesis [6, 7].

In this work, we examined mineral grains in the thin section of 60 μm thick by optical microscope and EPMA observations, and measured noble gases by mass spectrometer using laser microprobe (with laser beam of 50 μm in diameter and molten weight of 0.14-0.70 μg for 1 pulse depending on target mineral). In particular, we aimed mainly at orthopyroxene containing the tiny metal inclusions to confirm bubbles as a candidate for a noble gas trapping site.

Result of the laser microprobe analyses is given in Fig.1. Several grains such as pit 40, 42, 47, 48, 51 and 53 released large amounts of trapped gases. These pits were all orthopyroxenes containing the tiny metal inclusions. We observed bubbles of approximately 5 μm in diameter existing in pit 40, 51 and 53. Other pits were so dusty that we could not observe bubbles with transmitted light although

voids with 1 to several μm across were found by reflected light and back-scattered electron image on the surface.

In these spots, possible candidates of a noble gas trapping site are orthopyroxene, metal inclusions, chromite, apatite, troilite and bubbles. That orthopyroxene devoid of metal inclusions (pit 54) did not release trapped noble gases indicates orthopyroxene is not a trapping site. Because pit 38 containing the tiny metal inclusions released negligible amounts of trapped gases, metal inclusions are not trapping sites. Chromite (pit 50) released negligible amounts of trapped gases. The amounts of noble gases from apatite (pit 44) and troilite (pit 46) were low. To explain enormous amounts of ^{36}Ar for pit 48, they have to melt approximately 6.0 μg for apatite and 37 μg for troilite, respectively. Nevertheless, molten weight estimated on cosmogenic ^3He [7] and by measured diameter and depth of pit 48 is 0.35 μg . We observed chromite, apatite and troilite as accessory minerals.

For these reasons, we nominate bubbles as a candidate for a noble gas trapping site in orthopyroxene containing the tiny metal inclusions in Yamato-74063.

References

- [1] Takaoka, N. and Yoshida, Y. (1991) Proc. NIPR Symp. Ant. Met. **4**, 178-186.
- [2] Takaoka, N., Nagao, K. and Miura, Y. (1993) Proc. NIPR Symp. Ant. Met. **6**, 120-134.
- [3] Gobel, R., Ott, U. and Begemann, F. (1978) J. Geophys. Res. **83**, 855-867.
- [4] Wacker, J. F. (1986) Geochim. Cosmochim. Acta. **50**, 633-642.
- [5] Wieler, R., Anders, E., Baur, H., Lewis, R. S. and Signer, P. (1992) Geochim. Cosmochim. Acta. **56**, 2907-2921.
- [6] Takaoka, N., Motomura, Y., Ozaki, K. and Nagao, K. (1993) 18th Symp. Ant. Met. NIPR., Tokyo, (Abstract). 41-43.
- [7] Takaoka, N., Motomura, Y., Ozaki, K. and Nagao, K. (1994) Proc. NIPR Symp. Ant. Met. **7**, 186-196.
- [8] Nagao, K. and Abe, T. (1994) J. Mass Spectrom. Soc. Jpn. **42**, 35-48.

Yamato-74063

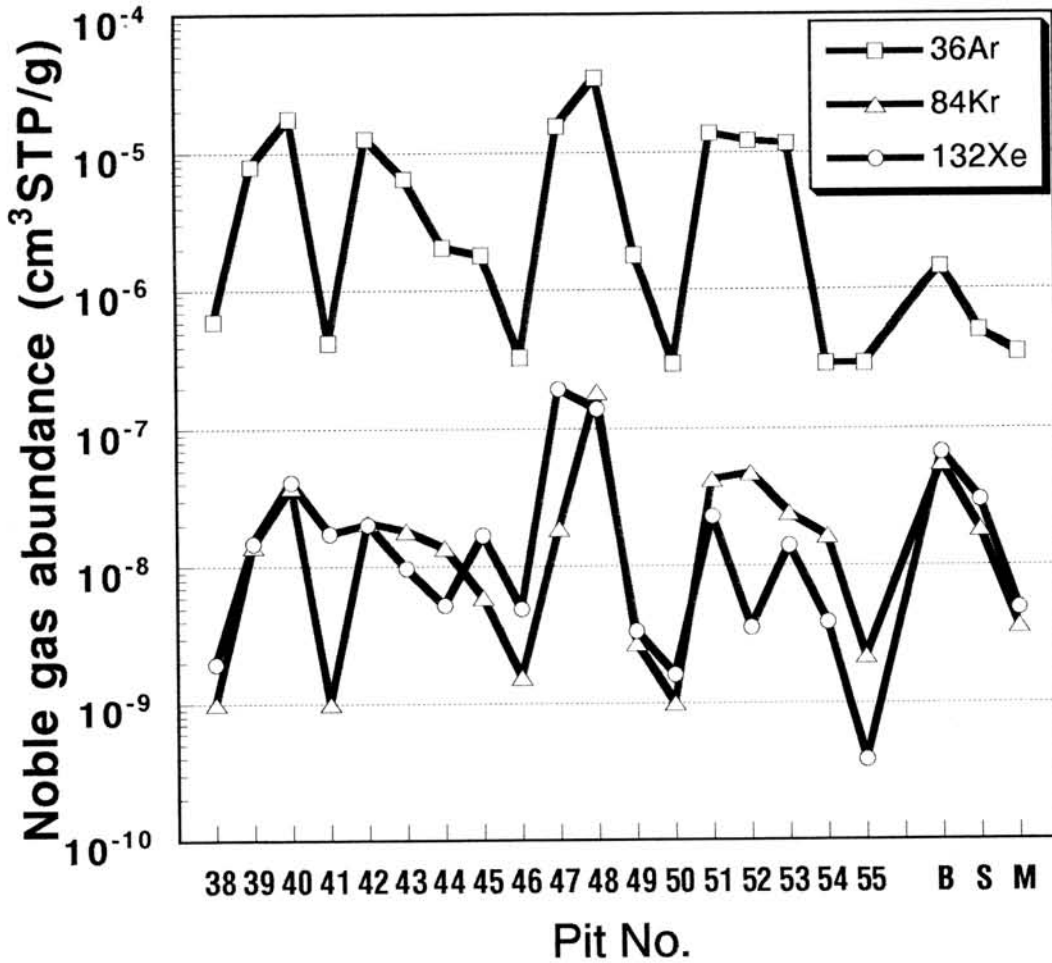


Figure.1 Noble gas abundances from pit 38 to 55 are given. The abundances for bulk (B), silicate (S) and metal (M) are also presented for comparison [2]. Typical blanks, dividing by molten weight ($0.4 \mu\text{g}$), are : $^{36}\text{Ar} = 3 \times 10^{-7}$, $^{84}\text{Kr} = 1 \times 10^{-9}$ and $^{132}\text{Xe} = 3 \times 10^{-10} \text{cm}^3 \text{STP/g}$.

Accretion of fine particles :Experimental study under the
atmospheric pressure.

Naoji Sugiura, Yukiko Higuchi and Tomoyuki Sakaguchi

Department of Earth and Planetary Physics, Univ. of Tokyo, Tokyo
Japan

Accretion of fine particles is an important process in the early solar system that determines 1) the settling of fine particles to the equatorial plane of the solar nebula and hence the formation of planetesimals, and 2) the thermal structure of the nebula that is dependent on the particle size through opacity. We review the present state of our knowledge on accretion of fine particles and suggest future directions of the study.

It is generally agreed that the sticking probability of fine particles is 1 for submicron particles, but at sizes larger than 1 micrometer, there exists almost no data on the sticking probability. A recent study (Blum and Munch, 1993) showed that aggregates (with radius from 0.2 to 2 mm) of fine particles did not stick when collided at a speed of 0.15 to 4 m/s. Therefore, somewhere between 1 micrometer and 200 micrometer, sticking probabilities of fine particles change from nearly one to nearly zero. We have been studying sticking probabilities of aggregates of fine particles in this size range using an optical sizing method. Our aggregates have a fractal structure and the relative velocity of collisions is of the order of 1 mm/s. Although we tentatively concluded that the sticking probability for 100 micrometer size aggregates is small under the experimental condition (Sugiura and Higuchi, 1993), there remain many uncertainties, such as 1) the method of optical sizing for fractal aggregates, and 2) the collision frequency of fractal aggregates. We will briefly describe these problems here.

The optical sizing method has been well established for spherical particles. This method utilizes the fact that the smaller the size, the larger the angle of scattered light. For spheres with various sizes, the size distribution is determined by solving $Y(i)=M(i,j)X(j)$, where $Y(i)$ is the scattered light intensity at angle i , $X(j)$ is the number density of spheres with size j , $M(i,j)$ is the scattering matrix which is determined by Mie theory. Dust aggregates which are formed in the chamber (or were formed in the early solar system) are not solid spheres but have a porous fractal structure. For such aggregates the scattering matrix $M(i,j)$ must be determined by taking account of all the interaction among constituent particles (discrete dipole approximation; DDA). We made such calculations for very small aggregates, and extrapolated the results to larger aggregates. This extrapolation involves many orders of magnitude,

and thus rather uncertain. In the near future, we intend to do the DDA calculation for larger aggregates, to reduce uncertainties due to the extrapolation.

Under the experimental condition at 1 atmosphere, the presence of air affects the collision rate between aggregates. In the case of collisions between solid spheres in the air, the collision rate is greatly reduced due to the presence of air when compared with the collision rate for ballistic trajectories. In our previous estimate of the sticking probability, such an effect has not been taken into account. In the case of fractal aggregates, this effect is expected to be not as important as in the case of solid spheres. Yet, in future studies we need to take it into account.

In terms of meteorite studies, the sticking probability of fine particles on larger objects is important. For instance, accretion features observed in chondrites are mainly the rims of fine particles around chondrules and other inclusions. We will in our future study examine the sticking probability of aggregates on walls on the chamber. Such a study will reveal whether the fine particle rims on chondrules and on inclusions represent the whole fine particles in the nebula, or they represent only a tiny fraction of fine particles. A related unsolved problem is the relationship between the rims and the matrix.

At the meeting we will report up-to-date results on these problems.

References

- J.Blum and M.Munch, Experimental investigations on aggregate-aggregate collisions in the early solar nebula, *Icarus*, 106,151-167, 1993
- N.Sugiura and Y.Higuchi, Accretion of fine particles: sticking probability estimated by optical sizing of fractal aggregates, *Meteoritics*, 28,445, 1993.

OPTICALLY STIMULATED LUMINESCENCE OF METEORITE

Syunji Takaki, Chihiro Yamanaka and Motoji Ikeya

Department of Earth and Space Science, Osaka University, Toyonaka, Osaka 560 Japan

1. Introduction

Lattice defects produced by natural radiation have been accumulated for a geological time. The cumulative defects whose concentration is proportional to the radiation dose or to the age can be detected by electron spin resonance (ESR)¹⁾ and thermoluminescence (TL)²⁾. Optically stimulated luminescence (OSL) can be also used to determine the concentration of defects¹⁻³⁾.

Historically, the luminescence dating using a nitrogen laser was proposed for cave deposits (CaCO_3) based on the principle of radiation effects used in TL dating. The method has been successfully applied to dating of quartz and feldspar in sediments taking advantage of the sun-light-bleaching effects.

Meteorites have been the object of ESR⁴⁾ and TL studies. An attempt to date the time of meteorite fall⁵⁾ and characterization of meteorites⁶⁾ have been reported. However, no work has been done on meteorites using OSL so far as we know. Hence, we have studied the meteorite using OSL, TL and ESR. Ca-Al-rich inclusions (CAIs) and matrix of Allende was measured in this study.

2. Experimental

A beam from a commercial He-Ne laser (JLH-1PS-B, 1mW) is used as the exciting light for the OSL as shown in Fig.1. TL can be measured with this apparatus by heating the sample holder. The laser light ($\lambda=633\text{nm}$) has been enlarged to $\sim 10\text{mm } \phi$ by a beam-expander so that the light irradiates uniformly on the powdered sample spreading on the aluminum holder. Optical filter (V-40, V-42, R-60) are used to cut the scattering light to the photomultiplier (Hamamatsu Photonics, Bialkali, R878). The photon counting method is used to detect the luminescence. Only the visible light can be detected with this system.

A piece of meteorite Allende was used for this study. The CAIs and the matrix portion were separated manually in a dark room. Gamma ray from the source of ^{60}Co were irradiated to calibrate the OSL intensity to radiation dose. TL was also

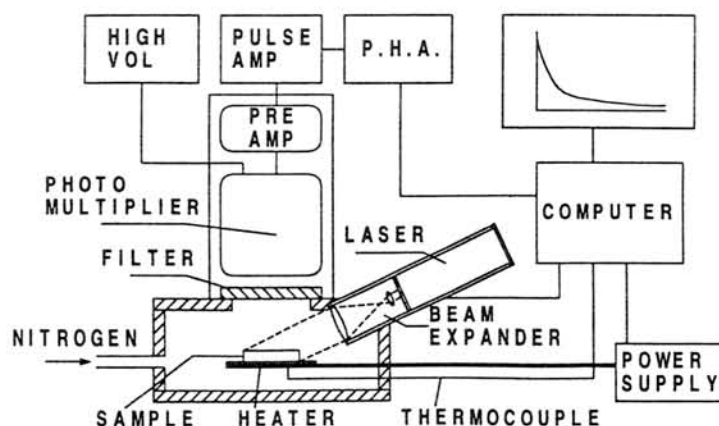


Fig.1. Used apparatus for optically stimulated luminescence (OSL) and thermoluminescence (TL).

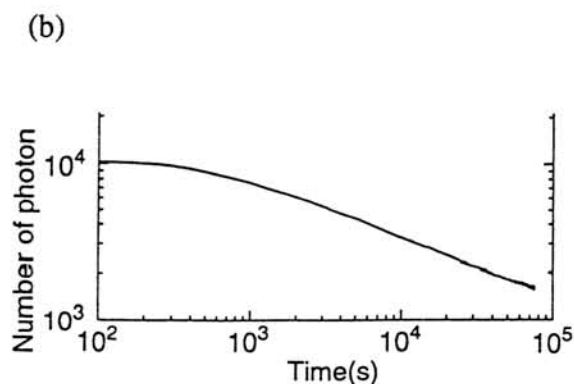
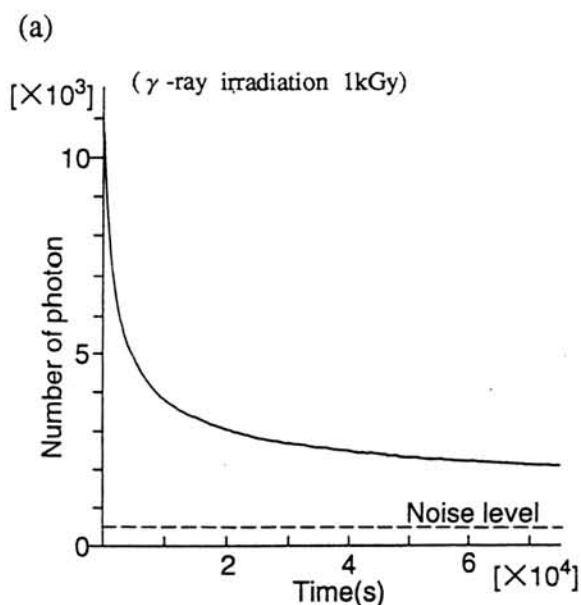


Fig.2 (a). Intensity of OSL as a function of the time after the exposure to the laser light. **(b)** Logarithmic plot of the OSL intensity as a function of the time.

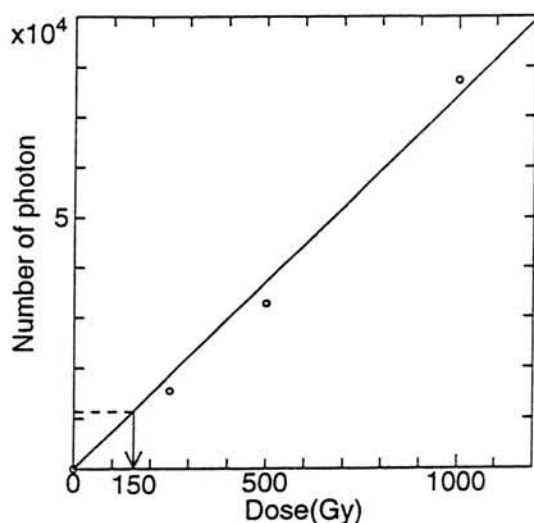


Fig.3. Growths of OSL intensity by gamma-irradiation as a function of the radiation dose.

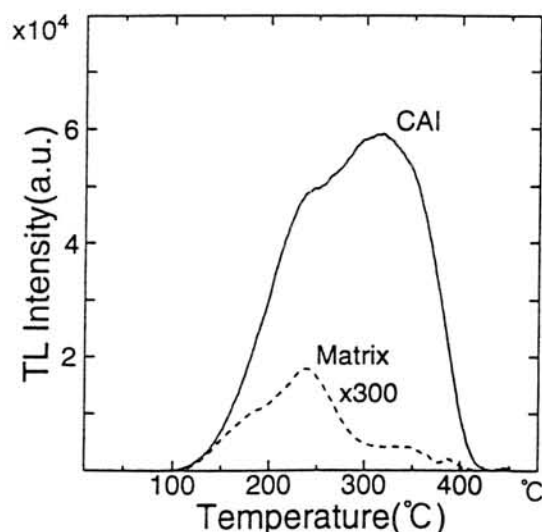


Fig.4. Thermoluminescence (TL) curve of CAIs and the matrix of the meteorite Allende. Note that the TL intensity for the matrix is multiplied by a factor of 300.

measured using the same apparatus at the heating rate of $5^{\circ}\text{C}/\text{s}$.

3. Result and Discussion

The OSL intensity after the irradiation of the laser light is shown in Fig.2-(a). The OSL intensity decayed after the exposure to the laser light. The OSL intensity decayed to the half of the initial value in $3 \times 10^3 \text{s}$ and to the quarter in $2 \times 10^4 \text{s}$. The logarithmic plot shown in Fig.2-(b) indicates in this case that the intensity changes nearly proportional to $t^{-1/3}$. The OSL continued more than 24 hours. It decreased to zero after the exposure to the sun-light for one-hour.

The OSL intensity was enhanced by γ -irradiation. The OSL intensity after γ -

irradiation is shown in Fig.3 as a function of the radiation dose. The OSL intensity observed in CAIs before γ -rays irradiation corresponded to the dose of 150 Gy. No OSL intensity was detected for the matrix even after γ -irradiation up to 500Gy.

TL curve for CAIs and for the matrix are shown in Fig.4. The intensity of luminescence from the matrix was extremely weak. The TL of CAIs appeared above 100°C. It showed double peaks at 210°C and 310°C. No change was observed after the OSL measurement in the shape of the TL curve. This indicates that the defects causing OSL are not directly related to TL. The equivalent dose(ED) of 150Gy obtained from the growth curve of OSL is now under investigation.

References

- 1) Ikeya M. (1993): *NEW APPLICATIONS OF ELECTRON SPIN RESONANCE* (World Scientific Publishing, Singapore).
- 2) Aitken M. J. (1985): *Thermoluminescence Dating* (Academic Press, London).
- 3) Ugumori U. and Ikeya M. (1980) *Jpn. J. Appl. Phys.* 19, 459-465.
- 4) Yamanaka C., Toyoda S. and Ikeya M. (1993) *Proc. NIPR Symp. Antarct. Meteorites.* 6, 417-422.
- 5) Ninagawa K., Miono S., Yoshida M. and Takoaka N. (1983) *Lett. Nuovo Cimento (Italy).* 38, ser.2, no.2, 33-6, 10 Sept.
- 6) D. W. G. Sears (1988) *Nucl. Tracks Radiat. Meas.* 14, Nos 1/2, 5-17.

Magnetic Properties of High Petrologic Grade L-LL Chondrites, Tenham, Tuxtuac, Willard and Forrest B

A. YAMANAKA¹, M. FUNAKI² and H. NAGAI¹

1:Shinshu University, Faculty of Science, 1-1 Asahi 3, Matsumoto 390

2:National Institute of Polar Research, 9-10 Kaga 1, Itabashi, Tokyo 173

Magnetic minerals in ordinary chondrites consist of iron-nickel alloys of various compositions. The principal components are kamacite and taenite. We have studied magnetic properties of high petrologic grade ordinary chondrites, Tenham(L6), Tuxtuac(LL5), Willard(L6) and Forrest B(L6). If a sufficiently strong magnetic field was present in the parent body; the chondrite has the possibility to record the cosmic magnetic field because of the higher petrologic temperature than Curie point of the magnetic mineral.

The magnetic hysteresis loops of small bulk samples and powder samples (magnetic composition and non-magnetic composition) of chondrites were measured from room temperature to 780° C. These measurements were performed with a heating rate of 50° C/h and 10⁻⁴Pa in pressure. From these results kamacite (7at.%Ni Fe-Ni alloy) was clearly identified in the J_s -T and X-T curves of Tenham, Willard and Forrest B chondrites (Fig.1, 2). Taenite containing about 50 at.% Ni was also clearly identified in the curves of three chondrites. In Tuxtuac, there is no (or slightly small amount of) kamacite and tetraetaenite with taenite containing about 50 at.% Ni was clearly identified in Hc-T and X-T curves of magnetic component powder sample (Fig.3).

The NRM (natural remanent magnetization) of subsamples of each chondrite are almost completely thermally demagnetized up to 580° C while about 15% of original NRM remained on the subsample of Forrest B over 600° C. This result suggest that taenite (and/or tetraetaenite) is the NRM carrier of these chondrites. The NRM stability against AF demagnetization up to 50mT in subsamples was different from each chondrite but might have a tendency which was that the bulk coercivity of these chondrites is not mainly determined by the amount of tetraetaenite. Tenham has the most stable NRM of four chondrites. Tuxtuac has most unstable one, though it contains tetraetaenite with high magnetocrystalline anisotropy ($K_1=3.2 \cdot 10^5 \text{ J/m}^3$, $K_2=2.3 \cdot 10^5 \text{ J/m}^3$) clearly. Willard has two types of the NRM (stable and unstable) and NRM of Forrest B was demagnetized with changing its intensity (Fig.4).

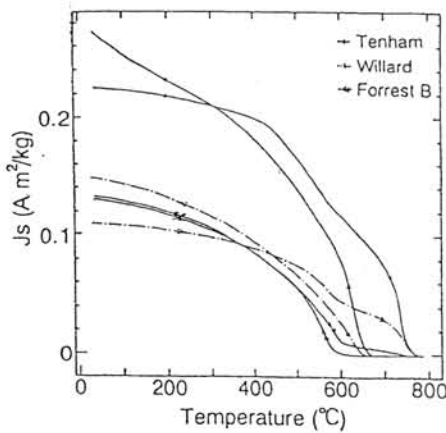


Fig.1 J_s -T curves of bulk samples of Tenham, Willard and Forrest B

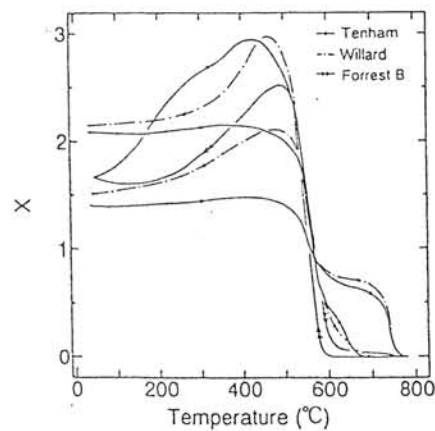


Fig.2 X-T curves of bulk samples of Tenham, Willard and Forrest B

These experimental results suggest that the stable NRM against AF demagnetization is carried by taenite (containing about 50 at.% Ni) and/or tetrataenite with high coercivity. But the high magnetocrystalline anisotropy of tetrataenite seem not to be important factors which determine the bulk H_c . And the magnetic field might be absent or negligibly small in their parents bodies during final thermal metamorphism because the directional changes of NRM exhibited a gradual thermal demagnetization with many variation of directional changes. The NRM carried by magnetic grains with high magnetic coercivity is hardly consisted of TRM (thermal remanent magnetization). We discuss some implications of these magnetic record of four high petrologic grade ordinary chondrites.

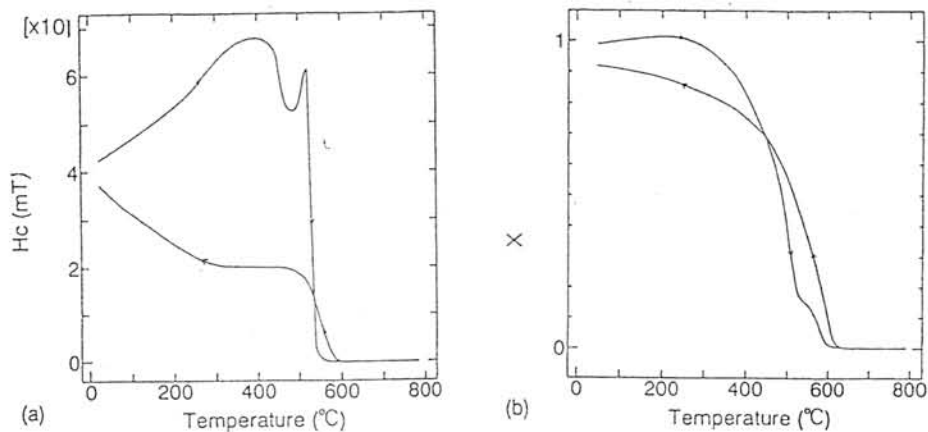


Fig.3 (a) H_c - T and (b) X - T curves of powder sample of magnetic component of Tuxtuac

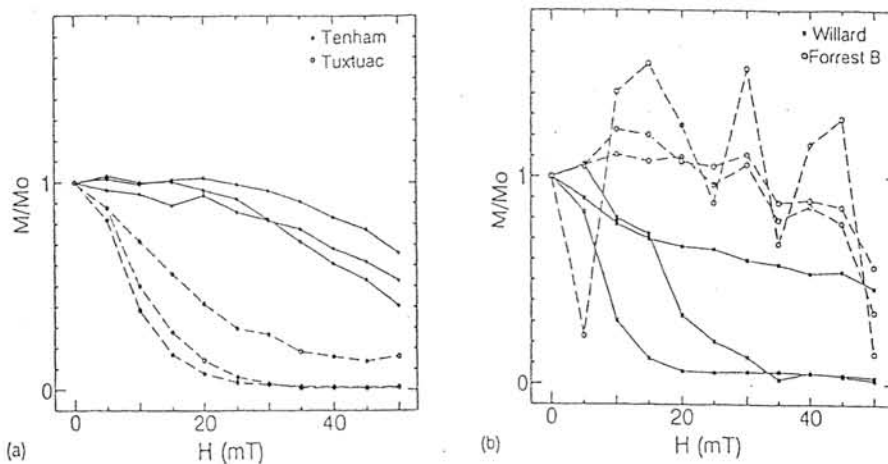


Fig.4 AF demagnetization curves of NRM of (a) Tenham and Tuxtuac bulks, (b) Willard and Forrest B bulks

References:

- BOZORTH, R.M. and WALKER, J.G. (1953) *Physical Review* Vol.89, No.3, 624-628.
 FUNAKI, N., NAGATA, T. and DANON, J.A. (1985) *Mem.Natl.Inst.Polar Res., Spec.Iss.*, 41, 382-393.
 NAGATA, T. and FUNAKI, N. (1987) *Mem.Natl.Inst.Polar Res., Spec.Iss.*, 46, 245-262.
 NEEL, L., PAULEVE, J., PAUTHENET, R., LAUGIER, J. and DAUTREPPE, D. (1964) *J.Appl. Phys.*, 35, 873-876.
 SUGIURA, N. and STRANGWAY, D.W. (1982) *Mem.Natl.Inst.Polar Res., Iss.*, 25, 260-280.

ELECTRONMICROSCOPICAL STUDY OF THE DISTAL EJECTA LAYER FROM FLINDERS RANGES IN SOUTH AUSTRALIA. Marek ZBIK & Victor A. GOSTIN, Department of Geology & Geophysics, University of Adelaide, Adelaide, South Australia 5005.

Introduction An extensive layer of a distal ejecta blanket has been found in the 600 million years old Precambrian Bunyeroo Formation and described by Gostin et al. [1]. The impact location creating this ejecta blanket is about 300 km west of the Flinders Ranges, at Lake Acraman, Gawler Ranges, South Australia [2]. A description of the ejecta composition and shock features, both in coarse clasts called "Flindersites" and in fine sediments were recently presented in [3, 4]. Here we present results of chemical analyses and electronmicroscopical study of three major sublayers of the ejecta blanket from Bunyeroo Gorge in the central Flinders Ranges. Samples have been collected from the rock layer as shown on Fig. 1. The genesis of shown sublayers have been described in [1 & 4].

Fig. 1- Impact ejecta layer from Bunyeroo Gorge in the central Flinders Ranges.

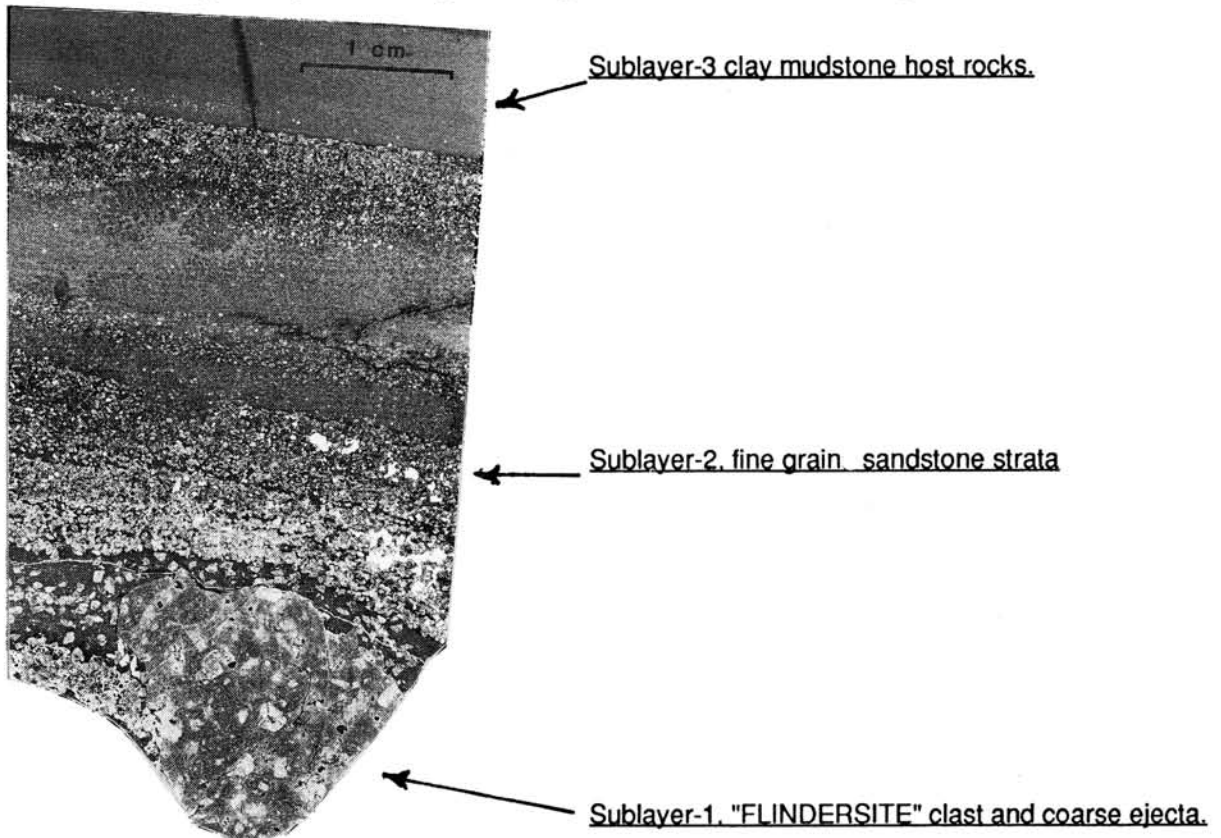


Table 1. Chemical composition of sublayers within the ejecta layer.

SAMPLE	whole rock			clay fraction		
	1	2	3	1	2	3
SiO ₂	69.7	67.4	61.5	36.8	31.3	50.2
Al ₂ O ₃	13.8	14.4	16.3	15.3	12.0	21.4
Fe ₂ O ₃	2.9	1.8	3.5	20.4	11.0	5.2
MnO	0.3	1.7	0.2	4.1	13.3	0.4
MgO	1.7	1.0	4.1	4.0	2.8	6.0
CaO	0.5	0.5	0.7	0.9	1.3	0.3
Na ₂ O	4.4	6.3	1.7	1.0	1.6	0.9
K ₂ O	2.8	1.2	4.3	3.3	2.2	5.8
TiO ₂	0.7	0.8	0.9	0.9	1.7	0.7
P ₂ O ₅	0.2	0.2	0.1	0.1	0.8	0.1

Results From the chemical composition presented in Table 1 can be seen that both coarse and fine ejecta sublayers (as whole rock and clay fraction) are depleted in potassium when compared to the host rock mudstone. The high sodium values in sublayers-1 and 2 result from their high albite content. Microprobe investigations determined two different types of albite. One, derived by impact from the target volcanic dacites, averages $Or_{5.7}Ab_{92.3}An_{2.3}$. Second, diagenetic albite crystals, formed as a secondary mineral inside the pores created by replacing primary material, probably glass. This new albite, developed especially around former glassy spherules and shard-like clasts, has an average composition of $Ab_{99.4}An_{0.6}$.

Photographs from Scanning Electron Microscope (SEM) presented on Fig.2a & b show the turbulent microstructure of diagenetically compressed sublayer-3 material. It is formed by clay chlorite and illite micro-aggregates, well oriented along the bedding and closely enveloping quartz silt grains (up to 50 μ m in diameter). According to [5] turbulent microstructure is formed during the course of lithogenesis, during compaction of clay sediments containing high porosity honeycomb, and possibly, matrix microstructure. Because of the high degree of microaggregate orientation, the pores usually have an elongated form and extend along the bedding, making permeability extremely low especially in a vertical direction .

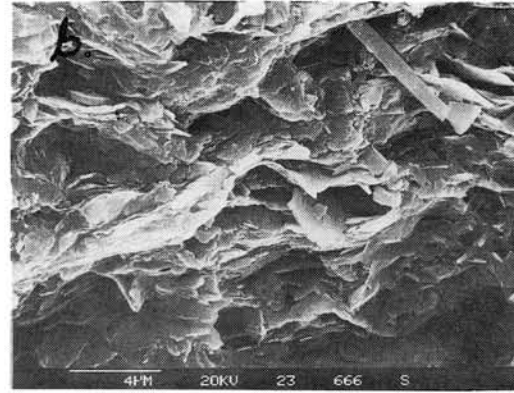
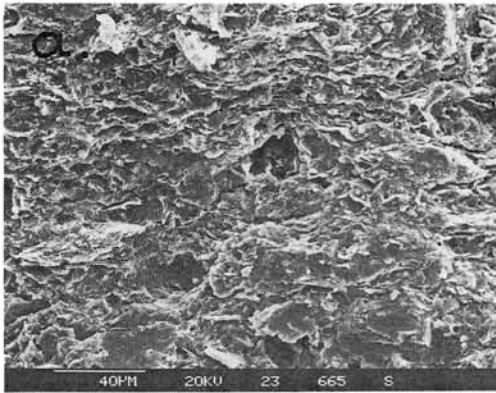


Fig. 2a & b,- Turbulent microstructure in the silty claystone sublayer-3

On Fig.2c & d fine grained sandstone from sublayer-2 (upper part) shows a typical well developed granular structure with a high intergranular porosity. Highly weathered sand size grains of feldspathic clasts are recognizable with difficulty because they are covered by an intergrowth of diagenetic albite and clays. These clays seen on Fig.2d, show a high porosity with an ultrafine cellular honeycomb structure developed on the diagenetic albite crystals. Such structures are characterized by high specific surface values.

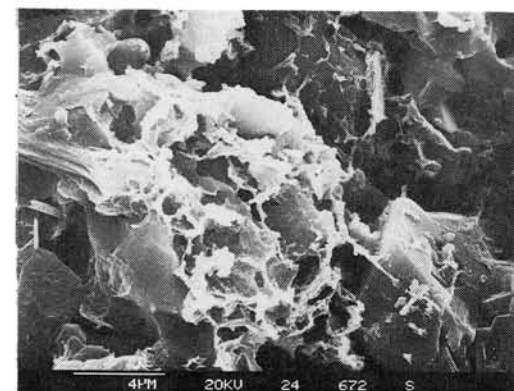
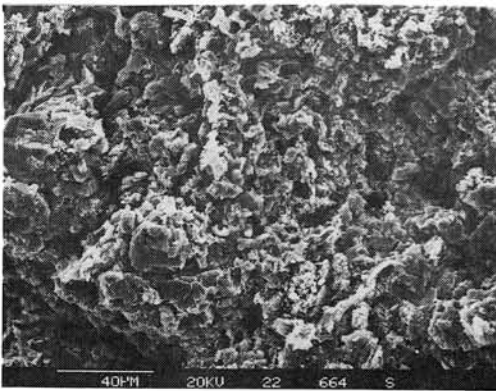


Fig. 2c,- Fine grained sandstone from sublayer-2.

Fig. 2d,- High porosity sheet silicates on albite.

Fig.2e & f show large pore systems developed inside and between highly weathered felspar grains in the coarse ejecta sublayer-1. Also in this sublayer, well developed diagenetic albite crystals as small as $10\ \mu\text{m}$ (Fig 2e) are seen inside empty spaces, while Fig.2f shows spongy clay aggregates cemented by iron and manganese minerals.

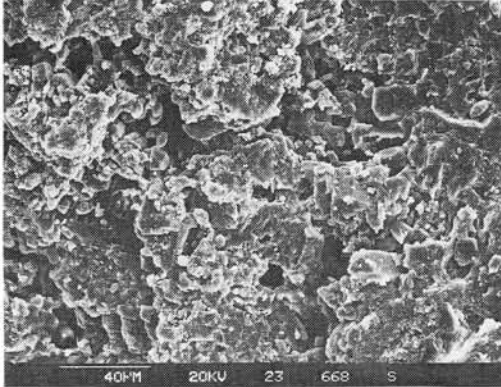


Fig 2 e,- Albite crystals in pore spaces sublayer-1.

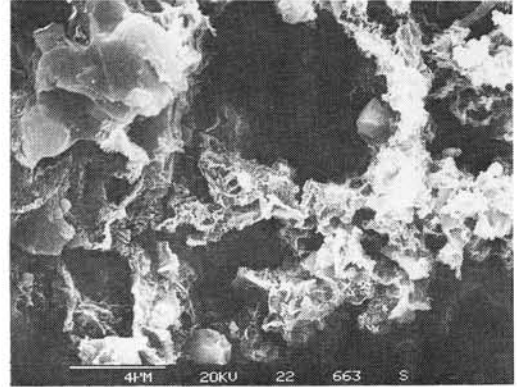


Fig. 2f,- Spongy clay aggregates in sublayer-1

Such manganese minerals, probably birnessite or vernadite, and other minerals like goethite with sheet silicates (illites and chlorites) shown on Fig.3a have been obtained by Transmission Electron Microscopy (TEM). Such a mineral assemblage is characteristic of both sublayers-1 and 2 which contrasts with the host rock sublayer-3 where only sheet silicates have been observed (Fig. 3b). The high Fe and Mn contents in the chemical composition of the clay fraction results from the presence of these observed minerals.

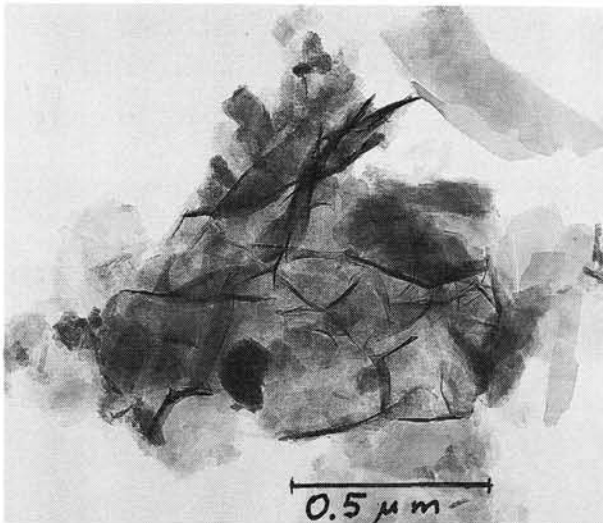


Fig. 3a- Mixture of goethite, sheet silicates, manganese minerals in sublayer 1 and 2.

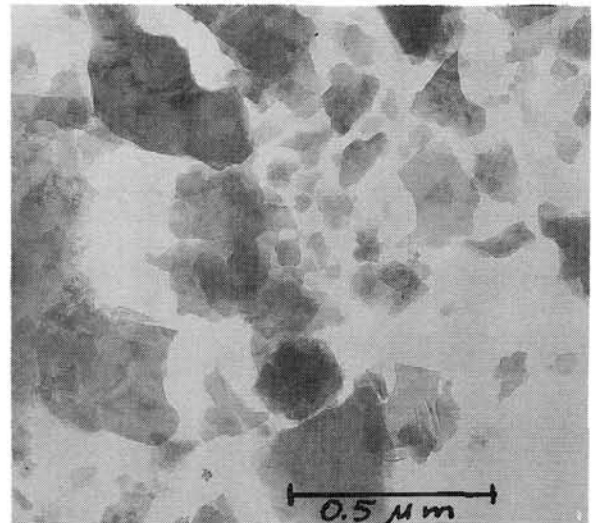


Fig. 3b- Sheet silicates; illite and chlorite in sublayer 3.

Among sheet silicates from sublayer-3, taken close to the coarse ejecta (sublayer-1) a tiny, $0.5\ \mu\text{m}$ diameter nickel particle has been found (Fig. 4). Such a particle could represent a remnant of the Ni rich core or a platinum rich nugget [6] from an FeNi spherule derived from the bolide explosion.

Discussion Ni rich particles, are more likely to be preserved in the impermeable and low porous sublayer-3 where sheet silicates are closely packed, and may also cover fragile remnants of cosmic spherules and microtektites. Such particles have been protected both against recent weathering and from tectonic forces when the Flinders Ranges were folded. These forces discharged their energy by

transforming the former highly porous sedimentary honeycomb structure to a compact turbulent one. Thus possible missile remnants could be found in the silty claystone layer that separates sublayers-1 and 2. In that layer well preserved spherules and shard-like clasts had been found and described in Gostin et al [1]. The absence of spherules and other glassy remnants in sandy sublayers-1 and 2 may be due their post-sedimentary mechanical destruction and chemical dissolution in these high porosity layers.

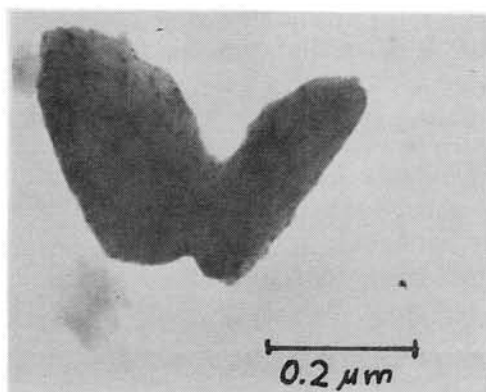


Fig. 4.- A nickel particle found in sublayer-3 close to sublayer-1 coarse ejecta.

REFERENCES: [1]- Gostin V.A. et al. (1986) *Science* Vol. 233, pp.198-200. [2]- Williams G.E. (1986) *Science* Vol. 233, pp. 200-203. [3]- Gostin V.A. and Zbik M. (1994) "Flindersites", distant ejecta impactites from South Australia, 25th, LPSC Houston. [4]- Gostin V.A. and Zbik M. [1994] "Flindersite" bearing impact ejecta layer from South Australia, 25th, LPSC Houston. [5]- Grabowska-Olszewska B. (1984) *Atlas of the Microstructure of Clay Soils*. PWN, Warsaw. [6]- Brownlee D.E et al. (1984) *Nature* Vol. 309, pp 693-695.

INFRARED ABSORPTION OF THE DIAPLECTIC GLASS. Lin Wenzhu, Institute of Geochemistry, Chinese Academy Sciences, Guiyang 550002, China

The diaplectic glass (or call shock glass), including nuclear explosive, impact crater, shock recovery experimental melts, and tektites, are amorphous solids formed by rapid release of ultra-high temperature and pressure. The thermodynamics system nearly doesn't exist thermal conductive and diffusion to be nonequilibrium dynamics. In space-time the rocks and minerals suddenly melted to occur order-disorder chaotic transition. The volcanic glass is quenched melts of the magma which is the phase equilibria. Water is one of the most important volatiles in magmas. A variety of magmas come from different depth to produce various temperature-pressure mineral assemblages. So, volcanic glass maintained primary crystal. The structural state of both diaplectic and volcanic glass apparently differs as Fig. 1,2. In a few words, Two species glass can be discriminated by the infrared absorption spectra.

Reference: [1]. Lin Wenzhu and Liu gaokui, CHINESE SCIENCE BULLETIN 38, 250-253, 1993 [2]. Stoffler, D., Fortscher. Miner. 51, 256-289 1974. [3]. Mysen, B. O., Virgo, D., Harrison, W. J. and Scarfe, C. M., American Mineralogist 65, 900-914 1980

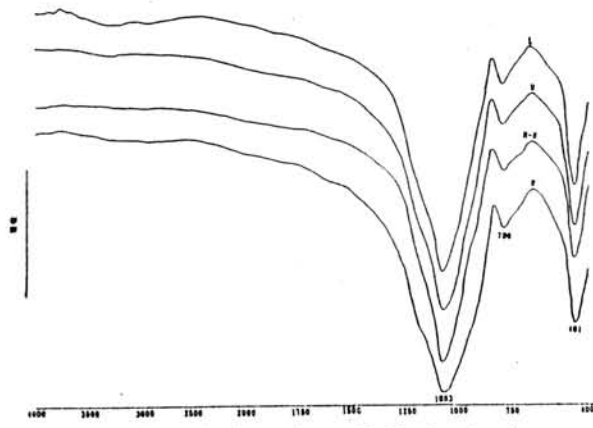


Fig. 1 Infrared absorption of diaplectic glass

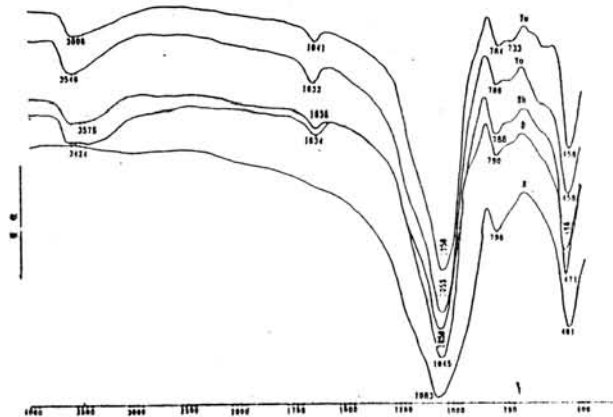


Fig. 2 Infrared absorption of volcanic glass

MORPHOLOGY OF ANTARCTIC COSMIC DUST SPHERULES, AND COMPARISON TO SPHERULES FROM THE TUNGUSKA CATASTROPHE.

Marek ZBIK & Victor A. GOSTIN Department of Geology & Geophysics, University of Adelaide, Adelaide, South Australia 5005.

Introduction. Cosmic dust spherules are the degassed and droplet-shaped ultimate products of atmospheric heating of micrometeorites [1], or products of atmospheric ablation/explosion of meteoroids that differ in size and composition [2]. Most micrometeorites have a CM-similar composition but some could possibly be planetary in origin, or represent interstellar matter [1]. However there is strong evidence that the 0.1-1 mm cosmic dust particles which survive atmospheric entry are predominantly and perhaps exclusively asteroidal in origin [3].

Twenty two spherules were separated from a few mg of mixed dust sample obtained from the "EUROMET". This sample was collected in Antarctica during the January-February 1991 field season. Spherules were coated by carbon and investigated by Cambridge Scanning Electron Microscope (SEM) equipped with EDAX system.

Results. Morphology of the investigated spherules shows different groups of morphology. There are five morphological types:

- 1.- Smooth glassy surface.
- 2.- Chain-olivine chondrule.
- 3.- Rough granular surface:
 - 3.a- glaze covered, stiff surface.
 - 3.b- dendrite decorated.
 - 3.c- octahedron decorated.

Five spherules of type 1 (Fig 1a, b) were investigated. They are 60 to 120 μm in diameter; one of the spherules (Fig. 1a) has a droplet shape, another, the largest spherule shown on Fig. 1b shows conchoidal fractures probably caused by cracking. Surface composition of these spherules is homogeneous and contains Mg, Si, Fe, Ca and some Al (Fig. 2).

There is one chain-olivine spherule (Fig. 3) containing a few skeletal olivines traversing a glassy material. Such a spherule seems to be very close to the first type because its surface is rather smooth.

The rough surface spherules could be divided into three subgroups. Most of the type 3 spherules present rough glaze surfaces (Fig. 4a, b). Sometimes such spherules are inhomogeneous like that on Fig. 4a where an Fe-Ni bead is seen inside a glassy matrix (Fig. 4b), or are covered by Ni rich troilite. The angular, stiff surface type represents several grains which display sharp angular grain borders covered by a glazed surface. In some places such a glaze displays holes and cracks with crystal structure inside.

There are two different subgroups of decorated spherules, dendrite decorated (Fig. 5a, b) and octahedron decorated (Fig. 6a, b). Dendrite decorated spherules type, have a regular rounded shape and a rough surface covered by needle-like magnetite dendrites crystals. It seems possible that this texture was derived from spherules with a smooth glassy surface after the glassy material was leached from between the dendrite needles. Type 3c is different, the rough granular surface of such spherules is covered by tiny Ni rich magnetite octahedrons held together by a rough glaze of Mg, Si, Fe, Ni rich composition (Fig. 7). Such an envelope could probably occur as a result of condensation of tiny magnetite crystalites from the postexplosion gas cloud.

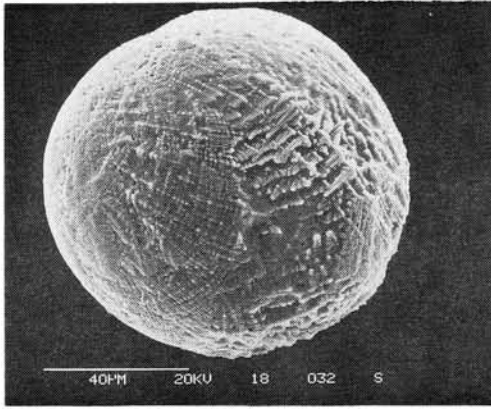


Fig. 5a- Dendrite decorated spherule

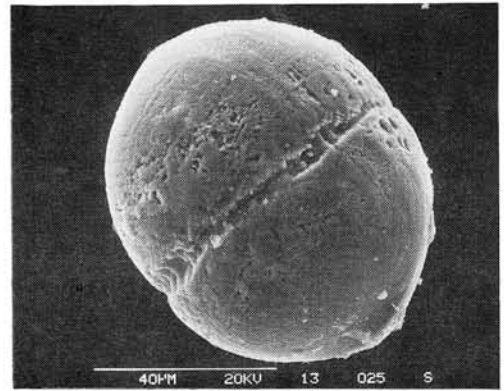


Fig. 5b- Twin dendrite decorated spherule



Fig. 6a- Octahedron decorated spherule

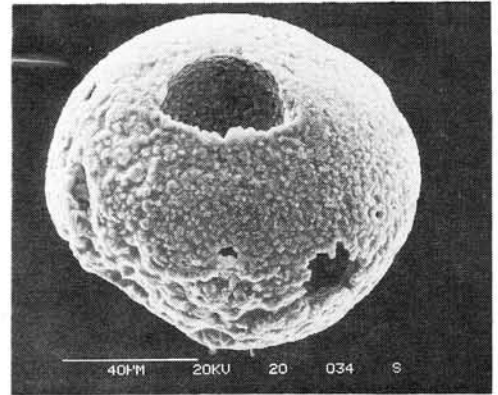


Fig. 6b- Octahedron decorated spherule

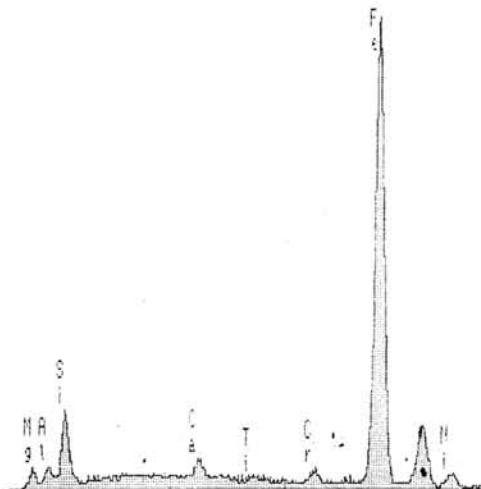


Fig. 7- EDAX composition of the Ni magnetite octahedrons

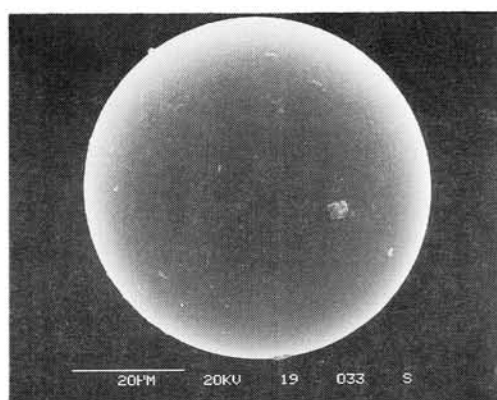


Fig. 1a- Smooth glassy spherule

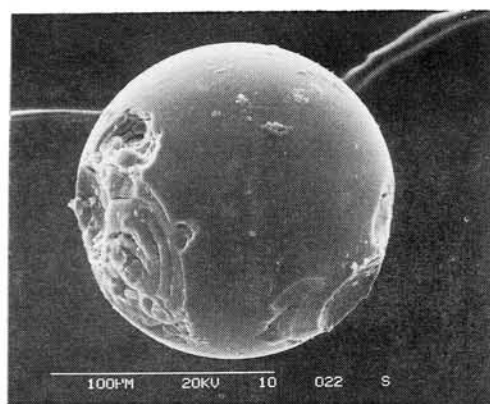


Fig. 1b- Cracked smooth spherule

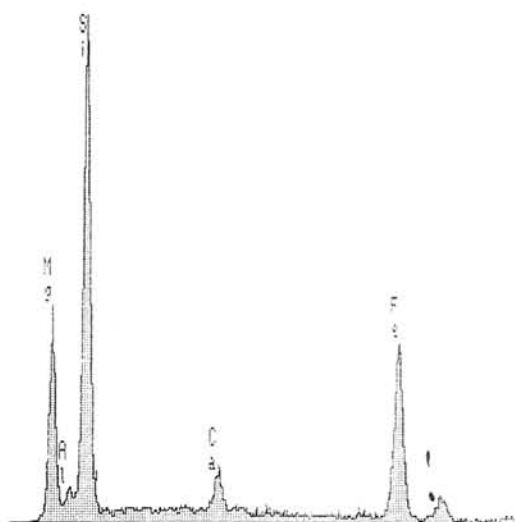


Fig. 2- EDAX composition of smooth spherule

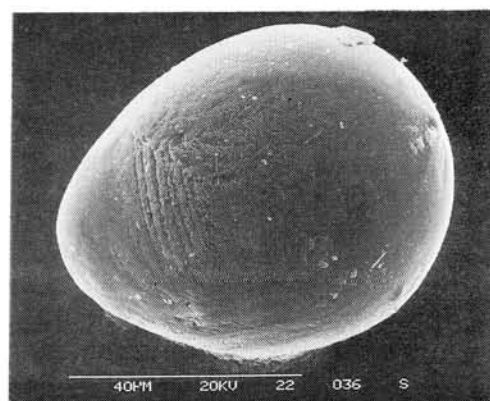


Fig. 3- Chain-olivine spherule

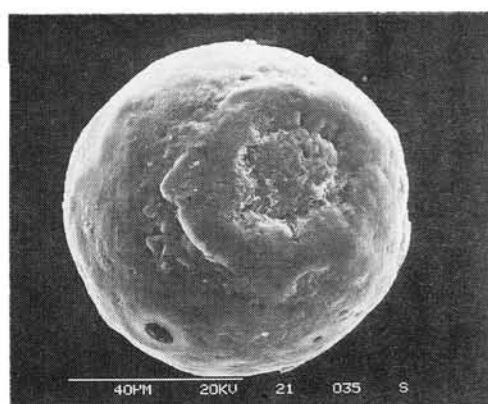


Fig. 4a- Fe-Ni bead inside glaze spherule



Fig. 4b- Ni rich glaze spherule

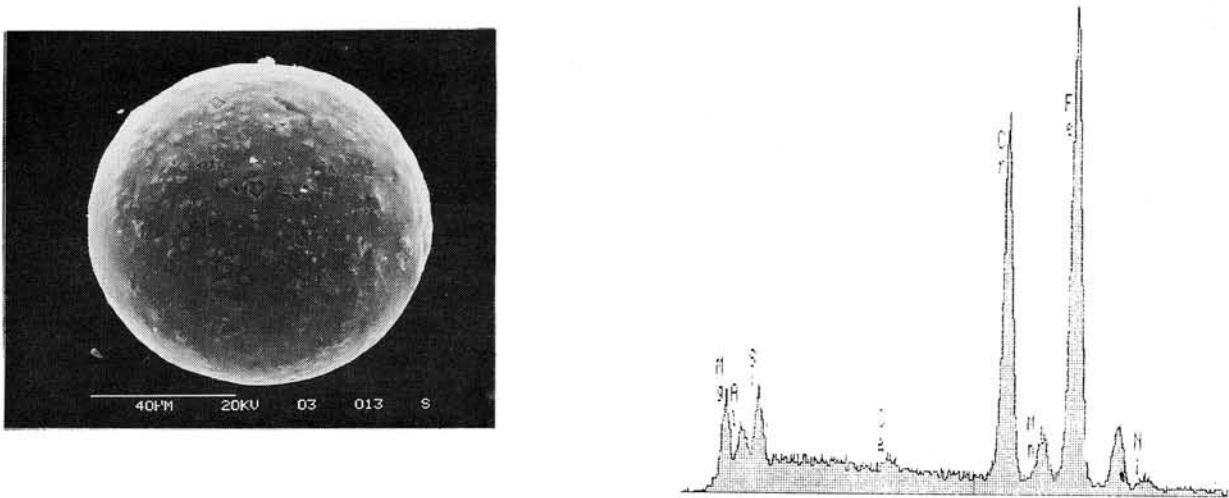


Fig. 8- Morphology and the EDAX composition of the industrial contaminate spherule.

Discussion. The above results represent a variety of melted cosmic matter in the form of micrometeorites and large meteoroids that ablated and exploded in the upper layers of our atmosphere. Some grains containing Fe, Ni, Cr and Mn (Fig. 8) probably correspond to the orbital debris originating mainly from spacecraft and their engines, or to other industrial contaminants. Detailed studies that are in progress on sections of these spherules should solve many present uncertainties.

Morphological study of the black magnetic spherules from the site of the 1908 Tunguska catastrophe was reported by Zbik [4]. SEM studies of these grains recovered from the topsoil represent five morphological types: compact smooth, rough, regolith-like, mosaic, and "astrakhan-coated". It was assumed that under circumstances of rapid explosive vaporization of the Tunguska body, which could be similar to CI-CM chondrite in composition, the surface of spherules became covered by a condensation envelope. In terms of the accepted classification, the candidates for the debris of the Tunguska body are most likely the regolith-like type spherules. Two regolith-like spherules found to be extraterrestrial in terms of their Ni contents seemed to argue in favour of such an assumption. These spherules are similar to the rough granular surface from our study and especially to the glazed covered and octahedron decorated.

Smooth morphological types of spherules exists in both studies. This is also true for spherules with polygonal mosaic fabric from Tunguska, and glazed stiff surface type from present work. These spherules correspond to S-type stony spherules in Taylor & Brownlee [5]. G-type spherules from [5] which are glassy spherules with dendrites could be related to our dendrite decorated glassy particles. Such spherules do not exist in Tunguska dust; however magnetite dendrites were developed inside the pores of "astrakhan-coated" type which correspond to the iron spherules [I-type] from Taylor & Brownlee [5]. Such spherules were absent in our study of Antarctic dust particles. Rough granular spherules similar to regolith like ones from Tunguska were found in the Cretaceous-Tertiary "fish clays" stratum (Denmark) [6]. But the rough morphology of these spherules could be due to weathering processes in such old strata.

REFERENCES: [1]- Kurat G., Koeberl C., Presper T., Brandstatter F. and Maurette M. (1992) 17th Symp. Antarct. Meteor., 53-1- 53-4. [2]- Zbik M. (1992) 17th Symp. Antarct. Meteor., [3]- Brownlee D.E., Love S. and Schramm L.S. (1991) LPSC XXII, 147-148. [4]- Zbik M. (1984) Proc. LPSC XIV, Jour. Geoph. Res. 89, B605-B611. [5]- Taylor S. and Brownlee D.E. (1991) Meteoritics 26, 203-211. [6]- Zbik M. (1984) LPSC XV, 955-956.

Studies on cosmic matter in the deep sea core sample.

Tsuneji Futagami
 Institute for Cosmic Ray Research, Univ. of Tokyo,
 Tanashi, Tokyo 188, Japan.

Deep sea sediments contain a high concentration of cosmic matter. I plan to investigate time variation of ratio of metallic elements in cosmic dust, using deep sea core samples. I used the core sample KH-68-4-22 [length: 316 cm] which was given by the Ocean Research Institute, University of Tokyo. The paleomagnetic data for the sample KH-68-4-22 is shown in Fig.[1]. Since boundaries between normal polarity and reverse polarity are not clear, age determination was not possible.

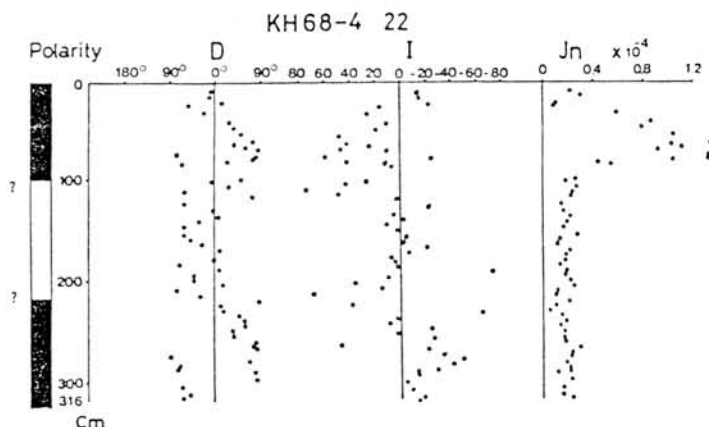
Sediments of 700-800 g were collected from six depths in the sample. Each sample was separated into two fractions by the sieve of 75 μ m. The magnetic fraction was collected from the fraction of $<75 \mu$ m. Since noble metal such as Ir, Os, Pt, Au, and Ni is enriched in extraterrestrial materials compared with terrestrial materials, I plan to investigate time variation in ratio of these elements.

It is recognized that He isotopic ratio in deep sea sediments shows much higher value than ratio for terrestrial air. It is attributed that cosmic dust in sediments retains He of solar wind origin [2]. I also plan to measure $^3\text{He}/^4\text{He}$ ratio in magnetic fractions in the core sample, and investigate time variation in $^3\text{He}/^4\text{He}$ ratio in solar wind.

Reference

1. Paleomagnetic results of deep-sea sediment cores collected by the R.V. Hakuho Maru in a period 1968-1977., Bulletin of the Ocean Research Institute, Univ. of Tokyo, No.13, 1980.
2. S. Amari and M. Ozima (1985): Search for the origin of exotic helium in deep-sea sediments., Nature 317, 520-522.

Figure



POYNTING-ROBERTSON EFFECT AND
COSMOGENIC ^{26}Al IN DEEP-SEA STONY SPHERULES

Hiroyuki Matsuzaki and Kazuo Yamakoshi

Institute for Cosmic Ray Research, University of Tokyo, Tanashi, Tokyo 188, Japan

Cosmogenic ^{26}Al activities in deep-sea stony spherules were calculated considering: 1)orbital evolutions by the Poynting-Robertson Effect in the interplanetary space, 2)capturing probabilities of the dust particles by the earth, and 3)size changes through atmospheric entry.

Solid bodies in the solar system all move on elliptical orbits in the gravitational field of the sun. In the case of small particles less than 1 *mm* in size, the orbits would changed gradually by the effect of the radiation pressure (this is the Poynting-Robertson Effect)[1]. The loci of the orbital evolutions of such particles are shown in (*a*, *e*) space in Fig. 1 by solid lines (where *a* represents the semimajor axis and *e* does the eccentricity of the elliptical orbit in the solar system). In this figure, the orbital elements of the asteroids, short period comets and major meteor streams are also plotted. We can see that dust particles of these different origins would have different paths of orbital evolutions.

Cosmogenic radio nuclide ^{26}Al (half life = 7.15×10^5 *yr*, which is comparable to the time scale of orbital evolution by the Poynting-Robertson Effect) is produced mainly by the solar cosmic ray, so its production rate in dust particles would be inversely proportional to the square of the distance from the sun. Then the ^{26}Al activities in dust particles would depend on their origins and the orbital evolutions. It seems possible to know the origin and the evolution of the interplanetary dust by measuring activities of ^{26}Al in samples such as deep-sea spherules.

But we must note that all available samples we can get are limited to those from terrestrial environment. That means our samples are all captured by earth among dust particles in the interplanetary space. Again see Fig. 1. The triangle region enclosed by broken lines is that in which the orbit satisfies the condition: $r_p < 1 \text{ AU} < r_a$ (r_p represents the perihelion distance and r_a does aphelion distance), i.e. the orbit has the point at which the heliocentric distance is just equal to 1 *AU*. That is, a dust particle has some probability to be captured by the earth in this region. However, dust orbits have inclinations to the earth's orbit generally. Orbital evolution rate is depend on dust size and density. Moreover, the earth is not always at the point at which the dust cross the earth's orbit. These factors make it somewhat confused to estimate the capturing probabilities of dust particles by the earth. So, dust particles of what origins or what orbital evolutions are easy to be captured by

the earth is not so clear.

Dust particles captured by earth then suffer from atmospheric entry. Heating and size change depend on the entry conditions i.e. entry velocity, entry angle and dust size and density, however, dust particles would melt and reduce their own sizes by evaporation in most cases. To extract informations about the interplanetary dust from data about the samples collected in terrestrial environment such as spherules, we must take the atmospheric entry effect into account.

Considering above mentioned points, we calculated ^{26}Al activities in deep-sea stony spherules. At first, three simple dust models, that is, the asteroids origin, the short period comets origin and meteor streams (or high eccentric dust) origin were set. Each model contains a combination of dust particles having initial orbital elements (a, e) consistent to each original group of celestial bodies. Then are calculated the ^{26}Al cumulations in the dust particles with each origin and along each orbital evolution, using data on the nuclear reaction cross sections and the cosmic ray flux proposed by Lal and Venkatavaradan[2]. Next step, the capturing probability by the earth of the dust which has each entry velocity and each ^{26}Al activity was calculated by our original method[3]. Finally, atmospheric entry effects were calculated mainly focusing on the size changes of dust particles according to the concept of Love and Brownlee[4].

The aim of these calculations is to examine whether the ^{26}Al activities of deep-sea spherules reflect the origin of the interplanetary dust. Some results are shown in figures below.

Fig. 2 shows what atmospheric entry velocities and what ^{26}Al activities dust particles of $100\mu\text{m}$ in size of three models have when captured by the earth. Fig. 3 and 4 are about spherules, i.e. after atmospheric particles. Fig. 3 shows the size dependences of averaged ^{26}Al activities in three dust model cases. Fig. 4 shows ^{26}Al activity distribution in each size spherule in the case of a) Asteroidal dust, b) Cometary dust and c) High eccentricity dust. This figure may give us a new point of view interpreting the AMS data such as given in Nishiizumi et al. (1991)[5].

References

- [1] Wyatt, S. P. and F. L. Whipple (1950) *Astrophys. J.*, 111, 134–141.
- [2] Lal, D. and V. S. Venkatavaradan (1967) *Earth. Plan. Sci. Lett.*, 3, 299–310.
- [3] Matsuzaki, H. and K. Yamakoshi (1994) *ICRR–Houkoku–109–94–1*, 126–141.
- [4] Love, J. J. and D. E. Brownlee (1991) *Icarus*, 89, 26–43.
- [5] Nishiizumi, K. et al. (1991) *Earth. Plan. Sci. Lett.*, 104, 315–324.

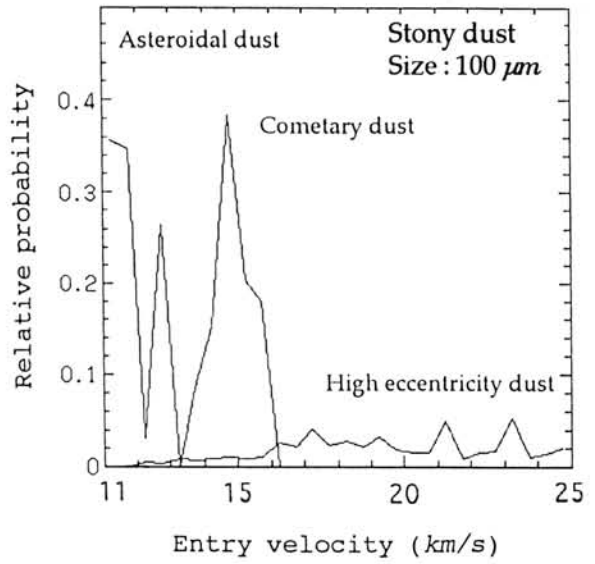
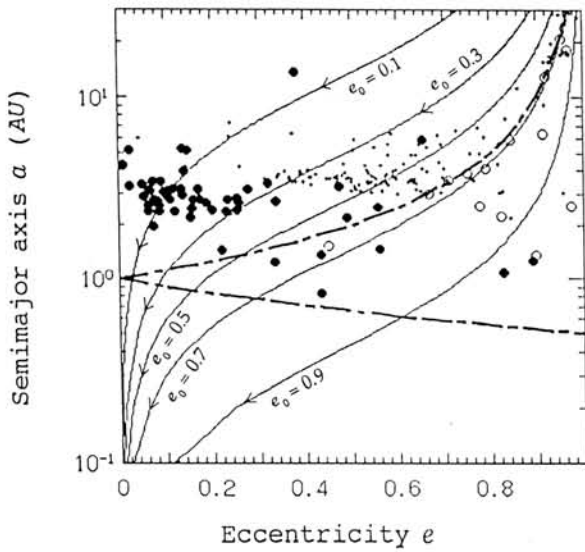


Fig. 1. (a, e) space of elliptical orbit in the solar system and the orbital evolutions of dust particles according to the Poynting-Robertson effect. e_0 represents the eccentricity when $a = 2.8$ AU. And the closed circles (\bullet), the fine dots (\cdot) and the open circles (\circ) represent the orbital elements of the asteroids, short period comets and major meteor streams, respectively.

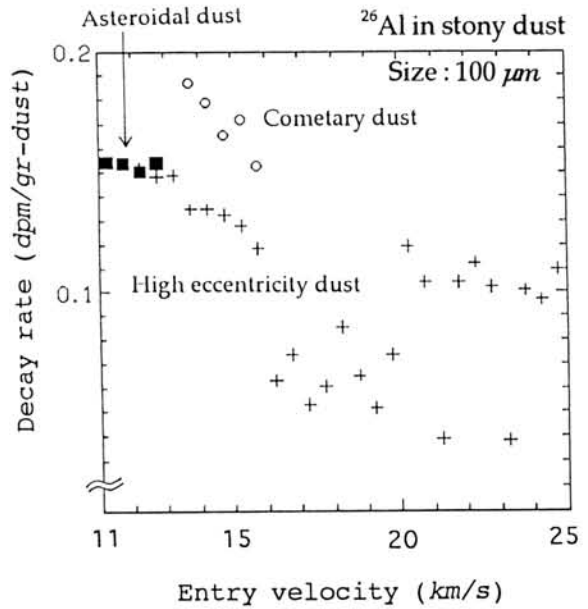
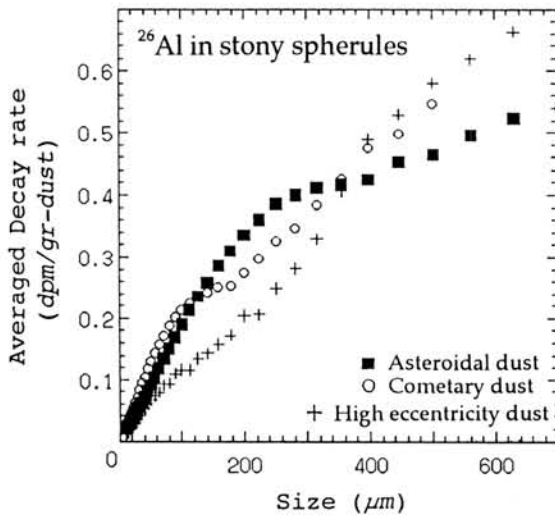


Fig. 2. What atmospheric entry velocities (upper) and what ^{26}Al activities (lower) dust particles of $100\mu\text{m}$ in size of three dust models have when captured by the earth.

Fig. 3. The size dependences of averaged ^{26}Al activities in three dust model cases.

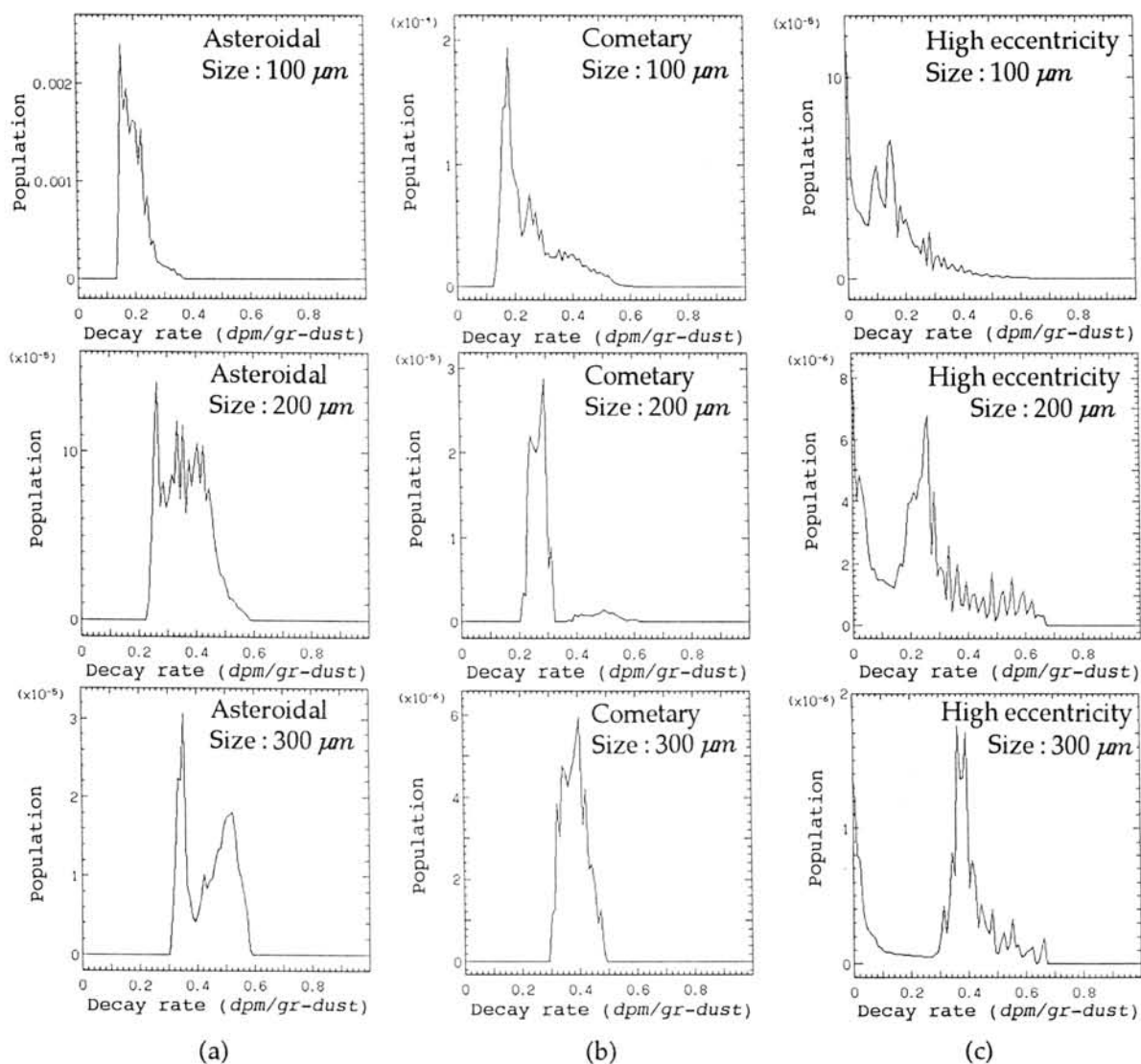


Fig. 4. ^{26}Al activity distribution in each size spherule in the case of a) Asteroidal dust, b) Cometary dust and c) High eccentricity dust.

Special Lecture (II)

Dr. D. Mittlefehldt

ALH84001 Orthopyroxenite: Comparison with Other Martian Meteorites and Yamato 75032-Type and LEW88xxx Ferroan Diogenites. David W. Mittlefehdt¹ and Marilyn M. Lindstrom²; ¹*Lockheed ESC, 2400 Nasa Rd. 1, Houston, TX 77058, USA;* ²*SN2, NASA-Johnson Space Center, Houston, TX 77058, USA.*

ALH84001 is a ferroan orthopyroxenite member of the martian meteorite clan [1]. Although it is clearly a martian meteorite, it is unusual compared to other martian meteorites and cannot be easily fit into petrogenetic models for them. Here, we will present the results of our continuing geochemical and petrologic study of ALH84001, and compare it to the other martian meteorites. ALH84001 was classified as a diogenite for 8 years. Because of this, it is also instructive to compare ALH84001 with ferroan diogenites, such as the Yamato 75032-type and LEW88008, LEW88011 and LEW88679 (hereafter LEW88xxx), in order to define the distinguishing characteristics.

Petrology and Mineralogy. ALH84001 is composed dominantly of orthopyroxene, with minor chromite, maskelynite and magnesite-siderite solid solution carbonates, and traces of apatite, pyrite and augite. Orthopyroxene occurs as equant grains up to 6 mm in size joined in 120° triple junctures. Chromite occurs as generally euhedral grains about 0.5 mm in size, both enclosed in, and interstitial to, orthopyroxene. These two phases represent the cumulus mineralogy of ALH84001. Interstitial to orthopyroxene are phases that likely crystallized from trapped melt: maskelynite and apatite. The maskelynite is highly angular and elongate in shape as it fills the spaces between orthopyroxene. Maskelynite areas are generally 0.2-0.5 mm in size, while apatite is about 0.3 mm in size. The maskelynite contains excess SiO₂, indicating that it was originally a mixture of plagioclase and quartz [1]. Augite may also have crystallized from trapped melt, or it could be granular exsolution from the orthopyroxene. Some of the orthopyroxene and chromite probably also crystallized from the trapped melt, although the textures don't demonstrate this. Magnesite-siderite solid solution carbonates were formed from a separate fluid phase. The early carbonates typically occur as zoned grains occupying spherical cavities 0.15-0.2 mm in size in the interstitial regions. Euhedral pyrite grains 10-20 μm in size occur in the interstitial regions and could have formed from either the trapped melt or a fluid phase.

Shock effects in ALH84001 include: (i) prominent crush zones, composed of comminuted primary mineral assemblage (grains a few tens of microns in size), sheared along the length of the crush zones, and sintered; (ii) conversion of plagioclase plus quartz to maskelynite; (iii) distortion of mineral grains (bent cleavage); and (iv) development of fine fractures offsetting grain boundaries.

The cumulus phases, orthopyroxene (Fig. 1) and chromite, are relatively homogeneous in composition. No systematic zoning in either major or minor elements was observed, although there is variation in the Fe₂O₃ content of the chromites (Fig. 2). The maskelynite shows some variation in composition from about Or₃Ab₅₈An₃₉ to about Or₁₅Ab₆₇An₁₈ (Fig. 3).

Geochemistry. We have analyzed five whole rock samples of ALH84001 by INAA. Incompatible trace lithophile elements confirm that the interstitial maskelynite represents trapped melt: bulk sample rare-earth element (REE) patterns are not those expected of an adcumulate orthopyroxenite, and the five samples show a wide variation

in light rare-earth elements (LREE) (Fig. 4). The La abundances vary from 0.27 to 2.7 times CI chondrites, and increase with increasing Na content. This suggests that much of the REE are in the trapped melt component, rather than in the carbonates, which are low in Na [1]. Note, however, that because the early carbonates are found in the interstitial regions with maskelynite, it is nonetheless possible that the REE were introduced by the fluid phase, and the correlation with Na is fortuitous. The correlation of LREE with Na is poorer than would be expected for mixing two components (cumulus assemblage and trapped melt). Therefore, it seems likely that the REE in ALH84001 require mixing of at least three components, one of which may be a metasomatic component. The sample with the highest Na content has a LREE-enriched pattern, with La/Yb ratio of 1.3 times CI. If the REE in this sample are dominantly from the trapped melt component, then this melt was LREE-enriched.

ALH84001 in Relation to Other Martian Meteorites. Martian meteorites can be divided into two clans: the basalts plus lherzolites (EETA79001, Shergotty and Zagami, and ALHA77005 and LEW88516, respectively) and the dunite plus clinopyroxenites (Chassigny, and Governador Valadares, Lafayette and Nakhla, respectively). These two clans are separated by the following three general petrologic characteristics. (i) The basalts and lherzolites crystallized low-calcium pyroxene (orthopyroxene ± pigeonite) with or without high-calcium pyroxene (augite), while the dunite and clinopyroxenites crystallized only augite as their pyroxene phase [2]. (ii) The feldspar component in the basalts and lherzolites is more calcic, with An_{36-63} , while that in the dunite and clinopyroxenites is more sodic (An_{2-33}) and includes alkali feldspar (Fig. 3). (iii) The inferred parent melts for the basalts and lherzolites are LREE-depleted, while those for the dunite and clinopyroxenites are LREE-enriched [3].

ALH84001 is like the martian basalts and lherzolites in that low-calcium pyroxene is the dominant pyroxene phase. The little augite we have so far identified is a later, interstitial phase. Hence, ALH84001 could not have crystallized from a parent melt like those estimated for the dunite and clinopyroxenites which are olivine+augite saturated [2], but could have formed by fractional crystallization from parent magmas like those of some of the basalts and lherzolites which are olivine+low-Ca pyroxene saturated [2]. However, the feldspar component of ALH84001 is more sodic than that of the basalts and lherzolites, and is more similar to feldspar in the dunite and clinopyroxenites, including fractionation to more potassic compositions (Fig. 3). We originally inferred based on one bulk analysis that, if later metasomatism did not affect the REE content in ALH84001, then the trapped melt, and thus the parent melt, was LREE-enriched [1]. Our additional bulk analyses have clouded this issue. There is not a simple two-component mixing model that will satisfy the REE and Na data on all bulk samples. Rather, there may be three components affecting their REE and Na contents: (i) the cumulus assemblage, (ii) a trapped interstitial melt, and (iii) a component which may be the late magmatic fluid or metasomatic assemblage. One of these components must be LREE-enriched, because one bulk sample is. Alternatively, we may have inhomogeneously sampled a REE-rich phase, such as apatite. In this case, only cumulus and trapped melt components are required. Regardless, additional analyses will be needed to determine whether the parent melt of ALH84001 was LREE-enriched like those of the dunite and clinopyroxenites, LREE-depleted like those of the basalts

and lherzolites, or unfractionated.

Petrogenesis. The primary textures and uniform major and minor element compositions of orthopyroxene and chromite suggest that the parent melt cooled slowly at depth, and that the cumulus grains chemically equilibrated with their parent melt during crystallization. The cumulus assemblage trapped variable amounts of the parent melt, presumably when open channelways became restricted. The amount of trapped melt is not easily determined, but if the parent melt had a Na₂O content like those of estimated martian melts [2], then the Na₂O contents of the bulk rock samples can be used to estimate between about 5-15% trapped melt is present. This trapped melt appears to have equilibrated with the surrounding cumulus assemblage, as there is no observable major or minor element zoning in orthopyroxene near maskelynite or apatite. A fluid phase separated from the trapped melt before it solidified as evidenced by the spherical cavities now filled by the zoned, early carbonates. These early carbonates formed before the shock event that affected ALH84001. Textures show early carbonates truncated by the crush zones, deformed in the maskelynite and containing fine fractures offsetting zoning. The textures do not allow us to determine whether the early carbonates were formed from primary magmatic fluids, or from fluids introduced later in a metasomatic event. The last event recorded in ALH84001 was an impact event which generated the shock features listed above. During or after this shock event, the late carbonates were formed as small grains in the crush zones and as fracture fillings. These late carbonates may be early carbonates that were remobilized as a result of the shock event, or a new generation of carbonates formed by metasomatism, perhaps induced by the shock event [1].

Comparison of ALH84001 with Ferroan Diogenites. ALH84001 was classified as a diogenite for eight years before its martian pedigree was established. During these eight years it was studied by several investigators, including ourselves, who did not detect its true origin because the major mineral, orthopyroxene, is so similar in composition to some diogenites (Fig. 1). Therefore, it is instructive to compare ALH84001 to similarly ferroan diogenites in order to define easily measured properties that distinguish martian from HED cumulate orthopyroxenites. The initial description of ALH84001 pointed out two unusual features of this meteorite: sodic maskelynite, and Mg-Fe-Ca carbonates [4]. Maskelynite is present in some eucrites, but plagioclase as sodic as that reported in ALH84001 is unknown. The ferroan diogenites (Yamato 75032-type, LEW88xxx) contain plagioclase that can be relatively sodic for HED meteorites, but these are much less sodic than those of ALH84001 (Fig. 3). Nonetheless, the diogenite Roda contains highly fractionated trace phases, including probable K-feldspar [5], so it is possible that sodic plagioclase could form from fractionated trapped melt in diogenites. Although carbonates in Antarctic achondrites might be dismissed as terrestrial weathering products, the carbonates in ALH84001 are Mg-Fe-Ca solid solutions [1, 4], and their compositions are unlikely to have formed at the low temperature conditions of Antarctica [1]. Hence, the initial report of carbonates should have made investigators suspicious. That this didn't occur probably reflects the general lack of carbonate expertise among most meteoriticists. Regardless, ALH84001 is unusually rich in carbonates compared to other martian meteorites, and, although the presence of these carbonates would serve to indicate possible martian origin, their

absence would not preclude a martian origin.

The first clue we had of martian origin for ALH84001 was in the compositions of spinels. Chromites in diogenites (and other HEDs) are low in Fe³⁺ (Fig. 2) due to the low f_{O₂} of formation; calculated Fe₂O₃ is <1 wt% [5, 6]. Spinel in ALH84001 contain between 4.5-9.0 wt% Fe₂O₃ calculated from stoichiometry [1, 7]. Other martian meteorites also contain either ferric iron-bearing chromites or magnetite [8]. The second definitive clue for a martian origin for ALH84001 was the occurrence of pyrite as the sulfide phase. HED meteorites contain troilite as the sulfide phase, while in martian meteorites, pyrite, marcasite pyrrhotite and/or pentlandite are the sulfides [8]. Spinel and sulfides are likely to be present in all martian mafic and ultramafic rocks, and electron microprobe analysis of these phases should allow easy, rapid identification of potential martian meteorites, even when the bulk of the rock is similar to asteroidal igneous rocks. Once probable martian meteorites have been so identified, the more time consuming oxygen isotopic analyses should be performed to confirm a martian origin.

References. [1] Mittlefehldt (1994) *Meteoritics* 29, 214. [2] Longhi and Pan (1989) *Proc. 19th Lunar Planet Sci. Conf.*, 451. [3] Longhi (1991) *Proc. 21st Lunar Planet Sci. Conf.*, 695. [4] *Ant. Meteor. Newslett.* 8(2). [5] Mittlefehldt (1994) *Geochim. Cosmochim. Acta* 58, 1537. [6] Mittlefehldt and Lindstrom (1993) *Proc. NIPR Symp. Ant. Meteor.* 6, 268. [7] Berkley and Boynton (1992) *Meteoritics* 27, 387. [8] McSween (1985) *Rev. Geophys.* 23, 391.

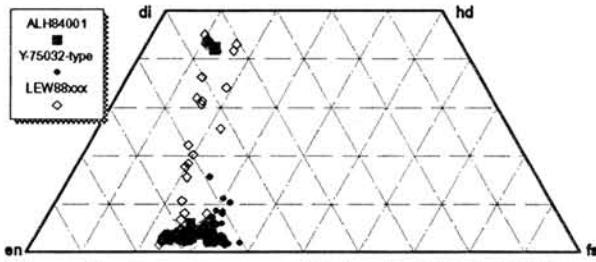


Figure 1. Pyroxene quadrilateral of ALH84001 and ferroan diogenites.

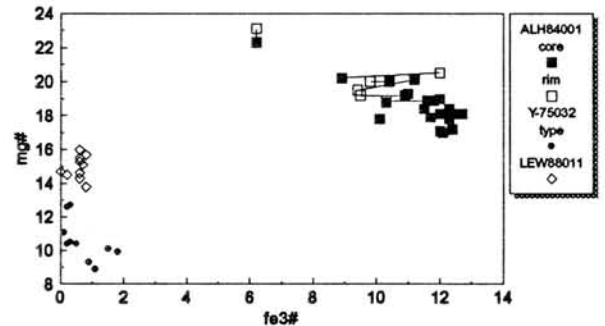


Figure 2. Mg# vs. fe3# (100 * molar Fe₂O₃/(Fe₂O₃+Al₂O₃+Cr₂O₃) of ALH84001 and ferroan diogenite spinels.

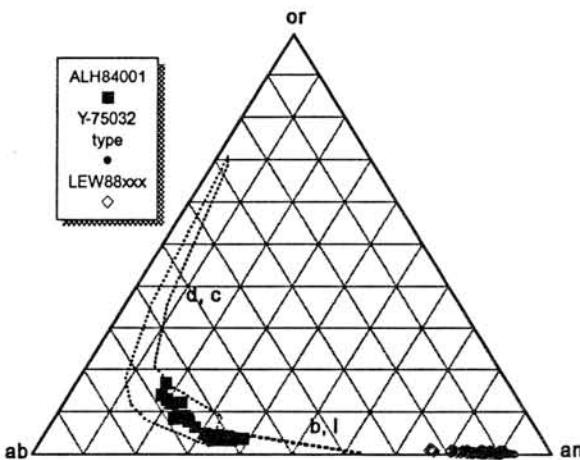


Figure 3. Plagioclase compositions of ALH84001, other martian meteorites and ferroan diogenites. d,c - martian dunite and clinopyroxenite feldspars; b, l - martian basalt and lherzolite feldspars.

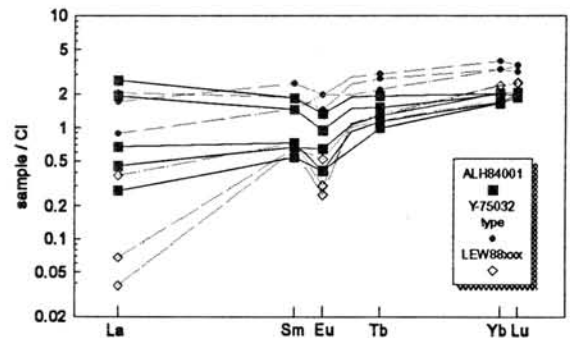


Figure 4. REE plot for ALH84001 and ferroan diogenites.

Abstract Only

TEM-AEM examination on impact glass from Henbury meteor crater in Australia

Junji Akai : Department of Geological Science, Faculty of Science
Niigata University, Ikarashi 2-8050, Niigata 950-21, Japan

Glass fragments can be formed by meteoritic impact on the earth. Mineralogical and geochemical studies may also be important for estimation of origin of glass, interaction between meteorite and country rocks and suggestion for origin of the more enigmatic natural glasses, e.g. tektites, etc.

Henbury meteor crater is situated in Northern Territory, Australia (24°35' S; 133°09' E). It was first described by Alderman (1932a). Iron meteorite found around the craters was described by Alderman (1932b). The main crater has oval shape which was considered to be due to overlap of two craters. Geology of the crater is mainly subgreywacke. Impact glass has been investigated by Taylor and Kolbe (1965), and Taylor (1967) for the first time. However, TEM investigations have not been carried out on glass specimens from Henbury until now. TEM investigation is very important for clarifying the state of the glass materials, their heterogeneities, identification of minute crystals in μm - to nm -scales included or neoformed. Now further cooperative study on the impactite glass with Dr. Koch of Technical University of Denmark is in progress. Specimen used in this study was sampled by Dr. Koch in our field excursion of 10th ICC to Henbury meteor crater. According to Koch (priv. comm.), results of Mossbauer spectra show that spectrum at 298 K appears may be interpreted as one component from an Fe(III) oxide, (at least) two different Fe(II) positions and one Fe(III) position- the latter two both being paramagnetic. Furthermore, he suggested based on additional low temperature Mossbauer spectra that the doublet with the small quadrupole splitting was due to Fe in a true glass phase, but on lowering the temperature most of this component order magnetically perhaps indicating a relation to a Fe poor olivine or Fe oxide clusters, and they may be formed rapidly after impact.

TEM investigation on Henbury glass specimens has not been carried out yet. Preliminary results of TEM - AEM investigation are shown here.

Small specimen of impact glass (2-3 mm in diameter) were crushed and prepared for TEM-AEM analysis, putting on carbon coated microgrid. TEM used is JEM 200CX with Novar detector and TN 2000 EDS system, operating at 200kV.

Fig.1a shows the TEM image of one of typical glasses. In the TEM image, many small crystals are found. Fig.1b shows AEM

spectrum of matrix glass phase. Fig.1c and 1d are AEM spectra of the small crystals contained in glass. Corresponded grains are marked in Fig.1a. Fe rich phase may be Fe-oxide (or Fe Ni metal). Composition of bulk glass phase may be fundamentally the same as those reported by Taylor and Kolbe(1965), and Taylor (1967) . Taylor (1967) reports the following composition of the impact glass assuming that FeO contents of glass are uniformly 4% in order to remove meteoritic material effects :SiO₂= 74-76%, Al₂O₃= 12-14%, FeO = 4%(assumed value), MgO= 2.1-2.4%, CaO = 0.4-0.7%, Na₂O = 0.9- 1.1%, K₂O=3.1-3.6%, TiO₂ = 0.9-1% The glass contain varying amounts of iron and nickel derived from the iron meteorite (Fe 91-93%, Ni 7.3-7.7%, Co 0.2-0.6%; Taylor and Kolbe, 1965) . Much of them have been estimated to be finely dispersed in the glass and be rarely in the form of spherules. However, concrete mode of occurrence in submicroscopic level has not been known. Some vague spherule extremely rich in Ni was found contained (Fig.2). Fe rich phase may be Fe oxide (or Fe Ni alloy). These phases contained may be consistent with the observation of cosmic Ni-Fe alloy spherules from sediments, Canada (Roger et al.,1993). These results revealed some types of occurrences of meteoritic Fe and /or Ni phases in glass although this is preliminary result
 References: Alderman (1932a) Min.Mag.,23,19-32. ;Alderman (1932b) Rec. S.Aust. Mus.,4,554-563. ;Roger, D.B., Morton,D. and Wang,K.(1993) GCA,57,4129-4136 ; Taylor and Kolbe (1965) GCA , 29,741-745, ; Taylor (1967) GCA, 31 961-968.

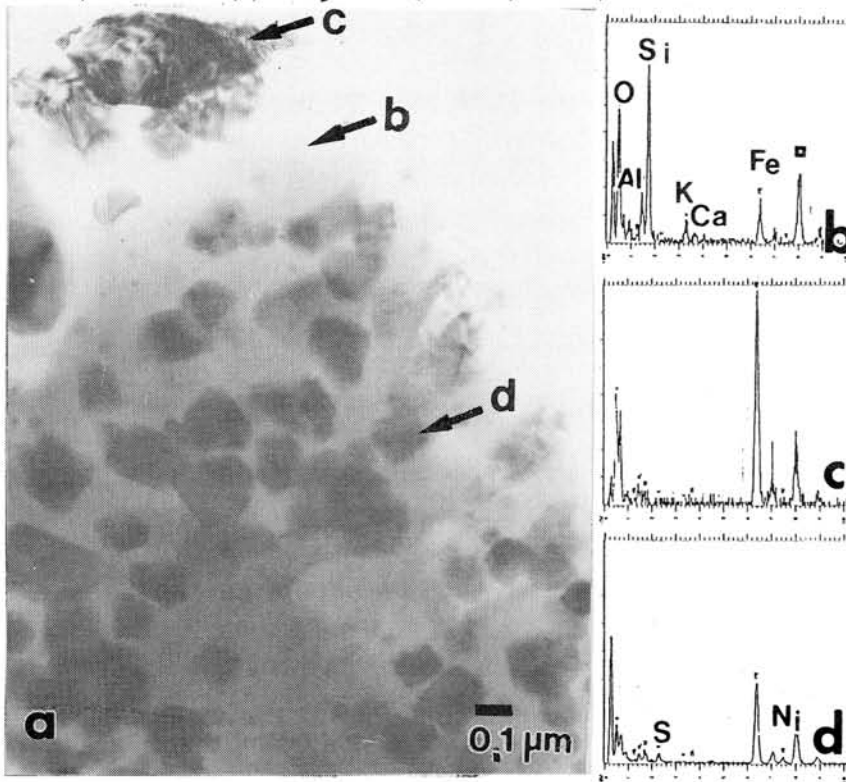


Fig.1 a: TEM image of impact glass
 b,c,d : AEM spectra (cf.arrows, in 1a)

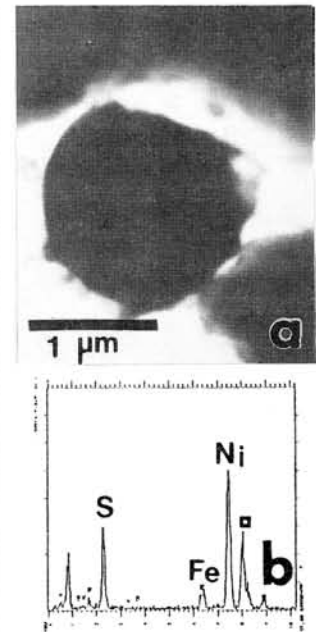


Fig.2 a:TEM image of spherule in glass
 b: AEM spectrum
 □:Cu from Mesh.

ICY METEORITES ON ANTARCTICA?Sz. Bérczi¹ & B. Lukács²¹ R. Eötvös University, Dept. of Astronomy, H-1083 Ludovika tér
2., Budapest, Hungary² Central Research Institute for Physics RMKI, H-1525 Bp. 114.
Pf. 49., Budapest, Hungary**Abstract**

On the basis of characteristics of some meteorites (cold meteorites after falling, fragility), of the chemical condensational model of the Solar System, and according to the main components of comets ICY-METEORITES can be suspected to exist. First the reasons are listed which make it plausible that icy-meteorites should be collected only in the conditions of Antarctica. Second: a method to find them on the ice-plains is suggested.

1. Introduction

There are at least five different reasons triggering the idea of search for ICY-METEORITES on Antarctica, because such meteorites should be in existence.

1. The chemical condensation models of the Solar System deduce an icy-belt far away from the early Sun, in the vicinity of the recent orbit of Uranus and Neptune. There water ice, ammonium and methane ices and their clathrates are expected (Lewis and Barshay, 1974, Larimer, 1967, Grossman, 1972).

2. There were at least two meteorites found in very cold condition when being collected immediately on the site of fall. One report is from Hungary and another from India (Török, 1882)

3. The Tunguz event had a material source, of which only traces remained, but most of it seems to have evaporated.

4. The fragile nature of carbonaceous chondrites suggest, and the hydrated silicates in carbonaceous chondrites corroborate the presence of water and other volatile components in these types of meteorites.

5. The main component of comets is contaminated water-ice.

Because of the request of survival of ICY-METEORITES in terrestrial conditions, the candidate place to collect them seems for us the ANTARCTICA. There very successful expeditions have already collected more than 10 000 pieces of meteorites. In this work a practice developed by the teams to ensure storing conditions of the deeply frozen state of the collected extraterrestrial material. We propose to search for icy meteorites, which, in case of success, promises a new achievement in the search for Antarctic Meteorites, on which the National Institute for Polar Research is successfully working on for more than three decades.

2. Implications from the condensation model for the Solar System

Different calculations on the chemical equilibrium for minerals condensed from the primitive Solar Nebula with cosmic (solar) chemical abundances were published in the late 60's and early 70's (Larimer, 1967, Lewis and Barshay, 1974, Grossman, 1972.). The main conclusion of such models was that three distinct material belts can be distinguished in the condensing solar nebula: the metal, the silicate and the ice ones.

Comparing the estimated mineralogy of these chemical models and the main types of meteorites, an important hiatus emerges.

Let us summarize the main meteorite types (anders, 1964) and mineral belts in a form which clearly exhibit this hiatus (Fig. 1.). The correspondence between mineral belts of the condensing solar nebula and the main (and intermediate) meteorite types shows sharply that representatives of ICY-METEORITES are missing.

Of course, most places on the Earth the icy-meteorites should have been evaporated. But there are places on the globe, which might preserve some pieces of them: especially Antarctica.

On the other hand, some descriptions of earlier meteorite falls may contain some important details referring somehow the existence of volatile components, which later were not found at all. One such event happened in Hungary, when not only the intensity of the phenomenon suggests that there were missing masses, but the condition of the found pieces (having been cold) is also in accord with supposed volatile components of the falling body.

3. Meteorites, found in cold condition right after fall

In his work about A MAGYAR BIRODALOM METEORITJEI, 1882 (The Meteorites of the Hungarian Realm) József Török describes a falling event of a meteorite, when the pieces of the meteorite were found in cold condition. This was the Zsadány Meteorite.

The falling happened on 31st March 1875, in the vicinity of the village of Zsadány, in Temes County, Hungary. (Recently belonging to Roumania.) Between 3 and 4 p.m. after a great thunder from the clear sky a swarm of rather small pieces of meteorites fell to the fields and gardens of the village.

It was very remarkable that when the pieces of the meteorites were taken into hands, they were found very cold. The author remarks, that there was another case, when meteorites brought the "coldness of outer space to the surface", where they were found. This event, he mentions, was in Eastern India, at Dhurmsala (Dharmasala, Punjab, India), on 14th July 1860. There was found six pieces of meteorites and those were so cold, that "people could not hold them for longer time in their hands".

The pieces of the Zsadány Meteorite are rather small like nuts; 7 pieces were found, representing chondrites. It is worthwhile to note that the Zsadány effect was well documented and investigated. The Lord Lieutenant of Temes County immediately reported the event to a scientific journal, enclosing two fragments: The meteorites fell in early afternoon to gardens, ploughfields and meadows, with many eyewitnesses. The Hungarian Academy of Sciences sent investigators to the site in 15 days, they questioned many eyewitnesses, and organised a systematic search with 30 persons after fragments in the area whither witnesses had seen several "stones" to fall, but only one tiny fragment was found.

We think that the data at least suggest that the Zsadány meteorites originated from an icy body with chondritic stony fragments embedded. The probable story is that the parent body fragmented during the fall, most fragments were ices and partly evaporated in fall, partly liquefied before finding them, and the stony fragments were preserved from heating by their icy covers.

4. On the possibilities of falling ices and of their observation

Here we only list the relevant points:

1) Origin

Ice is a substantial component in the outer Solar System, cf. e.g. the moons of the giant planets. Comet cores are stones cemented by ices. So ices entering the terrestrial atmospheres

may be frequent. The ices of the outer System may contain water, ammonium and methane.

2) Survival during fall

In the fall the evolution of a meteoritic body is governed by 3 coupled differential equations whose approximate form for a sphere of radius R and mass density μ is as follows:

$$(4\pi/3)\mu R^3 (dv/dt) = -F_{\text{drag}} \quad (1)$$

$$F_{\text{drag}} = F_{\text{drag}}(R, v, z) \quad (2)$$

$$(d(4\pi\mu R^3/3)/dt)cDT \approx W_{\text{heat}} = F_{\text{drag}}v \quad (3)$$

$$dz/dt \approx -v\cos\theta \quad (4)$$

where v is the velocity, z is the height, θ is the angle to vertical, c is the specific heat, and DT is the difference of the evaporation temperature and the original one. Depending on the original dustiness of the surface, the latter is 200-270 K, so $DT \approx 100-170$ K. As for the drag force, the simplest approximation, (which must be corrected at high velocities), is the Stokes law

$$F_{\text{drag}} \approx 6\pi\Gamma(z)R(t)v(t) \quad (5)$$

Now observe that for ice DT is roughly 1 order of magnitude smaller than for silicates but c is 1 orders higher. Therefore the total mass loss of ices and silicates during fall is roughly similar. If stones can reach the surface, ices can either.

3) Survival in the impact

This point is obscure. At the impact some part of the ice body can liquefy. However fragments may survive frozen.

4) Survival on the surface

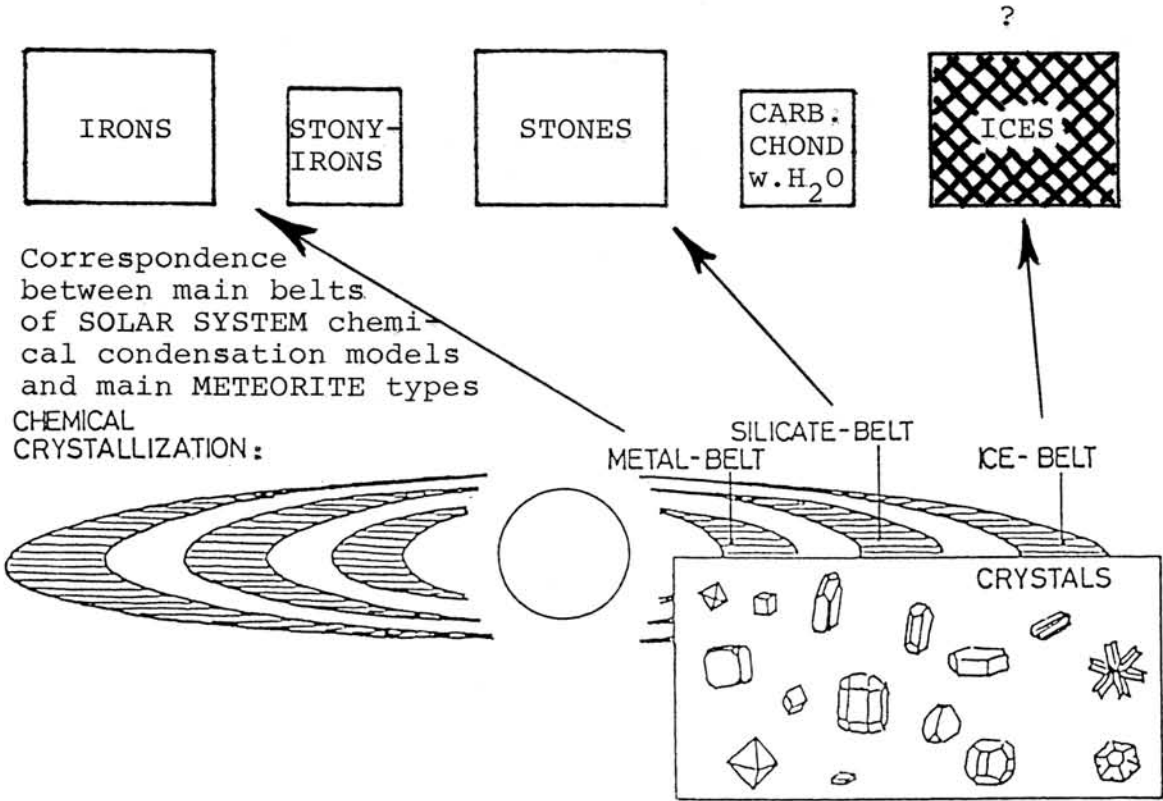
On the Dronning Maud Land, near Syoowa, which is an important site of meteorite search, the average midsummer air temperature at the ice is cca. -16 C°. So water ice can indefinitely long survive. As for mixtures: clathrates with high methane content are liquid at that temperature, but solved methane does not disturb survival, since its possible quantity is below 1 %. Ammonium may appear in great quantities. According to the Raoult law, 10 weight % NH_3 lowers the melting point to -11 C°, so this is the absolute upper boundary for surviving.

5) Chances of recognition

For pure water ice the meteorite cannot be identified. Water ice with stone core (see the Zsadány and Dharmasala meteorites) can be identified after collecting, but hard to find among similar terrestrial ice. Contaminated ices are easy to identify in laboratory because NH_3 and CH_4 are absent in the Antarctic interior. A possibility of identifying NH_3 -containing ices by reflection is under investigation.

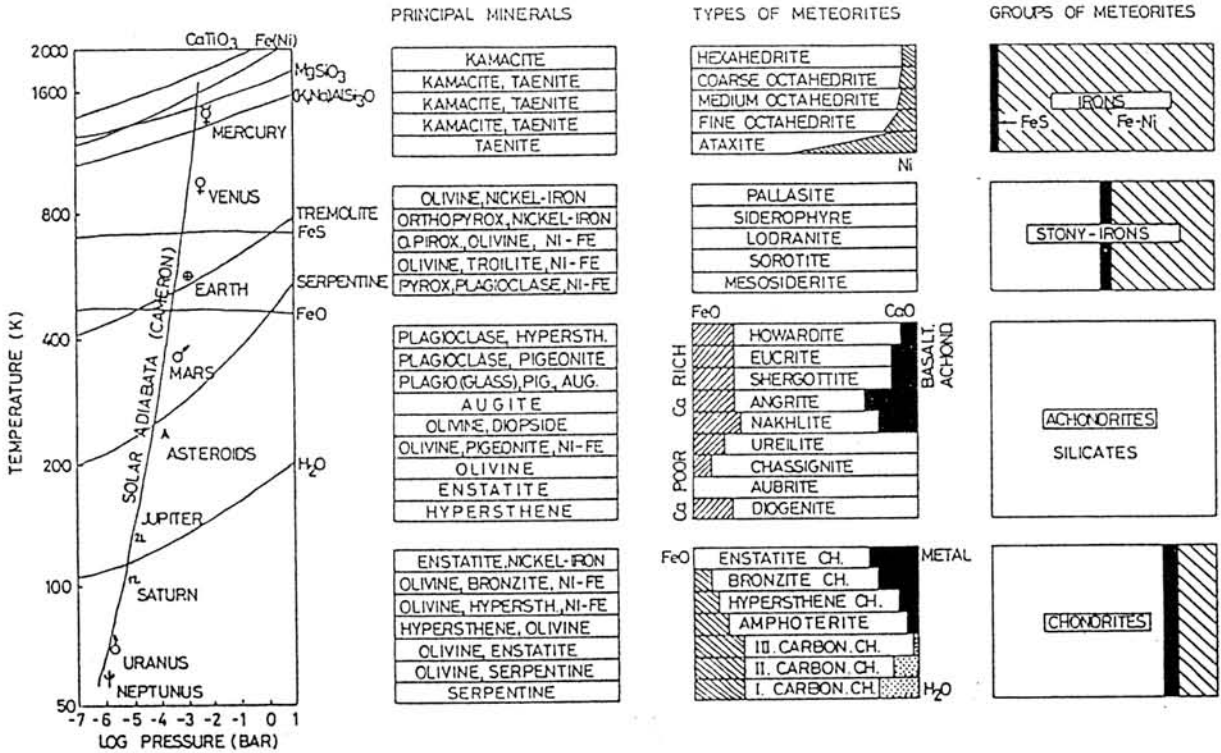
References

- Anders, E. (1964): Origin, age and composition of meteorites. Space Sci. Rev. 3. pp. 583-714.
- Grossman, L. (1972): Condensation in the primitive Solar Nebula. Geochim. Cosmochim. Acta. 36. pp. 597-620.
- Larimer, J. W. (1967): Chemical fractionation in meteorites. I. Condensation of the elements. Geochim. Cosmochim. Acta. 31. pp. 1215-1238.
- Lewis, J. S., Barshay, S. S. (1974): Chemistry of solar material. In: The Dusty Universe. (Eds.: Field, G. B., Cameron, A. G. W.) Neale Watson Acad. Publ.
- Török József (1882): A Magyar Birodalom Meteoritjei. (The meteorites of the Hungarian Realm). Természettudományi Közlöny. XIV. (159.füz.) 506.old.



LEWIS-BARSHAY MODEL

ROSE-PRIOR-MASON-ANDERS TABLE OF METEORITES



Summary of the chemical crystallization in the Solar System according to Lewis and Barshay /1975/ and meteoritic correspondence to these mineral bands. /Bérczi, 1991/

Fig. 1.

Microstructure analysis of the yamato 791694 antarctic meteorite

J.C. Bruno*, A.A.R. Fernandes* and R.B. Scorzelli, Centro Brasileiro de Pesquisas Físicas, Rua Xavier Sigaud 150, CEP22290-180, Rio de Janeiro, Brazil, *Instituto Militar de Engenharia, Rio de Janeiro, Brazil.

INTRODUCTION The metallographic study of meteorites is of great scientific interest, since besides giving information about the origin of the solar system allows the investigation of the metallic alloys properties that have been formed in pressure and temperature conditions difficult to reproduce in laboratories environments. In this context, samples of Yamato(Y)-791694 meteorite (a Ni-rich ataxite ~ 36% Ni) have been analysed. In this paper the results of our investigation on phase composition and structure of this ataxite is presented on the basis of optical microscopy, scanning electron microscopy (SEM), energy dispersive X-ray analysis (EDS) and compared with previous Mössbauer spectroscopy results [1].

EXPERIMENTAL The meteorite sample was mechanically polished and etched for metallographic examination. Different solutions were used in order to reveal the microstructure of the meteorite. Etching with Van NESTE [2] or nital (2%) revealed fine details of the microstructure. The samples were analysed by optical microscopy and also by SEM/EDS. Sample composition was determined using a computer program in the EDS software package based on ZAF technique. The volumetric fraction of some phases were estimated using the usual random point count method.

RESULTS AND DISCUSSION General aspects of the microstructure of Y-791694 are presented in this paper. EDS analysis on different points showed variation in chemical composition, as can be seen in Table 1, allowing the identification of different phases.

	ATOMIC %			
	Ni	Fe	P	
Matrix	36	64	-	taenite
Coarse phase	43	40	17	schreibersite
Fine grains (low relief)	9	91	-	kamacite

Table 1 - Elemental concentration of Y-791694 obtained by EDS analysis

The microstructure observed in a polished sample before etching showed mainly the presence of a coarse phase with light contrast with the matrix. Etching with nital 2% (fig.1) outlined a dark boundary in the coarse phase, and revealed the existence of deformation lines (Neuman bands) in the matrix. This chemical etching also disclosed the presence of fine grains with roughness, in low relief, and a fine dispersion of particles, in high relief. Applying the quantitative metallography using random count method, the estimate volumetric fraction of the coarse phase was 3.6%.

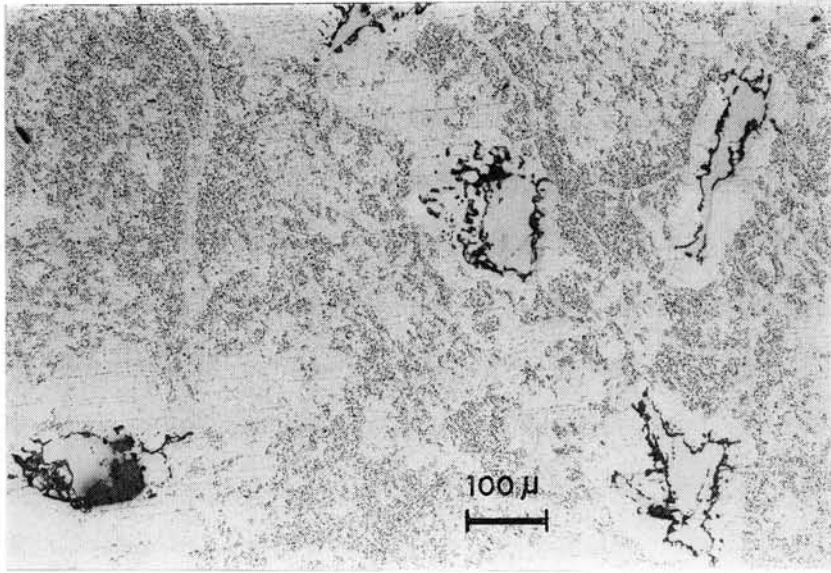


Figure 1 - Optical micrograph of Y-791694 etched with nital 2%, 110x

EDS analysis showed the presence of about 17 at.% P, 40 at.% Fe and 43 at.% Ni in this coarse phase, suggesting the presence of Schreibersite $(\text{Fe,Ni})_3\text{P}$. The phase in low relief was identified as an Fe-Ni alloy containing ~ 9 at.% Ni corresponding to kamacite. The matrix phase containing ~ 36 at.% Ni and 64 at.% Fe corresponds to a Ni-rich taenite (γ - FeNi). These compositions are similar to the ones observed by Shimamura et al. [3]; the other elements are below the detection limit of our technique. In fig. 2 the different phases are pointed out. The black region has a composition very close to schreibersite and the contrast can be due to sample preparation.

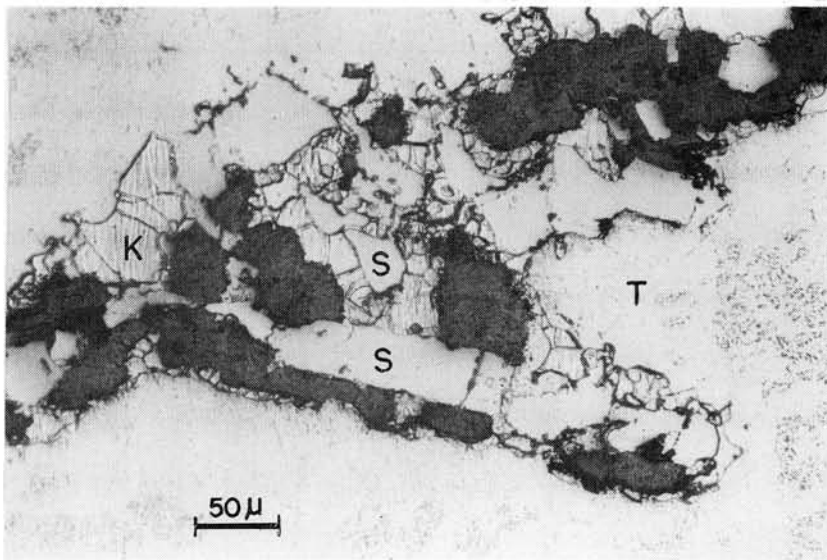


Figure 2 - Optical micrograph of Y-791694 etched with nital 2%, higher magnification (220x). The marked areas correspond to:
K (kamacite), S (schreibersite) and T (taenite)

Etching with Van Neste solution diminished these black areas as can be observed in fig. 3. In this figure the Neuman bands in the matrix are more evident.

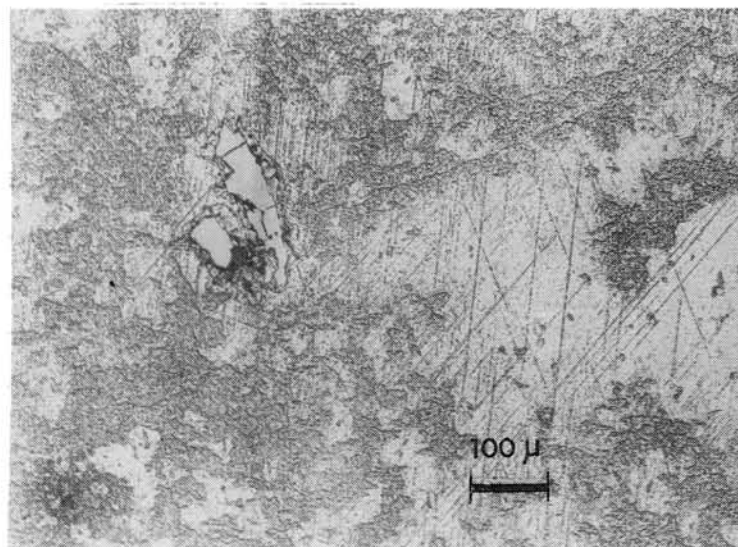


Figure 3 - Optical micrograph of Y-791694 etched with Van Neste, 110x.

The metallographic analysis of Y-791694 showed that this meteorite is a multiphased ataxite with matrix was identified as a Ni-rich taenite containing a low proportion of kamacite, dispersed cellular plessite and coarse particles of schreibersite. These results complement previous Mössbauer and X-ray diffraction analysis [1] that showed that the major component in this meteorite is a fully disordered Ni-rich taenite with a minor amount of kamacite. In spite of the high Ni content, the ordered Fe-Ni alloy (tetrataenite) was not observed suggesting a fast cooling rate for this meteorite.

REFERENCES [1] R.B. Scorzelli, R.A. Pereira, C.A.C. Perez and A.A.R. Fernandes, *Proc. NIPR Symp. Antarct. Meteorites*, 7, 293, 1994. [2] T. Shimamura, M. Honda, H. Nagai and Y. Yoshioka, papers presented to the 16th Symp. Antarct. Meteorites 79, 1991. [3] Van Neste and Krishnadev, *Metallography* 9, 63, 1976.

ACKNOWLEDGMENTS We thank Dr K. Yanai, curator of the Antarctic meteorites collection, for providing the meteorite sample.

EXPERIMENTAL ALTERATION OF A METEORITIC MODEL-GLASS IN DIFFERENT MEDIA

Bourdin Emmanuel *, Thomassin Jean-Hugues *, Le Coustumer Philippe * , Abrioux Marie-Françoise and Nakashima Satoru **

* Materials and Environmental Geology, Faculty of Engineering, URA CNRS 721, University of Poitiers, 40 avenue du Recteur Pineau, 86022 Poitiers Cedex, FRANCE.

** Geological Institute, Faculty of Science, University of Tokyo, Hongo 7-3-1, Bunkyo-ku, Tokyo 113, JAPAN.

The weathering of anorthosites is an important problem for the understanding of the earliest process alteration of the Earth. One of the best similar materials for this approach is lunar meteorite. But due to the rarity of the samples, an other way have to be investigated, comparing the alteration products of natural samples and the alteration products of experimental evolutions under conditions simulating those which may occurred during the cooling of the Earth's atmosphere.

Experiments were performed on glass with a composition close to the glassy matrix analyzed in Y-86032 lunar meteorite (SiO_2 : 46.43 ; Al_2O_3 : 26.74 ; MnO : 0.02 ; MgO : 5.35 ; CaO : 15.45 ; Na_2O 0.53 ; K_2O : 0.10 ; TiO_2 : 0.24 ; Fe_2O_3 : 5.67) . In order to simulate the evolution under oxidizing conditions and to explain the presence of sulphate minerals, experiments were realized in water, and in sulfuric acidic media (pH 4 and pH 1) for simulation of the solutions resulting of the reaction between water and sulfides present in meteorites. Chips of glass were disposed in a PTFE reactor, at 80°C between 1 day to 6 months. The ratio solid surface area / volume of solution (S/V ratio) was equal to 0.1. The medium was not stirred and not replenished.

The reacting solutions were characterized by measurement of pH and analysis of elements (Si, Al, Fe, Mg, Ca, K, Na, and S). The solid phases were studied by XRD, Infrared reflexion spectroscopy, SEM and TEM using ultrathin sections of materials which provide samples on which it is possible to study the relation between alteration products and glassy matrix.

From the solutions analyses, the main important results concern :

- the evolution of pH. In each case, pH is growing up to slight basic value (~ 8.2) for water and pH4 conditions, and 3.6 for pH 1 medium.

- some elements (Si, Al, K) are detected in solutions for water and pH4 conditions and Ca for pH4.

- for pH1, all the elements are detected in solutions, especially silicium at the beginning of the experiments.

The solids characterization indicate the quick development of an alteration layer whose composition and structure is quite different according to the altering medium :

- in water and pH4 conditions, the layer is enriched in iron. With time, this layer overlaps an other one mainly composed of Si and Al.

- in pH1 conditions, a silica gel layer growths with time. When hydrated, this gel layer contains also calcium and sulphate ions, which give gypsum crystallization during evaporation after extraction of the sample at the end of the experiments.

From the ultrathin sections analysis, one can underline the r

ole of iron for the development of the alteration layer in water and pH4 conditions, the relationship between the alteration layer and the transformed glassy matrix and the presence of sulfur in the alteration products of the highest acidic conditions.

The results obtained by experimental way, compared to those determined on natural samples, give some informations on the evolution of the glassy materials of meteorites under oxidizing conditions. In order to get a better comparison, other experimental conditions have to be investigated with a special insight on the effect of temperature and of S/V ratio.

MINERALOGY AND SPECTROSCOPY OF HEATED ALLENDE METEORITE AND A K-TYPE ASTEROID 221 EOS. Takahiro Hiroi¹, Michael E. Zolensky², and Michael E. Lipschutz³. ¹SN3, NASA Johnson Space Center, Houston, TX 77058, USA, ²SN3, NASA Johnson Space Center, Houston, TX 77058, USA, ³Dept. of Chemistry, Purdue University, West Lafayette, IN 47907, USA.

Introduction: A 110-km asteroid 221 Eos has a red UV-Vis reflectance spectrum similar to the S asteroids but a relatively flat IR spectrum similar to the C asteroids. The IRAS albedo [1] of Eos is 0.12 which is in between the average S and C asteroids. Eos is classified as a K-type asteroid [2]. The K asteroids have been believed to be similar to CV and CO meteorites [3]. This study attempts to characterize the surface mineralogy of Eos by comparing its reflectance spectrum with Allende (CV3) meteorite powder including the experimentally heated ones.

Experimental: Bulk samples of Allende were heated in low-pressure (initially 10^{-5} atm) H_2 atmosphere for 1 week at 400, 500, 600, 700, 800, 900, 1000, 1100, and 1200°C [4,5]. Polished thin sections were prepared from the above Allende chips, and the composition of their olivine grains were analyzed by an electron microprobe. Each of the heated and unheated Allende samples was ground with a mortar and a pestle and was sieved into grain size $<125 \mu\text{m}$. Bidirectional reflectance spectra (0.3-2.6 μm) of the samples were measured at 30° incidence and 0° emergence angles. Telescopic reflectance spectra of asteroid 221 Eos [6,7] were combined to cover the wide wavelength range 0.3-2.6 μm . The 8-color reflectance spectra were taken from [6] for many other asteroids whose classifications [2] were available.

Mineralogy of heated Allende samples: The Allende CV3 chondrite consists predominantly of olivine (Fe_{50-97}), with minor pyroxene, pyrrhotite, Fe-Ni metal, glass, refractory phases (in CAI), and rare saponite. Chondrules are large, well defined and matrix supported, frequently with fine-grained rims. There is a concentration of olivine and pyroxene compositions at Fe_{55} and En_{55} . The major progressive changes in the mineralogy and petrography of Allende with heating are (1) progressive diffusion of Fe into olivine and pyroxene, which has become apparent (in backscattering electron images) by 800°C, and (2) blurring of chondrule boundaries as chondrule rims and peripheral areas recrystallize (most apparent by 1000°C). By 1200°C the meteorite has melted, and the resultant sample is composed of an extremely vesicular mass of large (50-100 μm) equidimensional olivine crystals (Fe_{64-67}) with interstitial high-Ca pyroxene, Fe-Ni metal and sulfides, and a spinel (approximately $Hn_{52}Chr_{48}$). A histogram of Fo % of olivine grains in some of the Allende samples is shown in Fig. 1.

Reflectance spectroscopy of Allende: Reflectance spectra of Allende powders are shown in Fig. 2. Heating doesn't produce much change up to 700°C. After 800°C the shape of the UV absorption edge around 0.3-0.4 μm changes to a steeper one. After 1000°C the overall brightness greatly increases. The 1200°C sample shows a clear composite band around 2 μm which is probably due to high-Ca and low-Ca pyroxenes or spinel-group minerals.

Spectral comparison of Allende and Eos: Comparison of reflectance spectra between Allende samples and asteroid 221 Eos is shown in Fig. 3. Reflectance spectrum of unheated Allende powder is relatively similar to the Eos spectrum in the visible wavelength range but has stronger UV absorption and higher IR reflectances than Eos. The UV absorption becomes weaker for the 500 and 700°C samples, and the IR reflectances lower for the 400 and 500°C samples. The 800-

1000°C samples have IR spectra similar to Eos but UV-Vis spectra completely different from Eos. After 1100°C the composite 1- μm absorption band due to olivine becomes much stronger and the brightness becomes much higher than Eos (albedo 0.12). The reflectance spectrum of the 500°C sample is the closest to the Eos spectrum.

UV-Vis spectral profile: Because the UV-Vis spectral profile is the most important characteristics of the S and K asteroids, three of the 8-color bands (0.337, 0.437, and 0.701 μm) were used to compare Allende samples and many more asteroids. Shown in Fig. 4 is a plot of two reflectance ratios, $R(0.337\mu\text{m}) / R(0.437\mu\text{m})$ vs. $R(0.437\mu\text{m}) / R(0.701\mu\text{m})$. The S asteroids form a cluster in the lower-left and the C, G, B, and F asteroids in the upper-right region in Fig. 4. Eos (K) is located at the edge of the S-asteroid cluster near the CGBF-asteroid cluster. Allende is out of the S-asteroid region before heating, but moves toward the edge of the S-asteroid region after heating, becomes closest to Eos at 500 and 700°C, goes into the CGBF-asteroid region at 800, 900, and 1000°C, and goes away from any asteroid at 1100 and 1200°C.

Discussion: Because there are some variety in mineral composition among CV3 meteorites, the slight difference of the IR spectrum between the Allende samples and Eos may not be important. On the other hand, the change of the UV-Vis spectral feature of Allende by heating is very important. The fact that the UV-Vis feature is greatly changed by heating at temperatures higher than 700°C, may give the higher temperature limit of the K asteroids if they initially formed of CV3-like material. The result that the Allende samples heated at 500 and 700°C have the closest UV-Vis reflectance spectrum to Eos, is similar to the previous result that the Murchison sample heated at 600°C had the closest UV-Vis feature to some of the C, G, B, and F asteroids [8, 9].

Conclusions

1. Reflectance spectra of a K asteroid 221 Eos a CV3 meteorite Allende are similar, and heating of the Allende sample at 500°C makes its spectrum even closer to that of Eos.
2. If Eos initially formed of CV3-like material, it is unlikely that the surface of Eos was heated to the temperatures above 700°C.
3. The spectral comparison of the heated Murchison and Allende samples with the C, G, B, F, and K asteroids suggests that a moderate heating may have taken place on some of the observed main-belt asteroids.

Acknowledgments: Reflectance spectra of Allende powders were measured at RELAB in Brown University. We thank S. F. Pratt for the measurements. RELAB is a multiuser facility operated under NASA grant NAGW-748. This research was supported in part by NASA grant NAG 9-48 to M. L. and the NASA Origins of Solar Systems Program to M. Z. This work was done while T. H. held a National Research Council-NASA/JSC Research Associateship and was supported by the NASA Planetary Astronomy Program.

References: [1] Tedesco E. F. (1989) in *Asteroids II*, pp. 1090-1138. [2] Tholen D. J. and Barucci M. A. (1989) in *Asteroids II*, pp. 298-315. [3] Bell J. F. *et al.* (1989) in *Asteroids II*, pp. 921-945. [4] Ikramuddin M. and Lipschutz M. E. (1975) *Geochim. Cosmochim. Acta*, **39**, 363-375. [5] Bart G. *et al.* (1980) *Geochim. Cosmochim. Acta*, **44**, 719-730. [6] Zellner B. *et al.* (1985) *Icarus*, **61**, 355-416. [7] Bell J. F. *et al.* (1988) *Lunar Planet. Sci.*, **XIX**, 57-58. [8] Hiroi *et al.* (1993) *Science*, **261**, 1016-1018. [9] Hiroi *et al.* (1994) *Proc. NIPR Symp. Antarct. Meteorites*, **7**, 230-243.

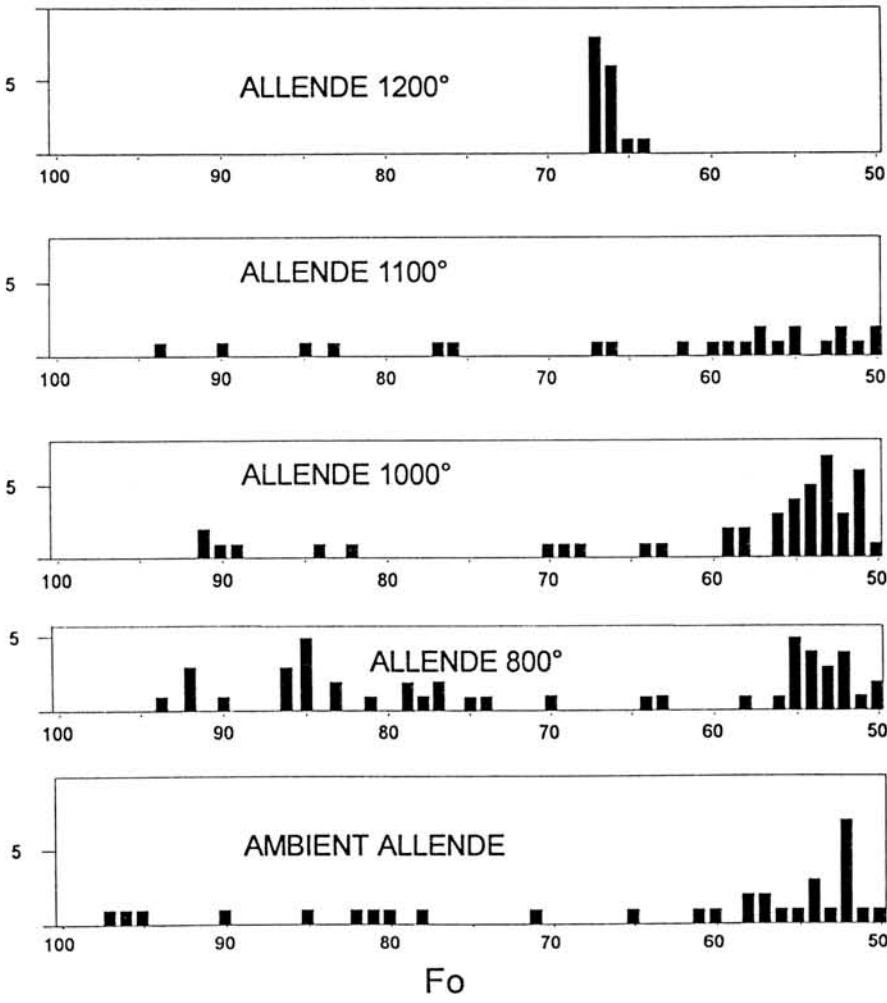


Fig. 1. The Fe contents vs. the number of olivine grains in the Allende samples measured by an electron microprobe.

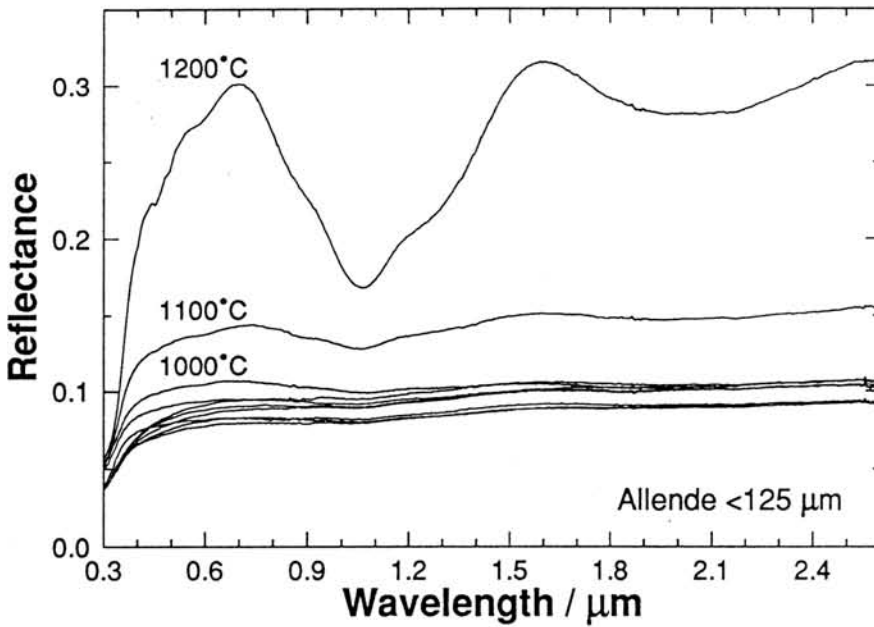


Fig. 2. Reflectance spectra of the unheated and heated Allende samples (<125 μm).

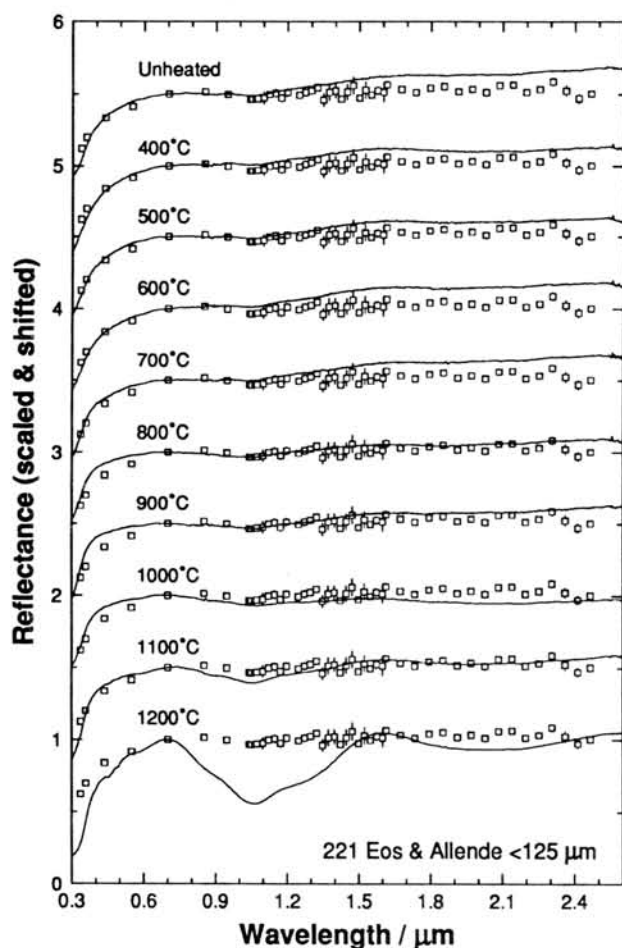


Fig. 3. Comparison of reflectance spectra of the Allende samples and asteroid 221 Eos. All the reflectance spectra are scaled to 1.0 at 0.7 μm and shifted from one another by 0.5.

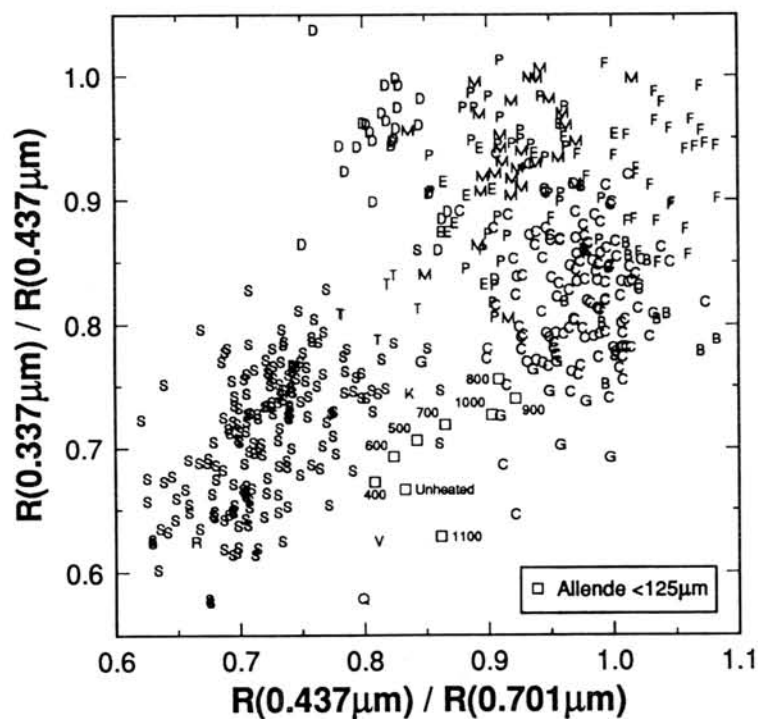


Fig. 4. A plot of the UV-Vis reflectance ratios of the unheated and heated Allende samples and the asteroids. The Allende samples are indicated by open squares and the asteroids by their class characters. The numbers indicate the heating temperatures ($^{\circ}\text{C}$) of the Allende samples.

MINERALOGY AND ULTRASTRUCTURE OF SOME ALTERATION PRODUCTS OF Y-86032 METEORITE.

Thomassin Jean-Hugues *, Le Coustumer Philippe * and Patrier Patricia **

* Materials and Environmental Geology, Faculty of Engineering, URA CNRS 721, University of Poitiers, 40 avenue du Recteur Pineau, 86022 Poitiers Cedex, FRANCE.

** ERM Society, Mérovée, 86320 Civaux, FRANCE

In order to characterize the alteration processes of anorthosites, we have got mineralogical data on lunar meteorite sample using some special analytical methods. We have studied one fragment of the meteorite Y-86032, provided by the Committee on Antarctic Meteorite Research. The sample is referenced as : Y-86032, sub n°123 (0.48g), received n° 724.

The results concern several kinds of preparation : direct study of the sample by XRD, powders diffraction on extracted materials at the surface of the sample, transmission microscopy on powders and ultrathin sections studied by TEM.

The two special technics we used for this study are:

- for XRD, linear localization detector which is very useful for diffraction of very small quantities of materials and which allows focussing of the X-ray beam on a small part of the sample by localization with a laser beam.

- ultrathin sections of materials which provide samples on which it is possible to study the relation between alteration products and minerals or glassy matrix. This preparation method provides ultrathin section with 50 nm thickness. At the difference of other technics, the confection is realized without ion bombardment and avoid any transformation of hydrous minerals.

The main results concern :

- the white products extracted at the surface sample and the mineralogy of the meteorite : olivine, pyroxene and plagioclase (labrador) and magnetite ? for the major components, with gypsum (XRD), calcite (XRD, TEM) , one phase with a d basal spacing equal to 1.02 nm (XRD) and kaolinite ? only observed by TEM and analyzed by EDS.

- the chemical composition of the alteration products determined on ultrathin sections with a special insight on iron-rich silicate phase and the relationships between Fe-Al / Fe-Al-S / Si - Al bearing phases.

The chemistry of some alteration products underline the accumulation of iron and the role of sulfur . For a better understanding of the evolution of the meteorite, other investigations have to be performed with a special emphasis on the complementarity of the presented method.

NASA Lunar Petrographic Thin Section Set in Hungary: Should Japan, NIPR prepare Thin Section Set of Antarctic Meteorites for education?

Dr. Imre Kubovics, Deputy State Secretary, Ministry of Culture and Education, Hungarian Republic, H-1055 Budapest, Szalay u. 10-14.
 Dr. Szaniszló Bérczi, R. Eötvös University, Dept. of Astronomy, H-1083 Budapest, Ludovika tér 2. Hungary

On 10th March, 1994, at Johnson Space Center, Houston, Texas, a Hungarian delegation could receive the famous NASA Lunar Sample Thin Section Set /No.6./ from Dr. James Gooding, Curator, for the Roland Eötvös University, Budapest, Hungary.

There are 20 packages of these thin section sets originally made for American Universities as educational materials. They consist of two parts: 12 thin sections and an epoxy disc with 6 lunar samples.

The 12 lunar sample thin sections for studies in microscope represent a nice cross section of materials collected by Apollo astronauts in the 1969-1972 years missions. They can be grouped to four parts: basaltic rocks, anorthositic rocks, breccias and soil samples.

The epoxy disc were made in 201 pieces for high school education. They can be studied with lupe. There are basalt, anorthosite, breccia samples /about 1 centimeter in size, each/ and three soil samples. The sets also contain a selection of papers on lunar samples, and a booklet: The Lunar Petrographic Thin Section Set written by Charles Meyer, earlier curator of lunar samples at JSC Houston.

We think, that NIPR has recently the one of the largest meteorite collection, which is "in hand" and is in continuous investigation like lunar samples. Both works are continuously published in the yearly conferences /NASA Lunar and Planetary Science Conference, 25th this year, NIPR Symposium on Antarctic Meteorites, 19th this year./ Seeing this noble competition the following idea emerged: it should be very interesting and useful for higher education and research, if an Antarctic Meteorite Thin Section Set should be prepared by NIPR, Japan. Both thin section sets could focus attention onto the planetary material exploration, and both could help international cooperation in education and research.

Moreover, these two types of sets /Lunar and Antarctic-Meteoritic/ could trigger the extension of cooperation in the form, that national collections should be prepared, from the most representative meteorites of the countries. Some meteorites are in governmental but some others are in private, or communal collections. Such thin section sets should be the units of international exchange, with international agreement control. Lunar Samples are the property of the Government of United States. Similarly, national thin section sets should be the properties of national governments, and an easy reaching of interesting rare meteorites this way could be arranged by loaning of them. /with governmental level guarantees/.

This proposal should initiate the reworking of old, almost forgotten meteorites, and also intend to find an easy, simple form and units of exchange of rare materials with high scientific value. Hungary has interesting meteorites: Kaba /c.c./, Mező-Madaras/c./, Zsadány /c./, see Bérczi, Lukács, this volume/, Mócs /c./ Knyahinya /c./, e.t.c. So Hungary offers cooperation. If this form of cooperation works, than the 20th Symposium of Antarctic Meteorites should be the excellent datum /after a year of preparation/ for beginning of this exchange of national meteorite collections.

**TWO STAGE EVOLUTION OF THE TERRISTRIAL PLANETS RECORDED IN
DIAMOND-BEARING CHONDRITES**

A. A. Marakushev

*Institute of Experimental Mineralogy, Russian Academy of Sciences
142432 Chernogolovka, Moscow district, Russia*

A cometary model for the origin of planets (Marakushev, 1992) shows a possibility to explain correctly the formation of chondrites and their diamondiferous mineralization. According to the model, origin of planets (including the parent chondrite planets) is resulted from accretion of the ice comet-like planetesimals, of hydrous composition at periphery of the Solar system (i.e. Neptun, Uranus) and hydrogen composition in the center of the system (i.e. Saturn, Jupiter, the parental terrestrial planets). As a result of gravitational compression all the planets had undergo a melting.

At the first stage of planetary evolution, melting has been followed layering and liquid iron-rock cores of chondrite composition formed. Ultra-high pressure caused by the fluid envelope in each planet promoted formation of diamond-bearing mineralization in a chondrite melt of the cores under strongly reduced conditions at high hydrogen pressure. At the second stage, a terrestrial planet lost its fluid envelope and oxidation reactions were predominated because dissipation of hydrogen from the planet. Low-pressure assemblages (i.e., the volcanic glass+plagoclase+olivine parageneses) were formed at this stage as well.

From the model proposed the following observations can be explain correctly.

1. Microdiamond as well as spinel and SiC are preserved in chondrites as relics (Levis et al., 1987) reflecting the earliest stage of evolution of a planet.

2. Microdiamond from the chondrites contains hydrogen (0.7 %), nitrogen (0.3 %), helium and other noble gases ($2 \cdot 10^{-3} \text{ cm}^3 \cdot \text{g}^{-1}$). High concentration of above gases causes relatively bulk density of diamond, $2.2 \text{ g} \cdot \text{cm}^{-3}$ (compare with regular density of diamond, $3.5 \text{ g} \cdot \text{cm}^{-3}$).

3. Isotopic composition of carbon, $\delta^{13}\text{C} = -38 \text{ ‰}$ reflects highly reduced conditions for the reactions $2\text{CO} = \text{C} + \text{CO}_2$, $\text{CH}_4 + 2\text{CO} = 3\text{C} + 2\text{H}_2\text{O}$ etc. Such conditions promoted formation of relic SiC associated microdiamond and graphite with a specific isotopic composi-

tion of the gases filled its porous: $\delta D = 180 \text{ ‰}$, $\delta^{15}N$ from -574 to -1000 ‰ etc. (Ash et al., 1983). This graphite differs from a regular graphite of chondrites ($\delta^{13}C = -18 \text{ ‰}$) crystallized from gases after the reaction $CO_2 + CH_4 = 2C + 2H_2O$ under relatively high f_{O_2} .

4. The diamond-bearing mineral assemblages show "highly anomalous isotopic ratios, varying more than 1000-fold for element such as C and N" (Anders, Zinner, 1993). These also reflect the early stage of the planetary evolution because of very high reduction of environment. At this stage the compounds with extremely low-degree of oxidation of metals (Al_2O , AlH , $AlCl$, SiO , SiH_2 , $SiCl_2$) were formed. The metals in such anomalous degree of oxidation have a strong affinity for the light isotopes of nonmetals. This causes the isotopic anomalies for diamond-bearing fractions of the chondrites. For example, the parageneses of silicium and olivine of high $^{16}O/^{18}O+^{17}O$ ratio was produced in the course of a reaction such as $2MgO + 2SiO = Mg_2SiO_4 + Si$, while Si and Al created the solid solutions with Fe. At the late stage of evolution, the $^{16}O/^{18}O+^{17}O$ ratio decreases and regular reaction $2MgO + SiO_2 = Mg_2SiO_4$ proceeds under relatively high f_{O_2} . In contrast to olivine, spinel ($\delta^{18}O = -38 \text{ ‰}$, $\delta^{17}O = -39 \text{ ‰}$) was formed at the first (low f_{O_2}) stage of the evolution only. For example, in the Allende meteorite two types of olivine with different oxygen isotope composition occur (Clayton et al., 1976; Weinbruch et al., 1989) $\delta^{18}O = -28,5 \text{ ‰}$ (-8,5) ‰, $\delta^{17}O = -23,0 \text{ ‰}$ (-4,5) ‰, reflecting above two stages.

Thus, studies of diamondiferous meteorites show clear evolution of fluid system of a planet from high reduction/high pressure to relatively low reduction/low pressure conditions. The evolution is caused by loss of the fluid envelope of a planet and dissipation of hydrogen.

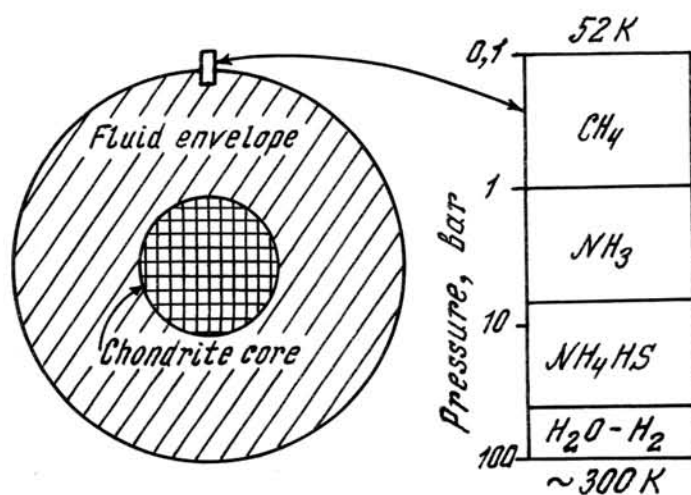
References

- Anders E., Zinner E. (1993) Interstellar grains in primitive meteorites: diamond, silicon carbide, and graphite. Preprint. California Institute of Technology. Pasadena, CA 91125.
- Ash R.D., Arden I.W., Grady M.N. (1988). Isotopically light carbon in the Allende meteorite. - *Meteoritics*. V.23. No 3.
- Clayton R.N., Onuma N., Mayeda T.K. (1976). A classification of meteorites based on oxygen isotopes. *Earth and Planet. Sci. Lett.* V.34. P.1607-1608

Lewis R.S., Bright D., Steel E. (1987) Presolar diamonds (C) in carbonaceous chondrites: size, distribution. - *Meteoritics*. V. 22. No 4.

Marakushev A.A. (1992) The origin and evolution of the Earth and other planets of the solar system. Moscow: Nauka (in Russian)

Weinbruch S., Zinner E.K., Steele I.M., et al. (1989) Oxygen isotopic composition of Allende olivines. 52-nd Annuale Meeting of the Meteoritical Soc. V.4. P.262.



Principal model of chondrite planet
at the early stage of evolution
(structure of Uranus is taken as an
example)

CARBON-14 DATA OF HETEROGENEOUS METEORITES AT HIGH-ENERGY-SIMS

Y. Miura

Faculty of Science, Yamaguchi University, Yamaguchi 753, Japan.

Accelerator mass spectrometry (AMS) with high current beam of Cs^+ for ultra-sensitive (sub-ppb) analysis of bulk sample is considered to be very high sensitive secondary ion mass spectrometry (SIMS) [1]. Radiocarbon data with the AMS have been obtained at homogeneous bulk samples by many researchers. But radiocarbon data of meteorite sample reveal significant difference between the AMS and counting methods. This is mainly because the counting method by large amount of sample with large errors cannot check heterogeneity of bulk sample.

Meteorite samples are originally the collision products from dust of the solar system, planetesimals, asteroids and meteoroids. Tiny fragments of meteorites broken by impact near the Earth (about 1 cm to 3 m in size on the Earth) reveal heterogeneous compositions and structures. The heterogeneous properties of various impact materials are confirmed by many systematic investigations of terrestrial impact craters and impact experiments [2]. As the petrographic and chemical classification of Antarctic meteorites is not uniform [3], isotopic data of the meteorites are also expected to be heterogeneous properties.

The main purpose of the present study is to elucidate heterogeneous ^{14}C isotopic age data of chondritic and achondritic meteorites determined by the AMS of high sensitivity SIMS and of achondrite determined by rare-gas (^{81}Kr) method.

1. Experimental procedures

The samples used in this study are Antarctic meteorites offered to the author as principal investigator by the National Institute of Polar Research (NIPR) of Japan. The Bruderheim (L6) and Kokubunji (L6) meteorites were used as standards of the recent definite fallen date. As Antarctic meteorites are not known for fallen date, the detailed carbon-14 data determined by the AMS data have been obtained to discuss the terrestrial ages, pairing problems and terrestrial histories of achondritic and chondritic meteorites [4,5,6,7].

In order to check the heterogeneity of meteorite, two experimental procedures of the AMS with Cs^+ ion have been applied in this study as follows :

1) IsoTrace-Toronto method: Chondrites of 0.5g were crushed and measured using the ^{14}C sensitivity of the AMS in Toronto [4]. Carbon species of CO_2 and CO were separated at different temperatures of a low temperature (500 to 900°C) and high temperature ($\sim 1600^\circ\text{C}$), respectively. The zero age was determined from saturated activity of ^{14}C in the Bruderheim chondrite, of mean value 54.6 ± 0.5 dpm/kg [4,5]. The terrestrial ages by ^{14}C AMS were used for the CO components of the melt fraction ($\sim 1600^\circ\text{C}$) which are mainly derived from cosmogenic carbon.

2) Tucson-Arizona method: Achondrites of 0.2-1.0 g were crushed and measured using the ^{14}C sensitivity of the AMS in Tucson [6,7]. For heavily weathered samples, the carbonates were removed with an acid etch. For cosmogenic ^{14}C , the sample was melted with iron, in a flow of oxygen. The zero age was determined from saturated activity of ^{14}C in the Bruderheim chondrite, of mean value 51.1 ± 1.4 dpm/kg [6,7]. High intensity ion-source of the AMS in Tucson was used due to the low contents of cosmogenic ^{14}C of achondrites.

2. Comparison with the various AMS data

The ^{14}C AMS data of several meteorites are listed in Table 1. Two Yamato Antarctic chondrites (used as Y- series) reveal consistence between the two analytical procedures of IsoTrace-Toronto and Tucson-Arizona [4,5,6,7], though there are still small differences between the two ^{14}C terrestrial ages. The different subnumbers, 62 and 64, of Y-791630 reveal different mean values of terrestrial ages (cf. Table 1). Two of the achondrites show remarkable difference between the AMS and counting (or $^{81}\text{Kr-Kr}$) methods, although these data are not direct comparisons with two different AMS data and long terrestrial ages by ^{81}Kr method should be checked by further cross-correlation with ^{14}C or ^{36}Cl .

Table 1. Comparison of the various AMS data of achondrites and chondrites.

Sample	Type	^{14}C dpm/kg	Age (kyr)	Remarks
1) Chondritic meteorites:				
Y-791717,55	C03	$25.74 \pm 0.19^*$	5.5 ± 0.1	IsoTrace-Toronto [4,5]
Y-791717,55	C03	28.0 ± 0.3	4.9 ± 1.3	Tucson-Arizona [6,7]
Y-791717,55HR**	C03	27.2 ± 0.4	5.1 ± 1.3	Tucson-Arizona [6,7]
Y-75271,51	L5	39.63 ± 0.22	1.9 ± 0.1	IsoTrace-Toronto [4,5]
Y-75271,51	L5	40.5 ± 0.6	1.9 ± 1.3	Tucson-Arizona [6,7]
Y-75271,51HR	L5	40.5 ± 0.3	1.9 ± 1.3	Tucson-Arizona [6,7]
Y-791630,62	L4	47.10 ± 0.35	0.5 ± 0.1	IsoTrace-Toronto [4,5]
Y-791630,64	L4	44.3 ± 2.5	1.2 ± 1.4	Tucson-Arizona [6,7]
2) Achondrites:				
Y-74097,66	Dio	15.22 ± 0.1	9.9 ± 0.1	IsoTrace-Toronto [4,5]
Y-74097	Dio	5.3 ± 1.1	19 ± 2	Counting method [8]**
ALH77256	Dio	17.7 ± 0.4	10.2 ± 1.3	Tucson-Arizona [6,7]
ALH77256	Dio	-	11.1 ± 1.5	Counting method [9]**
Y-790260,90	Euc	3.47 ± 0.16	23.6 ± 1.4	Tucson-Arizona [6,7]
Y-790260,90	Euc	-	140 ± 32	$^{81}\text{Kr-Kr}$ data [10]**

* 1σ errors (dpm/kg).

** Hydrolysis residue.

*** Counting or $^{81}\text{Kr-Kr}$ method for comparison.

3. Characterization of meteorites with AMS-SIMS method

The sources of ^{14}C ion in Antarctic meteorites can be affected by different factors (f) as follows [5]:

$$f(\text{total}) = f(\text{spallation}) + f(\text{contamination}) + f(\text{AMS method}) \dots\dots\dots(1)$$

Each factor of ^{14}C source can be described as follows:

1) Spallation of ^{14}C is generated predominantly of all ^{14}C sources (up to 70% of the ^{14}C level), which is divided into three types of ^{14}C sources.

(a) Factor of spallation-1 in cosmic rays is dependent on "sample chemistry" through nuclear-reaction $^{16}\text{O}(p,3p)^{14}\text{C}$ found in silicate or oxide phases of meteorites in the cosmic space [11]. Chemistry of meteorites is changed on classification of the major chemical groups (E, H, LL or C) of chondrites which

is difference in oxidation of primordial materials of the solar system dust. On the other hand, achondrites of evolved meteorites are considered to be impact fragments of planetesimals or asteroids which show also heterogeneous chemistry. Thus, we are now used correlated data of oxygen content for calculation of the AMS terrestrial ages. (b) Factor of spallation-2 is "shielding effect" or "heterogeneity" of meteorites. Sampling location of meteorites is dependent on depth from the surface of zoned or heterogeneous sample (i.e. shielding effects from the galactic origin). This factor is obtained as a trace difference of ^{14}C amount (a few percents of ^{14}C level). The depth profile can be checked easily by the conventional SIMS, because the depth profile of isotopic ratio by using the same SIMS method was established at heterogeneous layered structure of plagioclase minerals [12]. Heterogeneity of meteorites can be explained by the impact process in the cosmic space, atmosphere and on the surface of the Earth. The shock effects can be found by shock glassy veins, diaplectic glassy texture, and shocked crystalline phases of the meteorites. Light and volatile elements near the fusion-crust usually are largely depleted. There are two major structures of chondritic meteorites; onion-layer (concentric) structure [13], and brecciated rubble pile structure [14]. Although we can get isotopic ratio by the conventional SIMS from heterogeneous sample [12], the precise data of trace ^{14}C amount at small area and elevated temperature cannot be obtained by the same SIMS method. The factor of heterogeneity (up to several percents of ^{14}C level) cannot be discarded by the conventional AMS methods. Thus, it is now proposed to make newly development of the AMS with scanning SIMS device with fine collimeter-controlled primary beams in future [1]. (c) Factor of spallation-3 is terrestrial effects of sampling location, shielding and fission products by terrestrial radioactive isotopes (up to 11 % for ^{14}C level). This factor can be checked by the detailed recovery condition of the Antarctica.

2) Contamination on the Earth is a significant factor (up to 22 % for ^{14}C level), mainly from the atmospheric exchange and exposure on the Earth of recovery condition on ice-fields, and storage-weathering (within the glacier). Terrestrial weathering effect can be checked by the extraction fractions from low to high melted temperatures.

3) Factor of the AMS method is dependent on the AMS analytical procedure including laboratory contamination of sample preparation (i.e. combustion in the IsoTrace-Toronto method, or Fe-mixture in Arizona method), carrier gas, and the isotopic ratio ($^{14}\text{C}/^{12}\text{C}$ or $^{14}\text{C}/^{13}\text{C}$, respectively). The analytical errors of the AMS method are not so large (0.5 % for ^{14}C level), though the AMS data are checked by standards and blank tests in each run.

4. Summary

The present results are summarized as follows:

1) The ^{14}C AMS terrestrial ages of Antarctic achondrites and chondrites are compared with two different AMS methods of the IsoTrace-Toronto and Tucson-Arizona to elucidate the heterogeneity of ^{14}C amounts of meteorites.

2) The ^{14}C AMS data of three Yamato Antarctic chondrites reveal almost consistence between the two analytical procedures, although the two achondrites show remarkable difference between the AMS and counting (or $^{81}\text{Kr-Kr}$) methods. These data will be compared with two AMS and rare-gas (^{81}Kr etc.) analyses.

3) The various terrestrial ^{14}C ages of Antarctic meteorites can be explained by the various sources expressed by equation (1). Among these factors, heterogeneity of meteorite samples cannot be expected from the bulk sample analyzed by the conventional AMS method, though other major sources of ^{14}C are checked by the AMS analytical procedure of factors of spallation, contamination and the AMS analytical methods.

4) Heterogeneity of texture and minerals in meteorites should be checked by new development of the AMS attached with scanning SIMS device of fine collimator-controlled primary beam. The newly designed AMS with fine-focused beam-controller (AMS-SIMS method) can obtain difference in ^{14}C ratio of the depth-profile and various materials of meteorites which indicate aggregates in space of different formation condition and time.

References

- [1] A.E. Litherland, J.C. Rucklidge, G.C. Wilson, W.E. Kieser, L.R. Kilius and R.P. Beukens: SIMS IV (Chemical Physics 36), 170-174 (1984).
- [2] Y. Miura: Shock Wave (Springer-Verlag), 1, 35-41 (1991).
- [3] Y. Matsumoto, M. Hayashi, M. Daishi and Y. Miura : Mem. Natl Inst. Polar Res. (NIPR, Tokyo), Special Issue 12, 72-81 (1981).
- [4] R.P. Beukens, J.C. Rucklidge and Y. Miura : Proc. Symposium on Antarctic Meteorites (Natl Inst. Polar Research, Tokyo), 1, 224-230 (1988).
- [5] R.G. Cresswell, Y. Miura, R.P. Beukens and J.C. Rucklidge : Proc. NIPR Symp. Antarctic Meteorites (NIPR, Tokyo), 6, 381-390 (1993).
- [6] A.J.T. Jull, D.J. Donahue and T.W. Linick : Geochim. Cosmochim. Acta, 53, 2095-2100 (1989).
- [7] A.J.T. Jull, Y. Miura, E. Cielaszyk, D.J. Donahue and K. Yanai : Proc. NIPR Symp. Antarctic Meteorites (NIPR, Tokyo), 6, 374-380 (1993).
- [8] K. Kigoshi and E. Matsuda : Int. Workshop on Antarctic meteorites. Tech. Rep. 86-01 (LPI, USA), 58-60 (1986).
- [9] E.L. Fireman and T.L. Norris: Proc. Lunar Planet. Sci. Conf., 12B, 1019-1025 (1982).
- [10] L. Schultz : Mem. Natl Inst. Polar Res. (NIPR, Tokyo), Spec. Issue 41, 319-327 (1986).
- [11] R.C. Reedy and J.R. Arnold : J. Geophys. Res., 77, 537-555 (1972).
- [12] Y. Miura and T. Tomisaka : SIMS IV (Chemical Physics 36), 460-462 (1984).
- [13] M. Miyamoto, N. Fujii and H. Takeda : Lunar and Planet. Sci. Conf., 12, 1145-1152 (1981).
- [14] E.R.D. Scott and R.S. Rajan : Geochim. Cosmochim. Acta, 45, 53-67 (1981).

THE OPAQUE MINERALS IN IMPACTITE GLASSES FROM THE LONAR IMPACT CRATER, INDIA

V. K. NAYAK

Department of Applied Geology, Indian School of Mines, Dhanbad 826004, India

Several polished thin sections of impactite glasses from the Indian Impact Crater at Lonar ($19^{\circ}58'N$: $76^{\circ}31'E$), are examined in transmitted and reflected light. The objectives of this study are to understand whether the opaque minerals can be used as a reliable criteria for impact metamorphism and can we learn the behaviour of opaque minerals in basalt under impact environment.

The Lonar impact glass corresponds to Class 5 shocked category (Kieffer et al. 1976) where most of the mineral constituents of basalt have melted to produce impactite at 800 to 1000 kbar pressure. Generally, the glass is pale brown to deep brown in colour with magnetite, titaniferous magnetite and ulvospinel (?). The Fe-Ti oxide minerals occur in various shapes like skeletal, star and very minute grains and have a special significance. Sometimes the Fe-Ti oxide skeletal have a isometric symmetry. Breakdown textures are also documented and discussed. The opaques are marked by parallel, sub-parallel and folded structures and impart  extraordinary flow patterns. The arrangement and distribution of Fe-Ti oxide patterns are discussed to understand the nature of their formation in shock environment. On the whole, the Fe-Ti oxides in impactite glasses are closely comparable with those of unshocked basalts, although with minor variation. It is suggested that the presence of skeletal and other shapes of Fe-Ti minerals and their ornamentation patterns reflect a high temperature fusion of basalt followed by subsequent rapid rapid cooling in an impact environment.

REFERENCE

- Kieffer, S.W., Schall, R., Gibbons, R.V., Horz, F., Milton, D.J. and Dube, A. (1976) Shocked basalt from Lonar Impact Crater, India and experimental analogues: 7th Proc. Lunar Conf., pp. 1391-1412.

